Kent Academic Repository

Mackenzie, Cassidy (2017) *The Properties And Function Of Tropomyosin Dimers In Muscle Regulation.* **Doctor of Philosophy (PhD) thesis, University of Kent,.**

The Properties And Function Of Tropomyosin Dimers In Muscle Regulation

By Cassidy Mackenzie

A thesis submitted to the University of Kent for the degree of Doctor of Philosophy in Biochemistry

School of Biosciences

2017

Declaration

No part of this thesis has been submitted in support of an application for any degree or qualification of the University of Kent or any other University or Institute of learning.

Dedication

This thesis is dedicated in loving memory to my mother, Ira Mackenzie.

09.02.1962 – 11.06.2017

I always promised her I would become a doctor, I just wish she were here

to see it.

Peace, love & happiness

Acknowledgments

I would like to thank my supervisors Professor Michael. A. Geeves and Dr Wei-Feng Xue for their support and encouragement through my PhD. Their combined expertise, guidance and support enabled me to complete such an endeavour.

I am extremely grateful for the members of the Geeves and Xue labs, and colleagues in the School of Biosciences, past and present, for their support, friendship and pep talks over coffee; Dr Nancy Adamek, Samantha Lynn, Dr Zoltan Ujfalusi, Dr Alice Ward Racca, Dr Jonathon Walklate, Dr David Pearson, Dr Anja Schmidtmann and Jennifer O'Brien.

I would like to thank the University of Kent for my 50th Anniversary Scholarship and Associate Fellow Scheme training, without which I would not have been able to complete my work and teaching.

Finally, special gratitude goes to my wonderful family and friends, Michael and Alexander for always believing in me and being proud, even when they don't always understand precisely what it is I am doing!

Thank you all!

Abstract

Myosin binding to actin, and thus muscle contraction, is regulated by Tropomyosin (Tpm), Troponin (Tn) and calcium (Ca^{2+}). Tpm, is an α-helical coiled-coil dimer, which exists as a homo- or heterodimer. Two major isoforms of Tpm are found in striated muscle, α and β. Though it is known that different dimers exist, the mechanism by which they form and exchange is not fully understood.

The thermal stability and exchange between dimers was explored with the use of circular dichroism and SDS PAGE densitometry analysis. Homodimers showed little exchange to form heterodimers at temperatures up to 20 ℃ Dimer stability at these temperatures reduces the need for chemical cross-linking samples. While extensive exchange was seen at 37 ℃ Reverse exchange of WT and mutant (E54K – dilated cardiomyopathy mutant) containing heterodimers to form homodimers did not show the same extent of exchange, suggesting a dimer preference. Results showed the ability to determine dimer content of a solution with the use of polyacrylamide gels and chemical cross-linking.

The thermal melting curves of Tpm highlighted a significant destabilisation of β Tpm against the α isoform. Tpm heterodimer containing E54K mutant showed a decreased thermal stability. Notable differences were seen not only for isoforms and homo- and heterodimers, but also for buffer conditions and protein tags. Increased salt concentrations led to an increase in thermal stability. Cross-linking dimers increased thermal stability, whereas addition of His-tags led to a decrease in thermal stability. Changes in thermal stability highlighted the need for caution when tagging or cross-linking the protein. Dimer exchange on actin provided conflicting results between SDS PAGE cosedimentation assays and pyrene fluorescence cosedimendation assays, which highlighted limitations of cross-linking Tpm and using fluorescent labels.

The stiffness of Tpm dimers was explored using atomic force microscopy (AFM) to image Tpm particles. Significant differences were seen between the relatively stiff α Tpm and less stiff β isoform. Changes in stiffness of Tpm affect its ability to cooperatively activate the thin filament, and provides insight into the assembly of dimers in vivo.

Abbreviations

AFM	Atomic force microscopy
ARVC	Arrhythmogenic right ventricular cardiomyopathy
CD	Circular dichroism
DCM	Dilated cardiomyopathy
DTT	Dithiotreitol
EM	Electron microscopy
F actin	Filamentous actin
G actin	Globular actin
HCM	Hypertropic cardiomyopathy
HMW	High molecular weight
KPi	Potassium phosphate
L_c	Contour length
LMW	Low molecular weight
L_p	Persistence length
MD	Molecular dynamics
MOPS	3-(N-morpholino)propanesulfonic acid
Pi	Inorganic phosphate
Pyrene	N-(1-pyrenyl) iodoacetamide
S1	Myosin subfragment 1
SDS	Sodium dodecyl sulphate
STM	Scanning tunnelling microscopy
Tpm	Tropomyosin

Tn   Troponin

WT   Wild type

Table of contents

List of figures

XV

XX

List of tables

Introduction

1. Introduction

Tropomyosin (Tpm) is a 40 nm coiled-coil dimer that functions as a regulatory component of the thin filament in muscle tissue. Tpm is bound to actin, to regulate myosin binding and thus, muscle contraction. Non-muscle tropomyosins are important for motile processes such as cell migration, vesicle transport and cytokinesis, to name a few. Four genes encode the tropomyosin family. As a result of alternate splicing and post-translational modifications, up to 40 different isoforms of the protein exists. From these isoforms, tropomyosin is known to exist as homodimers and heterodimers. How these dimers form, and if partner exchange takes place, remains unknown. Mutations of tropomyosin are known to cause cardiomyopathies. The role of tropomyosin in regulating muscle contraction and the associated mutations make the protein of particular interest to study.

1.1. Tropomyosin gene structure and naming of isoforms

Mammalian tropomyosins are encoded by four genes; TPM1, TPM2, TPM3 and TPM4, which are located in different chromosomes; 15q22.1, 9p13.2-p13.1, 1q21.2 and 19p13.1, respectively. Alternate splice variants result in up to 40 different isoforms of the protein. The naming of isoforms in literature can be confusing at times, however

Geeves, et al. published a paper in 2015 outlining a systematic nomenclature for mammalian Tpm isoforms, which simplified and rationalised the naming system. Simply, TPM1 encodes α Tpm, TPM2 encodes ß Tpm, TPM3 encodes γ Tpm and TPM4 encodes δ Tpm. Many genes are expressed in multiple tissues, giving rise to multiple isoform expression. Tms are classified as either high molecular weight (HMW): containing 284-285 amino acids (excluding hTM1-1), including exons 1a – 2b, and low molecular weight (LMW): containing 245-248 amino acids, which exclude exons 1a – 2b and start from exon 1b instead.
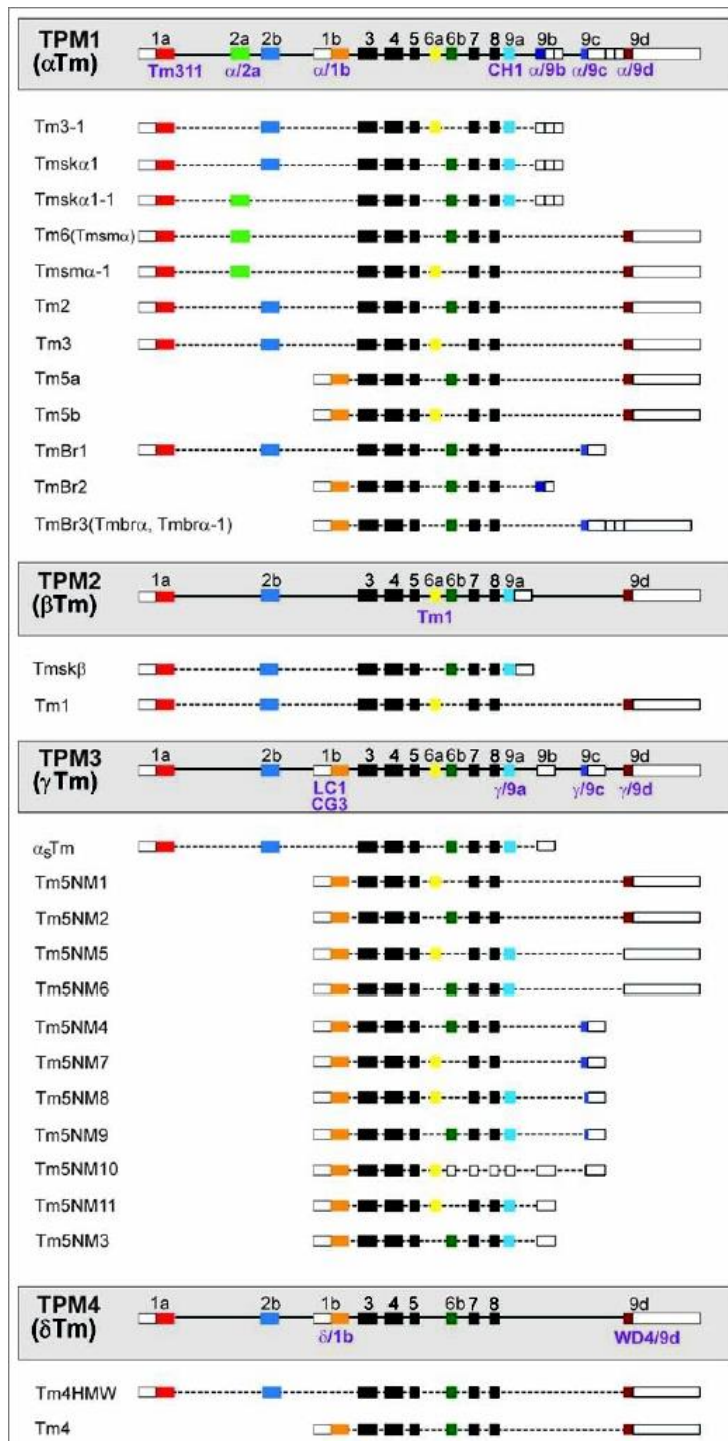
Figure 1.1.1 Organisation of mammalian Tpm genes and isoforms generated from alternative splicing. Protein coding exons 1 – 9 are shown by coloured boxes, while uncoloured boxes show untranslated sequences. Black boxes are common exons between all genes that have a high sequence homology. Tpm antibodies are listed (purple) below the exon containing the epitope. *Tropomyosin isoforms and reagents. Schevzov G1, Whittaker SP, Fath T, Lin JJ, Gunning P W (2011).*

SHORT NAME	COMMON NAME	ALTERNATE NAMES	FORMAL PROTEIN NAME	CODING EXONS
Tpm1.1	Tpm skα	αTm, fast skTm , cardiac Tpm, striated Tpm	Tpm1.1st (a.b.b.a)	1a, 2b, 6b, 9a
Tpm 1.2	Tpm skα1	κTm, Tmskα1-1	Tpm1.2st (a.a.b.a)	1a, 2a, 6a, 9a
Tpm1.3	Tpm smα-1	α smooth Tpm	Tpm1.3sm (a.a.a.d)	1a, 2a, 6a, 9d
Tpm1.4	Tpm smα	Tm6, α smooth Tpm, Tpm α1.2	Tpm1.4sm (a.a.b.d)	1a, 2a, 6b, 9d
Tpm1.5	Tm3-1	-	Tpm1.5cy (a.b.a.a)	1a, 2b, 6b, 9a
Tpm1.6	Tm2	-	Tpm1.6cy (a.b.b.d)	1a, 2b, 6b, 9d
Tpm1.7	Tm3	Tpm 1.4	Tpm1.7cy (a.b.a.d)	1a, 2b, 6a, 9d
Tpm1.8	Tm5a	-	Tpm1.8cy (b.-.b.d)	1b, 6b, 9d
Tpm1.9	Tm5b	-	Tpm1.9cy (b.-.a.d)	1b, 6a, 9d
Tpm1.10	TmBr1	-	Tpm1.10br (a.b.b.c)	1a, 2b, 6b, 9c
Tpm1.11	TmBr2	-	Tpm1.11br (b.-.b.b)	1b, 6b, 9b
Tpm1.12	TmBr3	Tmbrα, Tmbrα-1, Tpm α-1.6	Tpm1.12br (b.-.b.c)	1b, 6b, 9c
Tpm1.13	-	-	Tpm1.13 (b.-b.a)	1b, 6b, 9a

Table 1.1.1 Tropomyosin isoforms derived from human TPM1 gene (geneID: 7168), the mouse Tpm1 gene (geneID: 22003) or the rat Tpm1 gene (geneID: 24851). Formal name; st: striated muscle, sm: smooth muscle, br: brain, cy: other cytoplasmic. Letters in brackets reflect splicing of four codons, a dash indicates a missing exon and ergo a short form of the protein. The coding exons do not reflect splice variants in non-coding regions at the 3' end of mRNA transcripts. Modified from Geeves paper (Geeves, Hitchcock-DeGregori et al. 2015).

SHORT NAME	COMMON NAME	ALTERNATE NAMES	FORMAL PROTEIN NAME	CODING EXONS
Tpm3.12	Tpm skα-slow	γTm, αsTm1, slow skTm	Tpm3.12st (a.b.b.a)	1a, 2b, 6b, 9a
Tpm3.13	-	-	Tpm3.13cy (a.b.a.d)	1a, 2b, 6a, 9d
Tpm3.1	Tm5NM1	-	Tpm3.1cy(b.-.a.d)	1b, 6a, 9d
Tpm3.2	Tm5NM2	-	Tpm3.2cy(b.-.b.d)	1b, 6b, 9d
Tpm3.3	Tm5NM3	-	Tpm3.3cy(b.-.b.a)	1b, 6b, 9a
Tpm3.4	Tm5NM4	-	- Tpm3.4cy (b.-.b.c)	1b, 6b, 9c
Tpm3.5	Tm5NM5	-	- Tpm3.5cy(b.-.a.a)	1b, 6a, 9a
Tpm3.7	Tm5NM7	-	Tpm3.7cy (b.-.a.c)	1b, 6a, 9c
Tpm3.8	Tm5NM8	-	Tpm3.8cy (b.- .a.a/c)*	1b, 6a, 9a/c
Tpm3.9	Tm5NM9	-	Tpm3.9cy (b.- .b.a/c)*	1b, 6b, 9a/c

Table 1.1.2 Tropomyosin isoforms derived from human TPM3 gene (geneID: 7170), the mouse Tpm3 gene (geneID: 59069) or the rat Tpm3 gene (geneID: 117557). * Exon 9 includes 9a and five amino acids from 9c. Formal name; st: striated muscle, sm: smooth muscle, br: brain, cy: other cytoplasmic. Letters in brackets reflect splicing of four codons, a dash indicates a missing exon and ergo a short form of the protein. The coding exons do not reflect splice variants in non-coding regions at the 3' end of mRNA transcripts. Modified from Geeves paper (Geeves, Hitchcock-DeGregori et al. 2015).

SHORT NAME	COMMON NAME	ALTERNATE NAMES	FORMAL PROTEIN NAME	CODING EXONS
Tpm2.1	Tpm sm ß	ßTm Tm1, Tm1ß, smooth Tpm, smooth α-Tpm	Tpm2.1sm/cy (a.b.a.d)	1a, 2b, 6a, 9d
Tpm2.2	Tpm sk ß	ß skeletal Tpm, ß cardiac Tpm	Tpm2.2st (a.b.b.a)	1a, 2b, 6b, 9a
Tpm2.3	-		Tpm2.3 (a.b.b.d)	1a, 2b, 6b, 9d
Tpm2.4	-		Tpm2.4 (a.b.a.a)	1a, 2b, 6a, 9a

Table 1.1.3 Tropomyosin isoforms derived from human TPM2 gene (geneID: 7169), the mouse Tpm2 gene (geneID: 22004) or the rat Tpm2 gene (geneID: 500450). TPM2 genes in human, mouse and rat do not contain exon 1b. Formal name; st: striated muscle, sm: smooth muscle, br: brain, cy: other cytoplasmic. Letters in brackets reflect splicing of four codons, a dash indicates a missing exon and ergo a short form of the protein. The coding exons do not reflect splice variants in non-coding regions at the 3' end of mRNA transcripts. Modified from Geeves paper (Geeves, Hitchcock-DeGregori et al. 2015).

SHORT NAME	COMMON NAME	ALTERNATE NAMES	FORMAL PROTEIN NAME	CODING EXONS
Tpm4.1	Tm4HMW	δTm	Tpm4.1cy (a.b.b.d)	1a, 2b, 6b, 9d
Tpm4.2	Tm4	-	Tpm4.2cy (b.-.b.d)	1b, 6b, 9d

Table 1.1.4. Tropomyosin isoforms derived from human TPM4 gene (geneID: 7171), the mouse Tpm4 gene (geneID: 326618) or the rat gene Tpm4 (geneID: 248512). The mouse and rat genes do not contain exon 9a; human genes contain exon 9a, but it is not expressed. Formal name; st: striated muscle, sm: smooth muscle, br: brain, cy: other cytoplasmic. Letters in brackets reflect splicing of four codons, a dash indicates a missing exon and ergo a short form of the protein. The coding exons do not reflect splice variants in non-coding regions at the 3' end of mRNA transcripts. Modified from Geeves paper (Geeves, Hitchcock-DeGregori et al. 2015).

1.2.   Tropomyosin structure and dimer formation

Tpm can exist as a heterodimer (α – ß, or wt Tpm – Tpm* with one carrying a single point mutation) or a homodimer. How heterodimers form and if partner exchange takes place remains unknown. Yet the properties of the heterodimer (wt α – ß Tpm, or wt Tpm – Tpm*) are known to be distinct from the homodimer (Janco, Kalyva et al. 2012). Each α helix contains a heptad repeat of residues (*abcdefg*). These seven residues span across ~2 turns of the helix. Hydrophobic residues in positions *a* and *d* are responsible for maintaining the coiled-coil shape, while residues *b*, *c* and *f* are hydrophilic, polar or charged residues, and face the exterior of the coiled-coil. Residues *e* and *g* are responsible for ionic interactions and can form salt bridges. Protruding side chains from residues *a* and *d* in one α helix fill the gaps in the other and vice versa, described as "knobs in holes" packing, which helps to hold the structure together (Crick 1953).
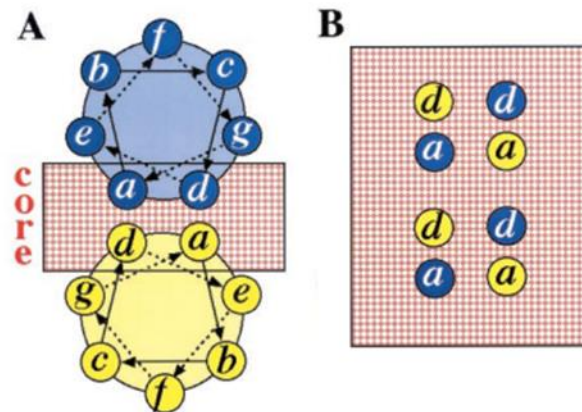
Figure 1.2.1 The interaction of two Tpm coiled coils. The heptad repeat is shown in A, looking from the N-terminus, end on. The "knobs in holes" packing is shown in B, highlighting the core interface (Stewart 2001).

Tpm polymerises head to tail along actin filaments at ~38.5 nm intervals. NMR studies have revealed that the N-terminal of one Tpm is inserted into the cleft of a partly unwound C-terminal on the following Tpm. The N-terminal is shown to contain positively charged residues, while the C-terminal contains negative residues (Corrêa, Salinas et al. 2008).

The shape of Tpm brings up many questions, as its structure is key to its role. It is not clear whether the shape of Tpm is defined by its primary structure, making it a complementary fit to actin, or if Tpm has a degree of flexibility that enables it to adapt to the actin and environment.

Holmes and Lehman proposed in 2008 a Gestalt-binding of Tpm to actin. In this, the form-function relationship of Tpm occurs as a result of the preformed shape of Tpm and its tendency to associate and polymerise head to tail. Gestalt binding also describes Tpm

and actin associations as more than just a simple lock and key binding mechanism, involving other weak interactions. This becomes an interesting theory in relation to disease causing mutations, wherein a single point mutation can cause a specific disease. Cardiomyopathy mutants D175N and E180G for example, were seen to affect local flexibility, but also conferred changes further down the filament (Li, Suphamungmee et al. 2012, Ly, Lehrer 2012).

The structure of Tpm is not a simple coiled coil, as it first may seem. Tpm contains regions of destabilisation, caused by alanine clusters and broken core regions. Strain created by the alanine clusters may be alleviated through the broken core regions. Indicating that Tpm has areas along the protein with more flexibility than others, which is communicated from end to end and influences the entire protein, rather than defining rigid and flexible areas separately.

Li et al. 2010 explored the structure of Tpm using EM and Molecular Dynamics (MD – a computational simulation of atomic trajectories of N particles). They uncovered six regions of the coiled coil that displayed a narrowing of the radius, which corresponded to alanine clusters on the Tpm. The alanine clusters affected Tpm at long range, rather than locally. A lack of changes in the local curvature and local deviations of Tpm was seen when comparing areas with and without alanine clusters. The triple mutant A74L–A78V–A81L showed an increase in local flexibility and an overall straighter structure, resulting in a longer persistence length, which is a measure of flexibility (Li, Holmes et al. 2010). This again highlights the interesting characteristics of mutations, which make their local and overall effects difficult to predict.

Overlapping head to tail regions of Tpm alongside Tpm – actin interactions, Tn and myosin, mediate Tpm binding to actin. These interactions are a result of the 14 quasi-equivalent repeats in Tpm containing charged and uncharged side chains. The heptad repeat of Tpm has been proposed to have a 14-fold periodicity that can be divided into two bands α and β. These have been proposed to bind to complementary sites along 7actins in the relaxed (α) and active (β) states (Stewart, McLachlan 1976).

1.3 What is muscle?

Muscle falls under two categories, smooth and striated. Smooth muscle is responsible for the involuntary contraction of hollow organs, such as the respiratory tract, blood vessels, the bladder and the uterus, where it is responsible for propelling the contents around or out of the body. The muscle fibres are tapered at both ends of the spindle and contain a single nuclei at the centre, they are arranged in bundles or sheets, and as such, do not appear striated. Striated muscle can be subdivided into cardiac and skeletal muscle. Skeletal muscle is made up of bundles of multinucleated fibres, whereas cardiac fibres (myofibrils) are branched and contain one or two centrally located nuclei. Cardiac fibres are connected by intercalated disks (Z disks), which enable the muscle to contract rapidly as a unit.
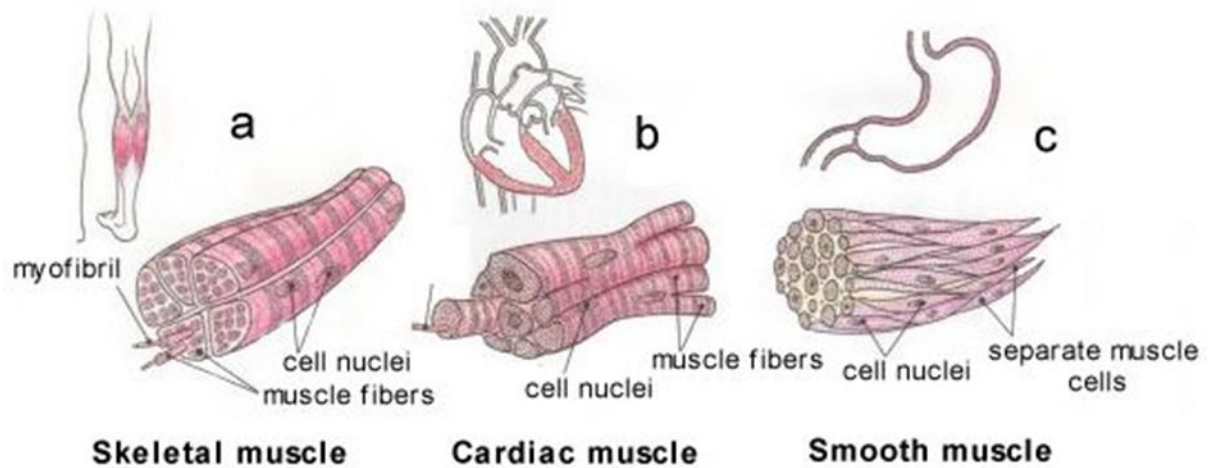
Figure 1.3.1. A comparison of muscle tissue, highlighting multinucleated fibres of skeletal muscle, single nuclei in smooth muscle and a couple of nuclei in cardiac tissue.

When striated muscle is studied under a light microscope, it appears to have stripes, called sarcomeres, shown in figure 1.3.2. Mutations of the sarcomeric proteins are responsible for hypertrophic cardiomyopathy (HCM) and dilated cardiomyopathy (DCM). Striated muscle is comprised of light bands (I bands), which contain thin filaments, and dark bands (A bands), which contain thick filaments and overlapping thin filaments. Within the A band there is an area in the centre, which is lighter and comprised purely of thick filaments, called the H zone, and the centre of this is highlighted by the M line. Z disks (Z line) are found in the centre of I bands and the section between two Z disks defines one sarcomere.
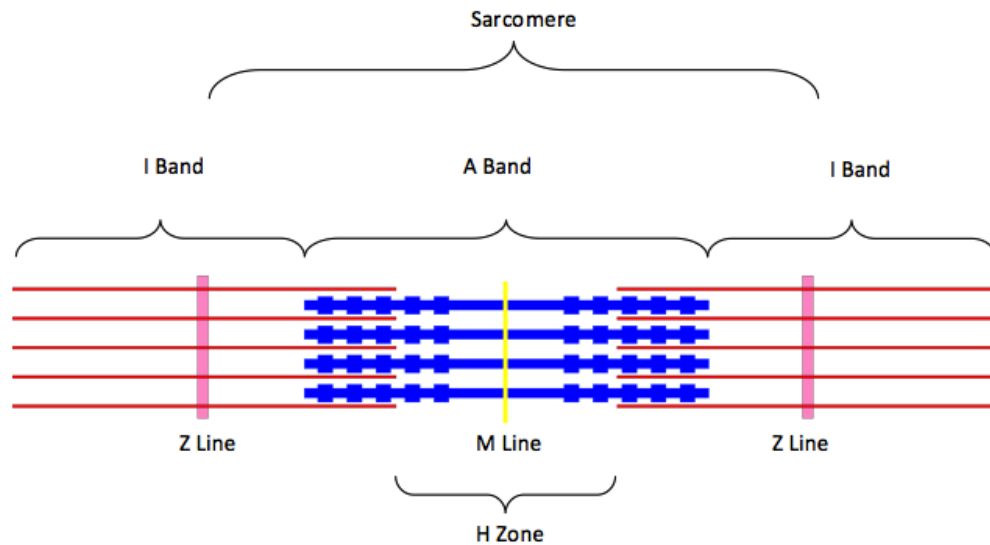
Figure 1.3.2. A schematic diagram of a relaxed sarcomere. Thin filaments are shown in blue and thick filaments are shown in red. A sarcomere is highlighted between the two Z lines (Image by Cassidy Mackenzie).

1.3.1 Components of muscle - Actin and myosin

Muscle contraction is described using the sliding filament model, in which thick and thin filaments slide along each other, bringing Z disks closer together and decreasing the size of the sarcomere. The thick filament is made up of polymerised myosin. This interacts with the thin filament, which is comprised of 2 filaments of actin alongside one troponin (Tn) and tropomyosin (Tpm), to induce muscle contraction.

Myosin is comprised of a globular head (subfragment 1, S1), neck domain and an elongated tail. The tails pack together to form the backbone of the thick filament and the heads protrude, allowing for interaction with actin. There are 35 classes of myosin, which vary in their biological function, from cytokinesis and muscle contraction to

organelle transport and cell shape maintenance. Sarcomeric myosins are class II myosins. Myosin II has two heavy chains and two pairs of calmodulin-like light chains. The heavy chain is formed of a head at the N-terminal, and a α-helical chain at the C-terminal. The α helical tail contains a heptad repeat that forms a coiled coil, responsible for linking the two heavy chains together. The linking of these tails results in S1 heads protruding from the surface of the thick filament at regular intervals. The coiled coil can be seen as repeats of a 28 amino acid unit and within the heptad repeats there are three of four "interruptions". These are inserted skip residues, which have been studied and found to play a key role in the molecular packing of myosin tails to form the thick filament. The neck domain on the coiled coil contains two IQ domains, which bind to one regulatory and one essential light chain. Non-muscle myosins are regulated via phosphorylation of the light chains, while skeletal myosin light chains are less important in the role of contractile force generation (Vicente-Manzanares, Ma et al. 2009).

The S1 head is comprised of 3 regions; a 25 kDa N-terminal region, a 50 kDa central region and a 20 kDa C-terminal region, also known as the lever arm. The central and N-terminal domains are linked by surface loop 1, while the C-terminal domain is linked to the central region by surface loop 2. The S1 contains the actin and nucleotide binding sites, and as a result it can bind to actin and act as a functional ATPase, without the rest of the myosin. This is useful experimentally, as it is easier to work with the smaller, soluble S1 head, than the whole myosin.
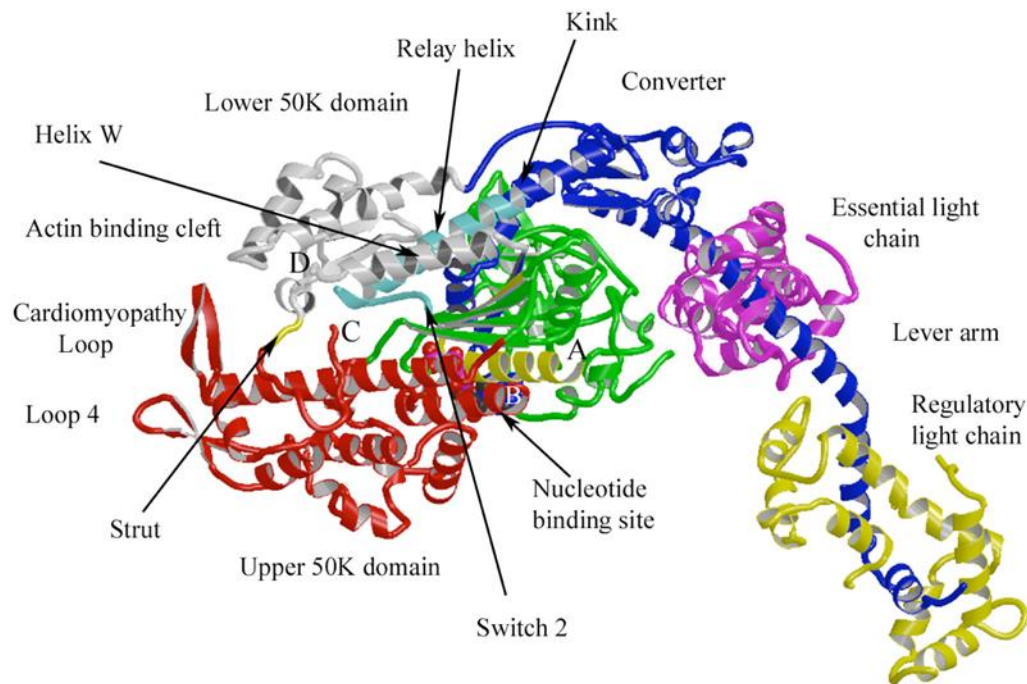
Figure 1.3.1.1. Ribbon diagram of myosin in the post rigor conformation. The C-terminal helix (dark blue) has two calmodulin like chains (pink and yellow). The N-terminus (green) is shown next to the nucleotide binding site and actin binding cleft, located between the upper 50K domain (red) and lower 50K domain (grey) (Geeves and Holmes, 2005).

The thin filament is made up of actin and regulatory proteins Tpm and Tn. In its monomeric, globular form (G actin), it has a mass of 42 kDa and is expressed in six isoforms; α cardiac, α skeletal, α aortic, ß cytoplasmic, γ cytoplasmic and γ enteric. While each actin is encoded on separate chromosomes, the amino acid sequence identity is over 90%, and most of the changes occur close to the N-terminal region. The initial crystal structure of G actin was solved with DNase I, but many have further explored this since. The 375 amino acid polypeptide chain of actin folds to form one small domain and one large, commonly known as the outer and inner, respectively, owing to their location. G actin is comprised of four subunits, which surround a nucleotide binding cleft (ATP or ADP) and divalent ion binding cleft (Mg^{2+} or Ca^{2+}). Monomeric G actin polymerises to form filamentous actin (F actin), the backbone of the

thin filament, with each monomer in contact with 4 others (one either side and two

from the opposite actin strand). F actin is comprised of two polymerised chains of actin

in a right-handed α helix. Monomers arrange with subdomains 3 and 4 facing inward to

interact with neighbouring subdomains 3 and 4, and subdomains 1 and 2 on the

periphery, exposed to solvents and enabling subdomain 1 to bind to a myosin head.

Subdomain 1 is responsible for myosin binding, owing to the fact that is contains the N-

and C-termini of actin.
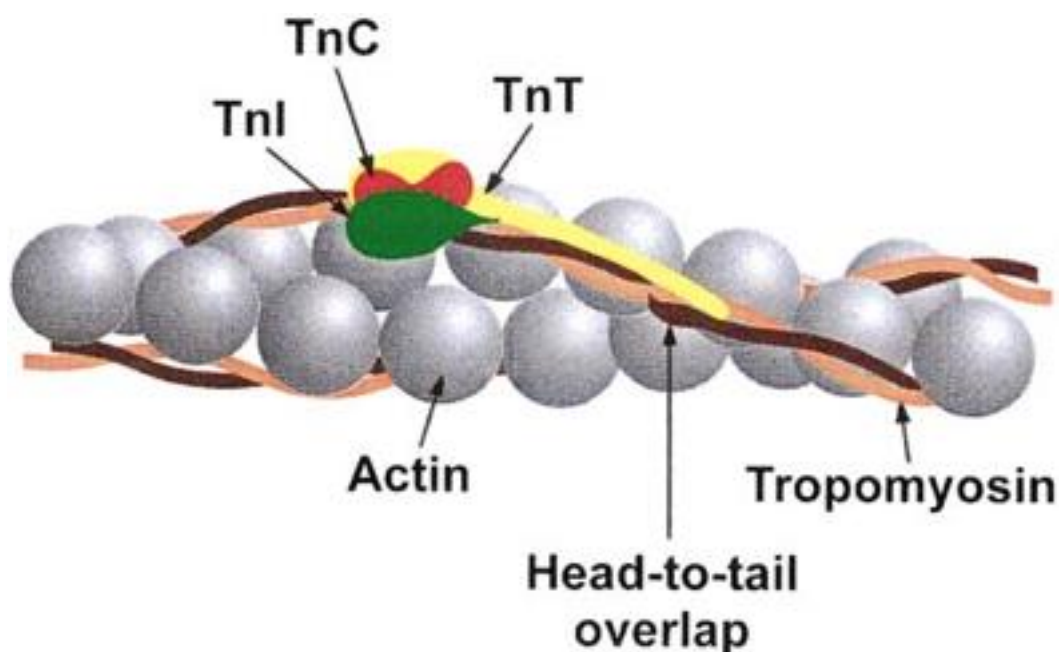
Figure 1.3.1.2. The thin filament; tropomyosin is shown as a αβ heterodimer in brown and orange, respectively. This lies along 7 monomers of G actin, shown in grey spheres. The three subunits of the troponin complex, TnI (green), TnC (red) and TnT (yellow) are shown holding tropomyosin in place along the actin filament. (Gordon, Homsher et al. 2000)

Actin in the filamentous form is a functional ATPase. G-actin on the other hand does not

have ATPase function. Crystal structures solved with ATP and ADP bound show

relatively little differences. As a consequence of adopting the filamentous form, the

outer domain rotates 20 °, flattening its conformation. This leads to the DNase I loop

forming an open loop, and Gly137, a key residue in the ATPase site, moving closer to the

γ-P of a bound ATP, enabling its hydrolysis.
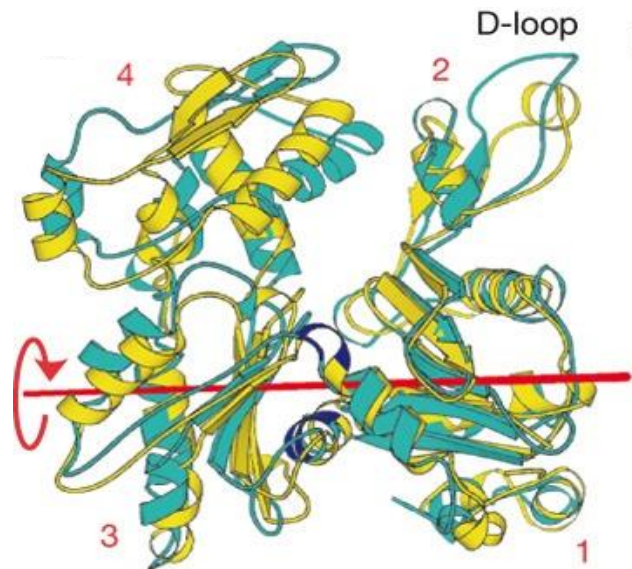
Figure 1.3.1.3. G actin (yellow) superimposed onto F actin (cyan) to show rotation (axis shown in red)
Subdomains 1 - 4 are highlighted (Oda, Iwasa et al. 2009).

1.3.2 Regulatory components – Tropomyosin

A single Tpm spans 7 actin subunits. Tpm exists as a dimer that polymerises head-to-tail

to form a filament that functions to regulate myosin binding, and thus muscle

contraction. In the relaxed state, Tpm sits along the actin filament, blocking myosin-

binding sites. It functions in conjunction with troponin (Tn), as a calcium sensitive

regulator. In the presence of calcium, the movement of the TmTn complex exposes

binding sites, which enables myosin to bind and releases contraction inhibition.

1.3.3 Regulatory components – Troponin

Troponin (Tn) is a heterotrimeric complex and consists of three subunits. Troponin C (TnC) is the Ca^{2+} binding domain, troponin I (TnI) is the inhibitory domain and troponin T (TnT) is the Tpm binding domain. Tn is essential in Ca^{2+} regulation of actin and myosin interactions (Filatov, Katrukha et al. 1999)and has been explored as markers used to identify cardiac risks in patients (Roppolo, Fitzgerald et al. 1999)
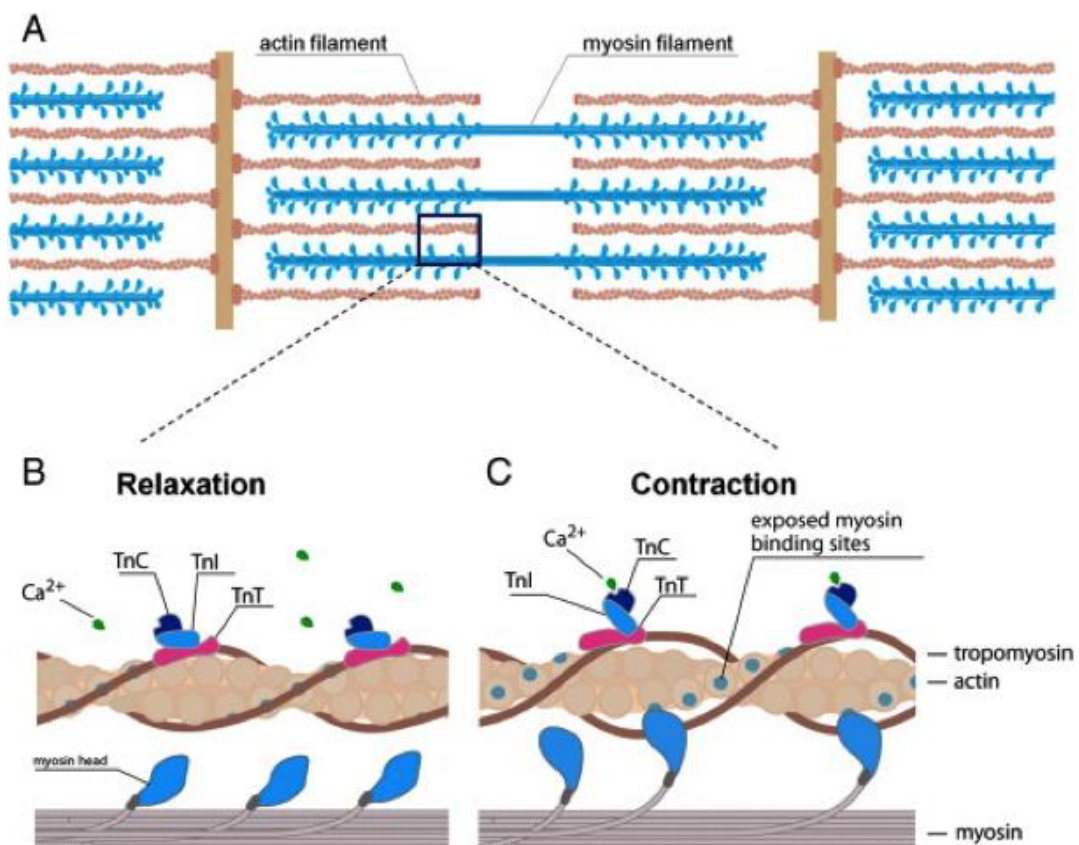
Figure 1.3.3.1. A schematic of the sarcomere, highlighting the relaxed and contracted muscle states and the role of calcium binding to troponin (Streng, de Boer et al. 2013)

TnC has four EF, helix-loop-helix, hands, which are responsible for its calcium binding function. The structure of TnC has two lobes (C and N) connected by a α helical linker,

and each lobe contains two EF hands (Nara, Morii et al. 2013) The C lobe is responsible for binding to the N domain of TnI and can bind calcium and magnesium. The N lobe is responsible for calcium binding only and binds to the C domain of TnI. When calcium binds to TnC it undergoes a conformational change, enabling it to bind to the C domain of TnI, releasing inhibition. This exposes the myosin binding sites and allows muscle contraction to ensue. Cardiac and skeletal TnC show 70 % sequence identity, with the most notable differences found in the first 40 residues.

Although all four EF hands in skeletal TnC are capable of binding calcium, in cardiac TnC, the first EF hand is unable to bind calcium as a result of several loop residue substitutions. This means that in cardiac TnC, there is only one calcium-binding site in its N domain responsible for the regulation of muscle contraction. The two EF hands in the C domain are thought to play a role in the structure of TnC, enabling it to bind to the Tn heterotrimeric complex (Davis, Tikunova 2008)Investigations on the TnC-G159D mutation, located in the C domain, uncovered a link between the mutation, calcium binding and cross bridge kinetics, when in the presence of TnI. The mutation resulted in increased calcium sensitivity, which provides novel data on thin filament mutations and myofilament function, leading to cardiomyopathies (Biesiadecki, Tachampa et al. 2010).

TnI is encoded and expressed in three isoforms; slow skeletal, fast skeletal and cardiac. The cardiac isoform has a 32 amino acid residue N-terminal extension, required for modulating cardiac contraction, resulting in it being the largest of the three isoforms (Biesiadecki, Tachampa et al. 2010)Phosphorylation of this N-terminus alters the TnI structure, resulting in diminished interaction with TnC. This decreased calcium

dependent muscle contraction and increased myosin cross bridge kinetics, is essential for increased cardiac muscle relaxation rates. TnI is known as the inhibitory subunit, because it binds to the C-terminal of TnT, 10-20 nm away from the Tpm overlap region called the IT-arm. It functions to inhibit myosin binding to actin by holding the actin-Tpm complex together, thus closing off the myosin binding sites. When calcium is present, it binds to TnC, which in turn affects TnI, causing it to detach from the actin-Tpm complex. Tn detachment allows Tpm to move on the actin filament and expose myosin-binding sites (Takeda, Yamashita et al. 2003)

TnT is encoded for by three genes, slow skeletal (T1), cardiac (T2) and fast skeletal (T3). Several isoforms of TnT exist as a result of splicing, and their expression is tissue specific (Geeves, Ranatunga 2012)TnT is a 30-35 kDa protein comprised of a α helical N-terminus and a globular C-terminus, arranged asymmetrically (Wei, Jin 2011)The C-terminal is more highly conserved than the hypervariable N-terminal. It is responsible for the binding of Tn to Tpm, and it helps to position the complex on actin filaments (Streng, de Boer et al. 2013)Tpm binding is important in the regulation of the actomyosin ATPase cycle. In the presence of calcium, TnT dissociates from Tpm, thus removing ATPase inhibition, allowing Tpm to adopt a different state (Farah, Reinach 1995)Tpm can adopt three states; closed, blocked and open, explained later on. TnT also interacts with TnI and TnC via its C-terminus, holding the complex together, while the N-terminus lies antiparallel along the C-terminal of Tpm. This positioning of TnT on Tpm covers the Tpm head to tail overlap and enhances Tpm affinity for actin (Zot, Potter 1987)
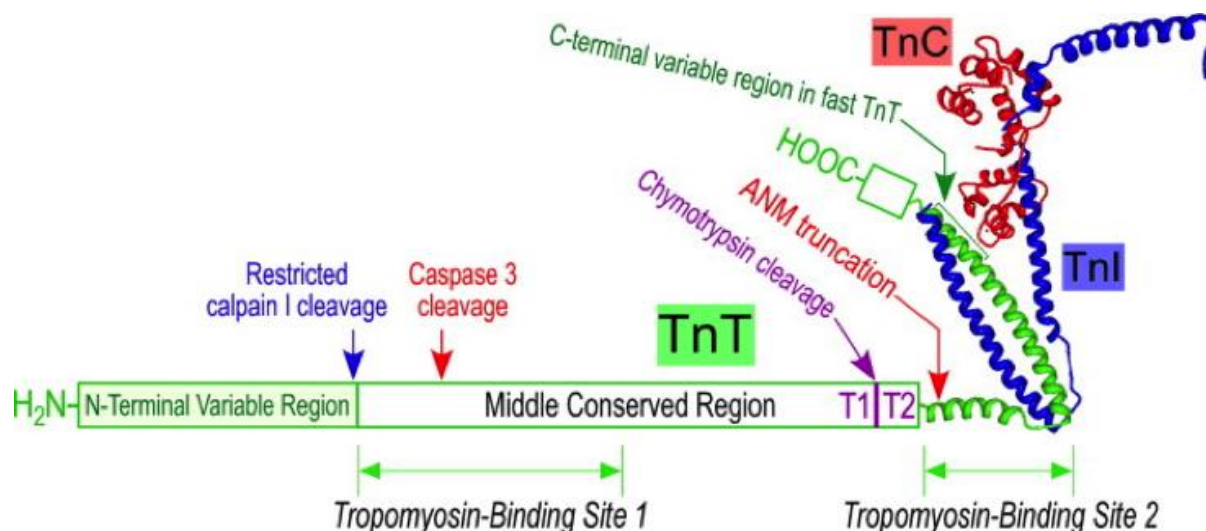
Figure 1.3.3.2. An illustration of troponin, showing the structural and functional domains of TnT (green) added to a crystal structure of troponin. Highlighting the hypervariable region, the tropomyosin binding regions and interactions with TnI (blue) and TnC (red) (Wei, Jin 2011)

1.4 ATP cycle

The interaction between myosin and actin is responsible for muscle contraction and many motile functions. ATP binding and hydrolysis provides the energy for thick and thin filaments to slide over each other as the sarcomere contracts and relaxes. When ATP binds to the actin and myosin complex, this triggers rapid dissociation to form actin (A) and myosin•ATP (M•ATP). Myosin subsequently cleaves ATP to form M•ADP•Pi, this step is very fast and is reversible. Actin can then rebind to myosin to form A-M•ADP•Pi. In this state, the actin and myosin are weakly bound until isomerised to a strongly bound state, AM•ADP•Pi. This form is further isomerised to form AM**•ADP•Pi and produces force, resulting in the lever arm motion. The lever arm motion is stabilised by the release of Pi. When ADP is released, myosin adopts the rigor

conformation and ATP binding triggers its release, taking it back to the start of the cycle. This is known as the cross-bridge cycle. These steps are still uncertain, but it is clear that changes from a weakly bound state (A-M•ADP•Pi) to a strongly bound state (AM**•ADP), results in a large change in free energy and produces force(Gordon, Homsher et al. 2000, Deacon, Bloemink et al. 2012)Lymn and Taylor initially proposed the cross-bridge cycle in 1971 and the basic principal still remains, but has been updated as new findings come to light. Geeves and Holmes produced a model in 2005 of the cross-bridge cycle using recent crystal structure findings. From this, three conformations were characterised and backed up with biomechanical and kinetic data (Geeves, Holmes 2005)

$$AM + ATP \xleftrightarrow{1} AM \cdot ATP \quad 3 \quad A\text{-}M \cdot ADP \cdot P_i \xleftrightarrow{5} AM \cdot ADP \cdot P_i \xleftrightarrow{6} AM^{**} \cdot ADP \cdot P_i \xleftrightarrow{7} AM^{**} \cdot ADP \xleftrightarrow{8} AM$$

$$2 \updownarrow \qquad\qquad 4 \updownarrow$$

$$M + ATP \xleftrightarrow{1'} M \cdot ATP \xleftrightarrow{3'} M \cdot ADP \cdot P_i \xleftrightarrow{5'} M + ADP + P_i$$
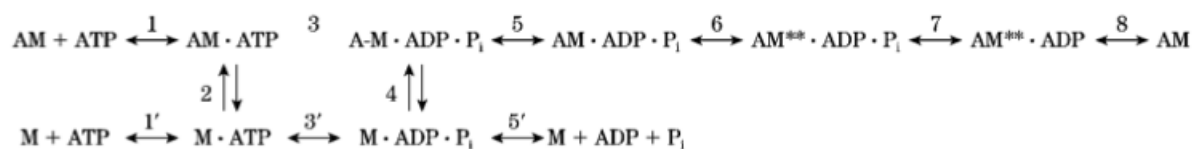
Figure 1.4.1. Cross-bridge cycle showing the ATPase cycle for myosin (M) interacting with actin (A), and phosphate (Pi) release (Gordon, Homsher et al. 2000)

The Geeves and Holmes cross-bridge cycle describes the myosin cross-bridge in four different states. Stage 1 shows the myosin strongly bound to actin in the absence of a nucleotide in the binding pocket. This is called the rigor conformation. When ATP binds to the ATP binding pocket, it causes myosin dissociation from the actomyosin complex, where it assumes the post rigor conformation (state 2). The cross-bridge makes a recovery stroke, where it is then in the pre-power stroke conformation (state 3) as ATP is hydrolysed and the products ADP and Pi remain bound in the pocket. In state 4, the cross-bridge takes on the top-of-power-stroke conformation, when actin binding

triggers the release of the hydrolysis products. Pi is released first, enabling the power

stroke to be executed, followed by ADP release. The cross-bridge is then back in state 1,

the rigor conformation, ready for the next cycle (Geeves, Holmes 2005)
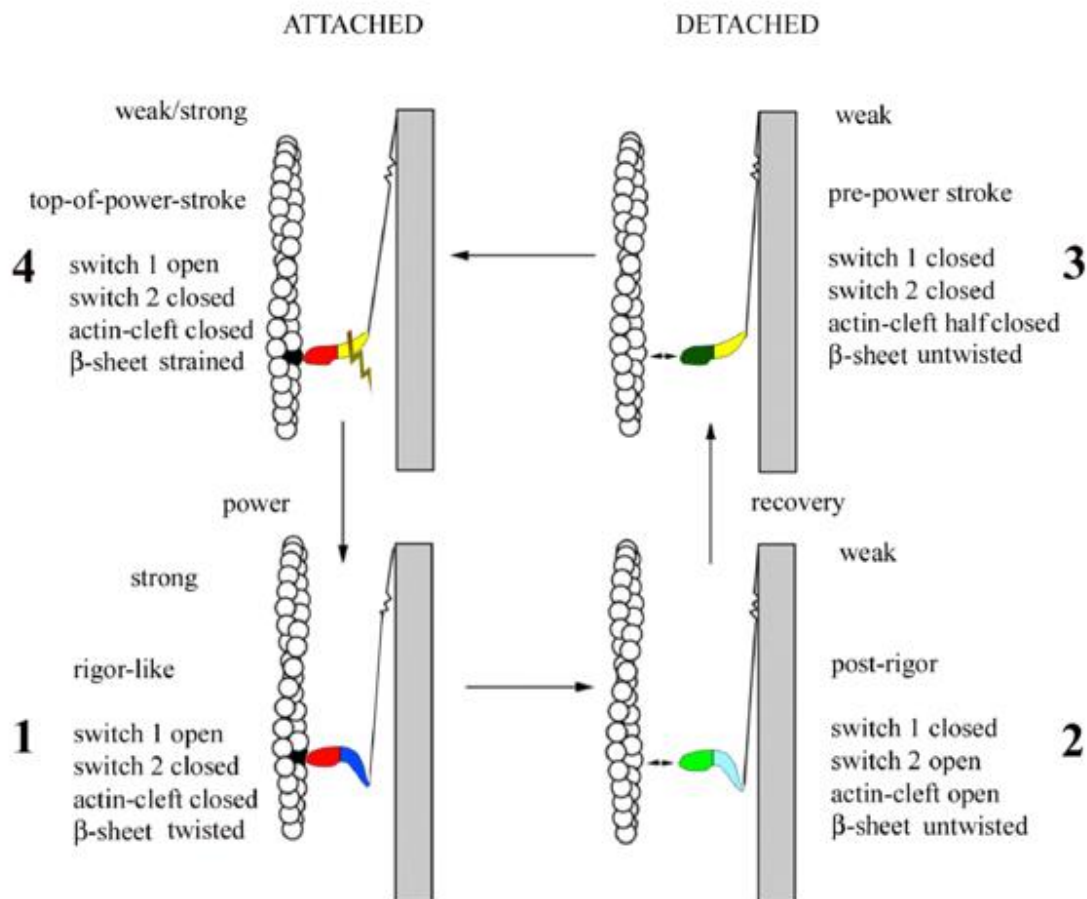
Figure 1.4.2. The cross-bridge cycle as proposed by Geeves and Holmes. State 1 is the rigor state, with strongly bound myosin. State 2 shows myosin in the post rigor conformation, this occurs after ATP binding to myosin dissociates it from the actomyosin complex. State 3 shows the cross-bridge recovery, assuming the pre power stroke conformation, wherein the myosin ATPase is active, hydrolysing ATP. State 4, previously undescribed by the Lymn-Taylor cycle, shows myosin rebinding to actin, in the top-of-power-stroke conformation. The transition from state 4 to state 1 involves the release of hydrolysis products and the execution of the power stroke (Geeves, Holmes 2005).

In order for the myosin cross-bridge to assume its various states, there are important

elements that must be conformationally flexible, which have a knock on effect on other

structures. In the rigor state (state 1), the 50K domain of myosin moves, closing off the

actin binding cleft and opening the nucleotide binding pocket. As a result, switch 1

(SW1) moves away from the nucleotide-binding pocket, thus opening the switch. ATP binding opens the actin-binding cleft, moving the switch back to the original closed position. This highlights the negative connection between actin affinity and ATP affinity. ATP binding also moves the P-loop into the down position and the β sheet is twisted.

The post rigor state (state 2) sees the opening of switch 2 (SW2), which causes the lower 50K domain to rotate inwards. This rotation causes a kink to form in the relay helix, which is the start of the pre power stroke. Removal of the kink means the lever arm rotates by 60°, which is the basis for the power stroke. As a result, SW2 closes, enclosing the nucleotide binding pocket and initiating ATP hydrolysis. The bound nucleotide means the P-loop remains down, and the β sheet remains untwisted. These conformational movements also close the inner actin-binding cleft.

Actin can bind to the pre power stroke conformation forming the top-of-power-stroke. This binding causes twisting of the β sheet, which in turn rotates the converter domain, removing the kink from the relay helix. The P-loop then assumes the up position. SW1 opens, closing off the outer cleft, while SW2 closes and closes the inner cleft. After this, Pi can be released and the cross-bridge can strongly bind, executing the power stroke of up to 10 nm, releasing ADP and assuming the rigor conformation again (Geeves, Holmes 2005).

1.5 Thin filament regulation – 3 state model

Initially it was postulated than thin filament regulation was controlled by a steric blocking mechanism, wherein Tpm physically blocked myosin-binding sites in the absence of calcium. Upon calcium addition, it would bind to Tn, which in turn affects Tpm, moving it to a non-blocking position on actin and allowing myosin to bind. This idea was supported by X-ray scattering studies, wherein a structural change on the thin filament was observed before cross-bridge formation. A flaw was discovered, however, when studies at a low ionic strength changed ATPase function but not actomyosin interactions. This led to the hypothesis that Tn and Tpm regulated actin and myosin interactions by controlling Pi release, which is the rate limiting step, as a two state model (Mijailovich, Li et al. 2012)In this, the cooperative unit, comprised of seven actins, bridged by one Tpm and one Tn (A_7TmTn), is predominantly in the off state (weak myosin binding), in the presence and absence of calcium. The thin filament can only be switched on by myosin binding. Kinetic data showed that in the presence of calcium, 90 % of the thin filament is switched on, compared to 30 % in the absence of calcium. Equilibrium data conflicted with this though, showing 20 % of the thin filament switched on in the presence of calcium and 5 % in the absence (Mijailovich, Li et al. 2012)These conflicts were resolved once a three state model was proposed (McKillop, Geeves 1993).

The three state model proposes three states of the thin filament in dynamic equilibrium; open, closed and blocked (McKillop, Geeves 1993)The closed state is predominant in the presence of calcium and the absence of strongly bound cross-bridges. The blocked state is predominant in the absence of cross-bridges and calcium, where Tpm blocks binding sites on actin, inhibiting myosin binding. The open state is predominant when myosin is strongly bound in the rigor state (R state). The transition from closed to blocked states in defined by K_B, and the transition from open to closed states is defined by K_T (Head, Ritchie et al. 1995) These

equilibrium constants are influenced by the presence of calcium. When calcium binds to Tn, the model shifts from the blocked to closed state, and releases its inhibition on Tpm. In the closed state, myosin can weakly bind, as Tpm has moved out of its blocking position, consequently exposing myosin-binding sites. The transition from closed to open occurs after weakly bound myosin is isomerized to strongly bound myosin, exposing further myosin binding sites, postulated as cooperative activation of the thin filament. ATP hydrolysis is not dependent on the thin filament state, because is occurs in state 2 and 3, as shown in figure 1.4.1.
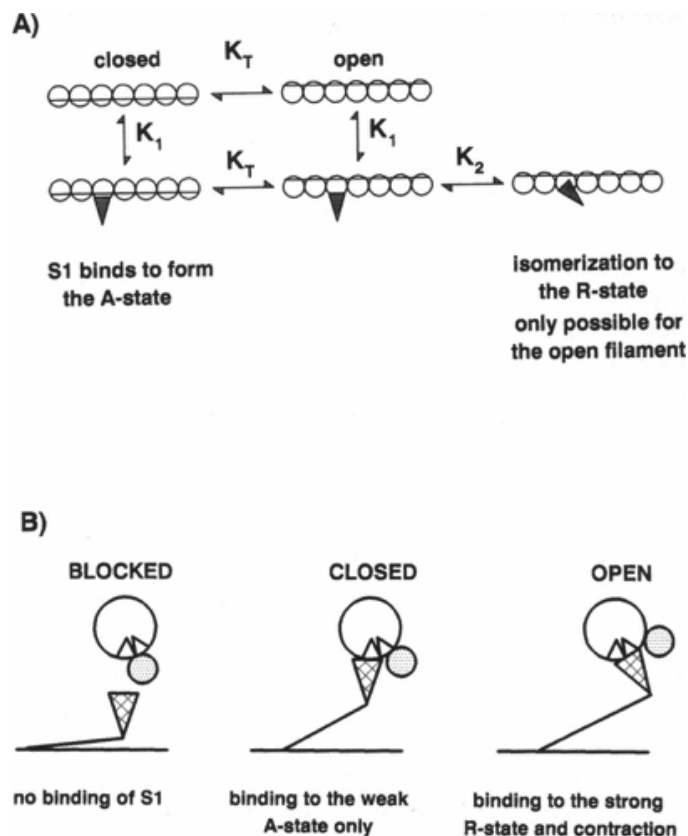
Figure 1.5.1. A. The two state model shows the cooperative unit (A_7TmTn) of 7 actins (spheres) connected by one Tpm (line). Myosin can bind to both states weakly with the same affinity (K_1) but only the open state is isomerised to form the strongly bound rigor state (K_2). B. The three state model shows the direct steric blocking of the thin filament. In the blocked state, Tpm blocks all myosin binding. In the closed state, myosin can weakly bind (A state) as the regulatory proteins have moved to expose some myosin binding sites. In the open state, all the myosin binding sites are exposed, enabling myosin to isomerise to form the rigor bound state (R state) (McKillop, Geeves 1993)

The McKillop and Geeves model found that in the presence of calcium, 20 % of the thin filament was open, 80 % was closed and 5 % was blocked, approximately. In the absence of calcium 2 % was open, 22 % was closed and 76 % was blocked. These data supports previous equilibrium data of 20 % in the 'on' state in the presence of calcium and 5 % in the absence of calcium.
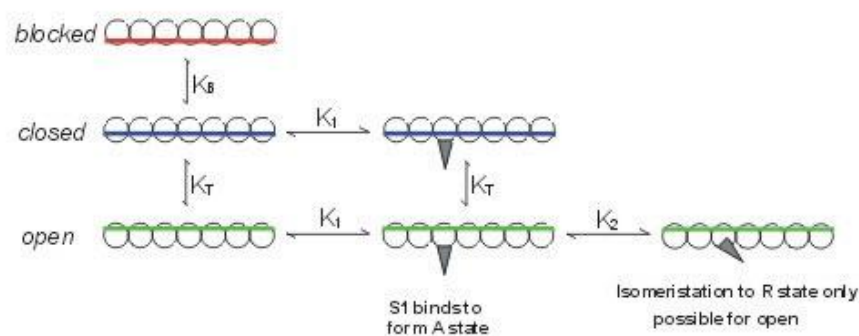
Figure 1.5.2. The three state model proposed by McKillop and Geeves. The blocked state shows no cross-bridge interaction, as Tpm is fully blocking the myosin binding sites. The closed state shows a small movement of Tpm, enabling weak binding of myosin (90° triangle, A state). The open state shows Tpm completely removed from the myosin binding sites, and as a result, myosin can bind weakly, and then isomerizes to form the strongly bound state (45° triangle, R state) (McKillop, Geeves 1993).

Tpm has been shown to propagate conformational changes over large distances via head-to-tail overlaps (Edwards, Sykes 1981) and phosphorylation of Tpm is required to cooperatively activate Tpm over multiple cooperative units. It has been postulated that cooperative activation can extend up to 500 nm (Vibert, Craig et al. 1997)and even over an entire thin filament, independent of length (<2 µM to 15 µM) (Fraser, Marston 1995)The position of Tpm on thin filaments in the presence and absence of calcium and S1 has been explored using EM. It was seen that both calcium and S1 were required to fully expose myosin binding sites, showing three positions of Tpm on the thin filament, thus reinforcing the three state model (Vibert, Craig et al. 1997).
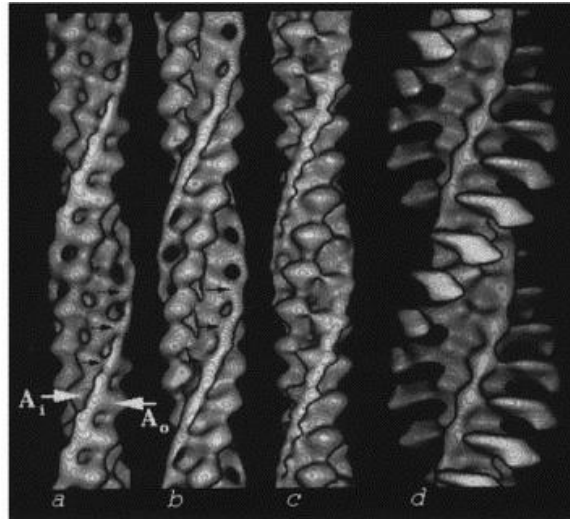
Figure 1.5.3. Surface view of frog skeletal muscle thin filament in EGTA; the thin filament is in the off state with Tpm in the outer domain, A_o (a). *Limulus* thin filament in calcium stimulates Tpm movement toward the inner domain, A_i (b). *Limulus* thin filament partially decorated with S1 (c) and *Limulus* thin filament fully decorated with S1 (d) show similar movement of Tpm to the centre of the thin filament, suggesting Tpm moves "as a whole" (Vibert, Craig et al. 1997).

Poole et al. (2006) explored the discrepancies between EM and X-ray fibre diagrams when looking at the positions of Tpm on the thin filament. Their work shows azimuthal movement of Tpm over actin, depending on whether it is in a blocked, closed or open state, with a small difference between data obtained from EM and X-ray diagrams. In the blocked state, Tpm can be seen to sterically inhibit myosin binding by sitting on the binding sites, and when in the closed state, Tpm moves 25 ˚ azimuthally away from the myosin binding sites, enabling weak binding. In the open state, Tpm moves a further 10 ˚ (35 ˚ from the original blocked state) across the actin, fully exposing the myosin binding sites, allowing myosin to strongly bind (Poole, Lorenz et al. 2006)This is similar to work completed by Lorenz et al 2007, supporting a three state model.
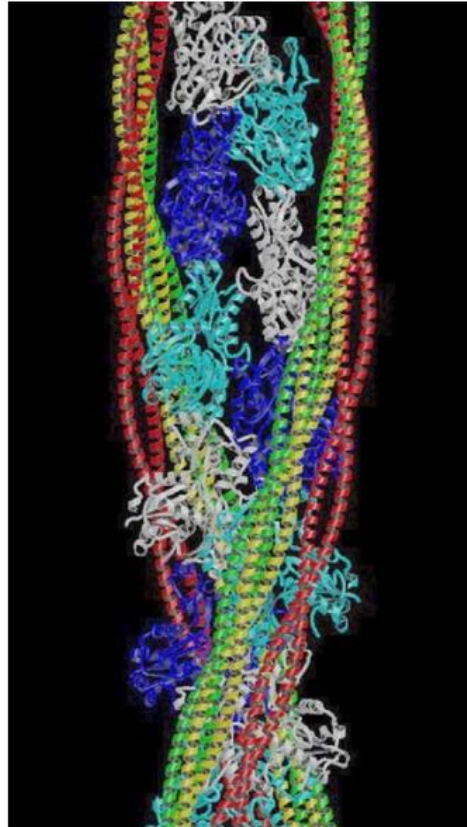
Figure 1.5.4. The three positions of Tpm on actin shown from EM reconstructions. Tpm can be seen in the blocking state (red) in the presence of EDTA. In the presence of calcium, Tpm can be seen to shift 25° (yellow) as it adopts the closed state. The open state is shown in green shows a further 10° shift of Tpm, where myosin can bind in the rigor state (Poole, Lorenz et al. 2006).

Steric blocking of Tpm was further explored by adding myosin cross-bridges to the reconstruction, enabling visualisation of steric interferences. In the blocked state, when a cross-bridge is added, much steric interference can be seen, particularly between Tpm and the 50K cross-bridge domain. Tpm is seen to lie in the cleft between the upper and lower 50K domain, splitting the binding sites in half. In the closed and open states, interferences are greatly reduced by the azimuthal rotation of Tpm.
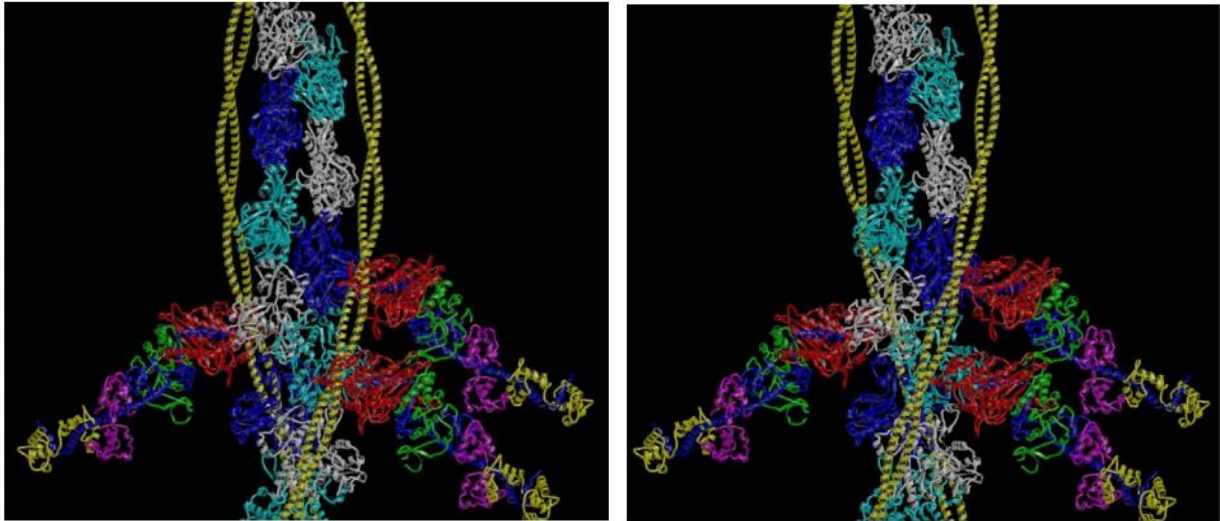
Figure 1.5.5. The blocked state, Tpm (yellow) is seen to conflict with the cross-bridge 50K domain (red) shown on the left. The thin filament in the open state shows the 25° azimuthal rotation of Tpm along actin, exposing actomyosin binding sites and thus reducing steric interference, shown on the right (Poole, Lorenz et al. 2006).

An 8 Å resolution structure of the thin filament in the rigor bound cross-bridge state has been reported, using cryo-EM (Behrmann, Müller et al. 2012). This provided a pseudo-atomic model of the thin filament cross-bridge interface, which gave evidence for the direct interaction of Tpm with the cross-bridge. A comparison of the rigor state and pre-powerstroke state showed an azimuthal shift of Tpm on the thin filament and conformational changes in the cross-bridge, but none were noted for actin. From this, a model was produced for Tpm dependent binding of myosin and actin induced nucleotide release from myosin. Their work provided high resolution information on the thin filament cross-bridge interaction, yet it is flawed, in that they applied helical symmetry to the actin to achieve the resolution, at a cost of smoothing the end to end Tpm overlap regions, losing crucial information (Behrmann, Müller et al. 2012).

Myosin binding to actin leads to cooperative activation of the thin filament. The role of Tpm in cooperative activation can be seen, as it is only once Tpm has moved from a closed state, allowing weak myosin binding, that strong binding of myosin can occur. This fully exposes actomyosin-binding sites and the thin filament can adopt the open state. Myosin binding only opens one section of the thin filament, preventing Tpm from rotating back to its original blocking position. Tpm itself transmits the movement along multiple end-to-end overlapping Tpm molecules, thus cooperatively exposing myosin-binding sites.

In striated muscle, α Tpm has a phosphorylation site at serine-283, near the C-terminus, that lies in the head-to-tail overlap region of neighbouring Tpm dimers. Phosphorylation is not seen in β Tpm, however (Mak, Smillie et al. 1980, Rao, Marongelli et al. 2009). The end-to-end overlap of Tpm plays an important role in detecting conformational changes in actin (East, Sousa et al. 2011, Heald, Hitchcock-DeGregori 1988, Mijailovich, Kayser-Herold et al. 2012). Dephosphorylated Tpm has been shown to behave like unregulated thin filament, highlight the role of phosphorylation on the regulatory role of Tpm (Rao, Marongelli et al. 2009). The α isoform is predominant in human hearts (95 %) and 25 – 30 % showed phosphorylation at serine-283. This was seen to be true for a healthy donor heart, as well as in hypertrophic obstructive cardiomyopathy samples (Marston, Copeland et al. 2013). Decreasing Tpm phosphorylation has been shown to "rescue" Tpm induced familial HCM (Schulz, Wilder et al. 2013).

1.6 The role of stiffness/flexibility

When Tpm binds to actin, the strength at which it binds, in conjunction with the degree of flexibility it has, varies depending upon the isoform bound. For example, smooth muscle Tpm is much more flexible compared to skeletal muscle. Early research into flexibility of smooth muscle Tpm showed a persistence length of 55 nm, compared to 150 nm of skeletal   (Swenson, Stellwagen 1989). However, later studies suggested the two had a similar L_p of ~ 100 nm, yet highlighted the twofold higher flexibility of the end-to-end linkage of smooth muscle (Sousa, Cammarato et al. 2010). This persistence length (L_p) defines the flexural rigidity of a semi-flexible linear molecule, as the length over which the molecule persists in that direction before changing course (Trachtenberg, Hammel 2010, Sousa, Cammarato et al. 2010, Loong, Badr et al. 2012). The "apparent" L_p of cardiac Tpm has been measured using EM to be ~ 100 nm and is relatively flexible over the end-to-end overlap. A degree of structural rigidity is gained once Tpm interacts with Tn (Sousa, Cammarato et al. 2010, Li, Holmes et al. 2010). A comparison of this value to those obtained using AFM show a large discrepancy with an L_p of ~ 40 – 50 nm (Loong, Zhou et al. 2012).

The flexibility of Tpm has been thought to correlate to disease propagation in cardiac hypertrophy. This is owing to the fact that if Tpm is more flexible, its calcium sensitivity is increased. In cardiac thin filaments, this corresponds to them becoming activated earlier in systole and staying activated longer, perhaps even remaining partially activated during diastole. These events undoubtedly affect the heart's function and

output. Hence, interest is increasing in the flexibility of Tpm in relation to its function and how this relates to Tpm isoforms carrying a known cardiomyopathy mutation.

1.7 Tropomyosin isoforms

As explained previously, it is known that Tpm can exist either as a homo or heterodimer, and each is shown to be functionally distinct. Studies into HCM mutations D175N and E180G on Tpm assembly showed little affect, ergo heterozygous affected are predicted to express homo and heterodimers. Therefore it is of interest to understand how and why these form and exchange. If isoforms have different functional properties, and dimers too, have different properties, does this affect preferential assembly or exchange? This also raises the question as to how a mutant behaves, whether it is present as a homodimer, or as one might assume given low expression and random assembly, a heterodimer.

The actin affinity, calcium sensitivity and thermal stability were explored for both HCM mutants, D175N and E180G. There was no significant trend, with each mutant having distinct properties, and homodimers and heterodimers also having different trends. There was no straightforward trend in either homo vs heterodimer or WT Tpm vs mutant. As the behaviour for each dimer is different, their relative abundance is of significant and interest to understand. As shown previously, the heterodimer may not be the most stable conformation overall, more a happy medium between the very stable and unstable homodimers. On the other hand, the effect of heterodimers was not always

an intermediate between WT and mutant homodimers, ergo it is not viable to use homodimers as a predictor of heterodimer properties (Janco, Kalyva et al. 2012).

Nemaline myopathy mutations in Tpm were studied and showed that dimer formation using the recombinant mutant proteins decreased assembly of heterodimers in vivo. This suggests altered dimerization and thus, altered sarcomeric thin filament dynamics, which would contribute to muscle weakness in the disease (Corbett, Akkari et al. 2005).

1.8 Cardiomyopathies

There are three main inherited forms of diseases of the heart; hypertrophic cardiomyopathy (HCM), dilated cardiomyopathy (DCM) and arrhythmogenic right ventricular cardiomyopathy (ARVC), as shown in figure 1.8.1. Cardiomyopathies reduce the ability of the heart to function normally. In HCM, muscle walls become enlarged. This increased thickness makes the heart muscles stiffer and may impede on the size of the chambers. DCM on the other hand, is characterised by enlarged chambers of the heart. In particular, the left ventricle becomes dilated, which affects the heart's ability to pump blood out and around the body. ARVC is caused by mutations to desmosomes (a protein that links muscle cells together), and leads to tissues becoming detached, dying and being replaced with fatty deposits and scar tissue. ARVC also leads to arrhythmias, as electrical impulses passing through the heart are disrupted when they encounter these areas of scarred or fatty tissue. Mutations in different muscle proteins lead to different forms of cardiomyopathies. There are 12 mutations in α Tpm linked to DCM and 15 mutations in α Tpm linked to HCM (Redwood, Robinson 2013).
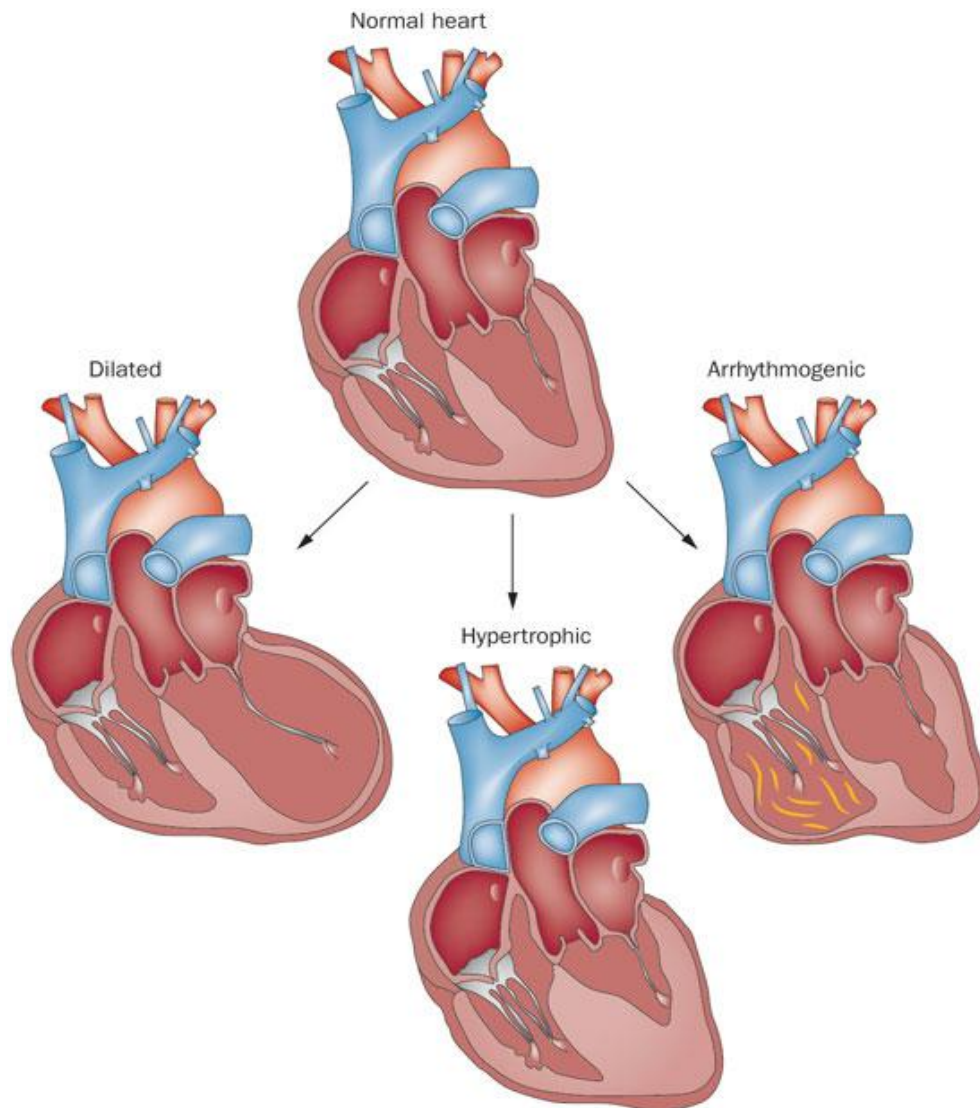
Figure 1.8.1. Morphology of HCM, DCM and ARVC, compared to a normal heart. HCM shows enlarged heart muscles, thickened septum and reduced chamber capacity. DCM shows enlarged chambers and thinned muscle walls of the heart. ARVC shows detachment of desmosomes and fibrofatty replacement of heart muscle, most notably in the right ventricle (Hershberger, Hedges et al. 2013).

1.9. Instrumentation – Circular Dichroism

Circular dichroism (CD) is a spectroscopic technique, which can be used to explore the secondary structures of proteins. It is defined by the unequal absorption of left handed and right handed circularly polarised light. Linearly polarised light oscillates

sinusoidally in a single plane. The circularly polarised vector will trace out a circle as a result of two vectors that are 90 ° out of phase to each other, which can be separated using a variety of cells and prisms that utilise Pockel's effect. The helix can either be left or right handed and are not superimposable mirror images. When asymmetric, chiral molecules interact with polarised light, they absorb left and right handed polarised light to different extents. This results in rotation of the plane of light and a change in the left and right-handed vectors, creating an elliptical shape, hence termed elliptically polarised light, figure 1.9.1.
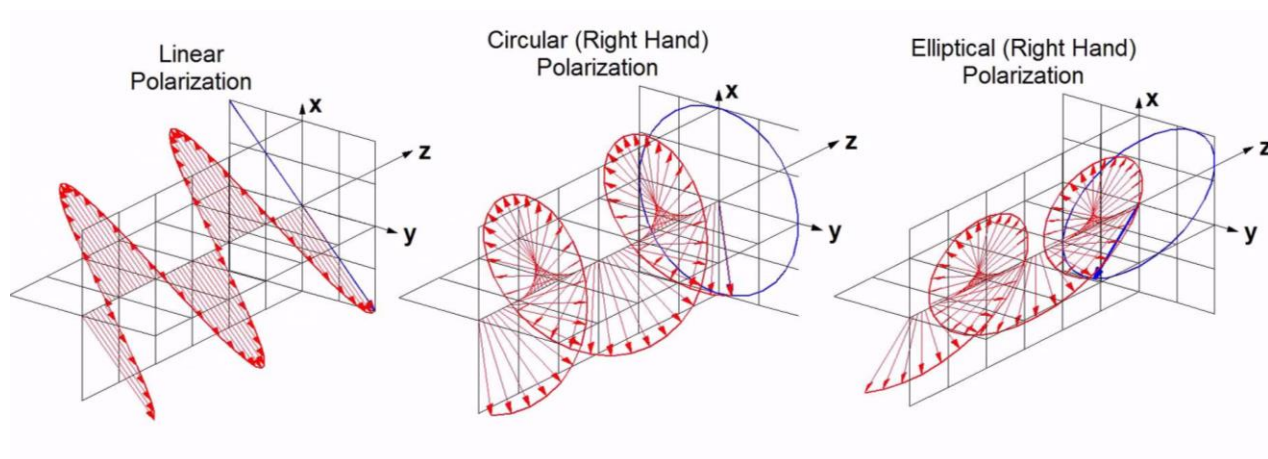
Figure 1.9.1. Linear, circular and elliptical polarisation of light. Image taken from https://i.ytimg.com/vi/Q0qrU4nprB0/maxresdefault.jpg.

Different structural elements in proteins have a characteristic CD spectrum, which leads to CD being a good tool for determining a protein's secondary structure. For example, α helices have a positive peak at 193 nm and two negative peaks at 208 and 222 nm, while β pleated sheets have a positive band at 195 nm and negative peak at 218 nm. CD spectrum as a function of temperature can be utilised to observe protein unfolding over a temperature range and thus determine the thermal stability.

1.9.1. Instrumentation – Atomic Force Microscopy

The first atomic force microscope (AFM) was developed in 1986, following work on scanning tunnelling microscopy (STM) (Binnig, Quate et al. 1986). A cantilever probe was employed to detect inter-atomic forces with a much higher level of sensitivity than STM offered (Binnig, Quate et al. 1986, Yurov, Klimov 1994). These advances have led to AFM becoming a widely used tool for high resolution imaging of biological systems, providing a three-dimensional representation of biological samples (Wang, Chen et al. 2013). It requires no chemical treatments, such as chemical fixation, to prepare the samples and samples can be scanned under ambient conditions in air or in liquid, minimising the damage to the sample and providing a means to image living organisms. However, the scan size is relatively limited (10 nm) and scan speed is slow, which can lead to thermal drifting of the sample. Alongside this, creep of the piezo scanner, and "cross-talk" between x-, y- and z- axes, means images require software filtering that can flatten out key topographical features. Imaging using a cantilever probe could also introduce artefacts, such as strangely shaped objects and alterations to the sharpness of the image (Ricci, Braga 2004). On the other hand, techniques are being continuously improved to provide better images with fewer secondary effects (Allison, Mortensen et al. 2010, Lapshin 2004).

Imaging can be done using three methods; contact, non-contact and tapping mode. Contact mode is best used on "hard" samples. The sample is mounted on a piezo scanner and the surface on the sample is scanned using a silicon nitride probe attached to a cantilever spring. As the probe moves over a sample, its deflection is measured via a

laser that is reflected off the probe and returned to the position sensitive photodiode detector. This laser detector is part of a feedback loop that adjusts the height of the sample, via the piezo scanner, to keep the deflection constant. A topography image is created using the height of the sample, while deflection images correspond to the deflection of the probe. Imaging with a static probe is done in contact mode, because the overall force on a sample's surface tends to be attractive, pulling the probe into the surface. Whereas, when the probe is in contact, the overall force is repulsive. On the other hand, friction and surface tension forces affect contact mode, as samples have a contaminant layer of gases and water that form a meniscus with the probe and also pull the probe towards the surface. Imaging in liquid instead of air can eliminate these problems, and also decrease Van der Waals forces. However, the process can be fiddly and subject to leaks and some samples become "vulnerable" when hydrated (Fotiadis 2012, Sokolov 2013).

Tapping mode is used instead of contact mode on soft samples that may be problematic for imaging due to issues with friction, force and adhesion. The tip oscillates close to resonant frequency across the surface, and the amplitude of this oscillation is the feedback signal, instead of spring and probe deflection as for contact mode. Non-contact mode is similar to tapping, but the tip is oscillated at resonance frequency and remains constant. This benefits from reduced tip degradation but the images produced are of lower resolution and are easily affected by surface contaminants such as water (Sokolov 2013, Veigel, Schmidt 2011). Non-contact AFM has been shown to produce high quality data, as shown in the work of Gross et al., wherein they achieved chemical structure resolution (Gross 2009). This example highlights the ever-evolving techniques and

limiting capabilities of systems that are being overcome, making their use in protein analysis increasingly desirable.

1.10 Aims

The aim of this study is to investigate the characteristics of Tpm homodimers and heterodimers. Tpm isoforms are complex in that, of the protein expressed, up to 40 isoforms are known in mammalian cells. Isoforms are cell specific and vary according to cell location and development. Homodimers and heterodimers are known to have distinct properties, but how these form and exchange are unknown. We intend to define the primary properties of Tpm isoforms with a variety of techniques. The thermal stability for tropomyosin will be determined using circular dichroism studies. This will explore the differences between isoforms and dimers, and also buffer conditions.

Previous biochemical studies have shown that smooth muscle α and ß Tpm have a preferential, thermodynamically favourable assembly to form a heterodimer, but how these heterodimers form and exchange has not been explored. We aim to study the exchange between homodimers to form heterodimers, under a variety of conditions. We predict that if exchange between dimers is seen at 37 °C in the absence of actin, this will be decreased when actin and troponin are present. We aim to explore the rate of tropomyosin exchange on the actin filament.

We aim to study tropomyosin dimers to gain insight into how they form and exchange as homo- and heterodimers. Exploring whether monomers exchange freely in solution or on the actin filament to form dimers, or if dimers are formed as they come off the ribosome. When looking at dimers, do they exchange readily on the actin filament or is there another system in place to assist the process?

The movement of Tpm between the three positions along actin requires a degree of flexibility, but also a degree of stiffness, so as to communicate cooperative movement along the Tpm chain. The flexibility of Tpm has been defined by measuring the persistence length of monomers. Studies using EM micrographs (Li, Lehman et al. 2010) give a persistence length of ~100 nm, while AFM images give ~40 nm (Loong, Zhou et al. 2012). Both studies describe a 30 % change in persistence length of monomers carrying a cardiomyopathy single point mutation, but have very different starting values for Tpm persistence length. We aim to investigate the discrepancies between EM and AFM studies on persistence length, following up on the idea of regulation of contraction by a continuous flexible chain. We predict that difference in persistence length may be caused not only by the technique used, but also the surfaces used to prepare and image the Tpm.

The difference between homodimers and heterodimers becomes increasingly interesting when looking at cardiomyopathy mutations in affected heterozygous individuals. We have developed a novel method to crudely extract tropomyosin from mouse cardiac tissue, without reducing tropomyosin dimers. Using this method, tropomyosin can be extracted from tissue and chemically cross linked to fix the dimer

population. This, in conjunction with mass spectrometry analysis, allows the native dimer content of a wild type mouse heart to be compared against a transgenic mouse heart containing a cardiomyopathy mutation. Given the random assembly of dimers, wherein a population of 50:50 homodimers after heating and cooling, will reassemble to form a 1:2:1 ratio (homo:hetero:homo), it is predicted that if a cardiomyopathy mutant is expressed <50 %, it will be present as a heterodimer, predominantly.

The interest behind cardiac disease causing mutations lies in their behaviour; do different isoforms have different properties to the wild type that might influence preferential assembly later, and how does it affect the dimers behaviour.

Chapter 2: Materials and method

2.1 Protein biochemistry materials & methods

2.1.1 Media recipes

LB: 35 g tryptone, 17.5 g $NaCl_2$, 17.5 g yeast extract dissolved in 3.5 l H_2O. Media was autoclaved and antibiotics added as required after cooling to room temperature.

Ampicillin: 300 mg ampicillin in 6 ml H_2O, syringe filtered with 0.2 μM Minisart filter.

IPTG: 0.47 g IPTG in 5 ml H_2O, syringe filtered with 0.2 μM Minisart filter.

2.1.2 Recombinant protein expression

Plasmid vector pJC20 is a small plasmid vector of 2.4 kbp, which is designed for the expression of recombinant proteins in *E.coli* (Clos and Brandeau 1994). The expression vector contains a T7 RNA polymerase dependent promoter, which is under the control of lacUV5 promoter. Protein expression is induced using IPTG. BL21 *E.coli* cells contain a gene for T7 RNA polymerase, making pJC20 a suitable vector for protein expression. The pJC20 vector is a desirable vector for high copy number plasmids, as it contains a multiple cloning region, restriction sites for commonly used enzymes and ampicillin resistance gene.
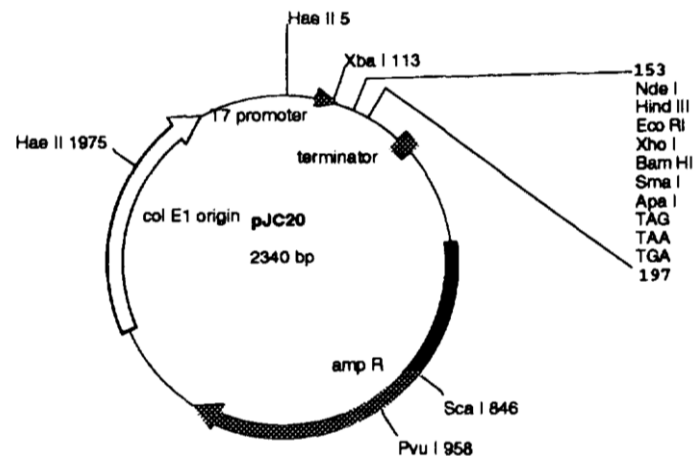
Figure 2.1.2.1 Schematic circular map of pJC20 vector. The sequence contains multiple cloning sites and ampicillin resistance gene. The vector contains a T7 promoter. Expression is induced by IPTG (image from Clos and Brandeau 1994).

An Alanine-Serine extension was added to the N-terminus of Tpm to mimic N-acetylation of the native protein (Boussouf et al. 2007, Kremneva et al. 2004, Monteiro et al. 1994).

Primers for the Ala-Ser extension addition:

Forward AS-αTm primer

5' GG CAT ATG GCG AGC ATG GAC GCC ATC AAG AAG AAG ATG CAG ATG 3'

       NdeI   AS   α-Tm

Reverse AS-αTm primer

5' CC GGA TCC TTA TAT GGA AGT CAT ATC GTT GAG AGC GTG GTC 3'

       BamHI   α-Tm

Glycerol stocks of BL21 *E.coli* cells containing the Tpm gene were used to inoculate 20 ml of LB media containing ampicillin (50 ug/ml) overnight at 37 °C shaking at 160 rpm. Overnight cultures were used to inoculate 750 ml of LB media containing ampicillin (50 ug/ml), which were incubated at 37 °C, 160 rpm, until an OD_{600} of 0.6 was reached. The

culture was then induced with IPTG (400 μM) and incubated for 3 hours at 37 °C, 160 rpm.

Cells were centrifuged at 5, 000 rpm (4412.2 x g) for 8 minutes at 4 °C and the pellet was centrifuged a second time at 4,500 rpm (357 3.8 x g) for 20 minutes at 4°C, before being frozen at – 20 °C until needed for purification.

2.1.3 Recombinant protein purification

Cells from recombinant protein expression were resuspended in 20 ml of ice cold buffer A (100 mM NaCl, 5 mM $MgCl_2$, 5 mM KPi, 1 mM NaN_3, pH7). Cells were then subjected to sonication to lyse the cells (2 minutes sonication, 1 minute rest, 2 minutes sonication). The lysate was heated at 80 °C for 10 minutes to denature contaminating proteins in the lysate, before being cooled on ice for 30 minutes. After cooling the lysate was centrifuged at 12,000 rpm (17371.6 x g) for 30 minutes at 4 °C to separate cell debris from the expressed protein.

The supernatant was subjected to pH precipitations by dropping the pH to 4.6 to precipitate Tpm, then centrifugation at 4, 600 rpm (2552.7 x g) for 10 minutes, and then resuspending the pellet in 25 ml buffer A, and adjusting the pH to 7 and left to stir for 10 minutes at 4 °C.

Tpm was then purified using FPLC using a 5 ml anion exchange HiTrap Q HP sepharose column. Samples were eluted using a linear salt gradient 0 – 100 % buffer B (1 M NaCl, 5 mM $MgCl_2$, 5 mM KPi, 1 mM NaN_3, pH7). Fractions containing Tpm were pooled and

subjected to pH precipitation as previously described. This was then purified using the FPLC a second time, as before, and Tpm containing elutions were pooled.

Tpm was purified a final time by being subjected to a pH precipitation again, but this time being resuspended in 3 ml buffer C (100 mM KCl, 20 mM MOPS, 5 mM $MgCl_2$, 1 mM NaN_3, pH7). The resuspended solution was ultracentrifuged at 100,000 rpm (434513 x g) for 20 minutes at 4 °C to remove any final contaminants. The concentration of Tpm was determined by measuring absorbance using a UV spectrophotomer at 280 nm and applying the Beer-Lambert law, A = E c l. the extinction coefficient, E, for α Tpm is 17,880 l mol^{-1} cm^{-1}.

2.1.4 His-tagged recombinant protein purification

Cells from recombinant protein expression were resuspended in 20 ml of ice cold buffer A' (300 mM NaCl, 50 mM KPi, pH8). Cells were then subjected to sonication to lyse the cells (2 minutes sonication, 1 minute rest, 2 minutes sonication). The lysate was centrifuged at 12,000 rpm (17371.6 x g) for 30 minutes at 4 °C to separate cell debris from the expressed protein.

The supernatant was subjected to pH precipitations by dropping the pH to 4.6 to precipitate Tpm, then centrifugation at 4,600 rpm (2552.7 x g) for 12 minutes, and then resuspending the pellet in 25 ml buffer A', and adjusting the pH to 7 after left to stir for 10 minutes at 4°C. The pH precipitation was repeated a second time and then left to stir for 30 minutes at 4 °C.

His-tagged Tpm was then purified using a TALON cobalt column. Samples were eluted using imidazole buffer B (300 mM NaCl, 50 mM KPi, 250 mM imidazole, pH8). Elution fractions containing Tpm were pooled and subjected to pH precipitation as previously described.

Flow through and wash elutions were subjected to pH precipitation and a further purification using the TALON cobalt column, and the elution products were added to the first purification pool.
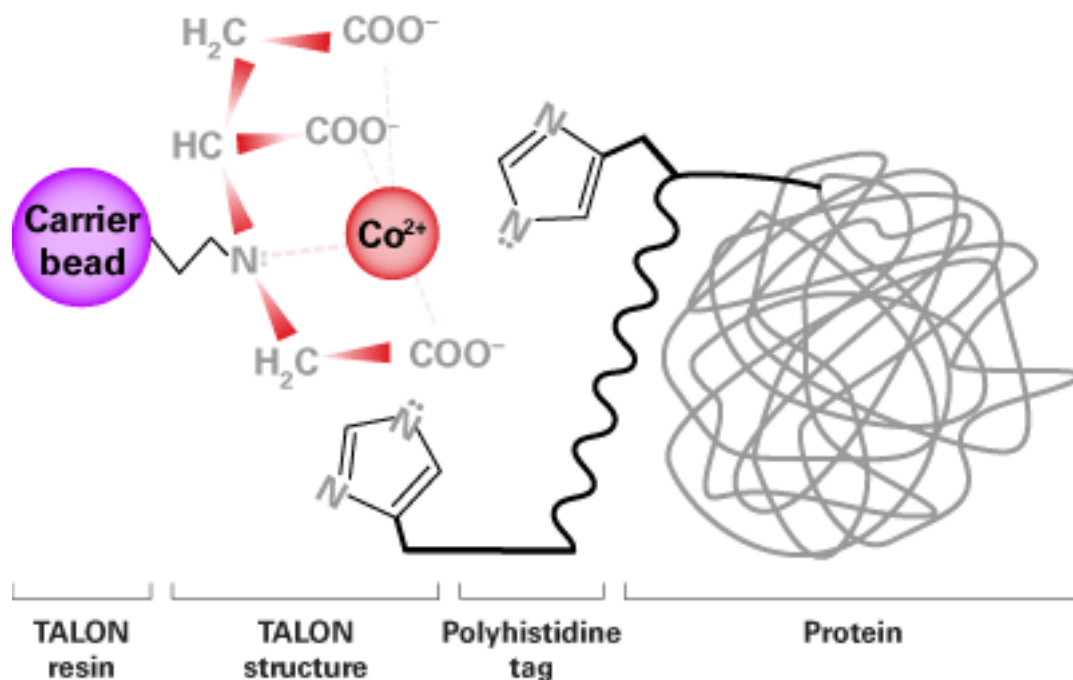
Figure 2.1.4.1 Highly specific interaction of His-tag with Co^{2+} of TALON resin (Image taken from http://www.clontech.com/US/Support/Applications/Tagged_Protein_Purification/Ni-NTA_Resin_vs._Talon)

TALON resin was chosen over NiNTA due to the increased specificity of His-tagged proteins and thus increased purity of protein elutions. Previous attempts of NiNTA purification resulted in poor binding of His-tagged Tpm and thus low yield of protein.

Tpm was purified a final time by being subjected to a pH precipitation again, but this time being resuspended in 3 ml buffer C (100 mM KCl, 20 mM MOPS, 5 mM MgCl$_2$, 1 mM NaN$_3$, pH7). The resuspended solution was ultracentrifuged at 100,000 rpm (434513 x g) for 20 minutes at 4 °C to remove any final contaminants. The concentration of Tpm was determined by measuring absorbance using a UV spectrophotomer at 280 nm and applying the Beer-Lambert law, A = E c l. the extinction coefficient, E, for α Tpm is 17,880 l mol^{-1} cm^{-1}.

2.1.5 Extraction of native Tpm from mouse cardiac tissue

Cardiac muscle tissue from mice was used to extract native Tpm. Half a mouse heart ($\sim$ 0.07 g) was minced and homogenised on ice in 500 μl wash buffer (100 mM KCl, 20 mM MOPS, 5 mM MgCl$_2$, 1 mM NaN$_3$, pH7) until smooth. The homogenised tissue was centrifuged at 4,600 rpm (2552.7 x g) for 4 minutes at 4 °C. The pellet was resuspended in 500 μl Guba Straub buffer (100 mM KH$_2$PO$_4$, 50 mM K$_2$HPO$_4$, 0.3 M KCl) and 5 mM ATP and incubated for 3 hours at room temperature, on a magnetic stirrer. The tissue was centrifuged at 4,600 rpm (2552.7 x g) for 4 minutes at 4 °C. The pellet was subject to a second Tpm extraction in Guba Straub, overnight at 4 °C on a magnetic stirrer. The supernatant was then analysed via SDS PAGE for Tpm content. Samples of the supernatant were chemically cross-linked and run on non-reducing gels. Tpm extractions from mouse cardiac tissue were stored at -20 °C.

2.1.6 Mass spectrometry

Proteins were explored via electrospray mass spectrometry to either verify the purified recombinantly expressed protein was the correct molecular mass, or to explore the dimer content of cardiac tissue, as in section 3.11. Mass spectroscopy was performed by Kevin Howland, the facility manager in the Biomolecular Science Facility at the University of Kent.

2.1.7 Pyrene labelling of Tpm

Protocol has been adapted from Ishii and Lehrer 1989. Tpm was reduced and desalted as per methods section 2.2.3. Tpm at 2 mg/ml was incubated in a pyrene containing buffer (5 M GuHCl, 10 mM HEPES pH7, 5 x molar excess pyrene) at 20 °C for 4 hours. The reaction is then quenched with 20 mM DTT and filtered to remove undissolved pyrene using a Zeba ™ Spin Desalting Column (7K molecular weight cut off). The eluent was then dialysed against a buffer containing 5 M GuHCl, 1 mM DTT pH7 overnight at 4 °C to remove unreacted pyrene. The Tpm was then dialysed again in a buffer containing 0.5 M NaCl, 10 mM HEPES pH7 over 8 hours at 4 °C, changing the dialysis buffer every 2 hours. The final dialysis was against a buffer of 2 mM HEPES pH7, 1 mM EDTA overnight at 4 °C.

2.2 Biochemical techniques for protein characterisation

2.2.1 Cosedimentation assays

Dimer exchange on actin could be monitored using cosedimentation assays. Tpm bound to actin will spin down to form a pellet during ultracentrifugation at 100,000 rpm (434513 x g), while Tpm free in solution will remain in the supernatant. Traditionally, cosedimentation assays were used to determine the affinity of Tpm for actin. Here, Tpm was pre-incubated with actin, before incubating with a tenfold molar excess of His-tagged Tpm. If exchange does occur, unlabelled Tpm will be found in the supernatant and His-tagged Tpm will be found in the pellet, as detected by SDS PAGE analysis.

In dimer exchange experiments, 7 uM actin was pre-incubated with 2.5 uM α Tpm, to saturate the actin filament, and incubated for 1 hours at room temperature in low salt (100 mM KCl, 20 mM KPi, 5 mM $MgCl_2$, 1 mM NaN_3, pH 7) buffer. The solution was then ultracentrifuged for 20 minutes at 100,000 rpm (434513 x g) at 4 °C to remove the unbound Tpm. The pellet was then resuspended in low salt buffer, with a 10 times molar excess of His-tagged α Tpm. The solution was then incubated at 20 °C and 37 °C and samples were taken at specified intervals. Samples were subjected to ultracentrifugation again for 20 minutes at 100,000 rpm (434513 x g) at 4 °C to separate Tpm bound to actin and Tpm free in solution. Pellets were resuspended in low salt buffer.

To enable clear visualisation and reduce interference of monomer exchange, Hisα Tpm was chemically cross-linked prior to use in cosedimentation assays. Samples were

analysed using non-reducing SDS PAGE due to the cross-linked Hisα Tpm. SDS Gels were then subjected to densitometry analysis to explore exchange.

2.2.2 Dimer reduction and exchange

Protein samples were reduced by the addition of 20 mM DTT and heating at 59 °C for 10 minutes. For use of reduced monomers, samples were cooled on ice and then subjected to desalting using a Zeba ™ Spin Desalting Column (7K molecular weight cut off). For dimer exchange, samples were incubated at desired temperature in the presence of DTT and then were desalted and stored on ice prior to use.

2.2.3 SDS PAGE – reducing conditions

Protein samples were analysed using Invitrogen NuPage Bis-Tris 4 – 12 % precast SDS polyacrylamide gels. Samples were mixed with 6X sample buffer and heated to 95 °C for 5 minutes before loading.

2.2.4 SDS PAGE – non-reducing conditions

Cross-linked samples were analysed under non-reducing conditions. Protein samples were analysed using 7.5 % SDS polyacrylamide gels. Samples were mixed with 6X sample buffer without betamercaptoethanol and loaded as quickly as possible onto the gel to prevent sample precipitation.

2.2.5 Chemical cross-linking

Cross-linking of Tpm dimers was used routinely to fix dimer populations for analysis. Samples of Tpm containing any DTT were first desalted using a Zeba ™ Spin Desalting Column (7K molecular weight cut off). Samples were mixed in a 1:1 volume ratio with oxidation buffer (10 mM MOPS, 2M NaCl, 2 μM $CuSO_4$, 10 mM $K_2Fe(CN)_6$, pH 7) and incubated overnight at 37 °C. Oxidation buffer is removed using Zeba ™ Spin Desalting Columns, normally twice, or until colourless. Samples were then stored short term at 4 °C or long term at -20 °C.

2.2.6 Densitometry analysis

Exchange between dimers was explored with the use of SDS PAGE and densitometry analysis. Dimers were visualised on gels and the content was determined for each band in each lane. Densitometry analysis was performed using ScionImage software.

Scanned images of SDS gels were imported into ScionImage. Macros GelPlot2 and LinePlot were loaded. When using GelPlot2, a box is drawn manually around each lane. The band densities are plotted as a histogram.

The area under the curve is proportional to the intensity of the band. For each lane, the peak densities are relative to the total area. Analysis band densities relative to the total area allowed comparison between lanes even if there were differences in loading.

The macro LinePlot was used in cases of unclear or curved bands. The analysis was similar to GelPlot2 and produces similar histogram profiles. The difference was that band densities were calculated through a line drawn through the gel, rather than the entire area within a box. This enabled the user to manually select the clearest section of a gel and avoid areas that would affect the histogram profile and thus, band analysis.

Results from this work are shown and discussed in Chapter 3.

2.2.7 Measuring the persistence length using atomic force microscopy

The stiffness of a protein can be explored by calculating its persistence length. Atomic force microscopy (AFM) images can be analysed to measure contour lengths of Tpm and determine the persistence length of the protein with the use of MATLAB.

Samples of Tpm were deposited onto freshly cleaved mica, that had been rinsed with distilled H_2O (dH_2O) and dried with N_2 gas. Tpm was incubated on the mica for 5 minutes and rinsed with 1000 μL dH_2O, before drying gently with N_2 gas. AFM images were collected in air using Bruker MultiMode 8 scanning probe microscope using a ScanAsyst-Air cantilever probe. Parameters of the scan were: spring constant 0.4 N/m, Auto z limit 1 μM, ScanAsyst noise threshold 0.1 nm, scan line 2048, scan angle 45 degrees. Larger scans scaled up the lines per scan accordingly, to preserve the xyz pixel/nm. Scans were performed at room temperature (20 °C) and each image was accumulated three times to minimise changes from thermal drift.

AFM images were processed in Bruker NanoScope software to flatten the background before exporting into MATLAB to be analysed using a semi-automated script, written by Dr Wei-Feng Xue, to trace particles.

Samples imaged on poly-lysine coated mica were performed as described by Loong et al. 2012.

Results from this work are shown and discussed in Chapter 5.

2.2.8 The use of circular dichroism to explore thermal stability

Circular dichroism (CD) as a function of temperature can be used to explore the thermal stability of a protein by studying the unfolding of its secondary structure. Here, CD was used to explore the thermal stability of WT and mutant homo and heterodimers, together with the effect of chemical cross-linking, His-tags and varying buffer conditions.

CD spectroscopy was collected on a Jasco 715-Spectropolarimeter. The thermal melting of 7 μM Tpm was observed in a 1 mm stoppered cuvette at 222 nm. Tpm was explored in buffer containing low salt (100 mM KCl, 20 mM KPi, 5 mM $MgCl_2$, 1 mM NaN_3, pH7) and high salt (500 mM KCl, 20 mM KPi, 5 mM $MgCl_2$, 1 mM NaN_3, pH7) buffers in the presence and absence of 1 mM DTT. Scans were performed from 5 – 65 °C, increasing at 1 °C / min, with readings every 0.2 °C using a Peltier device. Each sample was successively heated and cooled three times to ensure the protein refolded correctly. For heterodimer experiments, only the first melting curve showed a true profile for a

heterodimer, and the successive melts would be a mix of homo and heterodimers. For non-cross-linked homodimers, the first melting curve was discounted as this may be affected by any natural cross-linking.

Results from this work are shown and discussed in Chapter 4.

Chapter 3: Exchange of Tropomyosin dimers and monomers

3.1 Introduction

Tpm exists as both as a homo and heterodimer. It is not fully understood how these dimers are formed or if they exchange in the cell. The α and β isoforms are expressed in heart and skeletal muscle in varying amounts. The two isoforms dimerise to form homo and heterodimers. It was commonly thought that β homodimers were rarely found, however studies have shown its prevalence (Holtzer, Kidd et al. 1992, Corbett, Anthony Akkari et al. 2005, Bronson, Schachat 1982). Ratios of α homodimers to αβ heterodimers vary depending on muscle type, species and heart rates. Perry states that slower beating hearts, from larger animals such as pig, sheep and humans, contain up to 20% of the β isoform. While faster beating hearts from smaller animals, such as rats and rabbits express very small amounts of β isoform, and more α homodimer. When both isoforms are present in tissue, the β is often found as a heterodimer in preference to a homodimer (Perry 2001). Different tropomyosin isoforms have different properties that will affect their role and function in the cell, which require further exploration to understand their impact. These differences in properties could give explanation to their preferential dimerization and ratios in the cell.

Random assembly predicts that if you mix homodimers and mixed in a 1:1 ratio, they will assemble in a 1:2:1 ratio (homo:hetero:homo). If β expression is low, it

is more likely to form the heterodimer, thus limiting homodimer prevalence. As the ratio of α:β expression reaches 1, there must be some other process to assist assembly to ensure heterodimer preference, otherwise the ratio will be 1:2:1 (Kalyva, Schmidtmann et al. 2012). Previous studies have shown that overexpression of β Tpm can be lethal, highlighting the importance of expression and dimerization in its function (Wieczorek, Jagatheesan et al. 2008).

Understanding the stability of the Tpm heterodimer complex is important for studies in vitro. It is essential to be aware of any exchange that may be taking place while samples are being used. Studies in this chapter were designed to provide insight into the rate at which exchange occurs both in vivo and in vitro and further our understanding of how dimers are formed in vivo.

Work previously carried out by M. Janco and A. Kalyva was performed using chemically cross-linked forms of Tpm dimers, to ensure dimers did not exchange (Janco, Kalyva et al. 2012). While this guaranteed that heterodimers stayed pure throughout experiments, the effect this cross-link had on the protein during these experiments is unknown for heterodimers. The effect of cross-linking on homodimers was studied, and thermal melting curves showed a shift to biphasic unfolding depending upon the location of the cross-link (α has one cys, ß has two cys residues, able to form cross-links). In rabbit psoas muscle, the cys residue has been shown to be in the reduced state (Lehrer, Ly et al. 2011). Changes in the thermal stability of the protein were ascribed to the strain inflicted on Tpm at the site of the cross-link. This was attributed to weak and strong interchain interaction regions of the Tpm chain. However, it was also suggested that these

effects were amplified by the initial stability of the monomeric form of Tpm; α being more thermally stable than β, which provided evidence for long range effects of the cross-link (Wrabl, Holtzer et al. 1994, Holtzer, Kidd et al. 1992).

The aim in this chapter is to demonstrate the efficacy of SDS PAGE to visualise and establish the ratio of homo and heterodimers present in a solution by the addition of a His tag to one or both Tpm monomers. From this, the rate of exchange between dimers and their stability at various temperatures were explored. Principally, the stability of heterodimers was deduced, potentially removing the need for cross-linking in future experiments if the heterodimer proves stable in its absence. This same methodology was used to explore Tpm mutants linked to DCM. Dimer exchange in polymers was also monitored using fluorescent spectroscopy of a pyrene labelled Tpm, to explore exchange of dimers while bound to the actin filament, utilising cosedimentation assays.

Exchange will be explored of monomeric Tpm within a dimer (sections 3.4 – 3.8), and of dimeric Tpm within a polymer (sections 3.9 – 3.10), as shown in figure 3.1.1.
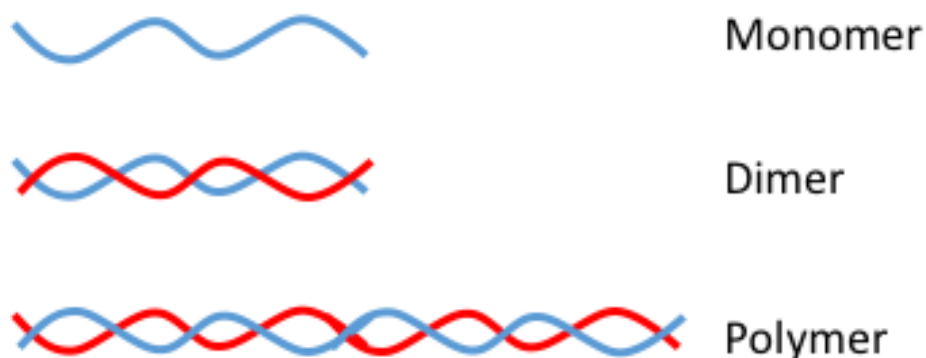
Figure 3.1.1. Illustration of Tpm dimerization. A monomer shown in blue on its own, and as part of a heterodimer, blue and red. Dimers polymerise head to tail to form polymers.

3.2 Method

Tpm dimers were reduced as described in the methods chapter 2.2.3. Conditions were either standard salt, 100 mM KCl, 20 mM KPi, 5 mM MgCl$_2$, 1 mM NaN$_3$, pH 7, or high salt, 500 mM KCl, 20 mM KPi, 5 mM MgCl$_2$, 1 mM NaN$_3$, pH 7. Previous work with Tpm has been performed under both standard and high salt buffers, but the effect of this salt concentration difference has not been fully explored.

The reduced dimers were then mixed in desired ratios and incubated at a range of temperatures, namely, 4℃, 20 ℃, 30 ℃ and 37 ℃ to explore the rate of exchange. At selected time intervals, samples were taken and either cross-linked to examine the dimers present, or reduced to explore the rate of degradation.

Incubations were performed in the presence of DTT, which was removed prior to cross-linking, using a Zeba spin column, as described in methods 2.2.3. The presence of DTT throughout the incubations not only prevented the formation of spontaneous cross-links, but also reduced protein degradation. The half-life of DTT is relatively short, however, at 20 ℃ for example at pH 7.5 its half-life is only 10 hours (Stevens, Stevens et al. 1983), which meant by the end of the incubations, especially at higher temperatures, the effect of DTT would be greatly reduced.

Samples taken over a time course were run under two gel conditions: 4 – 12 % precast gradient gels under reducing conditions, to assess the amount of Tpm

monomers present, while cross-linked dimer samples were run on 7.5 % gels under non-reducing conditions to assess dimer content. Gel bands were analysed as described, in figures 3.3.3 – 3.3.6. Reduced samples were run for 60 minutes at 150 V. Non-reduced samples were run for 240 minutes at 100 V.

Protein samples were visualised in their monomeric and dimeric form. Samples of Tpm were taken at specified time intervals and split in two. One half was reduced with the addition of sample buffer containing beta-mercaptoethanol (BME) and boiling at 80 ℃, which caused the disulphide bonds in the protein to be reduced. The second half were mixed with sample buffer that did not contain BME and were not subjected to boiling.

Non-reducing conditions were used for samples that were subjected to chemical cross-linking to fix a dimer population. These conditions were used to determine the amount of homo- and heterodimers in a solution. Reducing conditions were used to determine the ratio of monomer isoforms present in a population and to study the degradation of the protein over the time-course.

3.3 The addition of a His-tag enabled visualisation of homodimers and heterodimers

It was postulated that the addition of a His-tag to α Tpm would be sizeable enough to separate dimers containing 0, 1 or 2 tags on the protein. Wild type α Tpm and the His-tagged monomer samples were visualised on a gel under reducing conditions as explained in the methods, figure 3.3.1.
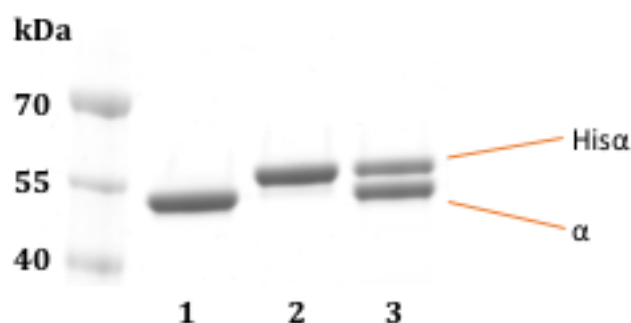
Figure 3.3.1. Tpm monomers run on a 4-12% gradient precast gel under reducing conditions. Prestained PageRuler ™ #26616, Lane 1: α Tpm, lane 2: Hisα Tpm, lane 2: α and Hisα Tpm mixed in a 1:1 ratio.

Lane 1 contained pure α Tpm and lane 2 contained pure Hisα Tpm. The addition

of a His-tag to Tpm added enough mass to the protein to make it

 clearly distinguishable against the untagged protein. Lane 3 shows a solution

that contained 1:1 α and Hisα Tpm, to highlight their separation on the gel.

The formation of a cross-link in vitro between monomers, as explained in

methods 2.2.6, enabled visualisation of dimers under non-reducing conditions. It

was hoped that the His-tag would allow separation not only of homodimers but

of heterodimers too. Samples containing either homo or heterodimers of α and

Hisα Tpm were chemically cross-linked to fix the dimer population and run

under non-reducing conditions. Sample 1 was pure α Tpm, sample 2 was pure

Hisα and sample 3 contained a mix of α and Hisα homodimers. Sample 4 was the

same as sample 3, however, this sample was subjected to heating at 59 ℃ for 20

minutes and cooling to 4℃ before cross-linking, to allow for dimer exchange.
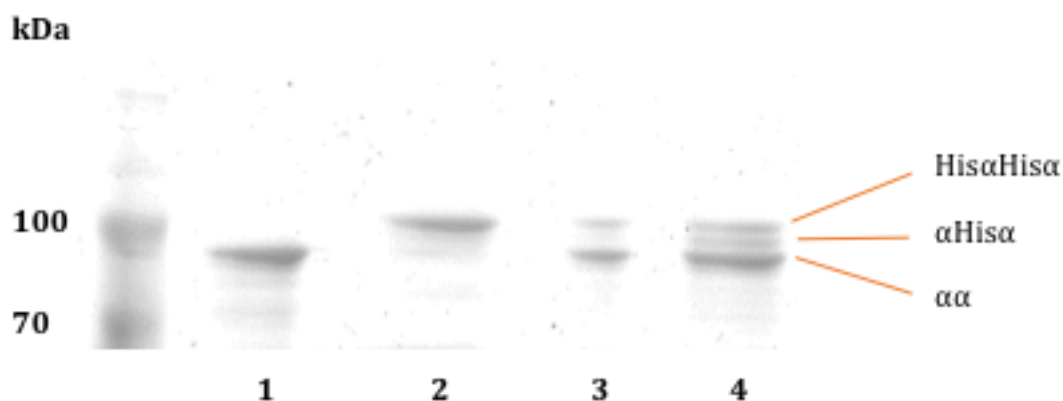
Figure 3.3.2. Cross-linked Tpm homo and heterodimers run on a 7.5 % SDS polyacrylamide gel, under non-reducing conditions (- betamercaptoethanol). Prestained PageRuler ™ #26616, Lane 1: αα Tpm, lane 2: HisαHisα Tpm, lane 2: αα and HisαHisα Tpm mixed in a ~2:1 ratio α:Hisα, lane 4: αα + HisαHisα + α-Hisα Tpm. Homo and heterodimers are indicated on the gel.

Cross-linked α and Hisα homodimers were seen to run distinct of each other on a 10 % polyacrylamide gel, as shown in lane 1 (α Tpm homodimer), lane 2 (Hisα Tpm homodimer) and lane 3 (α + Hisα homodimers). Lane 4 shows a mix of both homodimers and a third distinct band was seen that runs between the two, the α-Hisα heterodimer, as indicated on figure 3.3.2.

Cross-linked samples had a tendency to precipitate when mixed with sample buffer (-BME) and left for any period of time. As a result, cross-linked samples had to be run on a gel as soon as they were taken for each time point, to prevent smearing on the gels. Longer time course experiments required multiple gels to be compared, which can bring about a small discrepancy between loading and how the sample ran. The method of analysis used here calculated proportions of each dimer out of the total amount in each lane, so these changes between gels would not affect the analysis significantly.

SDS polyacrylamide gels were subjected to densitometry analysis with the use of Scion Image, to quantify the amount of protein in each band. Using macros "Gelplot2" and "Lineplot", bands were outlined and the change in density was plotted as a curve, shown in figure 3.3.3. The gel analysed is the same as shown in figure 3.3.2.
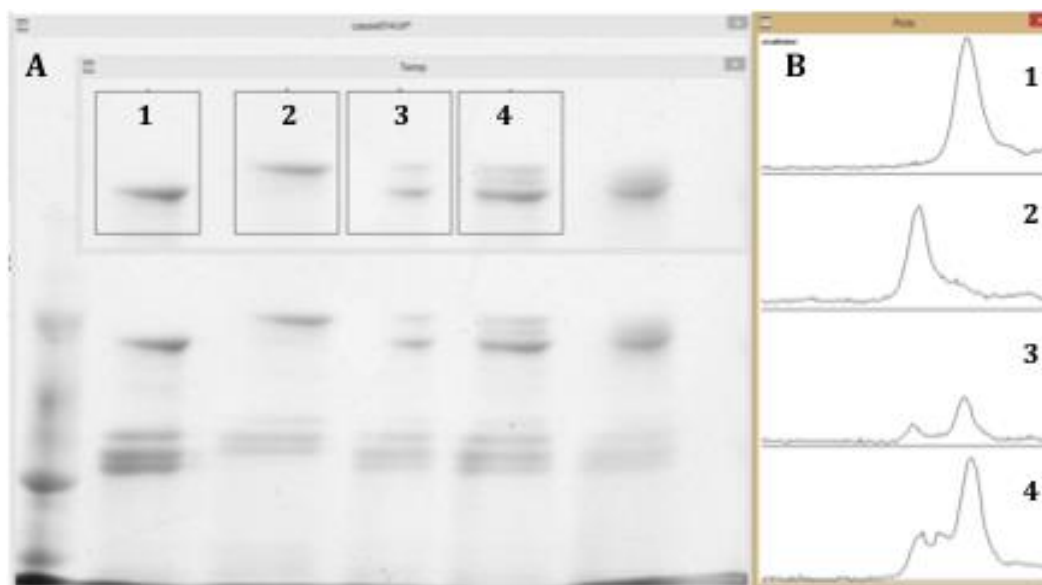
Figure 3.3.3. Scion Image densitometry analysis of an SDS polyacrylamide gel using **Gelplot2**. A: marking of lanes to be analysed, lane 1: α homodimer, lane 2: Hisα homodimers, lane 3: αα + HisαHisα, lane 4: αα + α-Hisα + HisαHisα. B: plots showing density of bands in each lane.

Using Scion, boxes were drawn around gel bands to be analysed. Each box was the same size, shown inset figure 3.3.3.A. From these selected areas, the band densities were calculated and shown as histogram plots, figure 3.3.3.B. This gel is the same as shown in figure 3.3.2. Lane 1 contained pure α homodimer, lane 2 was pure Hisα homodimer, lane 3 was a mix of Hisα and α homodimers (smaller peak and larger peak, respectively), and lane 4 was a mix of Hisα homodimer, α-Hisα heterodimer and α homodimer (small peak, small peak, large peak, respectively).

Total band densities were used, as this showed the entire loading of the sample more accurately, however, in some cases where a gel band may not run perfectly straight, Lineplot could be used in place to analyse the band densities through the line drawn, instead of over the boxed area, as in Gelplot2. This avoids errors through unclear bands, but showed a similar profile plot, as for Gelplot2. The profile plot for the band densities using Lineplot is shown in figure 3.3.4.
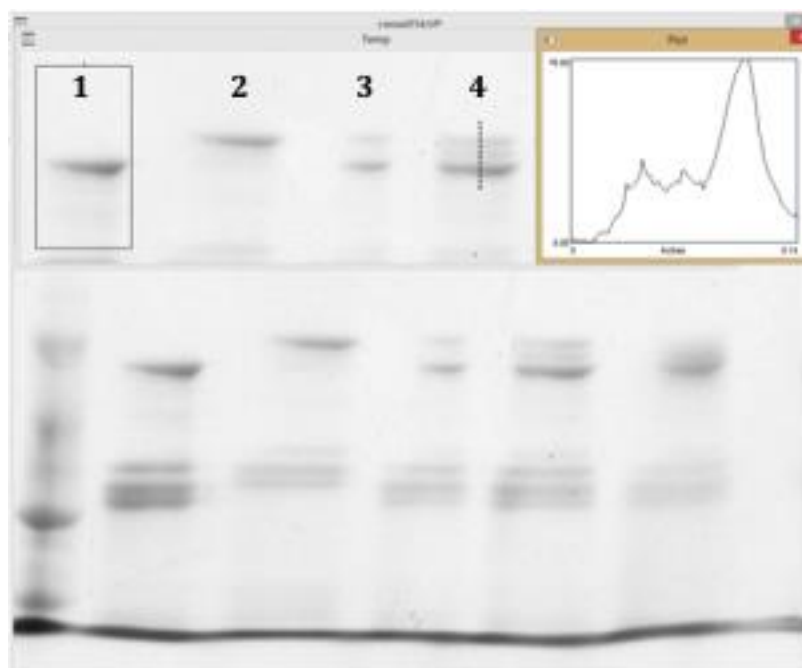
Figure 3.3.4. Densitometry analysis of lane 4 using **Lineplot** in Scion Image. Inset: density profile plot for HisαHisα + α-Hisα + αα bands.

The same gel was subjected to analysis using line plot, figure 3.3.4. For clarity, lane 4 was subjected to densitometry analysis, shown by the line drawn through the inset band areas. The histogram showed three peaks, corresponding to Hisα homodimer, α-Hisα heterodimer and α homodimer (small peak, small peak, large peak, respectively). This was the same profile as generated by Gelplot2, thus showing it was a reliable substitute in cases of imperfect gel images.

To accurately analyse these profile plots, the data points were exported into Microsoft Excel and fitted to Gaussian curves, shown in figure 3.3.5. From these fits, the area under the Gaussian plot was used to quantify the density of the band it represents.
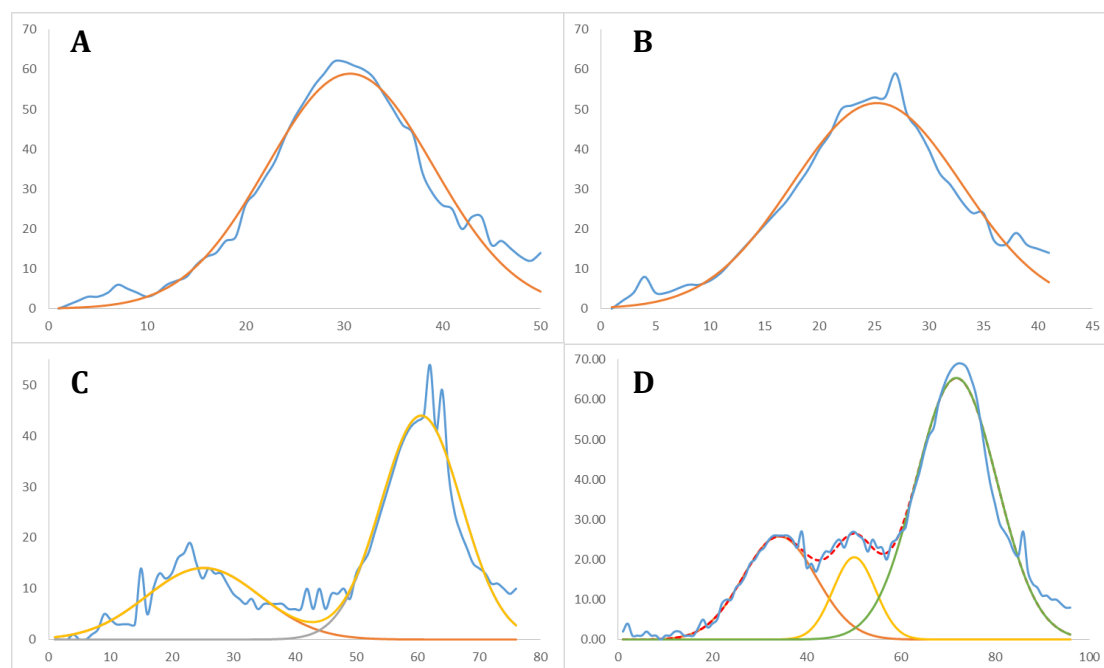
Figure 3.3.5. Densitometry analysis plots fitted to multiple Gaussian plots. 1: αα homodimer, one fit, 2: HisαHisα homodimer one fit, 3: HisαHisα + αα, two fits, 4: HisαHisα + α-Hisα + αα, three fits.

The area under the Gaussian represents the amount of protein in the band, which was then converted into a ratio to calculate the amount of exchange taking place. The amplitude is the peak of each Gaussian, which represents the intensity of the band, and the half width represents the half width of the Gaussian. Over time the amplitude, area and half width may decrease as the protein degrades. Conversely, protein degradation that leads to smearing of gel bands may also lead to an increase in the half width and area under the curve.

It was seen that the data in figure 3.3.5.1 and figure 3.3.5.2 was described by one Gaussian, while data in figure 3.3.5.3 requires two Gaussians and figure 3.3.5.4 was described by three, this was confirmed using MATLAB. MATLAB Curve Fitting Tool provides additional insight into the goodness of Gaussian fits on the gel band densities, shown in figure 3.3.6. This provided the means to analyse the statistical significance of fitting two Gaussians vs. three Gaussian plots to a curve, to more accurately define the appearance of a heterodimer.

The Gaussian model is given by:

$$y = \sum_{i=1}^{n} a_i e^{\left[-0.5\left(\frac{x-b_i}{c_i}\right)^2\right]}$$

<div align="right">Equation 3.3.1.</div>

Wherein a: amplitude, b: centroid location, c: peak half width and n: number of peaks to fit and $1 \leq n \leq 3$. This is the model for n Gaussian curves.

Curves were fitted in MATLAB to either two Gaussians or three Gaussians using equation 3.3.2 and 3.3.3, respectively, as shown in figure 3.3.6.

$$f(x) = a_1 e^{\left[-0.5\left(\frac{x-b_1}{c_i}\right)^2\right]} + a_2 e^{\left[-0.5\left(\frac{x-b_2}{c_i}\right)^2\right]}$$

<div align="right">Equation 3.3.2.</div>

Expanded double Gaussian fit from equation 3.3.1, shown in equation 3.3.2, wherein a: amplitude, b: centroid location and c: peak width, for Gaussians 1 and 2.

$$f(x) = a_1 e\left[-0.5\left(\frac{x-b_1}{c_1}\right)^2\right] + a_2 e\left[-0.5\left(\frac{x-b_2}{c_2}\right)^2\right] + a_3 e\left[-0.5\left(\frac{x-b_3}{c_3}\right)^2\right]$$

<div align="right">Equation 3.3.3.</div>

The expanded triple Gaussian fit from equation 3.3.1, shown in equation 3.3.3, wherein a: amplitude, b: centroid location and c: peak width, for Gaussians 1, 2 and 3.

Lane 4, shown in figure 3.3.5.4, was subjected to MATLAB analysis as outlined above, to test the goodness of fit of 2 Gaussian curves against 3 Gaussian curves, figure 3.3.6.
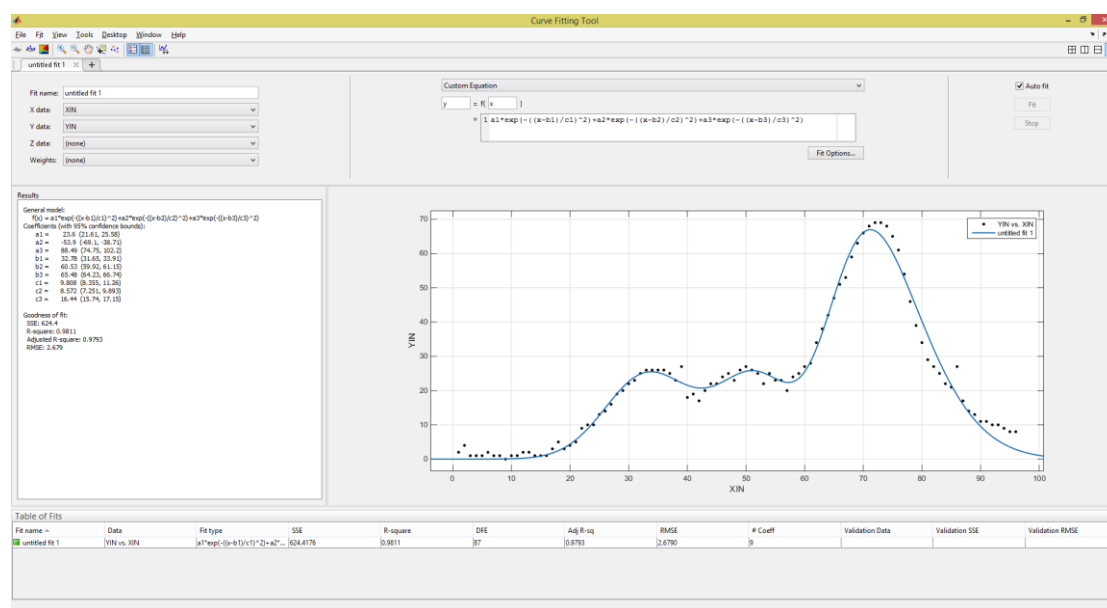
Figure 3.3.6. Multiple peak fitting to Gaussian plots shows three Gaussian fits to Lane 4 of the gel shown in figure 3.3.5. The three peaks correspond to the three band densities on the gel. The R squared value is 0.9811.

The output sum of squared errors (SSE) from MATLAB Curve Fitting Tool was used to perform an F test of the goodness of the fit, using equation 3.3.4. This model enabled comparison of the two fitted curves.

$$F = \left(\frac{SSE_1 - SSE_2}{SSE_2}\right)\Big/\left(\frac{df_1 - df_2}{df_2}\right)$$

Equation 3.3.4.

The F test, where SSE is the sum of squared errors for the simpler and complex models, model 1 (equation 2 – 2 Gaussians) and model 2 (equation 3 – 3 Gaussians) respectively. The degrees of freedom (df,) is defined by the number of samples – number of parameters for either the simpler or complex model, 1 and 2, respectively.

The P value is calculated for the F test using equation 3.3.5, to determine the significance of the goodness of the fit.

$$P = fcdf(F, df_1 - df_2, df_2)$$

Equation 3.3.5.

The P value of F test, as defined by MATLAB: If the F cumulative distribution function (fcdf) is > 0.05, we reject the null hypothesis (simpler model) and accept the alternate, complex model. F is the F test. The degrees of freedom, df, is

defined by the number of samples – number of parameters for either the simpler or complex model, 1 and 2, respectively.

In this example, figure 3.3.6, P = 0.9998, ergo the null hypothesis was rejected and the alternate, more complex model was accepted, and the data was therefore fitted to three Gaussian models.

Given that homo and heterodimer bands are clearly distinguishable on an SDS polyacrylamide gel, and are quantifiable using Scion and MATLAB, this technique provides a means to analyse the dimer content of a solution.

3.4 At 4 ℃ Tpm homodimers are stable and show no exchange over two weeks

Tpm α and Hisα homodimers were incubated at 4 ℃ in low and high salt buffers to explore the rate of exchange of monomers and the possible effect of salt on this rate of exchange. Two samples were taken every 24 hours to visualise using SDS PAGE. Samples were run under reducing conditions to assess the degradation of the protein and loading, and under cross-linked conditions, to assess the ratio of homo and hetero dimers present. The starting material for the experiment is shown in figure 3.4.1.
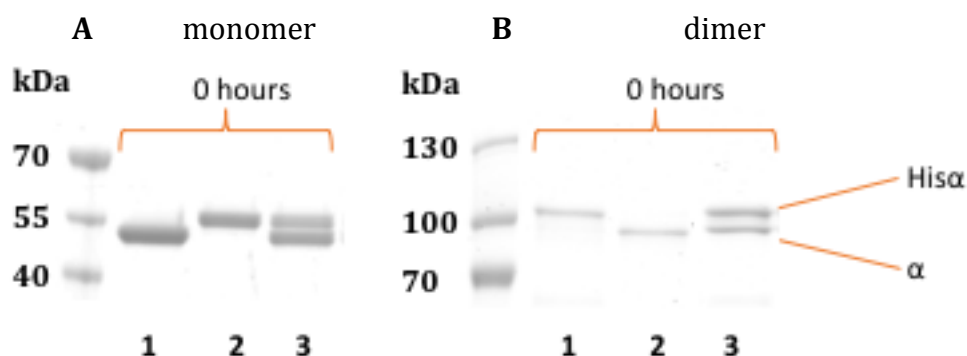
Figure 3.4.1. Tpm monomers run on a 4-12% gradient precast gel under reducing conditions (+BME), A, and cross-linked Tpm dimers run on a 7.5 % SDS polyacrylamide gel, under non-reducing conditions (- BME), B. Prestained PageRuler ™ #26616. A. Reduced monomers 1: α Tpm, 2: Hisα Tpm, 3: α + Hisα Tpm. B. Cross-linked dimers 1: Hisα Tpm, 2: α Tpm, 3: α + Hisα Tpm.

The reduced monomers shown in figure 3.4.1.A showed α in lane 1, Hisα in lane 2 and a mix of α and Hisα in lane 3. The cross-linked dimers shown in figure 3.4.1.B showed Hisα in lane 1, α in lane 2 and a mix of α-Hisα in lane 3. The His-tagged Tpm runs just above the non-tagged protein, allowing clear distinction between the reduced and cross-linked homodimers.

Tpm incubated at 4 ℃ showed no sign of exchange between the Hisα and α Tpm homodimers, shown in figure 3.4.2 at either standard salt or high salt conditions. Samples run under denaturing conditions show that there is no degradation of the protein over 72 hours, indicated by the clear bands in figure 3.4.2.A. and lack of change in band ratios, table 3.4.4. When cross-linked, it is clear that two homodimers exist in the samples, figure 3.4.2.B, with no heterodimer band appearing. This was confirmed by densitometry analysis, which indicated there was no change from the starting material band density ratios of the samples over the time course, table 3.4.2. Ergo, it was said that no exchange or protein

67

degradation occurred up to 72 hours at 4 ℃. There is no effect of salt

concentration on the stability or rate of exchange between the homodimers.
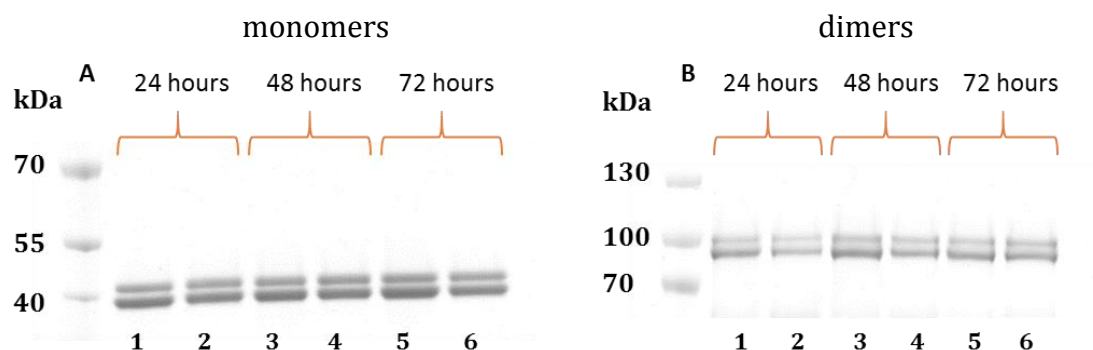
Figure 3.4.2. SDS gels of αα and HisαHisα homodimers incubated at 4 ℃ in standard and high salt (100 mM KCl and 500 mM KCl, respectively). Samples are as follows: 1. 4°C 24 hours standard salt, 2. 4°C 24 hours high salt, 3. 4°C 48 hours standard salt, 4. 4°C 48 hours high salt, 5. 4°C 72 hours standard salt, 6. 4°C 72 hours high salt. Gel A shows reduced monomers, and gel B shows cross-linked dimers under non-reducing conditions.

Samples showed no exchange up to 15 days at 4 ℃ (360 hours), figure 3.4.3.B.

Again, there is no difference in stability or exchange between standard salt and

high salt conditions. This was confirmed by densitometry analysis, which

showed no third peak appearing, table 3.4.1. Tpm showed some degradation at 2

weeks, seen on the gel in figure 3.4.3.A, by the bands becoming less distinct.

Overall, the protein stays as two stable homodimers, with no exchange seen,

figure 3.4.3.B. There is no observable difference between standard salt and high

salt conditions on exchange or protein degradation. This means the dimers can

be made and stored for at least two weeks and probably longer if frozen.
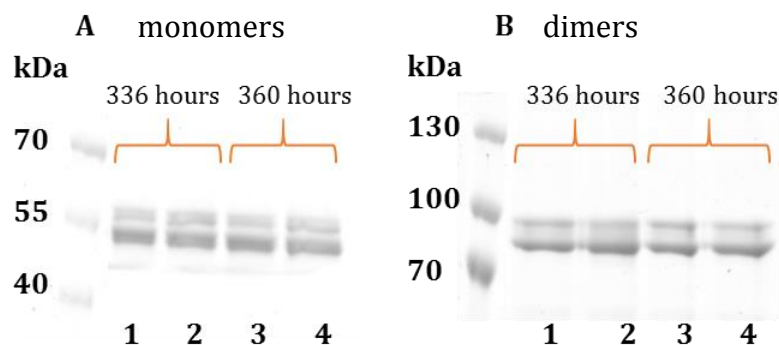
Figure 3.4.3. Samples at 4℃ taken after 14 and 15 days (336 hours and 360 hours, respectively) incubation in standard and high salt, run under denaturing conditions, A, and cross-linked, non-denaturing, B. Samples are as follows: Prestained PageRuler ™ #26616, 1. 4°C 336 hours standard salt, 2. 4°C 336 hours high salt, 3. 4°C 360 hours standard salt, 4. 4°C 360 hours high salt.

Scion Image densitometry analysis of the gels shows the ratio of both bands do not change significantly throughout the incubation, indicating there is little exchange taking place. Degradation of protein was noted by the decrease in amplitude over time for both the cross-linked and reduced samples, table 3.3.1. and 3.4.3. Towards the end of the incubation, the band width increases. This is as a result of protein degradation, because the bands start to smear, thus increasing the area covered, table 3.4.3.

Time (hours)		24		48		78		330		360	
Lane		1	2	3	4	5	6	1	2	3	4
Gaussian 1	amplitude	49.1	38.6	58.5	50.1	51.8	56.8	52.6	56.2	35.3	41.8
	SD	6.3	5.8	6.2	5.4	5.9	5.8	7.0	10.0	6.9	8.0
	area	760.7	556.2	902.8	666.7	748.6	826.4	923.6	1379.8	600.9	814.1
Gaussian 2	amplitude										
	SD										
	area										
Gaussian 3	amplitude	99.1	73.3	106.8	89.6	96.4	88.3	99.6	110.5	76.2	99.4
	SD	4.7	4.2	5.1	4.4	4.9	4.4	6.0	6.5	4.7	5.4
	area	1152.6	771.9	1347.9	981.2	1171.2	974.6	1498.0	1780.0	856.8	1314.3

Table 3.4.1. **Densitometry analysis of gel bands for <u>cross-linked</u> samples of Tpm incubated at <u>4 ℃</u> over 360 hours.** Lanes in grey show data for standard salt buffer conditions and white lanes show data for high salt conditions. Each Gaussian fit represents a band in the lane indicated of the corresponding gels shown in figure 8B and 9B. The lack of a third Gaussian indicates no exchange is taking place over the time-course. Gaussian 1 gives the area for Hisα and Gaussian 3 gives the area for α bands on the gel, while Gaussian 2 would correspond to α-Hisα heterodimer, not seen here due to a lack of exchange. As calculated from Figures 3.4.1 - 3.4.3 B.

Time (hours)		24		48		78		330		360	
Lane		1	2	3	4	5	6	1	2	3	4
	Gaussian 1	0.40	0.42	0.40	0.40	0.39	0.46	0.38	0.44	0.41	0.38
Ratio	Gaussian 2	0.00	0.00	0.00	0.00	0.00	0.00	0.00	0.00	0.00	0.00
	Gaussian 3	0.60	0.58	0.60	0.60	0.61	0.54	0.62	0.56	0.59	0.62

Table 3.4.2. **The ratio of the fraction of the total area for each lane for <u>cross-linked</u> samples of Tpm at <u>4℃</u>.** The starting ratio of α:Hisα is 0.6:0.4, which is consistent across the entire time-course experiment, as no exchange is seen to be occurring.

Time (hours)		24		48		78		330		360	
Lane		1	2	3	4	5	6	1	2	3	4
Gaussian 1	amplitude	107.3	102.9	105.6	108.2	112.8	98.9	56.3	78.1	62.5	72.4
	SD	5.1	5.6	5.5	5.6	5.8	5.1	10.9	9.5	9.8	11.3
	area	1361.2	1433.0	1457.4	1504.6	1640.9	1275.9	1511.4	1818.0	1495.4	2002.0
Gaussian 2	amplitude										
	SD										
	area										
Gaussian 3	amplitude	154.3	141.8	155.0	147.1	159.0	139.7	111.7	117.5	116.5	109.6
	SD	5.1	4.9	5.1	4.8	5.4	4.8	8.4	8.8	9.1	8.6
	area	1959.6	1721.6	1995.2	1752.3	2136.4	1669.9	2224.6	2465.6	2362.0	2173.7

Table 3.4.3. **Densitometry analysis for <u>reduced</u> Tpm samples incubated at <u>4 ℃</u> over 360 hours.** Grey lanes are standard salt conditions and white lanes and high salt buffer conditions. After 330 hours, Tpm shows signs of degradation. As calculated from Figures 3.4.1 - 3.4.3 A.

Time (hours)		24		48		78		330		360	
Lane		1	2	3	4	5	6	1	2	3	4
Ratio	Gaussian 1	0.41	0.45	0.42	0.46	0.43	0.43	0.40	0.42	0.39	0.48
	Gaussian 2	0.00	0.00	0.00	0.00	0.00	0.00	0.00	0.00	0.00	0.00
	Gaussian 3	0.59	0.55	0.58	0.54	0.57	0.57	0.60	0.58	0.61	0.52

Table 3.4.4. **Ratio of fraction of total area for each lane for <u>reduced</u> Tpm samples incubated at <u>4 ℃</u> over 360 hours.** The starting ratio of α:Hisα is ~0.6:0.4, which is consistent across the entire time-course experiment, as no exchange is seen to be occurring. Standard salt conditions are shown in grey lanes, and high salt conditions are shown in white lanes.

3.5 At 20 ℃, Tpm homodimers showed no exchange up to 48 hours,

whereas Tpm at 30 ℃ showed exchange after 24 hours

Tpm was incubated at room temperature (20 ℃) and 30 ℃ to observe the stability of the homodimers, as previously performed at 4 ℃. Both performed temperatures were under standard salt conditions, as salt showed no effect previously.

Tpm was stable up to 48 hours at both 20 ℃ and 30 ℃, but by 13 days (312 hours), it showed signs of degradation, as noted by the smearing of the bands, shown in figure 3.5.1 for the reduced samples.
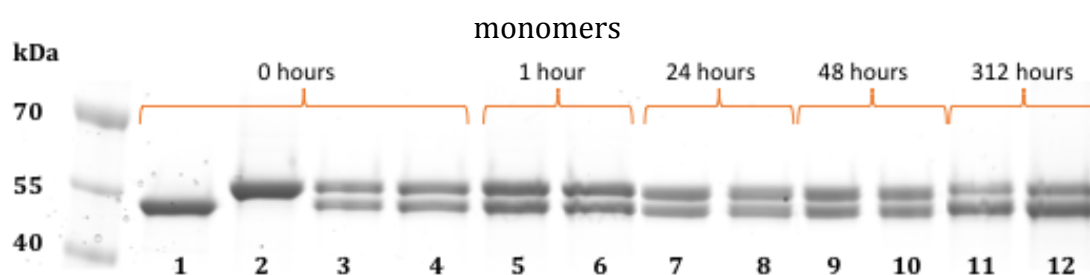
Figure 3.5.1. Reduced samples of Tpm incubated at 20 ℃ and 30 ℃, run under denaturing conditions. Samples are as follows: Prestained PageRuler ™ #26616, 1. α monomer, 2. Hisα monomer, 3. + 4. 20 ℃ and 30 ℃ 0 hours, 5. 20 ℃ 1 hour, 6. 30℃ 1 hour, 7. 20 ℃ 24 hours, 8. 30 ℃ 24 hours, 9. 20 ℃ 48 hours, 10. 30 ℃ 48 hours, 11. 20 ℃ 312 hours (13 days), 12. 30 ℃ 312 hours (13 days)

As at 4 ℃, Tpm incubated at 20 ℃ showed no exchange over the incubation period. The experiment was limited in time, owing to protein sample degradation. After 48 hours, the bands of cross-linked samples began to smear,

figure 3.5.2, lane 9, and after 13 days the sample bands were indistinguishable, lane 11.

Tpm incubated at 30 ℃ showed no exchange after 3 hours of incubation, figure 3.5.2, lane 6. After 24 hours, a small amount of exchange was clearly seen by the appearance of the third band in lane 8. After 48 hours, lane 10, the protein had degraded too much to analyse and by 13 days the bands were completely indistinct, lane 12.
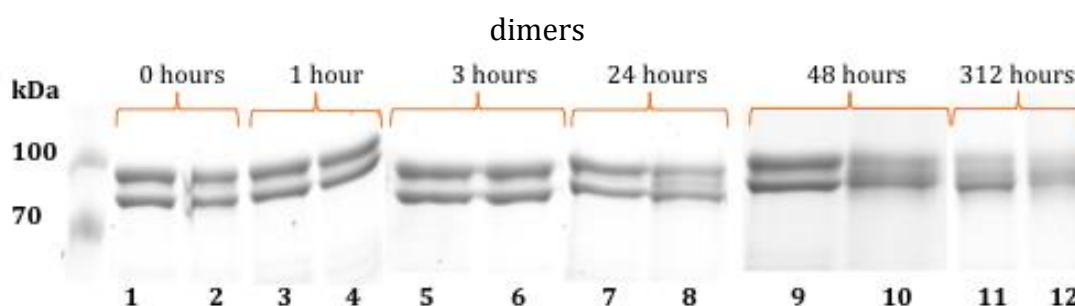
Figure 3.5.2. Samples at 20℃ and 30 ℃ incubated in standard salt, cross-linked, under non-denaturing conditions. Samples are as follows: Prestained PageRuler ™ #26616, 1. 20 ℃ 0 hours, 2. 30 ℃ 0 hours, 3. 20 ℃ 1 hour, 4. 30 ℃ 1 hour, 5. 20 ℃ 3 hours, 6. 30 ℃ 3 hours, 7. 20 ℃ 24 hours, 8. 30 ℃ 24 hours, 9. 20 ℃ 48 hours, 10. 30 ℃ 48 hours, 11. 20 ℃ 312 hours (13 days), 12. 30 ℃ 312 hours (13 days).

Over 24 hours, Tpm incubated at 20 ℃ showed no exchange, as indicated by the lack of a band that was fitted to Gaussian 2, table 3.5.4. The protein showed signs of degradation by the decline in the amplitude and area under the curve over time. After 48 hours incubation, the protein had significantly degraded, leading to the bands smearing. This smearing resulted in an increased area under the curve in regards to the total area analysed by densitometry, as the bands became less defined and more smeared over the total area, table 3.5.3.

The appearance of a heterodimer at 30℃ band was quantified via densitometry analysis, shown in table 3.5.3. The starting ratio of homodimers was ~0.5 : 0.5. After 24 hours incubation at 30 ℃, a third band (peak 2) appeared, shifting the ratio to 0.42 : 0.16 : 0.42 (α homo : α-Hisα : Hisα homo). The appearance of a third band resulted in a decrease in amplitude and area, and thus ratio, of each homodimer (Gaussian 1 and 3). These values decreased equally due to the formation of the heterodimer, which accounted for 16 % of the total protein dimer content after 24 hours, table 3.5.4.

After 48 hours incubation, the protein was significantly degraded, leading to smearing of the gel bands, rendering them impossible to analyse. For both 20 ℃ and 30 ℃, samples at 13 days post incubation were completely degraded and impossible to analyse.

It is interesting to note the difference in degradation between the reduced samples and the cross-linked samples, shown clearly in table 3.5.1 and 3.5.3. The cross-linked samples appeared to degrade at a faster rate and smear more on gels. This indicated that the cross-linking process was damaging the integrity of the protein.

Time (hours)		0		1		24		48		336	
Lane		3	4	5	6	7	8	9	10	11	12
Gaussian 1	amplitude	112.5	110.5	149.2	137.5	119.8	102.2	130.3	117.9	86.3	112.5
	SD	6.9	4.9	6.8	6.0	9.0	9.4	9.7	9.4	6.4	6.9
	area	1940.0	1358.3	2541.2	2053.4	2687.8	2393.3	3182.2	2774.2	1375.8	1940.0
Gaussian 2	amplitude										
	SD										
	area										
Gaussian 3	amplitude	154.1	87.9	147.2	138.0	114.0	99.2	128.7	120.7	139.4	154.1
	SD	6.8	6.9	5.1	4.6	6.4	7.0	6.9	7.3	6.0	6.8
	area	2551.6	1486.3	1881.5	1583.3	1820.5	1714.1	2239.6	2204.3	2098.8	2551.6

Table 3.5.1. **Densitometry analysis of <u>reduced</u> Tpm samples incubated at <u>20 ℃</u> and <u>30 ℃</u> in standard salt conditions over 336 hours**. 20℃ data in shown in the grey lanes, and 30 ℃ data is shown in the white lanes. By 48 hours, the protein shows degradation. As calculated from Figure 3.5.1.

Time (hours)		0		1		24		48		336	
Lane		3	4	5	6	7	8	9	10	11	12
	Gaussian 1	0.43	0.48	0.40	0.56	0.60	0.58	0.59	0.56	0.40	0.43
Ratio	Gaussian 2	0.00	0.00	0.00	0.00	0.00	0.00	0.00	0.00	0.00	0.00
	Gaussian 3	0.57	0.52	0.60	0.44	0.40	0.42	0.41	0.44	0.60	0.57

Table 3.5.2. **Ratio of fraction of total areas for each lane for <u>reduced</u> Tpm at <u>20 ℃</u> and <u>30 ℃</u>.** Starting ratio of α: Hisα homodimers is ~ 0.5:0.5, as shown by the ratio Gaussian 1:Gaussian 3. Grey columns indicate samples at 20 ℃ and white columns show data for 30 ℃.

Time (hours)		0		1		3		24		48	
Lane		1	2	3	4	5	6	7	8	9	10
Gaussian 1	Amplitude	100.8	77.6	100.0	95.4	102.4	91.5	84.7	50.5	105.8	46.1
	SD	7.7	7.7	7.9	7.8	7.2	7.2	6.7	6.4	11.6	13.1
	Area	1944.6	1502.4	1987.3	1871.8	1855.4	1643.5	1423.2	813.6	3061.9	1504.6
Gaussian 2	Amplitude								30.2		2.0
	SD								4.1		5.9
	Area								308.9		29.6
Gaussian 3	Amplitude	109.5	85.0	111.2	105.9	110.3	100.1	86.7	68.0	122.7	79.5
	SD	5.6	5.8	5.5	5.3	5.1	4.8	4.7	4.7	6.6	15.2
	Area	1544.7	1230.4	1519.6	1394.6	1399.7	1211.3	1030.5	801.9	2019.6	2991.8

Table 3.5.3. **Densitometry analysis of gel bands for <u>cross-linked</u> Tpm incubated at <u>20 ℃</u> and <u>30 ℃</u> over 48 hours**. Each Gaussian fit represents a band on the gel as shown in figure 9. Lanes in grey show data for Tpm at 20 ℃ and white lanes show data for 30 ℃ incubation. Heterodimer formation is indicated by the formation of a central band, fitted to Gaussian 2. Tpm shows no exchange at 20 ℃ up to 24 hours incubation. At 48 hours, the protein shows degradation at 20 ℃. Tpm shows no exchange at 30 ℃ up to 3 hours incubation. By 24 hours, some exchange is noted by the appearance of the third Gaussian. After 48 hours, the protein is highly degraded and unfeasible to analyse. As calculated from figure 3.5.2.

Time (hours)		0		1		4		24	
Lane		1	2	3	4	5	6	7	8
	Gaussian 1	0.56	0.55	0.57	0.57	0.57	0.58	0.58	0.42
Ratio	Gaussian 2	0.00	0.00	0.00	0.00	0.00	0.00	0.00	0.16
	Gaussian 3	0.44	0.45	0.43	0.43	0.43	0.42	0.42	0.42

Table 3.5.4. **Ratio of fraction of total areas for each lane for <u>cross-linked</u> Tpm incubated at <u>20 ℃</u> and <u>30 ℃</u> over 24 hours**. Starting ratio of α: Hisα homodimer is ~ 0.5:0.5, as shown by the ratio Gaussian 1:Gaussian 3. Grey columns indicate samples at 20 ℃ and white columns show data for 30 ℃. Tpm incubated at 20 ℃ shows no sign of exchange over 48 hours. At 30℃, exchange was seen after 24 hours incubation. After 48 hours incubation, samples were too degraded to analyse, as shown by the dramatic increase in the ratios.

3.6 Tpm homodimers incubated at 37 ℃ showed signs of exchange after 1 hour

As some exchange was seen at 30 ℃ after 24 hours incubation, it was expected that greater exchange would be seen at 37 ℃. As a result of this, the effect of salt on exchange and stability was explored again. Incubations were performed as per 4℃, in standard salt (100 mM KCl) and high salt (500 mM KCl) buffers. Tpm homodimers incubated at 37 ℃ showed monomer exchange after 1 hour incubation, which increased further by 24 hours, as shown in figure 3.6.2.

Tpm was stable up to 24 hours incubation at 37 ℃, showing no signs of degradation on the gel, figure 3.6.1, for either standard salt or high salt.
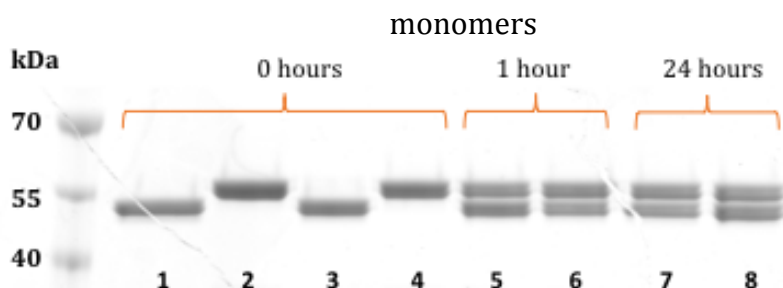
Figure 3.6.1. Reduced samples of Tpm incubated at 37 ℃ over 24 hours. Samples are as follows: Prestained PageRuler ™ #26616 1. 0 hours αα standard salt, 2. 0 hours Hisα homodimer standard salt, 3. 0 hours α homodimer high salt, 4. 0 hours Hisα homodimer high salt, 5. 1 hour α + Hisα standard salt, 6. 1 hour α + Hisα high salt, 7. 24 hours α + Hisα standard salt, 8. 24 hours α + Hisα high salt.

Tpm homodimers incubated at 37 ℃ showed clear signs of exchange after 4 hours incubation in both standard salt and high salt conditions. However, in high salt, Tpm homodimers showed some exchange after just 1 hour. After 24 hours

incubation, both salt conditions showed similar amounts of exchange and heterodimer formation, figure 3.6.2.
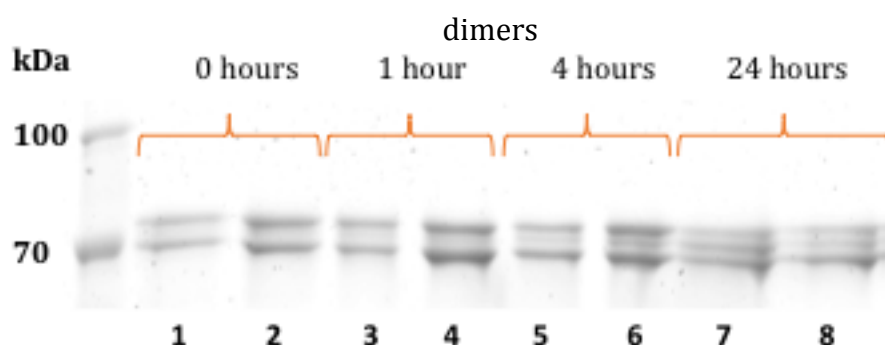
Figure 3.6.2. Exchange between α and Hisα Tpm homodimers at 37 ℃ under standard salt and high salt buffer conditions, 100 mM KCl and 500 mM KCl, respectively. Samples are as follows: Prestained PageRuler ™ #26616, 1. 0 hours standard salt, 2. 0 hours high salt, 3. 1 hour standard salt, 4. 1 hour high salt, 5. 4 hours standard salt, 6. 4 hours high salt, 7. 24 hours standard salt, 8. 24 hours high salt.

The rate of exchange appeared to be a slightly higher in high salt conditions within the first 4 hours of incubation, but by 24 hours, the standard salt and high salt conditions showed similar amounts of exchange.

Densitometry analysis of this gel was performed as before, and the areas of the bands were fitted to Gaussian curves, and the ratio of exchange was calculated, tables 3.6.1 and 3.6.2.

The starting ratio of homodimers was ∼ 0.5:0.5. After 1 hour incubation at 37 ℃ in high salt conditions, the ratio shifted to 0.42:0.05:0.5 (homo:hetero:homo), indicating the appearance of a heterodimer. However, as explained previously, the area and amplitude of the homodimer peaks would decrease equally to account for the heterodimer formation, but that was not seen here. This is largely down to an increase in loading of this sample, which increased the values. This

highlighted the importance of calculating band densities as a fraction of the total band area, not just comparing the raw data values. While this may explain the unexpected increased in amplitude and areas of peaks 1 and 2, the ratio of homodimer bands did not decrease equally, leading to some doubt over the appearance of this third band.

While the area of Gaussian 2 did not increase for each time point, owing to loading differences, the ratio of dimers did change significantly forming a 0.39:0.23:0.38 ratio after 24 hours at 30 ℃ in high salt conditions.

Exchange of Tpm was also seen under standard salt conditions, after 4 hours incubation at 37 ℃, wherein the Tpm shifted from a ∼ 0.5:0.5 ratio of α:Hisα to 0.38:0.15:0.48. After 24 hours incubation, the ratio of dimers has exchanged to 0.4:0.3:0.3. Exchange in standard salt buffer begun later than at high salt, however, the exchange to form a heterodimer is greater after 24 hours than at high salt. After 48 hours incubation, the samples at high and standard salt were too degraded to analyse.

Tpm degradation did not show any salt dependence over 24 hours. Very little change in amplitudes and areas were seen for both standard and high salt buffers, indicating that salt had little effect on the stability of the dimer over 24 hours at 37 ℃, tables 3.6.3 and 3.6.4.

Time (hours)		0		1		4		24	
Lane		1	2	3	4	5	6	7	8
Gaussian 1	Amplitude	37.0	61.9	42.4	87.9	62.1	54.7	47.0	57.1
	SD	5.5	6.3	6.0	6.5	5.0	4.7	12.6	7.0
	Area	506.4	975.3	634.0	1440.6	775.3	647.6	1364.2	998.1
Gaussian 2	Amplitude				25.2	28.8	27.1	47.7	41.7
	SD				4.2	4.2	3.2	8.6	5.6
	Area				265.4	300.7	214.6	1022.3	581.3
Gaussian 3	Amplitude	42.3	70.0	46.5	93.9	63.6	57.2	56.9	62.3
	SD	5.1	5.1	5.5	7.3	6.1	4.1	8.0	6.6
	Area	541.3	901.5	629.7	1687.3	977.1	584.2	1047.2	966.9

Table 3.6.1. **Densitometry analysis of gel bands for <u>cross-linked</u> Tpm incubated at <u>37℃</u> over 24 hours.** Each Gaussian fit represents a band on the gel as shown in figure 3.6.2. Lanes in grey show data for standard salt (100 mM KCl) and white lanes show data for high salt (500 mM KCl). Heterodimer formation is indicated by the formation of a central band, fitted to Gaussian 2. Tpm shows exchange after 1 hour incubation at high salt, and 3 hours incubation at standard salt. Protein shows minimal degradation over 24 hours for both standard salt and high salt. As calculated from Figure 3.6.2.

Time (hours)		0		1		4		24	
Lane		1	2	3	4	5	6	7	8
Ratio	Gaussian 1	0.48	0.52	0.50	0.42	0.38	0.45	0.40	0.39
	Gaussian 2	0.00	0.00	0.00	0.08	0.15	0.15	0.30	0.23
	Gaussian 3	0.52	0.48	0.50	0.50	0.48	0.40	0.30	0.38

Table 3.6.2. **Ratio of fraction of total areas for each lane for <u>cross-linked</u> Tpm incubated at <u>37℃</u> over 24 hours**. Starting ratio of α: Hisα is 0.5 : 0.5, as shown by the ratio of Gaussian 1:Gaussian 2. Columns in grey indicate standard salt conditions, while white columns show the data for high salt conditions. Exchange is first seen at high salt after 1 hour incubation and 4 hours after incubation at standard salt. After 24 hours, the amount of exchange to form heterodimers is similar for standard and high salt conditions.

Time (hours)	0		0		1		24	
Lane	1	2	3	4	5	6	7	8
Gaussian 1 Amplitude	125.3		135.8		109.0	102.7	109.5	106.4
SD	6.9		6.7		8.0	7.3	7.6	8.0
Area	2170.6		2239.9		2153.0	1865.6	2074.1	2123.8
Gaussian 2 Amplitude								
SD								
Area								
Gaussian 3 Amplitude		160.6		147.1	106.5	105.5	97.9	114.6
SD		7.7		6.9	5.2	5.5	5.3	5.7
Area		3069.0		2558.9	1383.7	1432.6	1286.3	1639.2

Table 3.6.3. **Densitometry analysis of gel bands for <u>reduced</u> Tpm samples incubated at <u>37 ℃</u> over 24 hours.** Lanes in grey show data for standard salt (100 mM KCl) and white lanes show data for high salt (500 mM KCl). The absence of a peak fit to Gaussian 2 indicates no exchange is taking place. Protein shows minimal degradation over 24 hours for both salt conditions. As calculated from Figure 3.6.1.

Time (hours)	0		0		1		24	
Lane	1	2	3	4	3	4	7	8
Ratio Gaussian 1	1.00	0.00	1.00	0.00	0.61	0.57	0.62	0.56
Gaussian 2	0.00	0.00	0.00	0.00	0.00	0.00	0.00	0.00
Gaussian 3	0.00	1.00	0.00	1.00	0.39	0.43	0.38	0.44

Table 3.6.4. **Ratio of fraction of total area for each lane, for <u>reduced</u> Tpm incubated at <u>37 ℃</u>.** Starting ratio at time 0 could not be compared as samples were loaded separately, however the ration of α : Hisα at 1 hour is ~ 0.6 : 0.4 for both standard salt and high salt conditions. After 24 hours, the ratio between dimers still ~ 0.6 : 0.4 for both salt conditions.

3.7 Reverse exchange of heterodimer showed minimal exchange after 24 hours

Tpm homodimers exchanged to form heterodimers after just 1 hour incubation at 37 ℃, so this raised the question as to how the heterodimer behaves in the reverse exchange. As our data showed Tpm did not exchange at 4 ℃, we were sure that the starting material of purified heterodimer would remain stable and pure, thus removing the need for cross-linking. Given that salt previously showed no effect on exchange at 4 ℃ and 37 ℃, Tpm α-Hisα heterodimers were incubated as previously, in standard salt conditions at 20 ℃ and 37 ℃. Heterodimers were made and purified as previously described by Janco et al, 2012.

The main difference for heterodimer incubations is that samples are not incubated in the presence of DTT, otherwise the heterodimer would be reduced (not an issue in monomer solutions). The down side to removing this is that the protein was more susceptible to degradation.

Tpm heterodimers were stable up to 24 hours, showing small amounts of degradation on the gel at 20 ℃ and 37 ℃, figure 3.7.1.
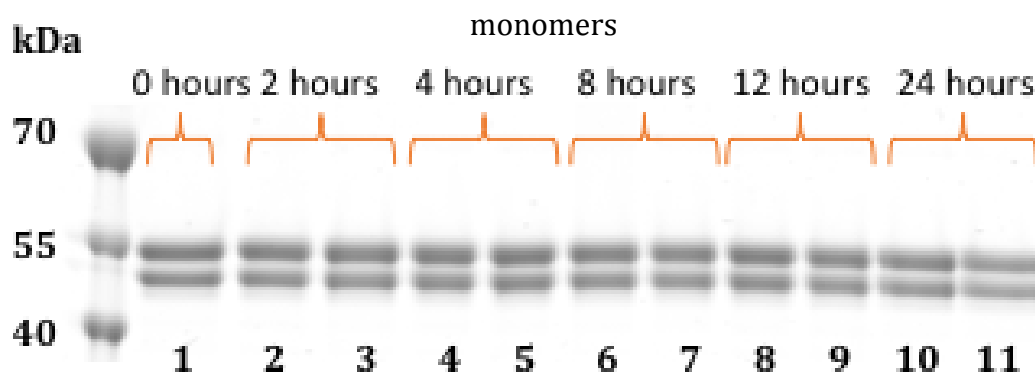
Figure 3.7.1. Reduced α-Hisα heterodimer Tpm in standard salt buffer (100 mM KCl) at 20 ℃ and 37 ℃ run under denaturing conditions. Samples are as follows: Prestained PageRuler ™ #26616, 1. 20/37 ℃ 0 hours, 2. 20 ℃ 2 hours, 3. 37 ℃ 2 hours, 4. 20 ℃ 4 hours, 5. 37 ℃4 hours, 6. 20 ℃ 8 hours, 7. 37 ℃ 8 hours, 8. 20 ℃ 12 hours, 9. 37 ℃ 12 hours, 10. 20 ℃ 24 hours, 11. 37 ℃ 24 hours.

Heterodimers incubated at 20 ℃ and 37 ℃ showed minimal amounts of exchange over 24 hours, figure 3.7.2. The starting sample unfortunately was not a pure heterodimer, so this was taken into account when analysing the gels.
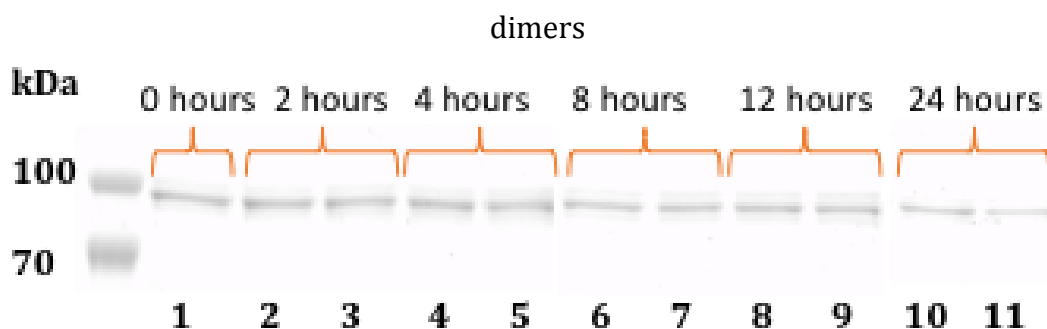
Figure 3.7.2. Heterodimer samples incubated at 20 ℃ and 37 ℃ in standard salt buffer, cross-linked, under non-denaturing conditions. Samples are as follows: Prestained PageRuler ™ #26616, 1. 20/37 ℃ 0 hours, 2. 20 ℃ 2 hours, 3. 37 ℃ 2 hours, 4. 20 ℃ 4 hours, 5. 37 ℃4 hours, 6. 20 ℃ 8 hours, 7. 37 ℃ 8 hours, 8. 20 ℃ 12 hours, 9. 37 ℃ 12 hours, 10. 20 ℃ 24 hours, 11. 37 ℃ 24 hours.

The rate of exchange from heterodimer to form homodimers appeared to be very small over the entire time course for both 20 ℃ and 37 ℃ in standard salt buffer. Samples after 24 hours incubation showed sign of degradation, as the bands were less intense. Densitometry analysis of the gel was performed as previously, to calculate band densities and ergo, ratio of exchange, tables 3.7.1 and 3.7.2.

Unfortunately, the heterodimer was not a pure sample to start the experiment and the ratio of α homo:α-Hisα:Hisα homo was 0.08:0.79:0.13. After 12 hours incubation, the ratio was 0.11:0.74:0.15 for both 20 ℃ and 37 ℃, which was only a 5% decrease in heterodimer ratio from the start. After 24 hours at both temperatures, the ratio increased of heterodimer, but this could be due to degradation affecting the intensity of already faint homodimer bands.

As seen previously for homodimers exchanging at 37 ℃, dimers did not exchange at 20 ℃. Therefore, what we were seeing as a small change in the ratio of densities was potentially just a human error, either loading and running of the gel, or when scanning and analysing the gel, not real exchange. Also, owing to the starting material not being a pure heterodimer, it is possible that small number of homodimers were forming heterodimers, while heterodimers are reverse exchanging at the same rate. However, the total amount of this exchange was 8% given the rate limiting factor in this scenario was the α homodimer.

Over 12 hours the band area for the heterodimer decreased for 20 ℃ and 37 ℃. There were small increases in band densities for Hisα homodimers at both

temperatures, but interestingly a decrease in densities for the α homodimers. The amplitude of heterodimer bands decreased over 12 hours, while homodimer peaks increased a small amount, owing to small amounts of exchange.

After 24 hours incubation, the band area and amplitudes for homo and heterodimer decreased drastically. The ratio of band densities decreased for homodimers and increased for heterodimers to 0.04:0.92:0.04 at 20 ℃ and 0.05:0.87:0.08 at 37 ℃. This apparent exchange to form heterodimers was most likely due to protein degradation and as the number of homodimers was so small to begin with, any degradation drastically impacts the densitometry analysis.

Time (hours)	0	2		4		8		12		24	
Lane	1	2	3	4	5	6	7	8	9	10	11
HisαHisα **Amplitude**	4.4	4.8	4.4	5.1	5.9	4.2	6.6	5.4	6.3	2.3	3.0
SD	6.3	6.2	5.7	6.0	5.8	5.2	4.9	5.4	4.3	1.5	2.0
Area	68.7	74.4	60.9	75.6	85.2	54.3	81.2	73.2	68.1	8.5	14.8
α-Hisα **Amplitude**	38.8	40.8	34.0	39.1	33.2	30.8	33.9	34.5	31.3	29.8	31.3
SD	4.3	4.4	4.1	4.4	4.3	4.0	4.1	4.2	4.2	3.0	3.2
Area	418.3	450.4	348.8	432.3	359.2	309.0	351.9	366.5	331.9	223.3	247.7
αα **Amplitude**	5.3	7.3	6.2	8.5	7.0	4.1	6.1	6.3	6.2	2.8	3.9
SD	3.0	3.8	4.0	4.3	5.0	3.4	3.2	3.5	3.3	1.6	2.2
Area	39.6	69.9	61.8	90.8	87.9	35.5	49.0	55.2	50.5	10.8	21.9

Table 3.7.1. **Densitometry analysis of gel bands for <u>cross-linked</u> α-Hisα Tpm heterodimer incubated at <u>20 ℃</u> (grey column) and <u>37 ℃</u> (white column) over 24 hours in standard salt buffer (100 mM KCl).** Homodimer formation is indicated by the formation and increase in band density for α or Hisα homodimers and a decrease in band density for the heterodimer α-Hisα. After 12 hours incubation at both temperatures, minimal exchange is seen. After 24 hours incubation, samples at both temperatures show signs of degradation. As calculated from figure 3.7.2.

Time (hours)	0	2		4		8		12		24	
Lane	1	2	3	4	5	6	7	8	9	10	11
HisαHisα	0.13	0.13	0.13	0.13	0.16	0.14	0.17	0.15	0.15	0.04	0.05
Ratio **α-Hisα**	0.79	0.76	0.74	0.72	0.67	0.77	0.73	0.74	0.74	0.92	0.87
αα	0.08	0.12	0.13	0.15	0.17	0.09	0.10	0.11	0.11	0.04	0.08

Table 3.7.2**. Ratio of fraction of total areas for each lane for <u>cross-linked</u> samples at <u>20 ℃</u> and <u>37 ℃</u>.** The starting ratio is not a pure heterodimer, at 0.13:0.79:0.08 (homo:het:homo). Column in grey show samples at 20 ℃ and white columns indicate samples incubated at 37 ℃. Minimal exchange is seen after 12 hours incubation at both temperatures. After 24 hours, the samples show signs of degradation, which affects the ratio calculated.

3.8 Reverse exchange of mutant heterodimer E54K-Hisα showed no

exchange over 11 hours at 4 ℃, 20 ℃, 30℃ and 37 ℃

Low level expression of mutant Tpm isoforms, such as DCM mutant E54K, are likely to form heterodimers over homodimers assuming there is no preferential assembly and it follows random assembly. The behaviour of the heterodimer relative to homodimers is of importance to heterozygous affected individuals.

A reverse exchange was performed, starting with an E54K-Hisα Tpm heterodimer, which was incubated at 4 ℃, 20 ℃, 30 ℃ and 37 ℃. Samples were then taken over a time course, as before, to see whether or not exchange takes place to form homodimers.

No exchange was seen for any of the samples across the temperature range. Even samples at 37 ℃, which showed extensive exchange from α and Hisα homodimers to form heterodimers previously after just 4 hours, showed no exchange up to 11 hours of incubation, shown in figure 3.8.1 lane 16.
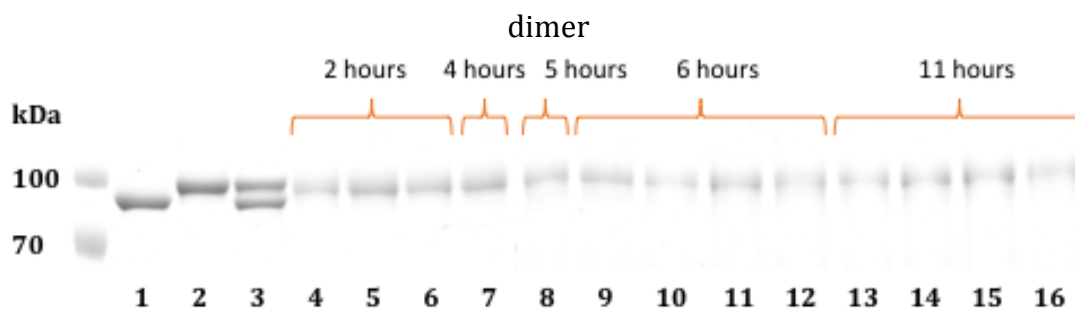
dimer

Figure 3.8.1. Cross-linked E54K-Hisα Tpm samples incubated at 100 mM KCl run on a 7.5 % SDS polyacrylamide gel, under non-reducing conditions (- BME). Samples are as follows: Prestained PageRuler ™ #26616, 1. α homodimer, 2. Hisα homodimer, 3. α + Hisα in 1:1 ratio, 4. 20 ℃ 2 hours, 5. 30 ℃ 2 hours, 6. 37 ℃ 2 hours, 7. 37 ℃ 4 hours, 8. 37 ℃ 5 hours, 9. 4 ℃ 6 hours, 10. 20 ℃ 6 hours, 11. 30 ℃ 6 hours, 12. 37 ℃ 6 hours, 13. 4 ℃ 11 hours, 14. 20 ℃ 11 hours, 15. 30 ℃ 11 hours, 16. 37 ℃ 11 hours.

The cross-linked E54K-Hisα heterodimer, figure 3.8.1, lanes 4 – 16, runs between α and Hisα homodimers, lanes 1 – 3. Over 11 hours incubation, the heterodimer band did not change significantly for all incubation temperatures, indicating exchange was not occurring, but did show increased blurring of the bands, indicating protein degradation. After 24 hours incubation, cross-linked samples were too degraded to analyse across the entire temperature range, shown in figure 3.8.2.

dimer
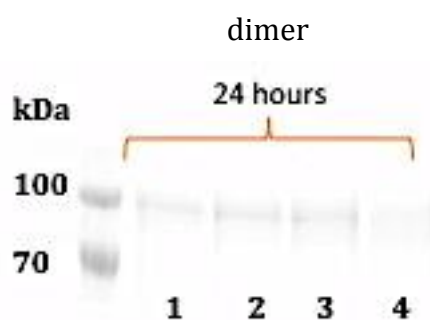
Figure 3.8.2. Cross-linked E54K-Hisα Tpm samples incubated at 100 mM KCl for 24 hours, run on a 7.5 % SDS polyacrylamide gel, under non-reducing conditions (- BME). Samples are as follows: Prestained PageRuler ™ #26616, 1. 4℃, 2. 20 ℃, 3. 30 ℃, 4. 37 ℃.

While the protein degradation was visible on the cross-linked gels, the reduced counterpart gels up to 11 hours incubation did not reflect protein degradation as previously described, figure 3.8.3. Two distinct homodimer bands were seen on the gel, with no obvious smearing or reduction of intensity, a striking difference between the cross-linked and reduced proteins. This indicated that protein degradation was accelerated after cross-linking.

Densitometry analysis of gels in figures 3.8.1 and 3.8.2 showed no appearance of homodimer band densities, just a single heterodimer band fitted to Gaussian 2, tables 3.8.1 and 3.8.2.
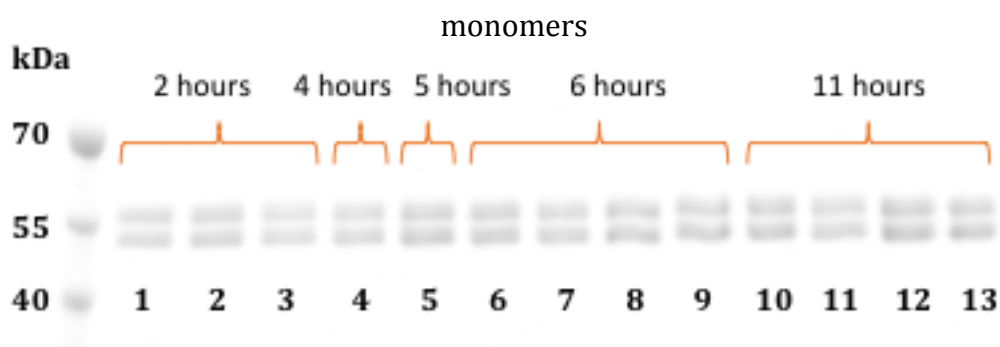
Figure 3.8.3. Reduced samples of Tpm mutant E54K-Hisα incubated at 4 ℃, 20 ℃, 30 ℃ and 37 ℃ in standard salt buffer. Samples are as follows: Prestained PageRuler ™ #26616, 1. 20 ℃ 2 hours, 2. 30 ℃ 2 hours, 3. 37 ℃ 2 hours, 4. 37 ℃ 4 hours, 5. 37 ℃ 5 hours, 6. 4 ℃ 6 hours, 7. 20 ℃ 6 hours, 8. 30 ℃ 6 hours, 9. 37 ℃ 6 hours, 10. 4 ℃ 11 hours, 11. 20 ℃ 11 hours, 12. 30 ℃ 11 hours, 13. 37 ℃ 11 hours.

The cross-linked protein showed signs of degradation over the time course, as the band intensity decreased and the bands became less distinct. After 24 hours incubation in standard salt buffer, Tpm incubated over all the temperature ranges from 4 ℃ to 37 ℃ showed too much degradation to be analysed. Degradation was most notably quantified by looking at the decrease in peak amplitude and increase in area across the time course, table 3.8.1. This

degradation may mean that homodimer formation could not be seen. The monomer gel however, did not reflect the E54K-Hisα protein degradation in the same manner up to 11 hour incubation. Densitometry analysis did not show a decrease in amplitude or increase in area over the time course, table 3.8.3.

It may be the case that the cross-linking process was too harsh for the mutant heterodimer, thus leading to degradation before loading on the gel. This appeared amplified with older, less stable samples, most notably if you look at the changes in the 37 ℃ incubations. Potassium ferricyanide was used, as a means of increasing the solutions redox potential, ($E^{\circ\prime} \sim 436$ mV at pH 7) (Dehnicke 1976, Pandurangachar, Kumara Swamy et al. 2010). Alternative cross-linking solutions might be sought, to reduce the protein degradation.

If reverse exchange of heterodimers was significantly slower than homodimer exchange, potentially, the experiment needed to be run for a longer time-course to detect homodimer formation, however due to degradation, this was not possible. Higher salt conditions could be explored to see if these increased the stability and/or exchange of the dimers. However, previous work in this chapter indicates this potentially will not have any effect, as no salt effect was seen at 4 ℃ or 37 ℃ for homodimer exchange. Data from chapter 4 on the other hand shows a significant salt effect for increasing thermal stability. This indicated that a change in thermal stability does not correlate with a change in exchange rate. Therefore, other chemicals, such as Tris(2-carboxyethyl)phosphine (TCEP) or protease inhibitors, need to be explored that will protect the protein from degradation without affecting the integrity of the heterodimer.

Data from thermal melting experiments using the E54K-α heterodimer, chapter 4, showed thermal destabilisation at temperatures above 50 ℃. At 37 ℃, however, the protein is not significantly less stable than the α WT homodimer under the same conditions. The E54K-Hisα heterodimer on the other hand, showed significant destabilisation at temperatures below 37℃, when compared to the α WT homodimer. This data provides insight into the reduced stability of the protein during the dimer exchange experiment and cross-linking process. This once again highlights the important effects that the addition of a His-tag can make on a protein.

Time (hours)		0			2			4	5	6				11			
Lane		1	2	3	4	5	6	7	8	9	10	11	12	13	14	15	16
Gaussian 1	amplitude	93.55		63.38													
	SD	16.37		17.25													
	area	4614.78		2733.06													
Gaussian 2	amplitude				24.44	40.80	28.87	39.14	31.59	25.70	20.81	15.19	10.49	10.17	8.60	12.45	16.23
	SD				22.05	25.80	23.98	26.44	23.94	20.75	21.43	18.82	22.03	16.40	15.07	18.22	24.77
	area				1348.19	2616.56	1720.35	2492.00	1895.67	1336.38	1117.31	716.62	579.00	418.30	324.94	568.46	1007.80
Gaussian 3	amplitude		93.43	76.17													
	SD		17.89	12.93													
	area		4974.94	2440.92													

Table 3.8.1. **Densitometry analysis for <u>cross-linked</u> E54K-Hisα Tpm samples incubated at <u>4 ℃</u> (white column), <u>20 ℃</u> (yellow column), <u>30 ℃</u> (blue column) and <u>37 ℃</u> (grey column).** The heterodimer showed no reverse exchange to form homodimers, by the lack of appearance of Gaussian 1 and 3. Lane 1 is α Tpm homodimer, lane 2 is Hisα Tpm homodimer and lane 3 is α-Hisα Tpm heterodimer. As calculated from figure 3.8.1.

Time (hours)		0			2			4	5	6				11			
Lane		1	2	3	4	5	6	7	8	9	10	11	12	13	14	15	16
Ratio	Gaussian 1	1.00	0.00	0.53	0.00	0.00	0.00	0.00	0.00	0.00	0.00	0.00	0.00	0.00	0.00	0.00	0.00
	Gaussian 2	0.00	0.00	0.00	1.00	1.00	1.00	1.00	1.00	1.00	1.00	1.00	1.00	1.00	1.00	1.00	1.00
	Gaussian 3	0.00	1.00	0.47	0.00	0.00	0.00	0.00	0.00	0.00	0.00	0.00	0.00	0.00	0.00	0.00	0.00

Table 3.8.2. **Ratio of fraction of total area for each lane for <u>cross-linked</u> samples of E54K-Hisα Tpm heterodimer.** Samples were incubated at 4 ℃ (white column), 20 ℃ (yellow column), 30 ℃ (blue column) and 37 ℃ (grey column). The heterodimer showed no detectable reverse exchange to form homodimers, by the lack of densities fitted to Gaussians 1 and 3.

Time (hours)	2			4	5	6				11			
Lane	1	2	3	4	5	6	7	8	9	10	11	12	13
Gaussian 1 amplitude	28.42	29.22	19.79	24.29	33.06	34.03	29.86	27.93	34.00	37.43	26.87	36.21	32.21
SD	11.13	12.55	12.69	11.85	13.11	12.94	12.12	12.67	12.45	13.26	13.54	13.56	12.77
area	792.75	918.55	628.83	721.03	1084.18	1102.38	905.09	886.96	1060.80	1243.53	911.15	1228.22	1030.40
Gaussian 2 amplitude													
SD													
area													
Gaussian 3 amplitude	30.98	34.75	25.59	30.81	41.95	41.14	35.97	35.43	42.57	45.93	33.73	46.29	42.45
SD	10.21	10.30	10.08	10.11	10.48	10.57	10.51	10.75	10.79	10.48	10.79	10.83	10.41
area	792.93	895.76	646.05	780.26	1101.33	1081.46	937.15	952.55	1148.46	1206.22	912.33	1245.42	1102.90

Table 3.8.3. **Densitometry analysis for <u>reduced</u> samples of E54K-Hisα Tpm mutant over 11 hours at <u>4 ℃</u> (white lane), <u>20 ℃</u> (yellow lane), <u>30 ℃</u> (blue lane) and <u>37 ℃</u> (grey lane).** The amplitude, area and peak width (SD) did not show significant changes over the time course for all temperatures explored. As calculated from figure 3.8.3.

Time (hours)	2			4	5	6				11			
Lane	1	2	3	4	5	6	7	8	9	10	11	12	13
Ratio Gaussian 1	0.50	0.51	0.49	0.48	0.50	0.50	0.49	0.48	0.48	0.51	0.50	0.50	0.48
Gaussian 2	0.00	0.00	0.00	0.00	0.00	0.00	0.00	0.00	0.00	0.00	0.00	0.00	0.00
Gaussian 3	0.50	0.49	0.51	0.52	0.50	0.50	0.51	0.52	0.52	0.49	0.50	0.50	0.52

Table 3.8.4. **Ratio of fraction of total band area for each lane, for <u>reduced</u> E54K-Hisα Tpm over 11 hours.** The starting ratio of monomers is ~ 0.5 : 0.5 and stays constant throughout the incubation across all temperature ranges. Samples were incubated at 4 ℃ (white column), 20 ℃ (yellow column), 30 ℃ (blue column) and 37 ℃ (grey column).

3.9 Exchange of Tpm dimers occurs on actin at 20 ℃ and 37 ℃

As shown in this chapter, Tpm monomers exchanged freely in solution at 37 ℃ and showed some monomer exchange at lower temperatures. Once bound to the actin filament, it is assumed that the rate of exchange will decrease, owing Tpm+actin interactions. Previous experiments have shown a 3 ℃ stabilisation of the C-terminus of Tpm when bound to actin (Kremneva, Boussouf et al. 2004).

Following on from our monomer exchange, exchange of Tpm dimers was explored in the presence of actin using cosedimentation assays. Tropomyosin exchange occurs not only as homo and heterodimers in solution, but while bound to the actin filament too. To explore the exchange of dimers on actin, tropomyosin homodimers were pre incubated and bound to actin, before adding tagged homodimers (for ease of visualisation on SDS gels as previously performed) in excess, to study the exchange of the Tpm dimers on the filament.

Actin was pre incubated with α Tpm homodimers for 1 hour at room temperature, before centrifugation at 100,000 rpm for 20 minutes at 4 ℃ to remove the unbound Tpm in the supernatant. The actin+αTpm pellet was resuspended and a 10 times molar excess of Hisα Tpm homodimers were added. The solution was then incubated at 20 ℃ and 37 ℃ and samples were taken, centrifuged to separate Tpm bound to actin in the pellet and free Tpm in the supernatant, and run on 7 – 12 % Precast gels under non-reducing conditions. The Hisα homodimers were chemically cross-linked at the start of the

experiment to enable clear visualisation as the Hisα monomers ran at a similar position to the actin on the gel. This also ensured that any exchange seen was of Tpm homodimers and took away the element of monomer exchange in dimers.

Due to the cross-linking of the Hisα Tpm, samples were not incubated in the presence of DTT, and therefore the protein was susceptible to degradation and oxidation. At 37 ℃ it is clear that the α Tpm was oxidised after just 2 hours, showing a cross-linked band on the gel, figure 3.9.1 lane 11. On the other hand, at 20 ℃ over 24 hours, α Tpm did not show signs of oxidation, figure 3.9.1 lanes 3 – 10.

At 20 ℃ there appeared to be a small amount of exchange taking place, with Hisα Tpm binding to actin and increasing band density in the pellet and α Tpm detaching from actin with a decreasing band density in the pellet. Samples incubated at 37 ℃ are more difficult to analyse, given that α Tpm is not only decreasing in band density due to exchange but also due to oxidation, creating the appearance of an additional band.
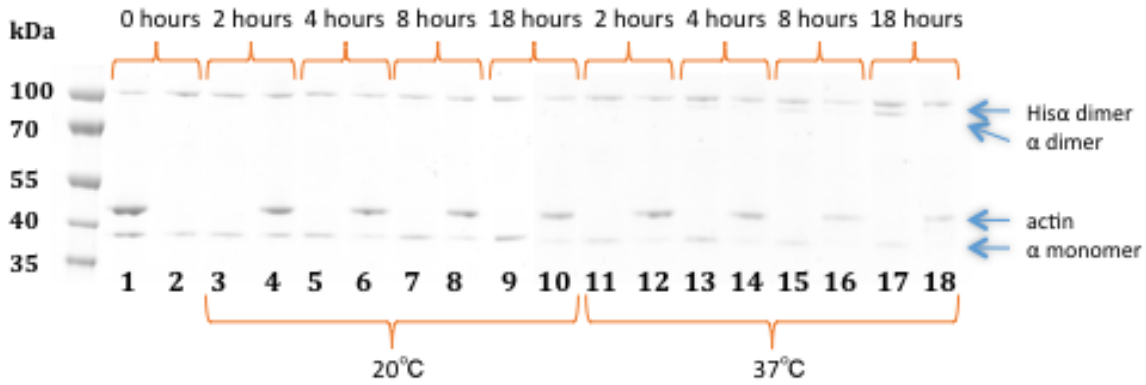
Figure 3.9.1. Non-reduced samples of actin+αTpm + 10 x molar excess Hisα Tpm incubated at 20 ℃ and 37 ℃ in standard salt (100 mM KCl). Samples are as follows: Prestained PageRuler ™ #26616, 1. 20/37 ℃ 0 hours pellet, 2. 20/37℃ 0 hours supernatant, 3. 20℃ 2 hours supernatant, 4. 20℃ 2 hours pellet, 5. 20℃ 4 hours supernatant, 6. 20℃ 4 hours pellet, 7. 20℃ 8 hours supernatant, 8. 20℃8 hours supernatant, 9. 20℃18 hours supernatant, 10. 20℃18 hours pellet, 11. 37 ℃ 2 hours supernatant, 12. 37 ℃ 2 hours pellet, 13. 37 ℃ 4 hours supernatant, 14. 37 ℃ 4 hours pellet, 15. 37 ℃ 8 hours supernatant, 16. 37 ℃ 8 hours pellet, 17. 37 ℃ 18 hours supernatant, 18. 37 ℃ 18 hours pellet.

Supernatant samples were diluted tenfold to enable clear visualisation on the gel, figure 3.9.1; otherwise their lanes were overloaded with protein. The rate of exchange of Tpm on actin was analysed as before, using densitometry analysis, as shown in tables 3.9.2 and 3.9.3.

It is clear to see that there appears to be Tpm "contamination" in the supernatant and pellet from the initial 0 hours time point. Given that α Tpm is preincubated with actin and centrifuged to remove the unbound, it is unusual for α Tpm to be present in the supernatant for the 0 hours time point. Samples taken were kept on ice when not in use, but while preparing solutions for incubations, there were periods when the samples were dealt with at room temperature (~20 ℃). Earlier work in this chapter showed a lack of monomer exchange at this temperature, so it was assumed that samples could be handled at room temperature without exchange occurring. However, data presented here showed

Tpm dimer exchange at 20 ℃ on actin. This provides insight as to why the 0 hours time point showed the presence of α Tpm not only bound to actin in the pellet, but also in the supernatant, and why Hisα was present in both too. The 0 hours time point is an approximate time, which excludes sample handling, ergo some exchange may have already begun during sample preparation.

The same is true for the 10 x molar excess of Hisα Tpm being present in both the supernatant and pellet. On the other hand, it could be an unexpected "contaminant" from centrifugation. To test this, a control was performed with a solution containing just Hisα Tpm at a high concentration (25 μM – solution 1) and low concentration (2.5 μM – solution 2), by subjecting it to centrifugation at 100,000 rpm for 20 minutes at 4 ℃, and visualising the supernatant and pellet content via SDS PAGE. Hisα Tpm was seen not only in the supernatant but also in the pellet, figure 3.9.2.
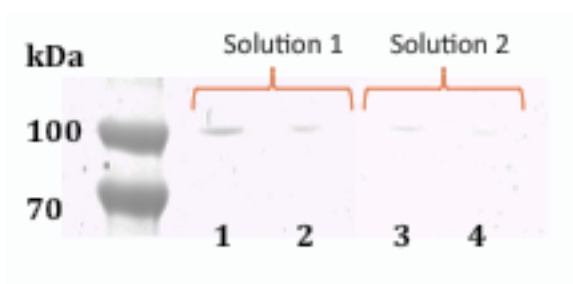
Figure 3.9.2. Non-reduced samples of cross-linked Hisα Tpm at 25 μM (solution 1) and 2.5 μM (solution 2), centrifuged at 100,000 rpm. Samples are as follows: Prestained PageRuler ™ #26616, 1. Solution 1 supernatant, 2. Solution 1 pellet, 3. Solution 2 supernatant, 4. Solution 2 pellet.

The high concentration of Hisα is the clearest to see in this test, solution 1, figure 3.9.2 lanes 1 and 2. After centrifugation, Tpm is seen on the gel not only in the supernatant, lane 1, but there is also a fraction in lane 2, the pellet. The same is true for the lower concentration test, however on paper it is not as clear. It was

seen that Hisα Tpm is unexpectedly being spun down during centrifugation.

Densitometry analysis was performed of the gel as previously, table 3.9.1 to

quantify the ratio of Hisα in the supernatant and the pellet.

Ratio	Supernatant 1	0.77
	Pellet 1	0.23
	Supernatant 2	0.68
	Pellet 2	0.32

Table 3.9.1. Ratio of band densities for supernatant and pellet of Hisα Tpm centrifuged at 100,000 rpm. Solution 1 contained 25 μM Hisα Tpm, and solution 2 contained 2.5 μM. The average amount of Tpm that spins down into the pellet in 27.5 %. As calculated from figure 3.9.2.

The high concentration solution (solution 1) showed 23 % of Tpm in the pellet,

and the low concentration solution (solution 2) showed 32 % of Tpm in the

pellet. This equated to an average of 27.5 % of Tpm being found in the pellet

unexpectedly. In future experiments, cosedimentation assays can be

standardised by either changing the duration or speed of centrifugation.

Unexpected pelleting of the tenfold molar excess Tpm in the supernatant may be

reduced by giving the solution a pre-spin, in the same manner that Tpm bound to

actin was pre-spun to remove the unbound. For the purpose of this analysis,

exchange was explored as change relative to the starting band densities.

Samples incubated at 20 ℃ showed a decrease in α Tpm bound to actin, table

3.9.2, over 18 hours, from 0.62 to 0.12. This was complemented by a change in

the ratio of Hisα: α found in the pellet, table 3.93. Over 18 hours, the ratio of Hisα

in the pellet increased from 0.31 to 0.72.

At 37 ℃, the ratio of α Tpm bound to actin decreased over 4 hours, after which the sample showed signs of significant degradation and densitometry analysis did not provide reliable data, table 3.9.4. After 8 hours incubation, the bands on the gel became faint and as such the densitometry analysis produced very inaccurate results. The amount of Hisα in the pellet increased significantly over 4 hours from 0.31 to 0.87 in ratio to α Tpm, table 3.9.5. Again, after 8 hours incubated, data could not be used.

The ratio of exchange appears to be twice as fast at 37 ℃ compared to 20 ℃, given the decrease in bound α Tpm from 0.62 to 0.12 and 0.28, respectively, for the first 4 hours incubation. This is confirmed by looking at the Tpm content in the pellet. Correcting the ratios found in the pellet for the initial Hisα contamination, samples at 37 ℃ increase by 0.56, while at 20 ℃ the increase is almost half that at 0.31.

20 ℃

Time (hours)		0	2	4	8	18
Ratio	Bound Tm	0.62	0.58	0.28	0.28	0.12
	Free Tm	0.38	0.42	0.72	0.72	0.88

Table 3.9.2. **Ratio of α Tpm bound to actin vs. α Tpm free in solution in the presence of 10 fold molar excess of chemically cross-linked Hisα Tpm, incubated at 20 ℃.** Samples were centrifuged to separate Tpm bound to actin in the pellet and free Tpm in the solution. Exchange was detected by movement of α Tpm band density from the pellet (bound) to the supernatant (free). As calculated from figure3.9.1.

Time (hours)		0	2	4	8	18
Ratio in pellet	HisTm	0.31	0.58	0.62	0.71	0.72
	Tm	0.69	0.42	0.38	0.29	0.28

Table 3.9.3. **Ratio of α Tpm to Hisα found in the pellet of samples incubated at 20 ℃.** There was a starting contaminant of Hisα at time ~0 hours. Exchange was detected by the decrease in α Tpm and subsequent increase of Hisα found bound to actin in the pellet. As calculated from figure3.9.1.

---

37 ℃

Time (hours)		0	2	4	8	18
Ratio	Bound Tm	0.62	0.28	0.12	0.67	0.09
	Free Tm	0.38	0.72	0.88	0.33	0.91

Table 3.9.4. **Ratio of α Tpm bound to actin vs. free α Tpm in solution in the presence of 10 fold molar excess of chemically cross-linked Hisα Tpm, incubated at 37 ℃.** Samples were centrifuged to separate Tpm bound to actin in the pellet and free Tpm in the solution. Exchange was detected by movement of α Tpm band density from the pellet (bound) to the supernatant (free). As calculated from figure3.9.1.

Time (hours)		0	2	4	8	18
Ratio in pellet	HisTm	0.31	0.78	0.87	0.23	0.90
	Tm	0.69	0.22	0.13	0.77	0.10

Table 3.9.5 **Ratio of α Tpm to Hisα found in the pellet of samples incubated at 37 ℃.** There was a starting contaminant of Hisα at time ~0 hours. Exchange was detected by the decrease in α Tpm and subsequent increase of Hisα found bound to actin in the pellet. As calculated from figure3.9.1.

An alternative method of exploring Tpm exchange on actin is to use fluorescent probes. Pyrene labelled Tpm can be detected in a solution using spectroscopy (Ishii, Lehrer 1990). Tpm was labelled as shown in methods 2.1.7. Incubations of Tpm and actin were set up, as for previous Tpm+actin studies, wherein labelled Tpm was pre incubated with actin before adding an excess of unlabelled Tpm and incubating the solution. Samples were taken and centrifuged to separate Tpm bound to actin and Tpm free in solution. These samples were then studied in the fluorimeter to detect pyrene fluorescence. Exchange of Tpm would be seen as a positive pyrene peak appearing in the supernatant, as well as a decrease in the signal of the pelleted Tpm+actin solution.

Samples of pyrene labelled Tpm bound to actin were incubated at room temperature for 96 hours in the presence of a tenfold molar excess of unlabelled Tpm to observe exchange on the actin filament. This was monitored utilising cosedimentation assay technique, as before. Tpm bound to actin will be found in the pellet of a solution once centrifuged. Unbound Tpm will be free in the supernatant. The presence of pyrene in the supernatant will be detectable using fluorescence spectroscopy.

To monitor the amount of exchange occurring, 3 μM pyrTpm (59% labelled) was incubated with 7 μM actin for 1 hour at room temperature to ensure an excess of Tpm to bind to the actin. This actin and pyrTpm solution was then centrifuged at

50,000 rpm for 20 minutes to remove any unbound Tpm. The pellet was resuspended and incubated with a tenfold molar excess of unlabelled Tpm. If any unlabelled Tpm exchanged with the pyrTpm bound to actin, pyrene would be detectable in the supernatant.

The experiment was performed under 4 conditions; unlabelled Tpm, pyrTpm, pyrTpm bound to actin and pyrTpm bound to actin with a tenfold molar excess of unlabelled. Each condition was incubated at room temperature in standard salt buffer (100 mM KCl, 20 mM MOPS, 5 mM $MgCl_2$, 1 mM NaN_3, pH 7) for 96 hours, with samples taken at time ~0 hours, 2 hours, 20 hours and 96 hours. Samples were centrifuged at 50,000 rpm for 20 minutes and the supernatant was scanned over 360 – 560 nm using Perkin-Elmer LS-5B. Fluorescence was excited at 340 nm and emission was monitored between 360 - 560 nm, as per Ishii and Lehrer 1990. Fluorescence and emission both used a monochromator bandwidth of 2.5 nm. The spectrum was then fitted to Gaussian curves as before, and the data for the peak height and area extracted and plotted in table 3.11.1.

The spectra of unlabelled Tpm was explored first to determine the background noise in the signal. The spectra showed 2 peaks at average positions of 384 nm and 409 nm. Spectra of pyrTpm showed peak 1 and peak 2, plus peak 3 at an average position of 442 nm, which is not present in the unlabelled control. Peaks 1 and 2 were attributed to Raman scattering. Ergo, peak 3 is the characteristic peak used to monitor the presence of pyrene.

Average data for peaks 1 – 3 were plotted as a pie chart for a visual aid to show which peaks were present and the relative amounts of each, to highlight the change between Raman scattering signal and a pyrene signal over the time course.

First the spectra of unlabelled Tpm was explored to determine the background noise of the signal. The fluorescence spectra showed small peaks at 383.4 nm (blue) and 409.3 nm (orange), with areas of 19.4 and 173.2, respectively, figure 3.10.1.
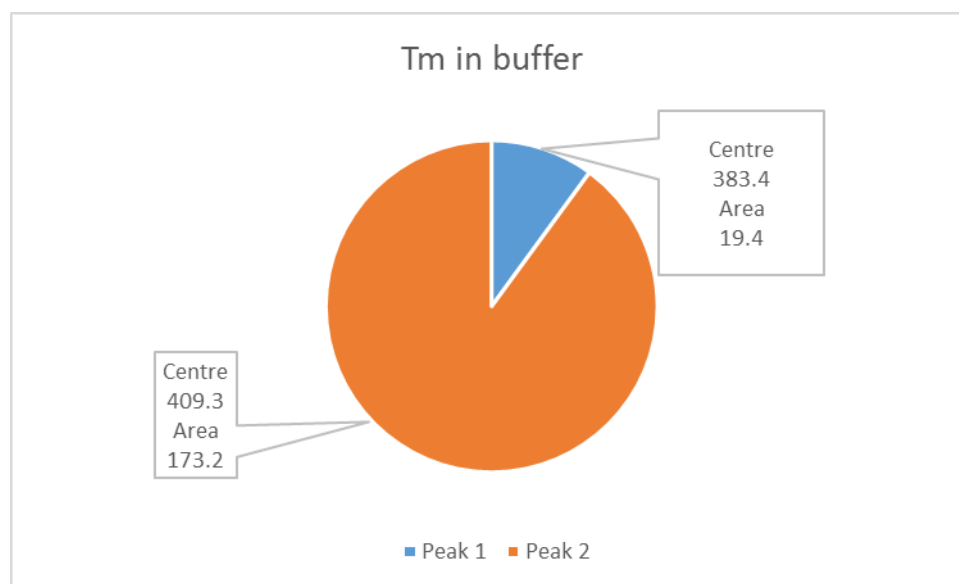
Figure 3.10.1. The supernatant of unlabelled Tpm in buffer fits to two Gaussian curves. There is no fluorescence in the solution, so it was assumed that the signal is from Raman scattering. There are two peaks; with average centres at 383.4 nm (blue) and 409.3 nm (orange) with an average area of 19.4 and 173.2, respectively.

As there is no pyrene label present, these peaks were attributed to Raman scattering. Spectra of water and buffer showed peaks in the same position, figure 3.10.2.
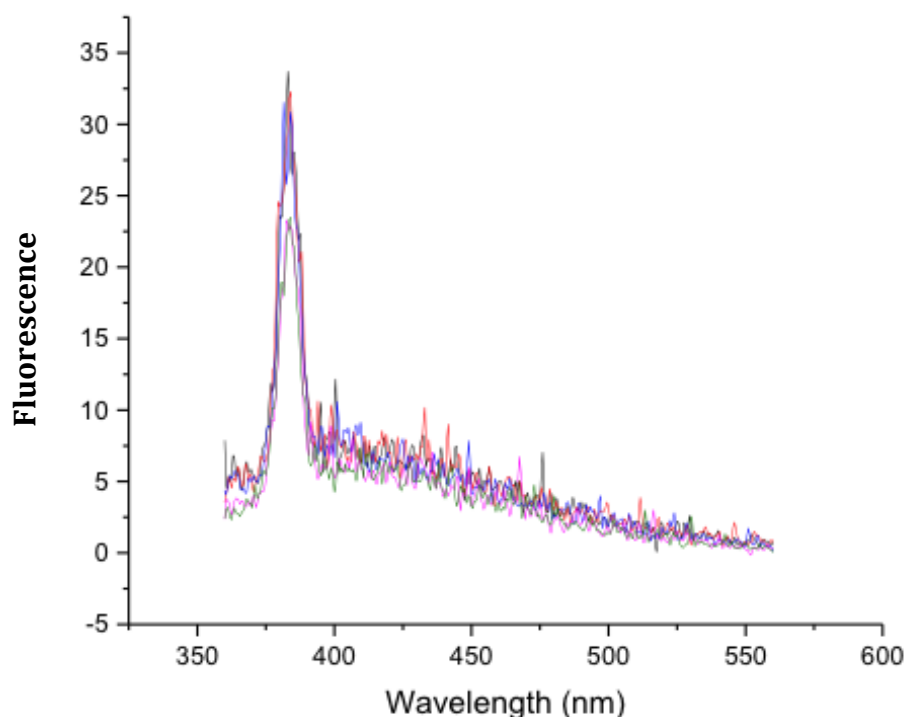
Figure 3.10.2. Spectra for standard salt (100 mM KCl) buffer, excited at 340 nm. There is a strong positive peak at ~ 383 nm and a smaller positive peak ~ 410 nm. Scans show multiple repeats of the same sample.

While the peak at ~384 nm corresponds to raman scattering, it is also a part of the pyrene spectra. Pyrene labelled Tpm fluorescence shows a ~ 10 x increase in the average signal at this peak when compared to the average for unlabelled Tpm. Labelled Tpm also has a peak at an average position of ~ 442 nm, corresponding to pyrene emission, figure 3.10.3. As this peak is the only one unique to the pyrene Tpm spectra, it is the one that will be used to detect the presence of the fluorescently labelled protein.
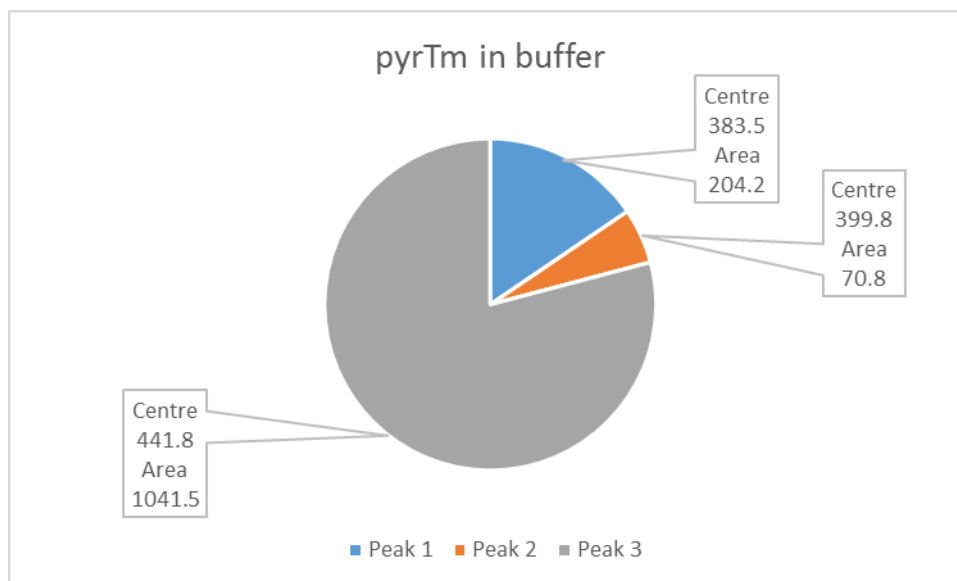
Figure 3.10.3. Pyrene labelled Tpm does not pellet down when centrifuged. So, the supernatant shows the fluorescence signal for pyrene. This is seen in the presence of peak 3 (grey) which has an average centre of 441.8 nm and area of 1041.5. Peak 1 (blue) and peak 2 (orange) are still present, with average centres at 383.5 nm and 399.8 nm, and average areas of 204.2 and 70.8, respectively.

The spectra of pyrTpm was explored over a range of dilutions to determine the level of detection. Samples were diluted from 100% pyrTpm (1 µM) to 5% (50 nm) and regular samples were taken and scanned between 260 nm – 560 nm, shown in figure 3.10.4.
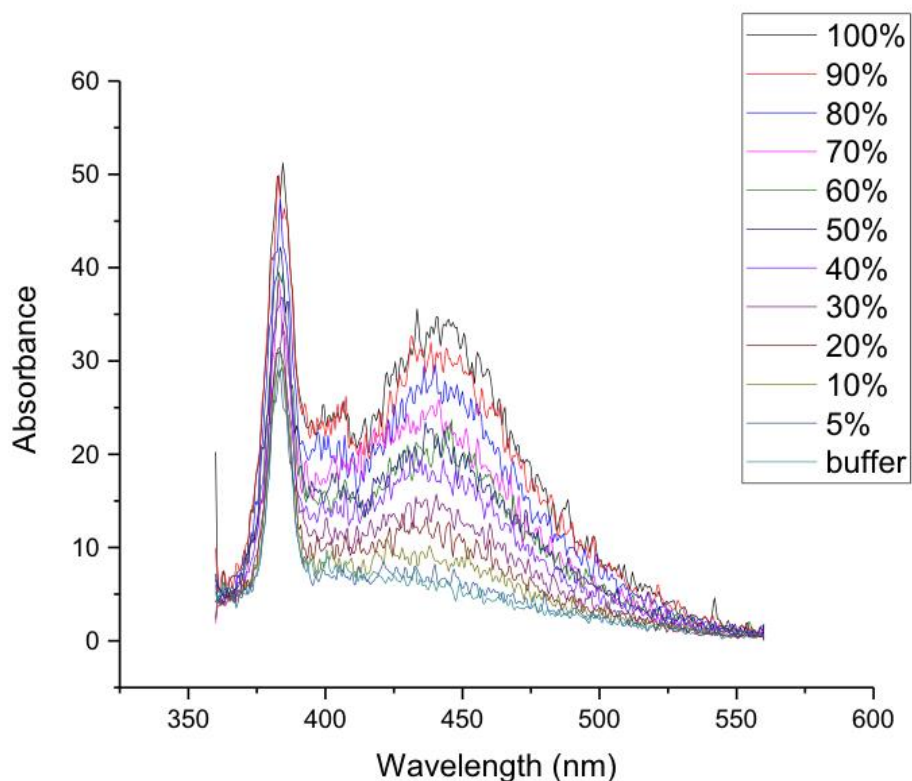
Figure 3.10.4. pyrTpm dilution spectra from 100 % (1 μM) to 5 % (50 nM). Pyrene spectra peaks are at ~ 383 nm, ~ 400 nm and ~ 440 nm for 100 % pyrTpm. Buffer spectra shows similar profile to 5 % dilution.

Pyrene labelled Tpm displays a spectra that fits three Gaussian plots, with peaks at at ~ 383 nm, ~ 400 nm and ~ 440 nm, as shown in figure 3.10.5. This data was used to determine the level of pyrene detection using the fluorimeter. Dilutions of pyrTpm fit three Guassian plots from 100 % - 10 % dilution, with peak averages at the correct positions as previously determined. The 5 % dilution was unable to fit three peaks and is therefore outside of the deteactable range.

The spectra for the buffer shows a positive peak at ~383 nm and a small, broad peak at ~ 410 nm. The spectra for the 5 % dilution is very similar to that of the buffer. This spectra is unable to fit three peaks.
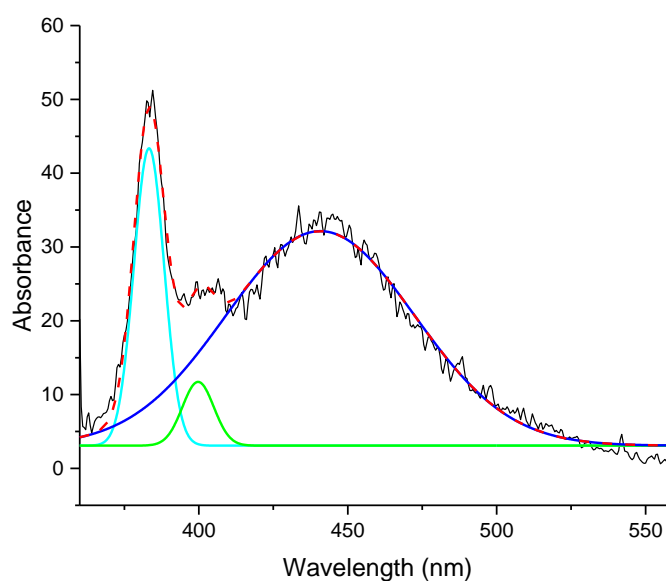
Figure 3.10.5. 100% pyrTpm (1 µM) fit to three Gaussian plots at peak positions ~ 383 nm (pale blue), ~ 400 nm (green) and ~ 440 nm (dark blue).

The positive peak for pyrene is that at ~440 nm, the other two peaks at ~383 nm and ~400 nm are present in the buffer and are attributed to Raman scattering. Therefore, it is the presence of this third peak that we are interested in.

Pyrene labelled Tpm was pre-incubated with actin for 1 hour at room temperature, before being centrifuged to remove any unbound Tpm. The actin and pyrTpm pellet was resuspended and incubated as per previous experiments to explore Tpm dissociation from actin. The spectra for the supernatant showed no presence of pyrene, by the lack of peak 3, figure 3.10.6, over 96 hours. The spectrum showed 2 peaks at an average position of 384.1 nm (blue) and 404.2 nm (orange), with areas of 48.8 and 675.2, respectively. These peaks correspond to the same peaks found in the supernatant of unlabelled Tpm and buffer, lacking a pyrene signal.
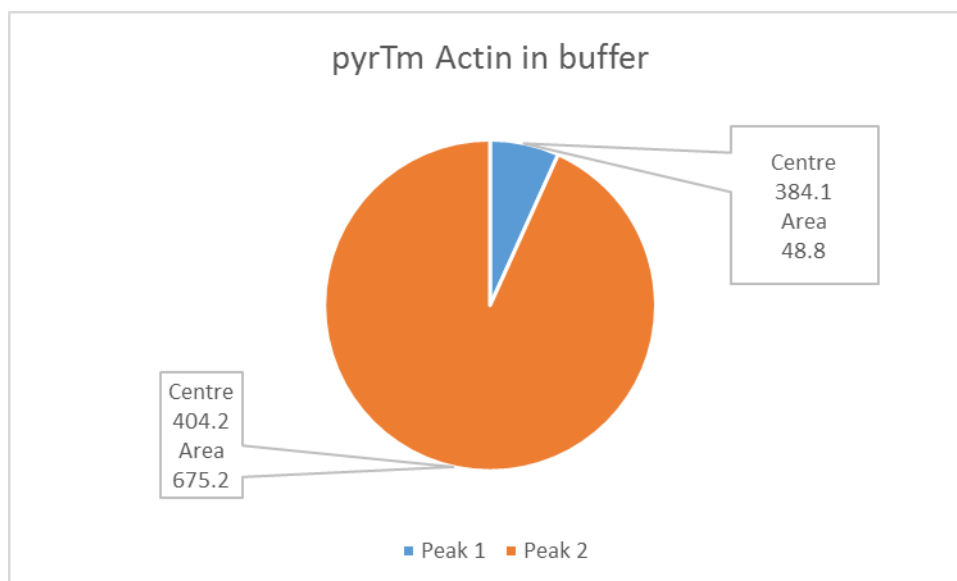
Figure 3.10.6. Pyrene labelled Tpm in the presence of actin shows no exchange off the filament, due to a lack of a pyrene peak in the supernatant. The signal shows similar noise to that of unlabelled Tpm. The average peaks are at 384.1 nm (blue) with an area of 48.8, and 404.2 nm (orange) with an area of 675.2.

The lack of peak 3 showed that once pyrTpm was bound to actin, dissociation did not occur or was too small to identify (<10 %) over the 96 hour time course, as no pyrene fluorescence was detectable in the supernatant.

To explore Tpm exchange, actin was pre-incubated and bound with pyrTpm as before, but for the time course incubation, a tenfold molar excess of unlabelled Tpm was added. If pyrTpm exchanged off the actin with unlabelled Tpm in solution, a pyrene peak will be seen in the supernatant spectra. Over 96 hours, there was no appearance of peak 3 in the supernatant. The spectra showed peak 1 at an average position of 384.5 nm, with an average area of 45.5, and peak 2 at an average position of 418 nm, with an average area of 766.1, figure 3.10.0. This lack of pyrene in the supernatant indicates that little or no exchange is occurring on the actin filament
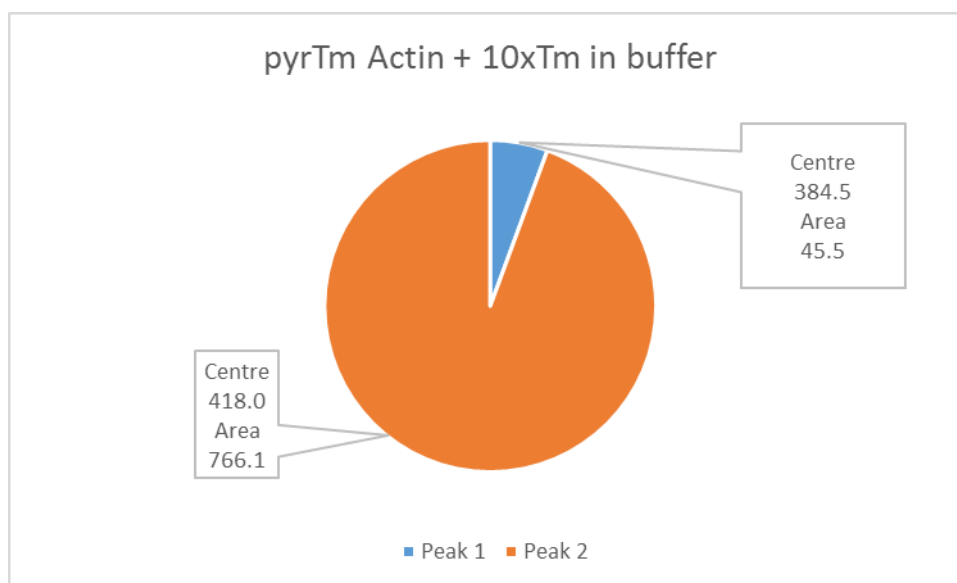
Figure 3.10.7. A ten times molar excess of unlabelled Tpm was added to pre-incubated pyrTpm and actin. The supernatant shows no pyrene signal. The average peaks are at 384.5 nm (blue) with an average area of 45.5 and 418 nm (orange) with an average area of 766.1.

A key change between all the spectra shown is the appearance of peak 3, which leads to a reduction in the signal for peak 2. Upon comparison, the only condition that gave a positive signal for pyrene was the pryTpm in buffer, figure 3.10.8, shown in yellow. This peak was the greatest area out of all the conditions explored. As a result of peak 3 appearing, the signal for peak 2 was greatly reduced to lower than that for unlabelled Tpm.

The signal for peak 2 increases for pyrTpm bound to actin and pyrTpm bound to actin in the presence of unlabelled Tpm, figure 3.10.8, orange and grey bars, respectively. This increased background peak could be as a result of the increased overall protein concentration producing more noise, or perhaps to low level pyrene detection, that is not enough to be detected by the third peak. As determined previously, the pyrene signal was detectable to 10 % dilution (50

109

nM) in solution. Pyrene present below this amount, whilst not quantifiable, may

increase background noise.
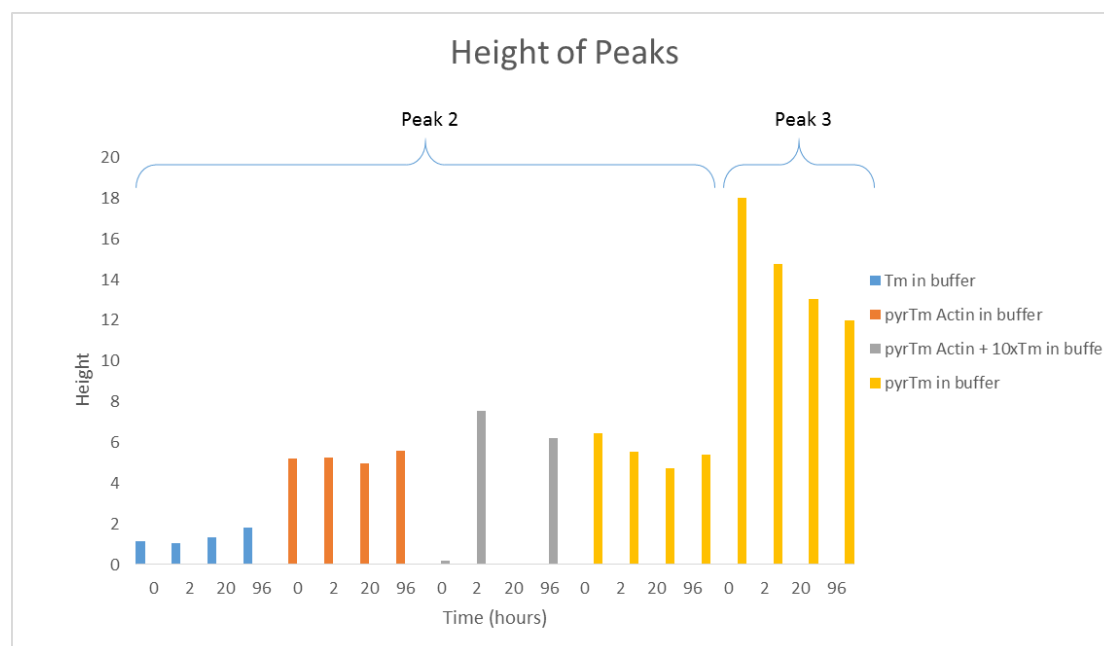
Figure 3.10.8. Comparison of the heights of peaks 2 and 3 for all 4 experimental conditions. Unlabelled Tpm (blue) shows a small peak 2, when compared to pyrTpm bound to actin (orange). pyrTpm bound to actin in the presence of a tenfold molar excess of unlabelled Tpm (grey), has a peak 2 area similar to that without the excess unlabelled. pyrTpm (yellow) shows a massive reduction in peak 2 and the appearance of peak 3, indicating the presence of pyrene in this solution.

Data for the three peaks for all experimental conditions is shown in table 3.10.1,

highlighting again the only conditions that fitted to a third Gaussian, the pyrene

peak, was free pyrTpm in buffer. The pyrene signal is shown to decrease over 96

hours by the decreased peak height from 18 to 12, showing the degradation of

the protein and label over this time.

Overall, it is clear to see that over 96 hours, there is no detectable exchange or

dissociation of Tpm on actin at 20 °C both in the presence and absence of a

tenfold molar excess of unbound Tpm. This indicates that heterodimer formation

is likely to occur in solution before binding to actin. However, if exchange of Tpm

was to happen along an actin filament under these conditions, one assumes another system must be in place to aid this exchange. Our previous work on Tpm monomer exchange between free dimers in solution, showed no detectable levels of exchange over 24 hours. On the other hand, Tpm dimer exchange on actin at 20 ℃ showed some exchange occurring at this temperature after 2 hours. Given the contamination problems of dimer exchange on actin, these results require further exploration. It may be that the cross-link on Hisα affects the binding constant (K_d) of Tpm, while the pyrene label does not have the same effect, thus showing a true result for exchange at this temperature.

For further exploration, performing the experiment again at 37 ℃, could provide insight on what happens under physiological temperature. Tpm showed monomer exchange between free dimers in solution at 37 ℃ after just 1 hour, and exchange of dimers on the actin filament after 2 hours at 37 ℃ when explored using SDS PAGE, ergo it was expected that pyrTpm exchange on actin at 37 ℃ would show similar degrees of exchange. It would also be important to explore the reverse experiment, and bind unlabelled Tpm to actin then add an excess of pyrTpm, to explore the effects of the pyrene tag on the binding affinity of Tpm for actin.

	Time (hours)	Peak 1				Peak 2				Peak 3			
		Centre	Width	Area	Height	Centre	Width	Area	Height	Centre	Width	Area	Height
Tpm in buffer	0	383.8	6.5	30.4	3.7	415.6	106.1	152.5	1.1				
	2	383.4	7.5	16.0	1.7	405.0	110.3	147.2	1.1				
	20	383.3	7.4	14.6	1.6	416.5	99.4	167.3	1.3				
	96	383.1	7.7	16.6	1.7	400.0	98.9	225.6	1.8				
pyrTpm Actin in buffer	0	384.3	7.9	43.6	4.4	409.3	96.7	632.6	5.2				
	2	384.0	6.9	47.7	5.5	405.9	94.5	619.2	5.2				
	20	384.3	7.8	41.6	4.3	402.8	110.5	689.4	5.0				
	96	384.0	9.6	62.3	5.2	399.0	108.3	759.6	5.6				
pyrTpm Actin + 10xTpm in buffer	0	384.9	6.9	50.8	5.9	422.2	88.3	769.6	0.2				
	2	384.2	6.6	47.1	5.7	423.8	86.3	812.9	7.5				
	20	384.4	8.2	43.7	4.3	415.5	90.7	716.4	0.1				
	96	384.5	6.5	40.4	4.9	410.7	98.1	765.5	6.2				
pyrTpm in buffer	0	383.8	11.7	212.1	14.5	400.2	8.1	65.0	6.4	443.7	53.8	1212.7	18.0
	2	383.1	11.8	193.3	13.1	399.6	10.1	70.6	5.6	443.1	59.9	1106.8	14.7
	20	383.9	12.3	197.3	12.8	400.2	10.2	60.6	4.7	442.9	57.0	930.8	13.0
	96	383.0	10.8	214.3	15.9	399.1	12.9	87.3	5.4	437.6	61.0	915.7	12.0

Table 3.10.1. Gaussian fits to fluorescence spectra. Peak 1 is centred at an average position of 384 nm. Peak 2 is centred at an average position of 409 nm. Peak 3 is centred at an average position of 442 nm. Data is from the supernatants of each solution. In the presence of actin, Tpm will bind and spin down into the pellet with the actin. Unbound Tpm will be free in the supernatant. Peak 3 is the corresponding pyrene fluorescence peak. As calculated from figure 3.10.8.

3.11 Extraction of Tpm from cardiac tissue

The stability of Tpm dimers up to 20 °C was exploited to explore the dimer content of mouse cardiac tissue. Previous Tpm extraction from cell cultures and tissue involve pH precipitations and heat denaturation to remove contaminants and purify Tpm. These stages break the bonds between Tpm dimers, meaning the pure product was subjected to significant exchange of monomers. While this may not be an issue when studying homodimers, it becomes important for studying heterodimers.

The aim was to extract Tpm from mouse cardiac tissue through standard salt washes, so as not to disrupt Tpm dimers. Then with the use of chemical cross-linking, the dimer population was fixed and explored through SDS-PAGE as before, and sent for mass spectrometry analysis (Bruker Daltonics micrOTOFQ) by Kevin Howland, University of Kent.

Cardiac tissue was homogenised in standard salt wash buffer (100 mM KCl, 20 mM KPi, 5 mM $MgCl_2$ pH 7) and then centrifuged at 4,600 rpm for 6 minutes at 4 °C to remove the supernatant. The pellet was then resuspended in ice cold Guba Straub buffer (100 mM KH_2PO_4, 50 mM K_2HPO_4, 0.3 M KCl, pH 6.6) + 5 mM ATP and incubated at room temperature for 3 hours while stirring to extract the Tpm. Guba Straub is traditionally used to extract myosin, however, upon standardisation of extraction buffers, it was found to also extract Tpm successfully. This was centrifuged again at 4,600 rpm for 6 minutes at 4 °C to separate the Tpm from the tissue pellet. The tissue was subjected to a second

extraction in Guba Straub buffer, stirring overnight at 4 ℃ before centrifugation

to separate the pellet and supernatant as before.

Tpm washes and extractions were cross-linked overnight, as before, then run

under non-reducing conditions on 7.5 % polyacrylamide gels. Results are shown

in figure 3.11.1.
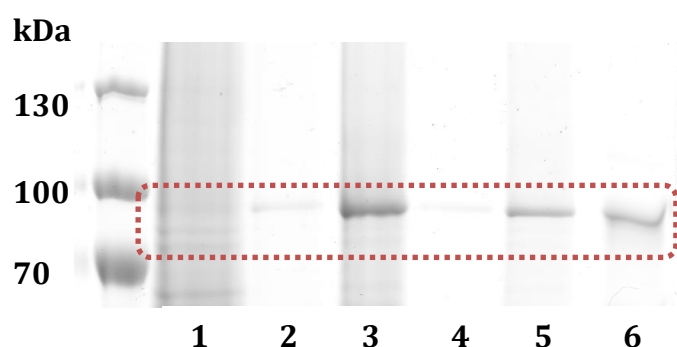
Figure 3.11.1. Tpm extracted from mouse cardiac tissue. Cross-linked, non-denatured samples are as follows: Prestained PageRuler ™ #26616 1. Wash supernatant 2. Extraction 1 pellet 3. Extraction 1 supernatant, 4. Extraction 2 pellet, 5. Extraction 2 supernatant, 6. α Tpm control. The Tpm band is highlighted by the red dashed box.

It was clear that Tpm was extracted from the cardiac tissue in the Guba Straub

buffer, figure 3.11.1 lanes 3 and 5, highlighted by the red box. The majority of

Tpm was extracted after 3 hours incubation in the first Guba Straub extraction at

room temperature, however, Tpm was further extracted by a second overnight

incubation at 4 ℃ in Guba Straub. Tpm was not significantly extracted during the

wash of the cardiac tissue.

Cross-linked Tpm extractions were then sent for mass spectrometry analysis.

The aim was to detect cross-linked Tpm dimers from within the crude extraction

from the cardiac tissue. Issues arose however in assigning mass peaks to Tpm, as

the electrospray displayed lots of heterogeneity.

To assess whether the issue lied within the sample or a limitation of the

equipment, a control was performed using α and Hisα Tpm. A mix of Hisα and α

Tpm homodimers were heated at 59 °C for 10 minutes, then incubated at 37 °C

for 45 minutes and cooled on ice. This heating and cooling allowed for dimer

exchange to take place, thus creating a mix of homo- and heterodimers. This was

then cross-linked overnight to fix the dimer population, figure 3.11.2.
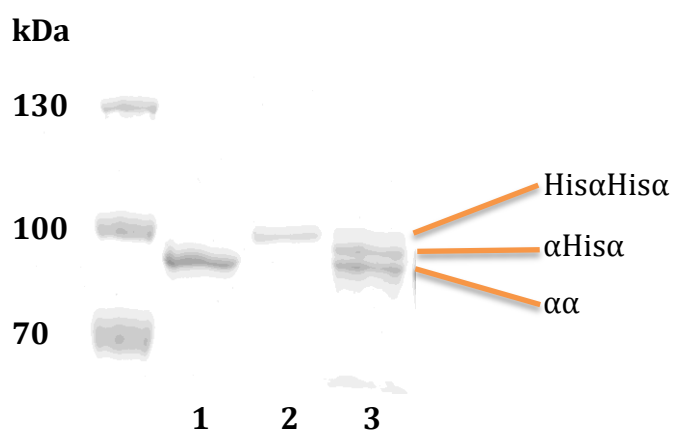
Figure 3.11.2 Cross-linked α and Hisα homodimers and α-Hisα heterodimer under non-reducing conditions on a 7.5 % polyacrylamide gel. Samples are as follows: Prestained PageRuler ™ #26616 1. α Tpm, 2. Hisα Tpm, α-Hisα Heterodimer.

It was seen that the α and Hisα homodimers exchanged and formed a

heterodimer, as indicated on figure 3.11.2, lane 3.

The cross-linked mixture of homo- and heterodimers was then sent for analysis

by mass spectroscopy. However, the sample did not show three clear peaks,

representing homo- and heterodimers, but revealed 5 different molecular weight

peaks, which did not correspond to expected values. The expected values for α homodimers, α-Hisα heterodimers, and Hisα homodimers were 65731.4, 67461 and 69151.2, respectively. It is clear that the mass spectroscopy data does not match expected values, with additional contaminants, and molecular weights generally lower than those expected, table 3.11.1.

Expected mass	Measured mass
65731.4	64728.5
67461	65675.2
69151.2	65864.2
	66077.9
	67429.8

Table 3.11.1 Expected mass values for Tpm α homodimer, α-Hisα heterodimer and Hisα homodimer (smallest to largest, respectively). Measured mass values displaying heterogeneity, revealing 5 mass peaks instead of 3.

It was possible that the cross-linking buffer may cause problems during mass spectroscopy, owing to the high salt content (2 M NaCl, 10 mM MOPS, 2 μM $CuSO_4$, 10 mM $K_2Fe(CN)_6$, pH 7). Samples were desalted using a ZebaSpin column as before and sent for mass spectrometry again to see if removal of the buffer would improve the signal. However, mass spectrometry results still did not display three peaks.

It was concluded that the cross-linking procedure of Tpm may be too harsh on the sample, thus creating heterogeneity when analysing using mass spectrometry. Degradation of Tpm through cross-linking was also noted in our earlier work, in particular with heterodimers.

Crude extraction of Tpm from cardiac tissue shown here provides an exciting method for potential future exploration of Tpm. If an alternate method was used to chemically cross-link Tpm that was less damaging, thus enabling clear distinction during mass spectroscopy, dimer content of transgenic mice hearts containing cardiomyopathy mutants, would give insight into the dimer expression and formation in heterozygous affected mice.

3.12 Conclusions

Tropomyosin exchange was explored on two levels: the exchange of monomers in dimers, and the exchange of dimers in polymers on actin.

The stability of monomer exchange and degradation at 4℃ and 20 ℃ allows us to be confident of dimer content in samples, as they are worked with at 4 ℃ and 20 ℃, and stored short term 4 ℃. As the rate of exchange decreases with temperature, we can also assume that samples in the freezer will not undergo any exchange.

The stability of the dimers at room temperature was exploited during thermal stability experiments of the protein using circular dichroism. Work previously carried out required Tpm dimers to be cross-linked to be certain of the dimer content on beginning the experiment. The effect of this cross-link on the heterodimer could not be judged, so the melting curves for the heterodimer had

to be estimated from three melting curves, accounting for random assembly of the dimers (1:2:1, e.g. αα* would reanneal to form αα:αα*:α*α*). From the dimer stability at 20 ℃, it was concluded that the first melting curve for a heterodimer in the presence of DTT will be a true melting curve for a heterodimer assuming it is not cross-linked at the start (Janco, Kalyva et al. 2012). Recent studies have shown that cross-linked α homodimers had decreased affinity for actin and decreased stability of the actin+Tpm complex. Cross-linking was also seen to increase the sliding velocity of regulated thin filaments during in vitro motility assays, more so for cardiac isoforms over skeletal, which they postulate to play a role in human cardiac disease mechanism (Matyushenko, Artemova et al. 2017). Also, the thermal stability of α Tpm was seen to increase upon cross-linking (Kremneva, Boussouf et al. 2004). Given the impact cross-linking has on Tpm, it is important to minimise its use experimentally(Kremneva, Boussouf et al. 2004).

The free exchange rate of dimers at 37 ℃ can potentially be exploited experimentally, for example, to exchange a label onto the protein, as a means of less intensive experimental conditions. Dimer exchange of monomers at 37℃ is already utilised experimentally during heterodimer formation, as explained in methods 2.2.3.

Even though exchange was seen at 37 ℃, it was still very slow, not even reaching the ratio of random assembly 1:2:1 (homo:hetero:homo) after 24 hours. This exchange was also in the absence of actin, which was expected to slow the rate down even further, indicating that there may be another method of dimer

formation and exchange. As Tpm exists as homodimers and heterodimers, exchange must take place between dimers, how this happens remains to be explained(Matsumura, Yamashiro-Matsumura 1985, Lehrer, Qian 1990, Lehrer, Stafford III 1991). Potentially dimers form off the actin filament in the cytoplasm after leaving the ribosome and bind to the actin preformed. On the other hand, if exchange does occur on the thin filament, another cellular system could be in place in order to aid this process e.g. chaperones.

This idea was further supported by the pyrTpm exchange data, which showed that pyrTpm did not dissociate from actin over 96 hours at room temperature and that pyrTpm bound to actin did not exchange even in a tenfold molar excess of unlabelled Tpm over 96 hours at room temperature.

Tpm dimer exchange on actin provided conflicting results between His-tagged Tpm SDS PAGE cosedimentation assays and pyrene labelled fluorescence cosedimentation assays. SDS PAGE visualisation of His-tagged Tpm cosedimentation assays showed exchange of Tpm on actin both at 37 ℃ and 20 ℃. The main limitation to the assay was the unexpected pelleting of Tpm when centrifuged, which required data to be normalised to starting measurements. Secondly, as explained before, it is known that cross-linking Tpm affects the properties of the protein; therefore, the cross-linked Hisα may have a different affinity for actin to the non cross-linked protein. This effect could be further explored by calculating the binding constants for Tpm with and without cross-linking, using the same cosedimentation assay techniques.

His-tagged Tpm exchange on actin showed approximately 50 % exchange between dimers over 4 hours at 20 ℃ and ~ 60 % at 37 ℃, in comparison to the pyrene labelled Tpm which showed no exchange over the same time period. It was calculated that pyrene level of detection was reliable to 10% dilution of the original. Therefore, if both experiments were exchanging at the same rate, exchange would've been detectable and quantifiable for the pyrTpm. This indicates a limitation of the experiment itself or the protein label. His-tagged Tpm suffered with unexpected pelleting, meaning data required standardisation. On the other hand, Tpm was only 59 % labelled in exchange experiments, this alongside detection levels of a very old piece of equipment, could explain the lack of detectable exchange. The His-tag and/or the pyrene label could affect Tpm affinity for actin, Tpm stability and therefore exchange of dimers.

In contrast, dimer exchange on actin using pyrene labelled Tpm revealed no exchange at 20 ℃. Given that the pyrene label was only detectable to 10 %, if low level exchange was occurring, this technique would not be sensitive enough to detect it. Exchange of monomers and dimers showed greatest exchange at 37 ℃, so repeating this experiment at physiological temperatures would provide greater insight into exchange on actin. As with cross-linked protein and His-tag, the effect of the pyrene label on Tpm affinity for actin should be explored to ensure the tag does not affect the exchange. This can also be verified by performing the experiment under two conditions; Tpm bound to actin with excess pyrTpm, and pyrTpm bound to actin with excess unlabelled protein.

The affinity and exchange of Tpm on actin will also be affected by other factors *in vivo*, such as the presence of Tn, which may reduce exchange further. As Tn sits on the Tpm-Tpm overlap region, it potentially acts as an anchor for Tpm. Recent 3D reconstructions from EM have shown that TnI interacts with Tpm or TnT1 by azimuthally bridging between adjacent actin subunits. The C-terminal domain of TnI interacts with actin and in turn TnT1 positions Tpm to block cross-bridge binding, thus leading to muscle relaxation. In this blocked state, Tpm is wedged between the TnI C-terminal domain and the Tn core domain, which they attribute to "functional interaction between the two sides of the filament" (Yang, Barbu-Tudoran et al. 2014). The presence of ions, such as calcium, may influence exchange *in vivo* by reducing Tn regulation of myosin binding, which in turn relieves its inhibition of the azimuthal movement of Tpm over actin.

Calcium is known to not only permit myosin binding to actin by relieving Tn inhibition (McKillop, Geeves 1991), but also shows an effect on Tpm function. At high calcium it is proposed that Tpm follows the long pitch helix of actin in either the closed or open state and does not swivel, however at low calcium, Tpm is required to swivel at the head-to-tail overlap region to accommodate the azimuthal shift and adopt the blocked state (Murakami, Stewart et al. 2007, Miki, Kobayashi et al. 1998, Miki, Miura et al. 1998). At different positions on the actin filament, Tpm may be more as less likely to exchange, given steric pressures and relaxed states. It would be interesting to see whether or not the swivel encourages Tpm exchange or if in the blocking state, Tpm is less likely to exchange.

As homodimers and heterodimers behave differently thermodynamically, it is interesting to note that their rate of exchange is different too. Tpm α-Hisα heterodimers showed minimal reverse exchange to form homodimers over 24 hours at 37 ℃ unlike the homodimers under the same conditions. This could give an indication to preferential assembly for dimers.

Early studies into homodimer exchange showed under physiological conditions *in vitro,* homodimers slowly exchanged to preferentially form heterodimers, which was attributed to thermodynamic equilibrium (Lehrer, Qian 1990, Lehrer, Stafford III 1991, Lehrer, Qian et al. 1989). On the other hand, studies performed under high salt conditions showed a preferential assembly of β homodimers from an original mixture of α homodimers and αβ heterodimers after denaturation-renaturation (Holtzer, Kidd et al. 1992). Once again, different studies have revealed very conflicting and contrasting results. Data presented here does not reveal any salt dependence of dimer exchange, but does support a heterodimer preference, which requires further investigation.

The DCM mutant, E54K, is located within the actin-binding motif of the N-terminal region of Tpm. In the heptad repeat, this mutant is located at the *e* position, interacting with a residue, K49, at position *g* on the opposite chain, through electrostatic forces. Changing the charge of this residue from glutamic acid to lysine will undoubtedly affect its interchain interactions and potentially affect its affinity for actin (Brown, Kim et al. 2001). In vitro motility assays using skeletal muscle show the E54K mutation increases the sliding velocity of thin filaments but does not alter the calcium sensitivity, (Kopylova, Shchepkin et al.

2016), however earlier work with cardiac isoforms suggested the inverse (Mirza, Marston et al. 2005). While other explored DCM mutants, such as E40K, are more simply and directly explained, the E54K mutant is often referred to as having a "complex effect" of Tpm structure and function, which means its disease causing mechanism is not truly understood (Mirza, Robinson et al. 2007). It is interesting that both DCM causing mutations located in the *e* position, both cause the DCM phenotype, but both alter Tpm role and function in almost opposing ways. E54K is located in the second α band rather than the β band (E40K), which has been proposed to correspond to On and Off states of the thin filament (McLachlan, Stewart 1976) hence its destabilisation of the Off state, compared with E40K, which destabilises the On state.

Here it is seen that the E54K – Hisα heterodimer did not exchange over 11 hours, even at 37 ℃, unlike the WT α and Hisα homodimers, which showed extensive exchange under the same conditions. The effect of the two positive charges may be balanced by the location of the residue, as it sits between two alanine clusters, which cause bends in the protein structure. Perhaps the repulsion of the two positive charges strengthens the shape of the Tpm, thus giving it a greater conformational stability, and less exchange occurs. Previous work has shown that E54K has two opposite effects of the stability of the N-terminal region of Tpm (Mirza, Robinson et al. 2007).

It is also possible that the heterodimer is the most stable conformation overall, in comparison to a solution containing the two homodimers. This was reinforced by the heterodimer control α-Hisα experiment, which showed little exchange over

24 hours at 37 ℃. The Hisα homodimer may be the most stable, but an E54K homodimer may be significantly destabilised as it will have two sites of interchain repulsions, encouraging heterodimer formation of an intermediate stability. It would be interesting to do the reverse exchange of the experiment, starting with E54K and Hisα homodimers to see if they exchange to preferentially form a heterodimer.

Interestingly, previous work with HCM mutants, D15N and E180G, showed no preference for dimer assembly, when a starting ratio was ~ 0.5 : 0.5, following random association instead, resulting in a ratio of 1 : 2 : 1. Actin binding assays showed a weaker affinity of mutant homodimers of ~ 2.5 fold, and small changes for the mutant-WT heterodimers affinity (Janco, Kalyva et al. 2012). However, these differences in affinity are apparent at low working concentrations of Tpm and actin, ergo under high physiological conditions, these changes are likely to be negligible. This furthers questions into how dimers are formed and exchange in the cell.

It would be interesting to study Tpm homo and heterodimer exchange over different temperatures to explore physiological conditions of other animals, for example ~ 40 ℃ to be closer to the body temperature of rabbits, pigs and chickens.

The effect of chemically cross-linking the protein led to faster protein degradation, most notably for heterodimers during reverse exchange experiments. This was seen by the smearing of samples during a time course

smearing on cross-linked gels, while the same samples on reducing gels did not show degradation of the protein at the same level. It was apparent that samples were more fragile once cross-linked, as once prepared to load onto polyacrylamide gels, samples very quickly precipitated. This meant that samples had to be run on a gel as soon as a time point was collected, otherwise gel bands were indistinguishable. Potentially, different salt buffer conditions could be explored to try to minimise precipitation, however, it would be better to find cross-linking conditions that were less detrimental to the protein.

The detrimental effect of cross-linking was also seen for samples sent for mass spectroscopy analysis. Analysis of cross-linked α-Hisα heterodimers showed differences in mass peaks to expected values, in conjunction with additional peaks being present. We concluded that cross-linking was detrimental to the structure of Tpm and therefore to continue exploration of Tpm dimer content in cardiac tissue, alternate methods for fixing a dimer population needed to be explored that was not detrimental to the sample.

The data presented here provides insight into dimerization and exchange of Tpm isoforms. The stability of Tpm isoforms with and without tags and cross-linking was also explored during exchange experiments alongside cardiomyopathy mutants. To further explore the thermal stability of Tpm and better understand the primary properties, which could explain the exchange seen here, the following chapter explores Tpm through the use of circular dichroism (CD) as a function of temperature.

Chapter 4: Investigating the thermal stability of tropomyosin using circular dichroism spectroscopy

4.1 Introduction

The thermal stability of a protein can shed light on its properties and function. Changes in thermal stability may occur as a result of changes to inter and intrachain interactions within the protein. The thermal stability of Tpm may link to its function, by affecting the stiffness or flexibility of the protein. Changes within tropomyosin will not only alter the protein but how it functions with actin and troponin, as well as its role in regulating myosin binding and its calcium sensitivity (Robaszkiewicz, Ostrowska et al. 2015).

As mentioned before, previous work with Tpm heterodimers required chemical cross-linking of the protein to ensure no exchange occurred and the starting sample remained a pure heterodimer. However, previous studies have showed that cross-linking the protein affects its stability (Kremneva, Boussouf et al. 2004). On a similar note, during protein purification or dimer assembly, a His-tag is often used to aid purification or visualisation of the protein. Again, it is important to understand the impact this tag may have on the properties of the protein and therefore its function.

Previous thermal stability studies with Tpm were performed under high salt buffer to conditions to ensure that the protein did not polymerise, but the effect of this high salt buffer was not explored against more physiological salt concentrations (Janco, Suphamungmee et al. 2013, Janco, Kalyva et al. 2012). Early dimer assembly worked showed no change in preferential assembly of skeletal β homodimers in high and standard salt conditions (Holtzer, Kidd et al. 1992, Brown, Schachat 1985), which raises the interesting question of if the thermal stability is affected, why does this not alter dimer interactions.

It is known that different isoforms of Tpm have different properties, therefore their expression and dimerization in vitro and in vivo is of great interest (Janco, Kalyva et al. 2012). This is of particular importance when looking at cardiomyopathy mutants and heterozygous affected individuals.

Here, properties of Tpm isoforms were explored as homo and heterodimers, together with the effect of chemical cross-linking, protein tagging and buffer conditions, as well as looking into the effect of known cardiomyopathy mutations.

Measurements of CD spectrum as a function of temperature were used to investigate the thermal stability of Tpm homo- and heterodimers. To explore the secondary structure of Tpm, CD spectra was studied at wavelengths 190 – 250 nm. Spectra were collected at 5 ℃ for the fully folded protein, and at 65 ℃ for the fully unfolded protein.

4.2 Method

The secondary structures of proteins have characteristic spectral properties in CD. CD measurements of α Tpm reveal the structure to be α-helical at 5℃, owing to the fact that it has a positive peak at ~193 nm and two negative peaks at ~208 nm and ~222 nm, as previously described by N.J. Greenfield (Greenfield 2006), Figure 4.2.1, shown in red. Upon heating to 65 ℃, the spectra of the same sample showed a loss of signal across the entire spectrum, indicating the protein is fully unfolded, shown in blue. A control scan of the buffer without any protein showed it had no effect on the spectra, shown in purple.

Parameters for the spectra scan were: sensitivity (standard), wavelength range 190 – 250 nm, temperature as per experiment (5 ℃ or 65 ℃), data pitch (determines how often data points are collected) 0.5 nm, scanning mode continuous, scanning speed 50 nm / min, response 1 sec, accumulation (number of repeated scans) 4.
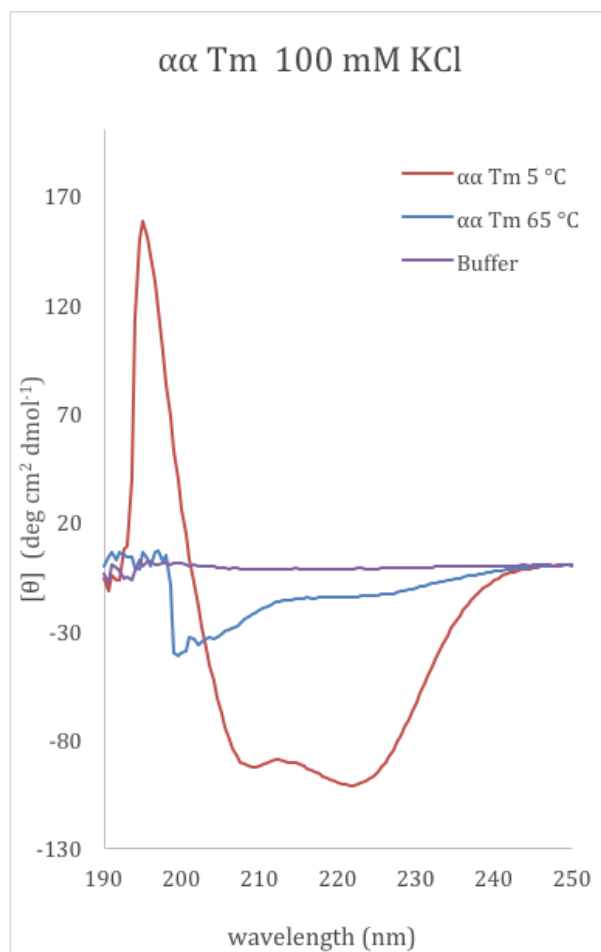
Figure 4.2.1. CD spectra of αα Tpm at 5 °C (red) and 65 °C (blue) and of the buffer alone (purple) under standard conditions: 7 μM Tpm, 100 mM KCl, 20 mM KPi, 5 mM MgCl$_2$, 1 mM NaN$_3$ pH 7.

To investigate the thermal unfolding of Tpm, CD intensity was measured at 222 nm, as this is the most negative peak, giving the strongest signal to measure. CD thermal melts were performed over a temperature range of 5 ℃ – 65 ℃, increasing at 1 ℃ / min, with readings every 0.2 ℃. For each experiment, the sample was heated and cooled multiple times, to check that the protein refolded into an α-helical structure after each cycle.

The first example shown here is of α Tpm homodimer in standard salt (100 mM KCl) buffer in the presence of 1 mM DTT. The same sample was heated and cooled three times. The three identical melting curves are shown in figure 4.2.2.
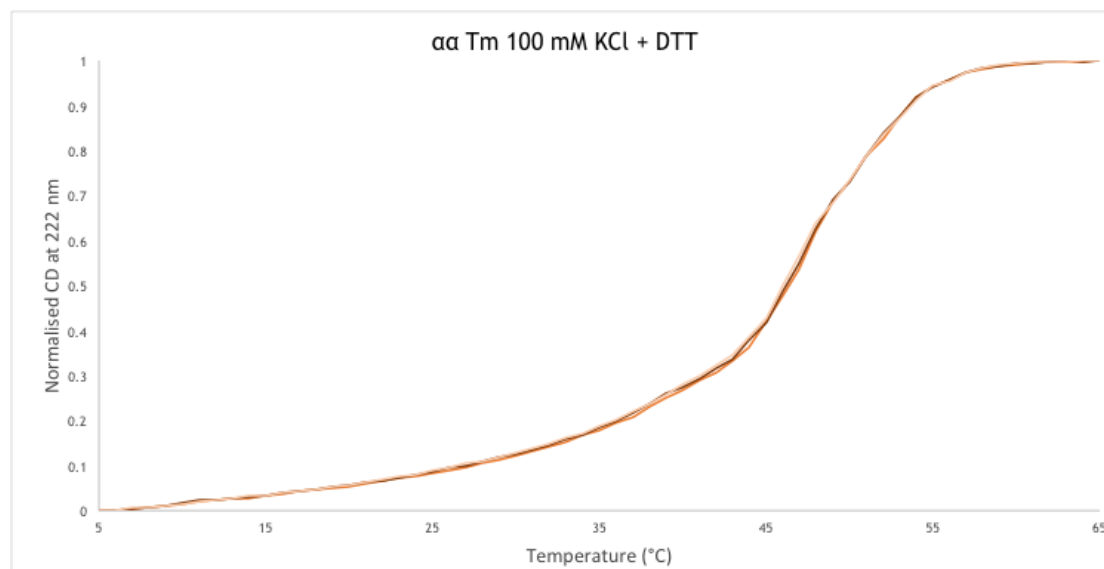
Figure 4.2.2. Melting curves for repeated heating and cooling of the same α Tm sample in 100 mM KCl, 20 mM KPi, 5 mM MgCl$_2$, 1 mM NaN$_3$, 1 mM DTT, pH7, from 5 ℃ - 65 ℃.

Melting curves for each experiment were normalised to enable ease of data comparison using equation 4.2.1. Min-max normalisation performs a linear transformation on the original data values, as shown in figure 4.2.3.

$$Y' = Y - Y_{min} / (Y_{max} - Y_{min})$$

Equation 4.2.1.

Min-Max normalisation of data, where Y_{min} is the minimal data value and Y_{max} is the maximal data value.
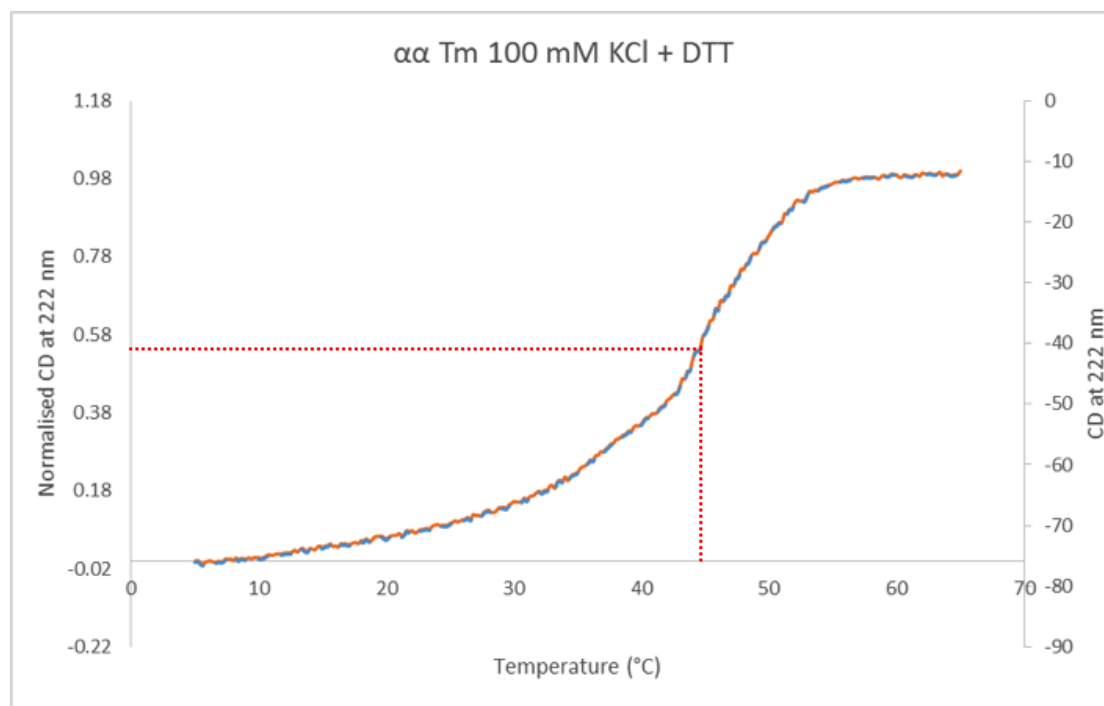
Figure 4.2.3. Thermal unfolding of αα homodimer under standard salt conditions. The melting curves for the raw and normalised data are displayed on the primary and secondary x axis. The data is scaled by the same factor, so the curves are identical. The melting point of the αα Tpm is estimated by the midpoint of the curve; here ~ 44 °C, shown by the red dotted line.

The melting point for α Tpm is ~44 ℃, as indicated on figure 4.2.3 by the red dotted line. Studying this melting curve, it is clear that this is a complex curve, with multiple changes in the slope. Ergo, a single melting point is not sufficient and does not reveal enough about the thermal unfolding of the protein. To explore these inflection points further, the normalised melting curves were differentiated to reveal multiple melting points at which the slope of the curve changes, shown in figure 4.2.4.a.

The first derivative is calculated using the gradient of the slope, change in y divided by change in x, shown in equation 4.2.2.

$$\Delta Y / \Delta X = (Y_2 - Y_1) / (X_2 - X_1)$$

<div align="right">Equation 4.2.2.</div>

To find the derivative of a function $Y = f(X)$, the slope formula changes to equation 4.2.3.

$$\Delta Y / \Delta X = (f(X + \Delta X) - f(X)) / \Delta X$$

<div align="right">Equation 4.2.3.</div>

First differential plots were processed in OriginLab. Firstly, plots were smoothed using the Savitzky-Golay method (25-point smoothing), figure 4.2.4.b This is a built-in tool in OriginLab software that performs local polynomial regression over the data set to determine the smoothed value for each data point. These smoothed plots were then subjected to the Peak Analyser, figure 4.2.4.c, which automatically finds positive and negative peaks that can then be fitted to multiple Gaussian peaks, figure 4.2.4.d. From these Gaussian fits, the midpoints, peak area and half peak width were defined for each unfolding event, which allowed for a quantifiable data set comparison.
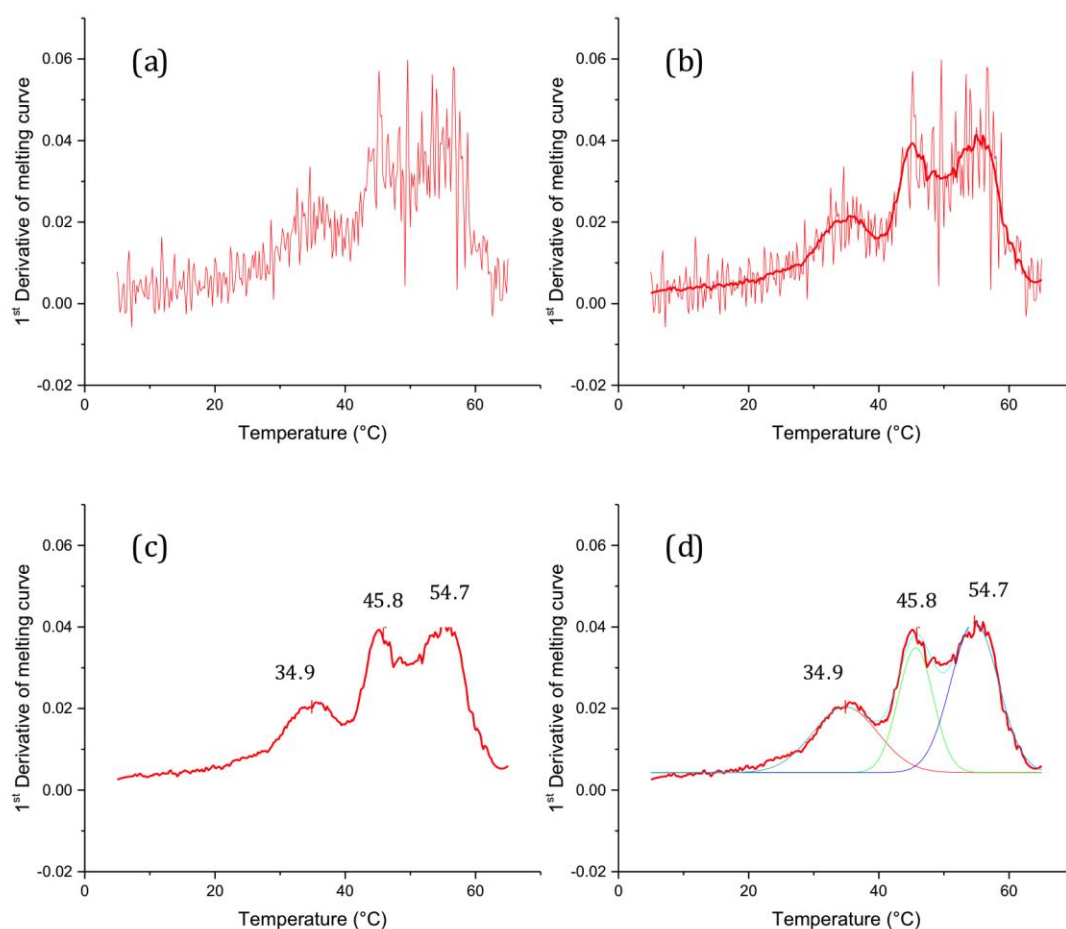
Figure 4.2.4. First differential plots of the melting curve for α-Hisα heterodimer in the absence of DTT. The first differential is shown in the top left (a), which is then smoothed (b). The smoothed plot is then subjected to the Peak Analyser (c) and the peaks detected can then be fitted to multiple Gaussian fits (d).

The multiple Gaussian fits represent multiple unfolding events of a protein during a thermal melt. These unfolding events may represent localised unfolding of the protein, for example, the C-terminus, N-terminus and global unfolding, however, it is difficult to accurately assign these events. During this chapter I will discuss these events and regions of unfolding with respect to the protein being studied, to hypothesise what these events may relate to. To begin, homodimers of α and β Tpm were explored, before exploring the effect of His-tags, buffer and salt conditions and a DCM mutant E54K.

4.3 The use of DTT to explore monomeric Tpm

Thermal melts were performed in the presence and absence of 1 mM DTT, figure 4.3.1. The presence of DTT reduces the disulphide bond in the dimer, which can mean the first melting curve is different to the subsequent melting curves, as the bond is initially broken and then the DTT maintains the protein in a reduced state. However, if the starting material is monomeric, without any spontaneous, or chemically formed cross-links, all three melting curves should be identical.

In the absence of DTT, the melting curve of a cross-linked dimer can be determined. Under these conditions, all the melting curves should be identical, assuming 100% cross-linking at the start of the experiment; as no disulphide bonds are reduced by the DTT during the thermal melts. Cross-linking of Tpm occurs naturally, but can also be chemically induced, as previously described in materials and methods chapter 2.2.6.

Thermal melts of α Tpm homodimers were performed under standard salt buffer conditions in the absence and presence of DTT. In the absence of DTT, shown by the purple dotted line, figure 4.3.1, α Tpm has a notably higher thermal stability at temperatures above 45 ℃, and slightly decreased thermal stability at temperatures below 45 ℃ when compared to α Tpm in the presence of DTT, shown by the solid purple line. The changes between the presence and absence of DTT indicated that the starting solution had oxidised and formed some natural cross-links, which were subsequently reduced upon addition of DTT.
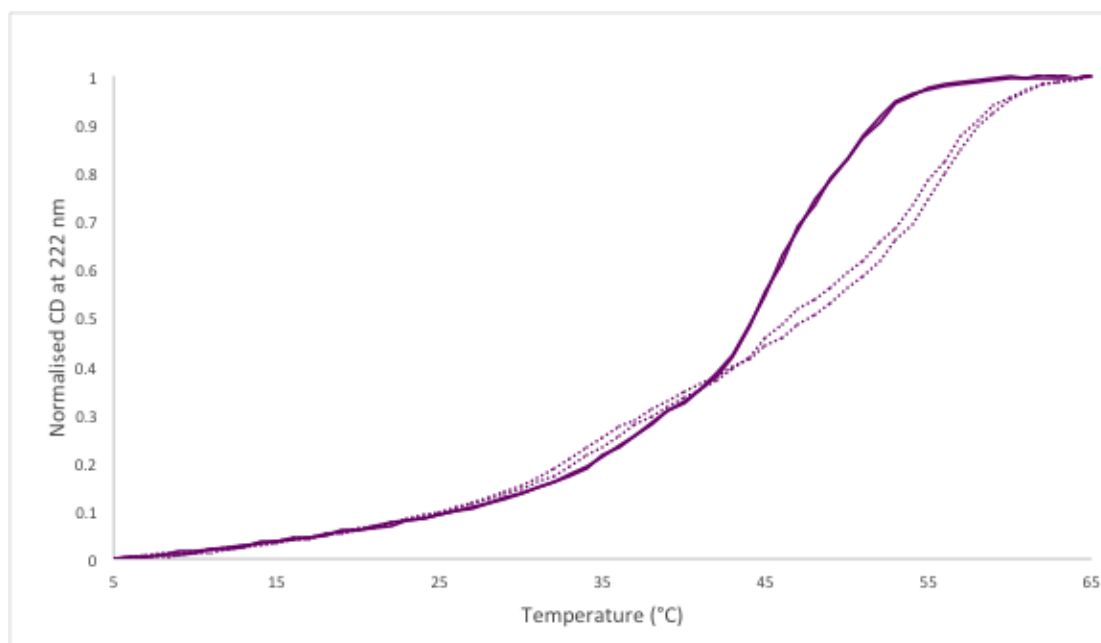
Figure 4.3.1. Melting curves of α Tpm in the presence (solid line) and absence (dotted line) of 1 mM DTT, in standard salt conditions.

In order to ascertain whether or not a change in thermal stability is significant, thermal unfolding events are subjected to a quantitative analysis. The variance between Gaussian peaks (unfolding events) was calculated for each replicate melt of α Tpm in standard salt, high salt and buffers containing either KPi or MOPS. From this variance, the standard deviation was calculated to be 0.49. Using this value, the confidence interval at 95 % was found to be 0.95 ℃. Given this analysis, a baseline of 1 ℃ was used to define the significance of change in thermal stability, opposed to fluctuations between repeated melts of the same protein. This baseline is indicated by a red dotted line, figure 4.4.2.

4.4 Changes in pH during a thermal melt have little effect

Changes in pH may affect Tpm structure and unfolding. It is known that the pH of a buffer will change with temperature. As experiments were performed over

such a wide temperature range (5 – 65 ℃), it was important to determine the pH

changes that occurred over this temperature range and what effect, this may

have on the thermal melts of the protein.

The change in pH for buffers containing MOPS and KPi between 5 – 65 ℃ was

calculated using the temperature coefficient. Given the buffer was adjusted to pH

7 at room temperature, the pH fluctuations between 5 ℃ and 65 ℃ for MOPS

was calculated to be pH 6.7 and 7.6, for KPi, the changes were pH 7.1 and 6.9. The

calculated changes are relatively small for KPi and likely to not affect the protein

significantly. To explore the effect of these changes, thermal melts of α Tpm were

performed in both buffer conditions in the presence of 1 mM DTT, shown in

figure 4.4.1. As before, each sample was heated and cooled three times.
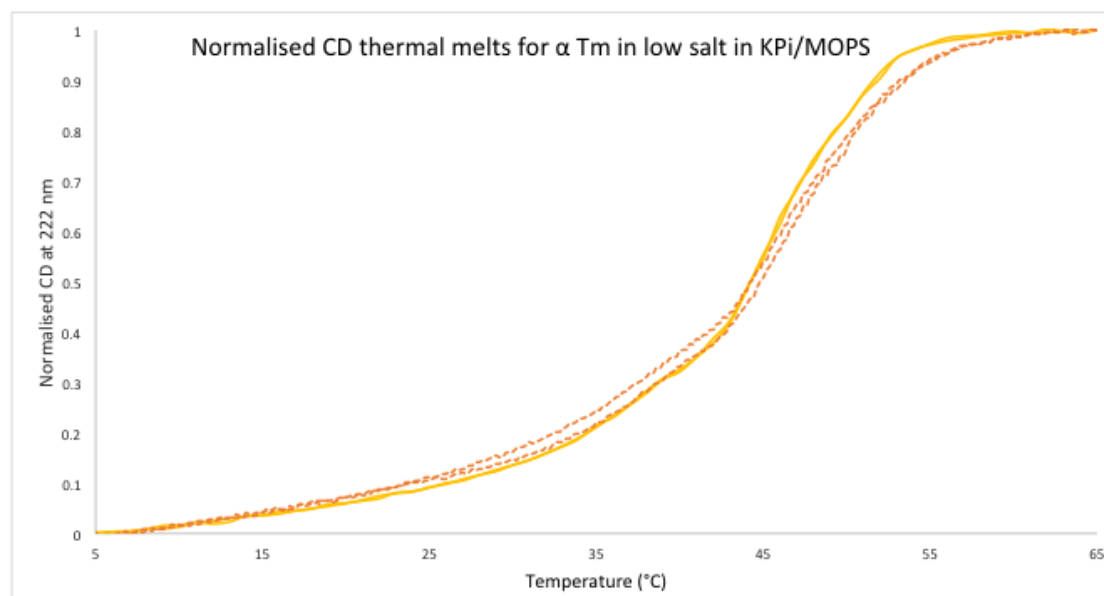
Figure 4.4.1. Substituting KPi (solid yellow line) for MOPS (dashed orange line) on the thermal
stability of α Tpm in standard salt conditions in the presence of DTT

The melting curves for α Tpm under standard salt conditions were very similar in shape across the entire range for buffers containing either MOPS (dashed orange line) or KPi (solid yellow line), shown in figure 4.4.1. The repeated melts of the same sample show similar melting curves, indicating that in both buffer conditions, the protein refolds correctly once cooled.

To determine whether or not any of the slight changes in thermal stability were significant between the two buffer conditions, the melting curves were subjected to first differential analysis as explained in figure 4.2.4. The three Gaussian curves for each experimental condition were then compared as a change in temperature in ℃ (ΔT) for each peak height. Peak 1, 2 and 3 relate to the three Gaussian fits on the 1st differential plots. These peaks correspond to unfolding events at low, middle and high temperatures, respectively.
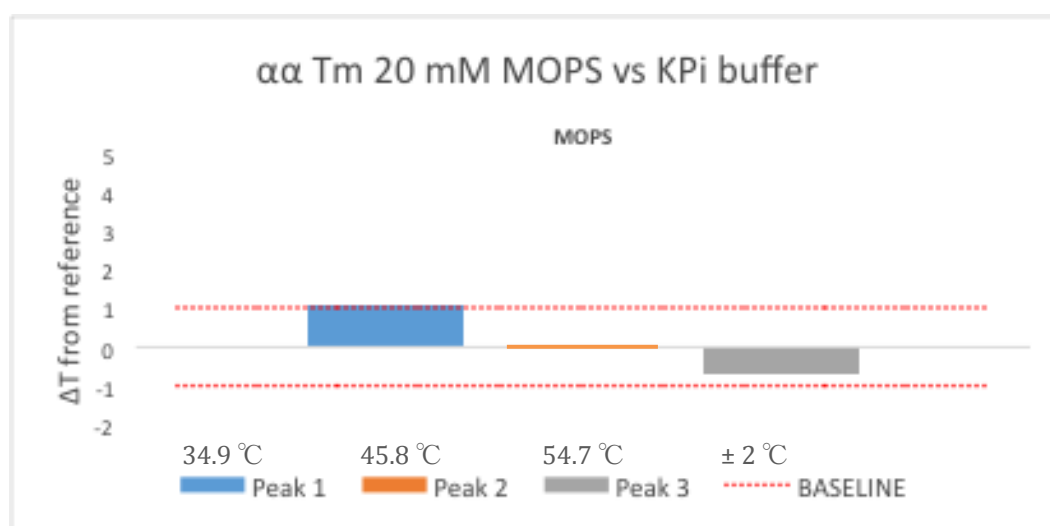
Figure 4.4.2. First differential analysis of α Tpm in standard salt buffer containing MOPS, against α Tpm in standard salt buffer containing KPI, in the presence of DTT. The red dotted line indicates the baseline for significant changes in thermal stability. Peak 1 – 3 represent the three unfolding events at low, mid-range and high temperatures.

The change in ΔT of α Tpm in standard salt buffer containing either KPi or MOPS for peaks 1 – 3 was less than 1 ℃, indicating that this change in thermal stability was not statistically significant over the entire temperature range, shown by the red dotted line, figure 4.4.2. The peak height data is shown in table A1 (Appendix) for clarity.

4.5 β Tpm homodimers have a significantly lower thermal stability than α Tpm homodimers

The thermal properties of α and β homodimers were explored first. Previous work on the thermal stability of Tpm by Miro Janco was completed at 400 mM KCl. The high salt conditions prevented Tpm polymerisation and thus limited Tpm-Tpm interactions. This experimental data was reproduced for α and β homodimer. Homodimers were heated and cooled three times sequentially for each sample in the absence of DTT from 5 – 65 ℃. Following this, 1 mM DTT was added to the sample and the protein was subjected to three further heating and cooling cycles. The melting curves for these are shown in figure 4.5.1.
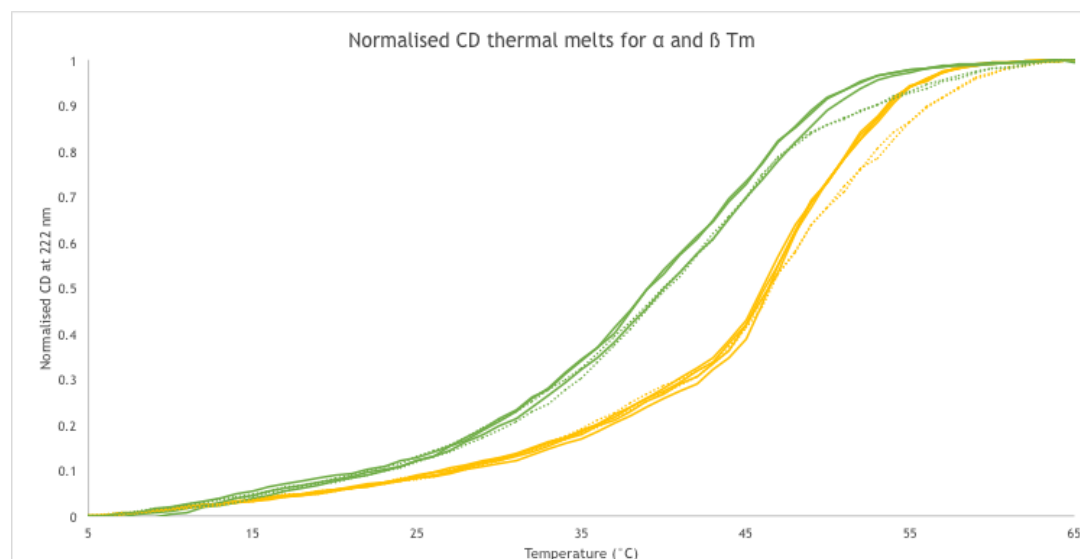
Figure 4.5.1. α Tpm (yellow) vs. β Tpm (green) melting curves in 400 mM KCl, 20 mM KPi, 5 mM MgCl$_2$, 1 mM NaN$_3$ pH7, in the presence (dotted) and absence (solid line) of 1 mM DTT.

Thermal melts for α Tpm shown in yellow, figure 4.5.1, display similar melting curves between each repeated melt, for samples in the presence and absence of DTT, showing the protein refolds and the data is reproducible. The first melting curve in the presence of DTT is omitted here because it shows the breaking of any disulphide bonds present in the protein, which are reduced in melts 2 and 3 of the protein. Thermal melts for β Tpm also showed the protein refolded correctly, both in the presence and absence of DTT, although the overall stability for both conditions was significantly lower than that of α Tpm homodimers.

In the absence of DTT (solid yellow line), the α homodimer showed a decrease in thermal stability at temperatures above 45 ℃ compared to α Tpm in the presence of DTT, (dashed yellow line) figure 4.5.1, shown by the shift right in the curve. At temperatures below 45 ℃, there is little difference between the two melting curves in the presence and absence of DTT. These observations are also

true for the β homodimer; shown in green, figure 4.5.1. Thermal stability was decreased for β Tpm in the absence of DTT at higher temperatures, compared to the thermal melt in the presence of DTT, solid and dotted lines, respectively. Overall, β Tpm showed a dramatically lower thermal stability over the entire temperature range. The shape of the melting curve was also different for β Tpm, with a much more gradual unfolding of the protein, compared to the steep slope of α Tpm.

The shapes of the melting curves were further analysed after differentiation, as explained previously in figures 4.4.1 and 4.4.2 From the Gaussian fits, the mid-points of these curves were compared to find the difference in thermal stability between the β and α isoforms, figure 4.5.2. The peak height data is shown in table A2 (Appendix) for clarity.
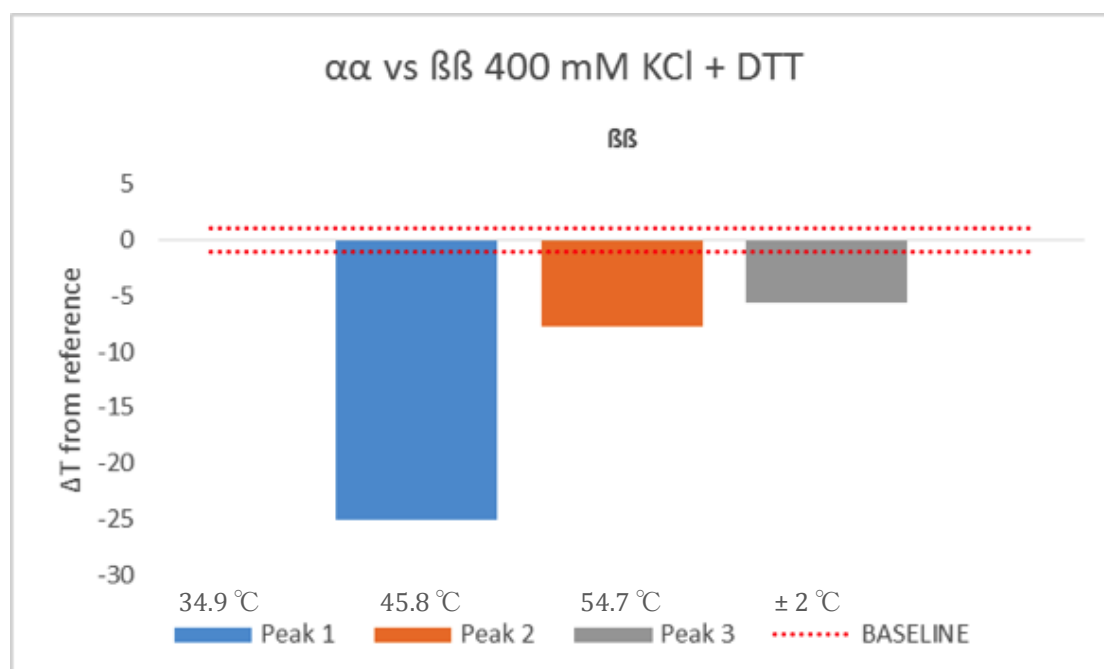
Figure 4.5.2. Changes in thermal stability of β Tpm in reference to α Tpm in 400 mM KCl, 20 mM KPi, 5 mM MgCl2, 1 mM NaN3 pH7. Peaks 1 – 3 represent thermal unfolding events at low, middle and high temperature ranges. The baseline significant change in thermal stability is indicated by the red dotted line.

Comparisons of the two isoforms show that β Tpm is significantly less stable than α Tpm. It is clear that all three peaks are outside the baseline range, indicating that the change in thermal stability is significant. Peak 1, in blue, is the greatest affected peak, with three times the temperature difference, compared to peaks 2 and 3, orange and grey, respectively. All three peaks are significantly destabilised for β Tpm compared to α Tpm. Suggesting at physiological temperatures, the β homodimer may be significantly destabilised or partly unfolded. If β Tpm is expressed and forms a homodimer in the body, it can be postulated that the protein may be stabilised by interactions with actin or Tn, as previous studies have shown up to 3 ℃ stabilisation of Tpm on binding actin (Kremneva, Boussouf et al. 2004).

4.6 His-tags have a small destabilising effect at higher temperatures

Occasionally, the use of a tagged Tpm is necessary, such as in dimer exchange experiments to aid visualisation and purification, ergo it is important to understand what affect, if any, this might have on the protein. Thermal melting curves of His-tagged α homo- and heterodimers in standard salt buffer containing 1 mM DTT were acquired and compared to α Tpm. Melting curves were subjected to first differential analysis, as before, and the change in temperature between the three peaks were compared, figure 4.6.1. The peak height data is shown in table A3 (Appendix) for clarity.
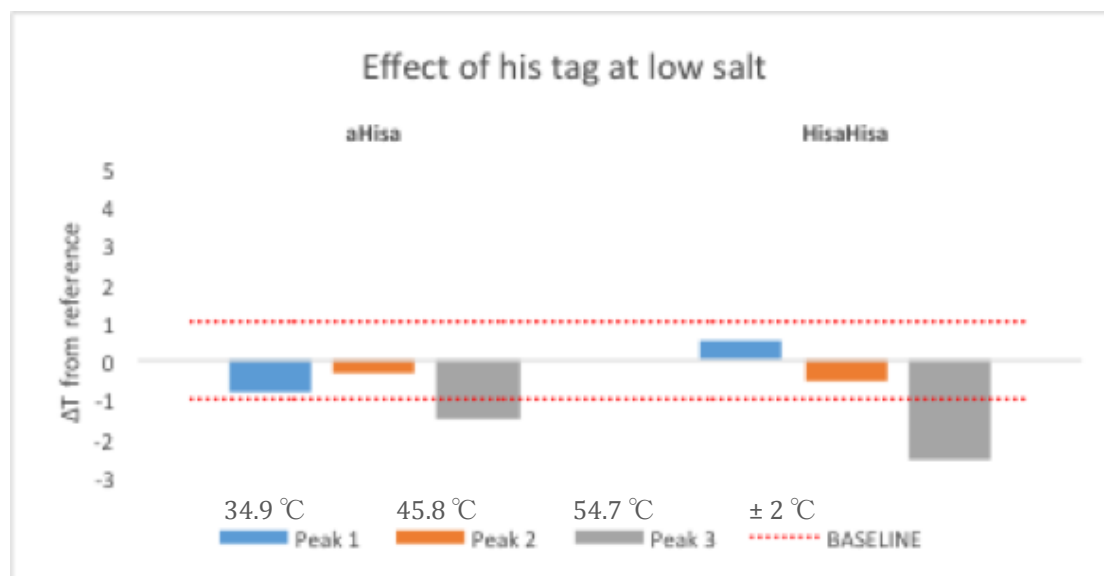
Figure 4.6.1. Changes in thermal stability of Hisα homodimer and αHisα heterodimer Tpm in reference to α Tpm in 100 mM KCl, 20 mM KPi, 5 mM MgCl2, 1 mM NaN3 pH7, 1 mM DTT. Peaks 1 – 3 represent thermal unfolding events at low, middle and high temperature ranges. The baseline significant change in thermal stability is indicated by the red dotted line.

The addition of a His-tag, either as a homo- or heterodimer to Tpm, showed no significant effect on the thermal stability of the protein at low and mid-range temperatures (5 – 50 ℃), showed by peaks 1 and 2 of the first differential analysis of the thermal melting curves. The His-tag destabilises the thermal stability of the protein at high temperatures however, shown by the large decrease in peak 3, shown in grey, figure 4.6.1. This destabilisation is amplified by the addition of a second His-tag on the protein. Though the destabilisation is statistically significant, the changes are only small, 1.5 – 3 ℃. The His-tag is located on the N terminus, with that in mind, one is able to suggest that any changes in the properties of the protein upon addition of the His-tag, would be linked to a change in either the N-terminal region or as a global effect. Ergo, this small destabilisation of peak 3 might attribute this peak to the N-terminal unfolding event, or to the global unfolding of the protein.

4.7 Salt increases the thermal stability of Tpm

Previous work carried out by Miro Janco was performed under high salt conditions to prevent polymerisation. It is of importance to understand what effect, if any, this would have on the thermal stability of the protein.

CD thermal melts from 5 ℃ to 65 ℃ at 100 mM KCl (standard salt) and 500 mM KCl (high salt) were compared as before. Interestingly, increased salt concentration showed an overall stabilising effect on the protein.

The melting curves for standard salt and high salt buffers were very similar in shape, but the high salt conditions showed an increased thermal stability at middle to high temperatures (> 35 ℃). Standard salt buffer conditions displayed a melting point of 44 ℃, while high salt showed a melting point of 47 ℃. The salt effect on stability is the same for the protein in the presence and absence of DTT. In the absence of DTT, the thermal stability of Tpm is increased, as shown by the dotted lines for both buffers, figure 4.7.1.
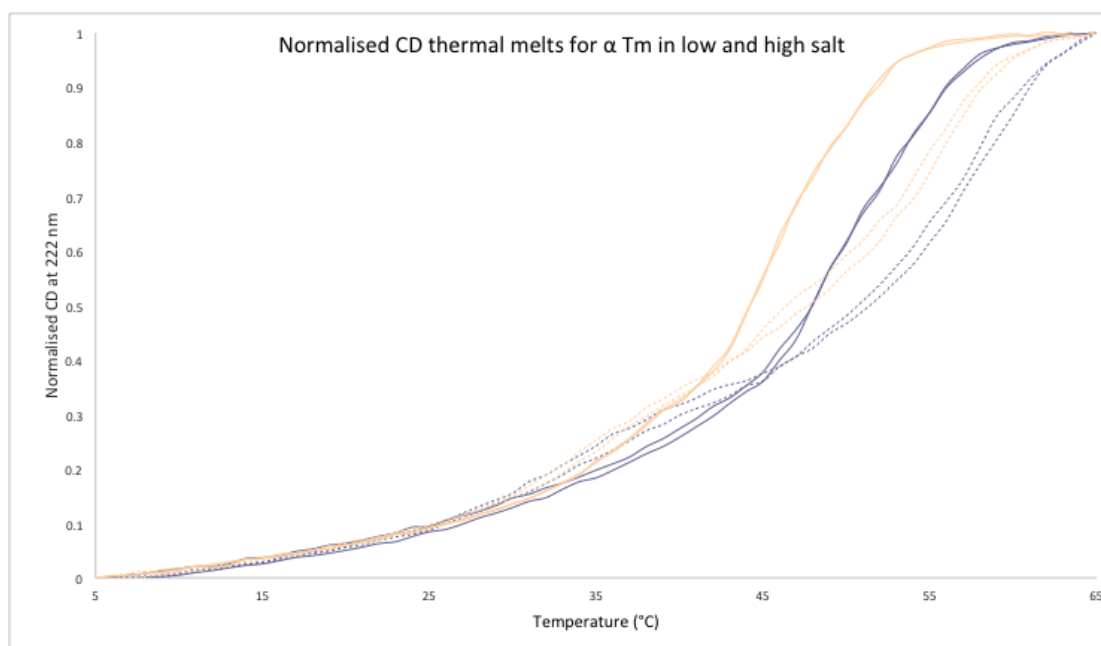
Figure 4.7.1. Melting curves of αα Tpm in low (yellow lines) and high (blue lines) salt buffers, from 5 ℃ to 65 ℃, in the presence (solid lines) and absence (dashed lines) of DTT.

Previous thermal melting data of α Tpm at 400 mM KCl (figure 4.5) was incorporated into this data set, and first differential analysis revealed a cumulative stabilising effect of increasing salt concentration, shown in figure 4.7.2. The peak height data is shown in table A4 (Appendix) for clarity.
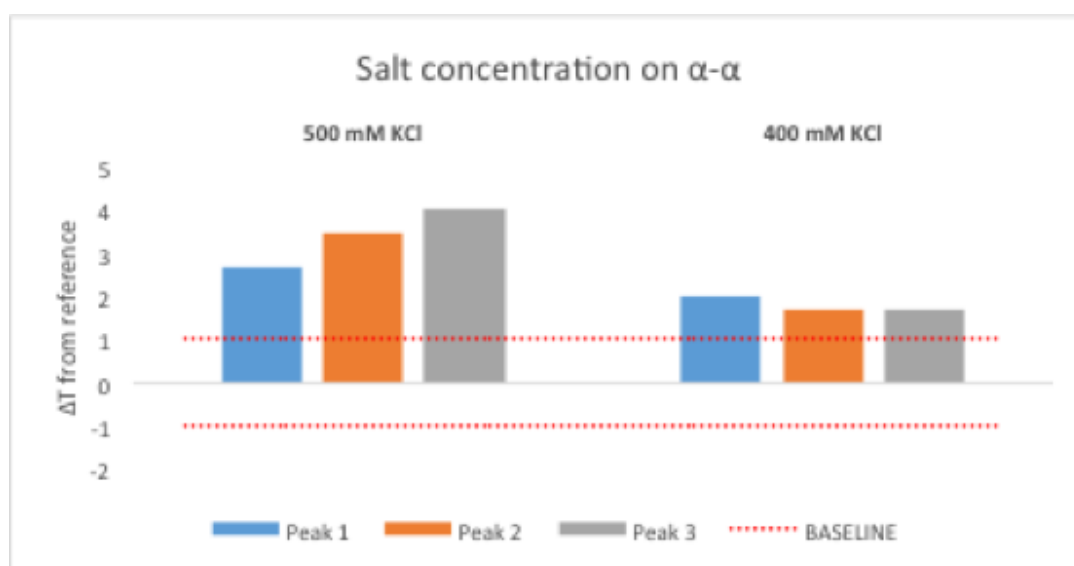
Figure 4.7.2. First differential analysis of α Tpm in 500 mM KCl and 400 mM KCl compared to 100 mM KCl. Thermal stability is increased across all three peaks, and increases with increased salt.

Increased salt concentrations showed a significant increase in thermal stability across the entire temperature range, figure 4.7.2. Thermal stability at 500 mM KCl had an increasing effect as temperature increased, showing the strongest stabilising effect of peak 3 (~4 ℃). The thermal melting curves of Tpm at 400 mM KCl also showed a significantly increased stability across the entire temperature range, but to a lesser extent than that of 500 mM KCl, averaging at ~2 ℃ increase.

The same salt effect was compared for αHisα heterodimers, to explore the effect of the His-tag in these conditions. Thermal melts were performed as before in the presence of 1 mM DTT. Interestingly, the addition of a single His-tag to Tpm reduced the salt stabilisation effect, shown in figure 4.7.3. The peak height data is shown in table A5 (Appendix) for clarity.
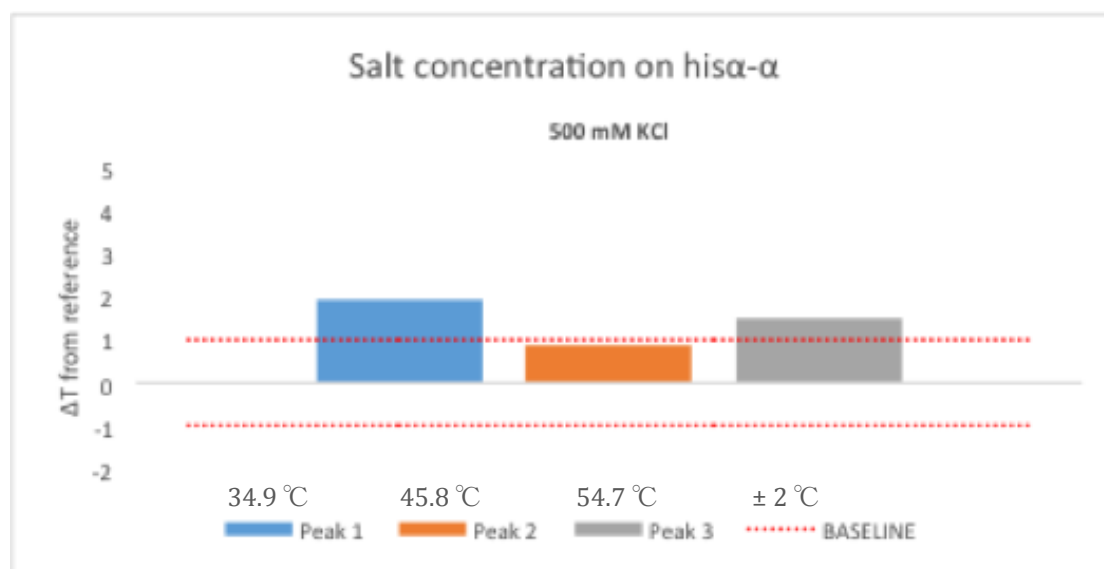
Figure 4.7.3. Changes in thermal stability of Hisα Tpm in 500 mM KCl against α Tpm in 100 mM KCl. High salt buffer increased the thermal stability overall, most significantly peaks 1 and 3.

High salt still had an overall stabilising effect on αHisα, however the extent to which it stabilised the protein was reduced. Peak 1 and 3 showed significant

increased thermal stability of ~ 2 ℃ and ~ 1.5 ℃, respectively. On the other hand, the slight increase in thermal stability of peak 2 was not significant (<1 ℃). This suggests that the destabilising effect of the His-tag, explored earlier, is still prevalent at high salt conditions, but the stability of Tpm could be rescued under high salt conditions.

4.8 The effect of salt on Tpm stability follows the Hofmeister series

To explore whether or not the salt stabilisation is an electrostatic effect, the Hofmeister series must be tested. Salts are organised according to their ability to salt in or salt out proteins, shown in figure 4.8.1. Experimental data thus far has been collected using KCl as the salt component of buffers, which sits in the middle of the Hofmeister series. Salts from either end of the series were chosen to explore their respective effects on protein thermal stability, which were ammonium chloride, NH_3Cl and calcium chloride, $CaCl_2$. As $CaCl_2$ is a divalent ion, it was studied at 33 mM concentration, to ensure the ionic strengths were comparable.
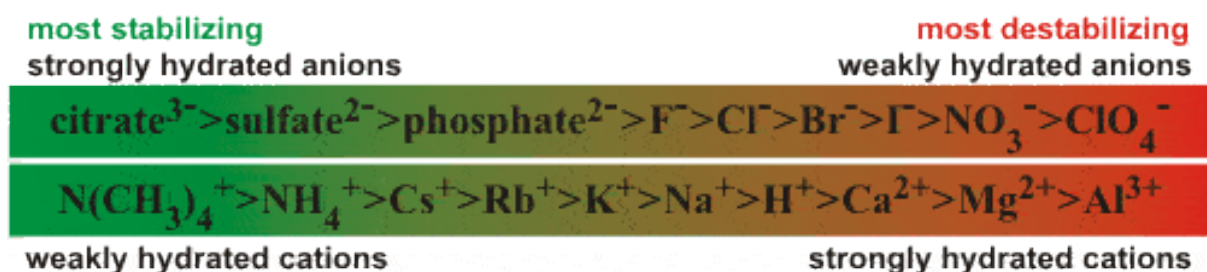
Figure 4.8.1. Hofmeister series of salts; anions and cations that lie on the green side (stabilising) of the scale salt out proteins, while those that lie on the red side (destabilising) of the scale salt in proteins

Thermals melts of α Tpm were performed as previously, with substituted salts in the buffers, and their first differentials were compared to the standard standard salt buffer melting curves, figure 4.8.2. Tpm in the $CaCl_2$ buffer had an extended thermal melting range from 5 ℃ - 85 ℃, as it was seen that the protein was not fully unfolded at 65 ℃.
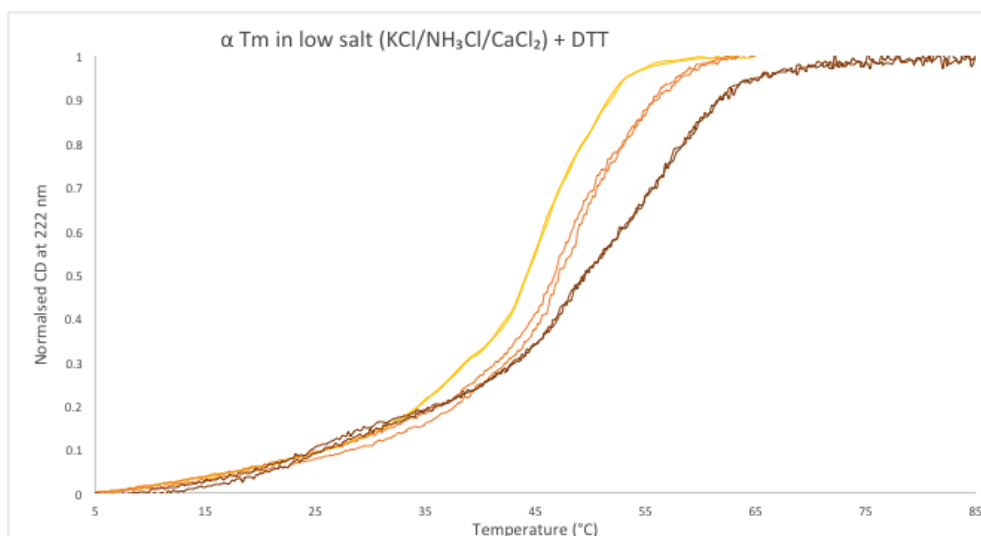
Figure 4.8.2. Melting curves of α Tpm in 100 mM KCl (yellow), 100 mM NH_3Cl (orange) and 33 mM $CaCl_2$ (brown) in the presence of 1 mM DTT.

When KCl is substituted for NH_3Cl, it is clear that there is an increase in the overall thermal stability of the protein, which is similar across the entire temperature range. When KCl is substituted for $CaCl_2$, the thermal stability of Tpm is decreased at lower temperatures but increased at higher temperatures.
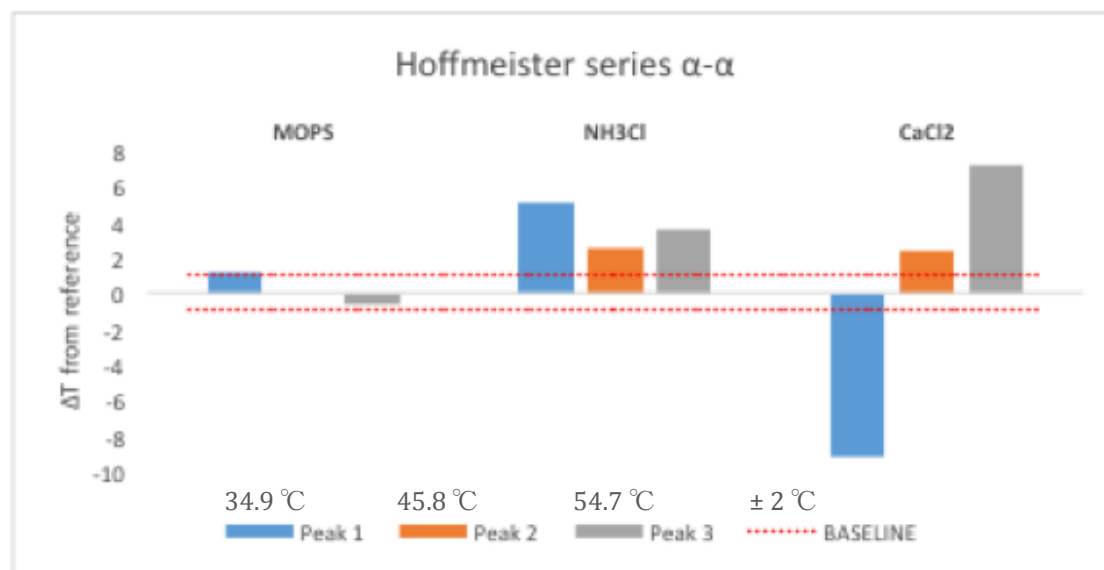
Figure 4.8.3. Changes in thermal stability when 100 mM KCl was substituted for 100mM NH$_3$Cl and 33 mM CaCl$_2$. NH$_3$Cl increased thermal stability over the entire temperature range, which CaCl$_2$ decreased thermal stability of peak 1 and increased thermal stability of peak 2 and 3.

The ammonium cation is weakly hydrated and sits on the stabilising side of the Hofmeister series. These will salt out proteins by increasing their surface tension and therefore decreasing the solubility of non-polar molecules. This effect is commonly utilised in protocols such as ammonium sulphate precipitations. This stabilising effect of this salt was shown clearly in the melting curves, with a 2.5 ℃ - 5 ℃ stabilisation across the entire temperature range, figure 4.8.3. The peak height data is shown in table A6 (Appendix) for clarity.

Calcium is on the opposite end of the Hofmeister series. It is a strongly hydrated cation. Ions at this end of the scale weaken hydrophobic interactions, and as a result, salt in proteins. This salting in of peptide groups mean their ions are strong denaturants. They tend to interact more strongly with the unfolded form, against the native form, which shifts the equilibrium of the reaction towards the unfolded form. The destabilising effect of calcium was clearly seen at lower

temperatures, but the inverse effect was seen at higher temperatures, figure 4.8.3. The valency of calcium increases the potency of precipitation.

The salt effect showed that the thermal stability followed the Hofmeister effect up to physiological temperatures, but also that increasing salt concentration increased thermal stability, which indicated it was not an electrostatic effect. The salt effect at temperatures above peak 1 (~35 ℃) did not follow Hofmeister predictions, most notably for $CaCl_2$. However, these predictions were from previous studies performed at 25 ℃, ergo it is unsurprising the effect is not consistent at higher temperatures. (Baldwin 1996). Studies on the temperature dependence of the Hofmeister series have shown that at temperatures above 37 ℃, ions had different stabilising effects to those previously predicted. For example $[Me_4N]^+$ was the most stabilising cation at low temperatures, but the least stabilising at high temperatures. (Senske, Constantinescu-Aruxandei 2016). The study suggested that ion rankings are temperature dependent, and couple explain the results seen here for calcium.

4.9 Chemical cross-linking of Tpm significantly increases thermal stability at higher temperatures

Before investigating the properties of heterodimers, it is important to understand the effect of cross-linking dimers and to explore the difference between thermal melts in the presence and absence of DTT.

Thermal melts of cross-linked α Tpm homodimers were performed in standard salt conditions, in the presence and absence of DTT, shown in figure 4.9.1. The addition of DTT reduced the cross link, shown in figure 4.9.1. Cross-linked dimers, shown in yellow, showed an increase (∼7 ℃) in thermal stability at temperatures above 45 ℃ and a small decrease (∼ 3 ℃) at temperatures below 45 ℃ when compared to the reduced protein. In the presence of DTT, the slope of the curve was much steeper than the cross-linked Tpm slope. Upon addition of DTT, the cross-link is reduced. The first thermal melt showed the transition from cross-linked to reduce Tpm, and showed an intermediate thermal stability, shown in light blue. The subsequent repeated melting curves showed the fully reduced proteins, dark blue lines.
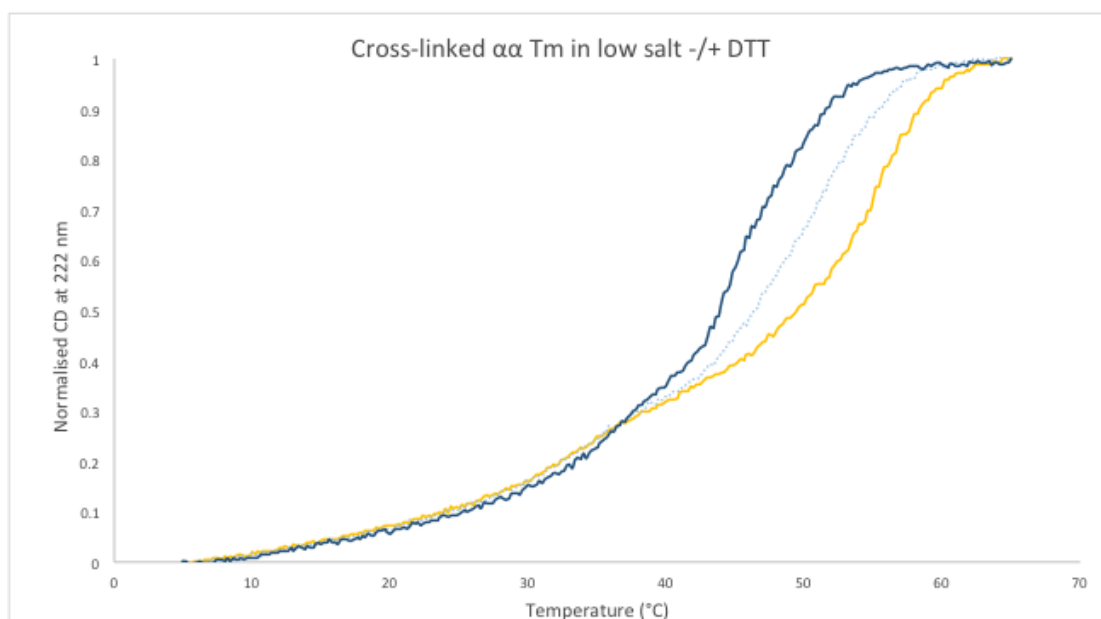
Figure 4.9.1. Cross-linked α Tpm thermal stability upon addition of 1 mM DTT, and reduction of the cross-link. In the absence of DTT (yellow line) the thermal stability is significantly higher at high temperatures and slightly lower at low temperatures, than in the presence of DTT (dark blue line). The first melt upon addition of DTT (light blue line) shows an intermediate thermal stability.

The same pattern of thermal stability can be seen for the His-tagged homodimer, shown in figure 4.9.2. The addition of a His-tag to the protein exaggerates the destabilising effect of the cross-link at low temperatures and stabilising effect at mid to high temperatures, when compared to α Tpm. The Hisα homodimer behaves similarly to αα Tpm, in that upon addition of DTT, the thermal stability of the protein is decreased at high temperatures and increased at lower temperatures, dark blue line compared to yellow line. There is also a transition between the two melting curves for the first thermal melt in the presence of DTT, which lies between the curves in the presence and absence of DTT, shown by the light blue line.
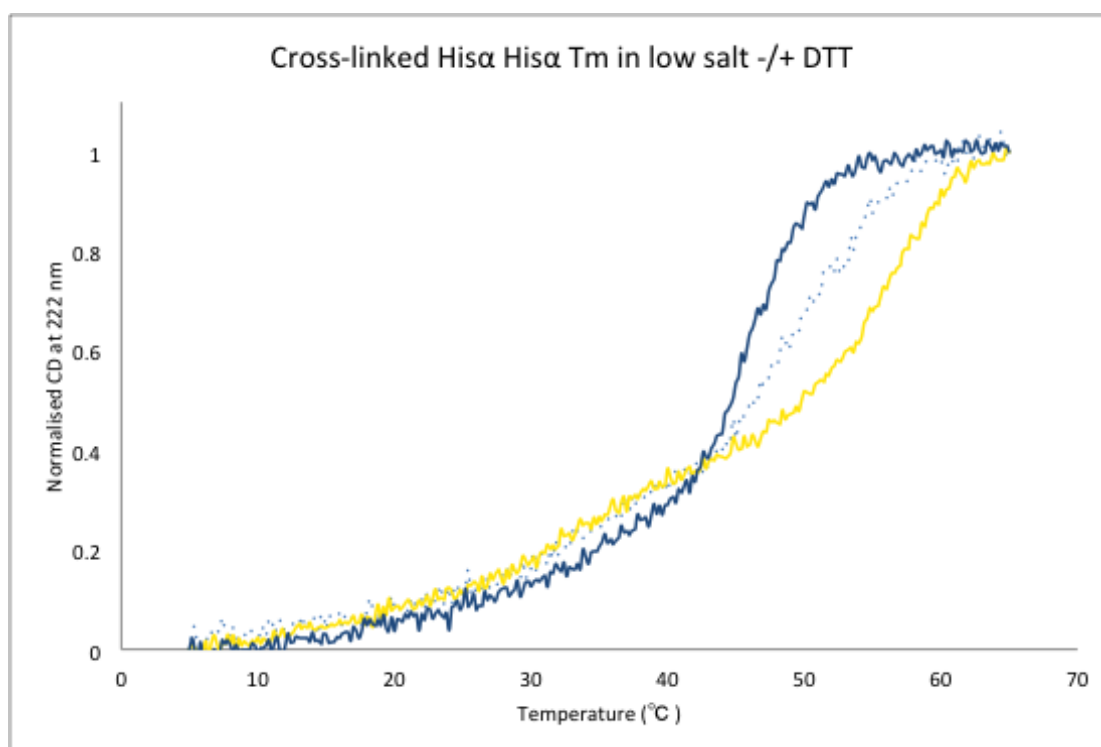
Figure 4.9.2. Cross-linked Hisα Tpm upon addition of 1 mM DTT and reduction of the cross-link. In the absence of DTT (yellow line) the thermal stability is higher at high temperatures and lower at low temperatures, than in the presence of DTT (dark blue line). The first melt upon addition of DTT (light blue line) shows an intermediate thermal stability.

Cross-linking of αα Tpm stabilised the protein at lower temperatures and destabilised the protein at higher temperatures, showed by the analysed first differential data, plotted in figure 4.8.3. Upon addition of DTT the cross-link was reduced. The first melting curve of Tpm after DTT addition was representative of this cross-link breaking, while melts 2 and 3 were the reduced forms of Tpm. Cross-linking appeared to increase the thermal stability of Tpm for peaks 2 and 3, but caused destabilisation of peak 1. The peak height data is shown in table A7 (Appendix) for clarity.
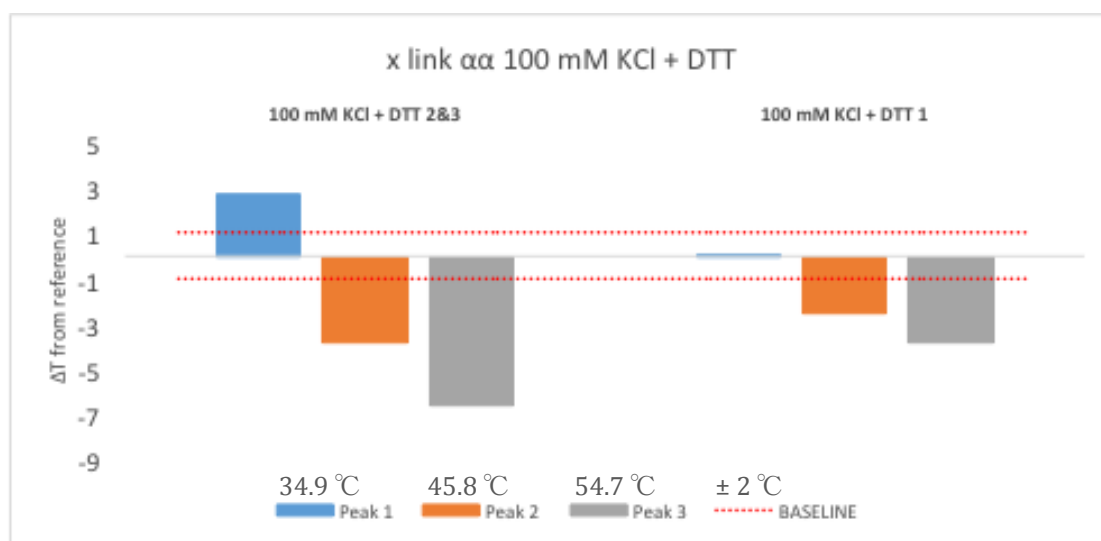
Figure 4.9.3. The effect of cross-linking α Tpm on thermal stability in standard salt buffer (100 mM KCl). The first melt after addition of 1 mM DTT (reducing the cross-link) showed a decrease in thermal stability of peaks 2 and 3 (mid to high temperatures). There effects were amplified for melts 2 and 3 of the same sample (fully reduced). Peak 1 (low temperature) showed an increase in thermal stability, only upon full reduction of the cross-link.

The His-tagged protein showed the same effect of cross-linking. However, the addition of a His-tag amplified the stabilising effect of the cross-link most notably for peak 2, and amplified destabilisation of peak 1 to approximately double that of the untagged protein, figure 4.9.4. The peak height data is shown in table A8 (Appendix) for clarity.
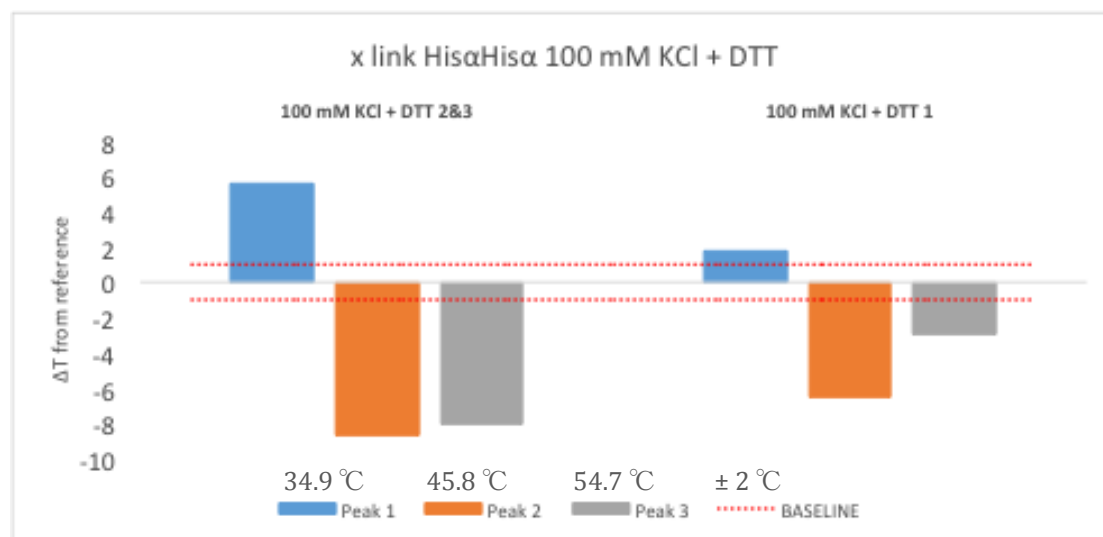
Figure 4.9.4. The effect of cross-linking Hisα Tpm on thermal stability in standard salt buffer (100 mM KCl). The first melt after addition of 1 mM DTT (reducing the cross-link) showed a decrease in thermal stability of peaks 2 and 3 and an increased thermal stability of peak 1. There effects were amplified for melts 2 and 3 of the same sample (fully reduced).

Cross-linking Tpm increased the thermal stability of the protein significantly for mid to high range temperatures, as the chemical process of forming and fixing the disulphide bond adds extra structural stability. Upon addition of DTT, the cross-link is broken, and thus, the first melting curve in the presence of DTT showed this reduction of the disulphide bond. As the bond is broken, the thermal stability of the protein decreased at mid to high range temperatures, and increased slightly at low temperatures. The consecutive melting of the same sample in the presence of DTT then displayed melting curves for the reduced Tpm, which highlighted further reductions of thermal stability at mid to high range temperatures and an increase in thermal stability at low temperatures. This data showed the effect of the cross-link was very significant and therefore not ideal to use during experiments.

4.10 E54Kα heterodimer is less stable at high temperatures

As wild type Tpm is stable and does not show exchange up to 20 ℃, chapter 3, it can be assumed that the first melting curve of a pure heterodimer will be a true heterodimer melt, without the need to cross-link the protein to fix it in the dimer form. The subsequent melts of the same sample however will be a mix of homo and heterodimers, in a random assembly.

Heterodimer samples of DCM mutant E54Kα Tpm were subjected to thermal melting as before, but in the absence of DTT. Only the first melting curve was subjected to first differential analysis. Interestingly, the effect of the mutant is very small. Only changes in thermal stability of peak 3 were significant. Peak 3 of E54Kα were destabilised by ~2.5 ℃ compared to α homodimers under the same conditions, figure 4.10.1. The peak height data is shown in table A9 (Appendix) for clarity.
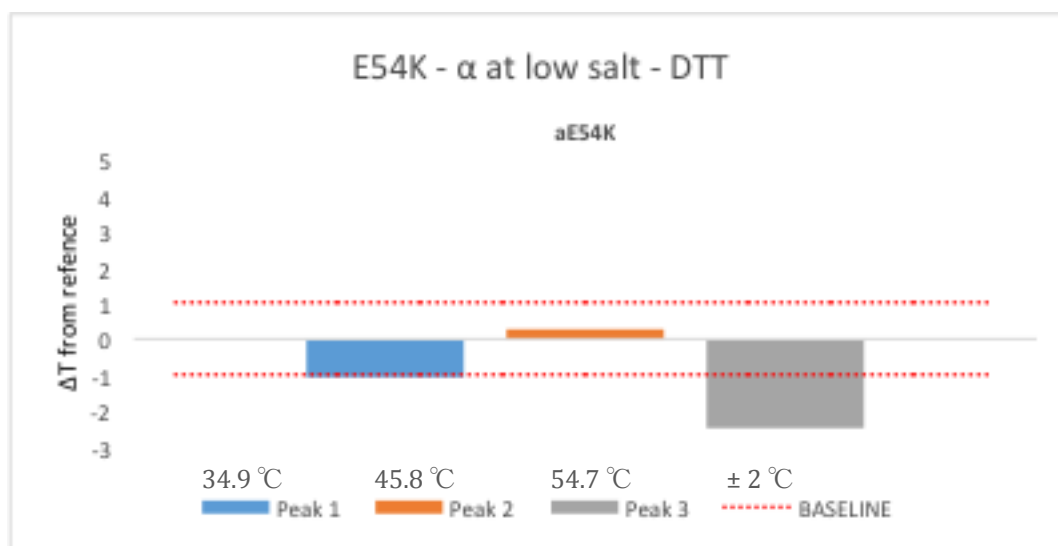
Figure 4.10.1. Changes in thermal stability of E54Kα Tpm in standard salt buffer (100 mM KCl) in the absence of DTT, against αα Tpm under the same conditions. The mutant heterodimer decreased thermal stability of peak 3.

The E54K mutation changes a negative glutamic acid to a positive lysine. E54 is located at position *e* in the heptad repeat and interacts with K49 of the of the opposite Tpm chain, located at position *g* in the heptad repeat. These positions in the heptad repeat are responsible for electrostatic binding between the coiled coil dimer. Therefore, the E54K mutation will result in repulsion of the two positive amino acids and destabilisation of the coiled coil structure.

As the E54K mutation is located in period 2 a of the actin binding motif on the N-terminal region of Tpm, to further study the destabilising effect, the mutant was explored again, as E54KHisα, as the His-tag was also located on the N-terminus of Tpm. Previous data on the effect of the His-tag showed a decrease in thermal stability, notably for peak 3. Whilst one might assume that the mutation in conjunction with the His-tag would show a stronger decrease in thermal stability of peak 3, the inverse was true.

The addition of a His-tag appeared to recover the thermal stability of peak 3 caused by the DCM mutation, but in turn caused a decrease in thermal stability of peak 1, figure 4.10.2. The peak height data is shown in table A10 (Appendix) for clarity.
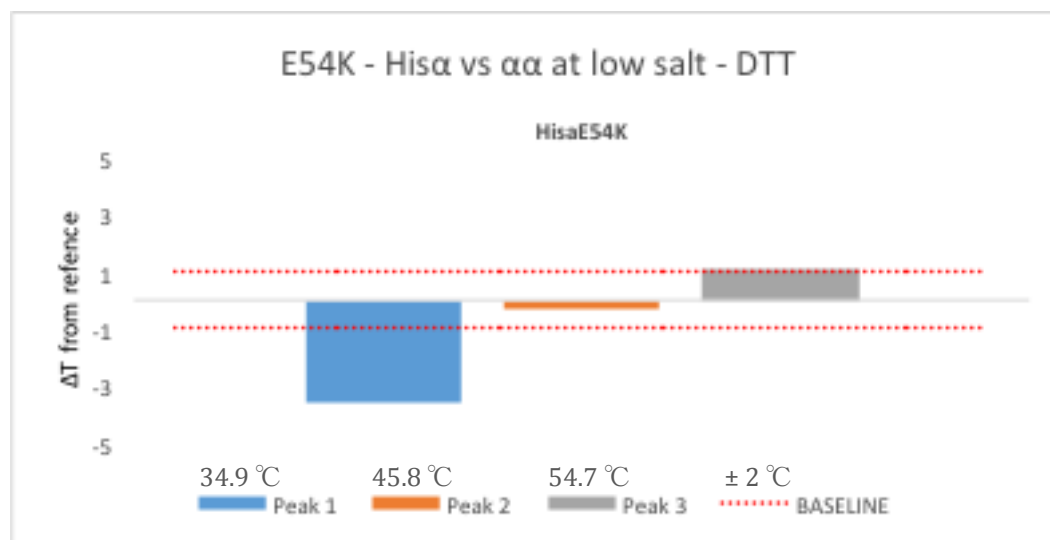
Figure 4.10.2. Changes in thermal stability of E54KHisα Tpm in standard salt (100 mM) in the absence of DTT, against the thermal stability of αα Tpm under the same conditions. The mutant heterodimer showed a significant decrease in the thermal stability of peak 1.

4.11 Conclusions

Different isoforms have different thermal stabilities, for example α and β homodimers, which could give rise to their dimer prevalence. Previous studies, along with data shown here, reveal different characteristics of homodimers and heterodimers. This difference in properties for dimers becomes particularly important when looking at heterozygous affected individuals with cardiomyopathy mutations.

The thermal melting curves for α and β Tpm in 400 mM KCl buffer showed a dramatic difference between the two isoforms. Over the entire temperature range, β homodimers were destabilised, but most notably at low temperatures, wherein peak 1 was destabilise by ∼25 ℃. The shape of the curves was also very

difference, as α Tpm followed a slower more gradual unfolding, while β Tpm had a steeper slope.

The sequence identity between α and β human Tpm is 85.6%, with 243 identical positions and 34 similar positions, out of 284 amino acids, as calculated by UniProt. Of the amino acid changes, 25 occur in the C-terminal region, which is responsible for TnT binding and the Tpm overlap region. The overlap region involves the last 10 amino acids of Tpm, in which there is an amino acid change between α and β, His 276Asn. This change means β is more negatively charged. There is a second negative amino acid change at Ser229Glu for β Tpm. Previous studies have shown that β Tpm binds weaker to TnT than α, which may be explained by this charge change between the two isoforms (Mak, Smillie et al. 1980). Overexpression of β Tpm in cardiac tissue induced severe cardiac abnormalities, including lethality at 10-14 days postnatally (Muthuchamy, Boivin et al. 1998, Smillie 1996).

The thermal stability of cys-containing regions of Tpm, and therefore C-terminal domains, have been previously explored and showed decreasing stability from α homodimers, αβ heterodimers and β homodimers in that order (Lehrer, Joseph 1987). With the significant destabilisation of the C-terminal region and the large destabilisation of peak 1 for β Tpm, it can be postulated that peak 1 in the thermal melt may represent the C-terminal domain unfolding event. The significant differences in thermal stability between isoforms, it is clear that isoform expression and dimerization is a delicate balance for it to function normally.

At physiological temperatures, Tpm is shown to be partially unfolded. The structure of Tpm is designed for its role in actin regulation. Local instability along Tpm has been shown to be required for cooperative actin binding. As explained previously, local destabilisation in conferred along Tpm long range. Ergo, mutations will have a global effect on the proteins structure and stability, which will alter its function. So, a disease-causing mutation such as E54K, which is shown to change the stability of Tpm, will affect the Gestalt binding of Tpm to actin, and thus alter its function in regulating muscle contraction.

The effect of mutations can be hard to predict, as shown from the data collected here. This is as a result of different behaviours of homo and heterodimers, but also due to the communication of destabilisation not only locally but also globally along the Tpm coiled-coil. The use of CD to explore thermal stability of Tpm might be able to shed some light on how different mutations of the protein affect its function, whether just locally or globally. This might shed some light as to how mutations of the same protein can cause very different diseases such and DCM and HCM.

It is known that the thermal stability of Tpm will be affected when bound to actin. Previous studies have shown that actin stabilises the C-terminus of Tpm by up to 3 ℃ (Kremneva, Boussouf et al. 2004). In order to study this, Tpm would need to be bound to actin in a 7:1 ratio in order to saturate the filament. At these high concentrations, our CD spectrophotometer would not be able to give an accurate reading. The signal for the high actin concentration would drown out

the signal of Tpm. The experiment was tested using thermal shift analysis (TSA), but the results were inconclusive.

Aside from CD and TSA using fluorescent binding dyes, thermal stability of proteins can be explored using nuclear magnetic resonance (NMR), optical rotary dispersion (ORD), viscosity and other hydrodynamic methods (Pace, Shirley et al. 1989). Differential Scanning Calorimetry (DSC) has been previously used to study Tpm interactions with actin. Results stated that Tpm unfolding curves were altered when in the presence of F-actin, but not phalloidin stabilised F-actin (Levitsky, Rostkova et al. 2000, Kremneva, Boussouf et al. 2004). The phalloidin stabilised actin had an increased thermal stability which enabled separation of the Tpm melting curve signal. On the other hand, unlabelled F-actin overlapped the Tpm signal, which meant the Tpm melting curve was not clearly distinguishable. Changes in the thermal stability of Tpm while in the presence of actin were associated with Tpm dissociation from actin (Kremneva, Boussouf et al. 2004). These methods may provide an alternative means to explore Tpm stability while bound to actin.

The addition of a His-tag to Tpm caused destabilisation of peak 3. This destabilisation of peak 3 for αHisα Tpm was compounded for His-tagged homodimers. The His-tag is located on the N-terminus, indicating that peak 3 can be linked to the unfolding of the N-terminus or a global unfolding event.

As the His-tag does not significantly alter Tpm thermal stability at low to mid-range temperatures, it can be concluded that it should not have a significant

impact of the protein during experimental conditions within this range, e.g. protein purification at 4 ℃, or exchange experiments up to 37 ℃.

The cross-link is formed at cys190 in α Tpm. Cross-linked α Tpm showed destabilisation at low range temperatures, but significant stabilisation at middle to high range temperatures. The cross-link is formed on the C-terminus of Tpm. Previous studies on the effect of this cross-link were explored using DSC, showed just 2 unfolding events (calorimetric domains), which were attributed to C- and N-terminal unfolding events. Kremneva, Boussouf et al. 2004, stated that the N-terminal region unfolds at a lower temperature than the C-terminal region of Tpm, when cross-linked, 50 ℃ and 55 ℃, respectively. However, the reduced protein melts at the C-terminal first with 12 ℃ difference in thermal stability, while the N-terminal showed no change in thermal stability (43 ℃ and 50 ℃, respectively). When a mutant C190S was explored, which prevents cross-linking, the melting profile was similar to reduced Tpm, with unfolding events at 38 ℃ and 50 ℃. However, it was seen that there was a third unfolding event at much lower temperatures (~32 ℃) (Kremneva, Boussouf et al. 2004). This new peak at lower temperatures could be assigned to the C-terminal unfolding event, as the mutation is located in this domain. The signal for C-terminal unfolding may not be strong enough to detect until significantly affected by introducing the C190S mutant.

The data presented here does not fit the previous data well. Given that our study reveals three unfolding events, the two are not directly comparable. It may be

the case that the CD studies and analysis provide a more sensitive method of the thermal unfolding of Tpm. Firstly, we cannot report a lack of change in thermal stability that matches previous data for the N-terminus of Tpm, as each unfolding event showed a significant change. The first melt of cross-linked Tpm in the presence of DTT showed the breaking of the cross-link. This melting curve showed the cross-link stabilised peaks 2 and 3 but had no significant effect of peak 1. The breaking of the cross-link is irrelevant here though, as we are studying the changes between reduced and cross-linked. Once fully reduced, melts 2 and 3, it was seen that peak 1 was stabilised by 3 ℃, indicating that the cross-link had a destabilising effect at low range temperatures. This suggests that the cross-link could negatively affect the protein at experimental temperatures, and thus should be avoided. However, at high temperatures, the cross-link stabilised the protein by 7 ℃, which may be useful, for example during purification when the protein is heated at 59 ℃.

This data provides new light on Tpm thermal stability. It is difficult to assign the three peaks to unfolding events. Earlier work with the His-tag suggests that peak 3 is the N-terminal unfolding event, leaving peak 1 and 2 as global and C-terminal unfolding events. Peak 2 corresponds somewhat to the previous study for C-terminal thermal unfolding, suggesting it can be assigned to a C-terminal unfolding event. On the other hand, data with the C-terminal C190S mutant displayed a new peak similar to that of peak 1 here (Kremneva, Boussouf et al. 2004), suggesting this peak may represent the C-terminal unfolding event, or perhaps a global unfolding event. It may be that the signal for changes in the C-

terminal region are too small to be detected by DSC, however the changes for the

C190S mutant is large enough to create a detectable signal for the C-terminal

unfolding event.

As mentioned previously, Tpm transmits stabilisation/destabilisation long range,

therefore it is difficult to predict how such a modification will affect the protein

locally and as a whole. It is clear here that the cross-link, while located at the C-

terminal region of the protein, affects the protein as a whole, by having both

stabilising and destabilising effects.

The His-tagged homodimer showed very similar effects of the cross-link, with

the exception of peak 2. Peak 2 showed significant stabilisation of 9 ℃ for the

cross-linked protein. As noted before, the addition of a His-tag caused significant

destabilisation of peak 3. It can be postulated that the cross-link might rescue

this local destabilisation, and therefore peak 2 can be attributed to a global

unfolding event. It is interesting to note that while the His-tag has a significant

effect on the protein stability, previous studies have shown that the addition of a

His-tag did not affect Tpm dimerization (Janco, Kalyva et al. 2012).

The thermal stability of α Tpm may be influenced by pH changes during thermal

melts. The changes in pH of buffering components MOPS and KPi were calculated

using their temperature coefficients to be pH 6.7 – 7.6 and 7.1 – 6.9, respectively.

The small variations in pH from 5 – 65 ℃ was explored using CD and was shown

to not have a significant effect on the thermal stability of α Tpm.

The concentration of salt was also explored, as previous work carried out by Miro Janco was performed using high salt buffer conditions to prevent Tpm polymerisation. A high salt concentration could disrupt salt bridges within the protein and thus decrease the thermal stability. However, upon investigation it was seen that under physiological conditions, the thermal stability of the protein was significantly reduced across the entire temperature range, when compared to high salt buffers. Increasing salt concentration was shown to positively correlate with thermal stability.

The salt effect was further explored by substituting KCl for salts from either end of the Hofmeister series. These salts (NH_3Cl and $CaCl_2$) mostly behaved according to their Hofmeister ranking, within which, KCl is in the middle, neither stabilising nor destabilising (Baldwin 1996). The nature of KCl should not contribute to the thermal stability of α Tpm, according to Hofmeister rules.

Previous work on ionic strength dependent stability calculations showed that at standard concentrations, the salt effect was exerted through electrostatic interactions, while high concentrations exerted the effect through non-polar solvation (hydrophobic interactions) (Date, Dominy 2011). The hydrophobic interactions may act to increase thermal stability by stabilising electrostatic repulsions within the protein or exposed charged surfaces.

Tpm is not alone in being stabilised by increased salt concentrations. Previous work with HIV-1 protease showed enhanced stability and catalytic activity with

increased salt concentration. The authors attribute this increased stability of the structure to "preferential hydration" (Szeltner, Polgár 1996).

High salt was shown to also have a stabilising effect on Hisα Tpm, although less pronounced than for α Tpm. Peaks 1 and 3 were significantly stabilised, while peak 2 did not show significant stabilisation. Salt concentration was able to rescue thermal destabilisation by the addition of a His-tag. It is interesting that peak 2 showed no significant stabilisation by increased salt concentration. This is another example of how local and global effects are communicated in the protein, which does not appear to follow any particular pattern, thus making it difficult to predict. The implication of ionic stabilisation of Tpm requires further investigation to understand how and why this happens, which may provide a useful tool for exploring cardiomyopathy mutations.

The effect of the E54K mutation on α Tpm shows a thermal melting curve similar to that of the His-tagged heterodimer. Given its location in the N-terminal region of Tpm, this furthers the idea that peak 3 of a thermal melting curve can be attributed to the N-terminal unfolding event. Interestingly, the addition of a His-tag to the E54K-α mutant showed recovery of peak 3 destabilisation, but significant destabilisation of peak 1. This indicates that potentially one change balances out the other at the N-terminus of the protein, but communicates the destabilisation long range. Peak 1 destabilisation may therefore be linked to either the global unfolding event or to the C-terminal unfolding event. It would be interesting to explore the effect of high salt buffer conditions on the thermal

stability of the E54K mutant, to see whether or not it could recover the destabilisation, as seen previously for the His-tagged protein.

Data presented here reveal numerous changes in Tpm thermal stability, which are likely to affect the function and role of the protein. It is interesting to note that for some isoforms and changes e.g. β homodimers and the addition of a His-tag, although a change in thermal stability is seen, previous studies have shown these do not alter assembly of dimers (Janco, Kalyva et al. 2012, Holtzer, Kidd et al. 1992). This raises further questions as to how these changes are stabilised and what other effects they may have, if not on dimerization, perhaps calcium sensitivity or actomyosin interaction.

As mentioned previously, the three peaks fitted from the first differential analysis of thermal melts can be attributed to unfolding events of Tpm. Given the N-terminal location of the mutation and the destabilisation of peak 3 when compared to α Tpm, this peak could be the unfolding of the N-terminus of Tpm or a global unfolding event. Previous thermal stability data of the effect of the His-tag also showed significant destabilisation of peak 3. As the His-tag and the E54K mutation each affected peak 3, this peak can be attributed to the N-terminal unfolding event. The α/β comparison showed β destabilisation of the C-terminal region of Tpm, and this was reflected in the destabilisation of peak 1, ergo attributing this peak to the C-terminal unfolding event of a global unfolding event. The ability to assign peaks to specific unfolding events provides a platform with which to further explore the protein and how modifications alter structural stability. However, as seen during these experiments, it is not always clear cut as

to which peak can be assigned to which unfolding event, given the communication of stabilising and destabilising effects both locally and globally.

The unfolding events of Tpm have been comprehensively explored over the years, with the number of unfolding events varying from one to four (Sturtevant, Holtzer et al. 1991, Williams, Swenson 1981, Ishii, Hitchcock-Degregori et al. 1992, Ishii 1994). Studies employed CD and DSC, but struggled to resolve discrete stages from the smooth curves. Melting curves of Tpm were shown to have smaller "cooperative blocks", which correspond to the unfolding events of the protein (Potekhin, Privalov 1982). The smaller broad overlapping Gaussian fits proved difficult to analyse and it was postulated that the melting was cooperative, i.e. each unfolding event was dependent on the neighbouring unfolding event stability. It is clear to see, as we further push the boundaries of technology and analytical techniques, the sensitivity and information acquired is ever improving, and as a result, experimental data is subject to changes in deduction.

Chapter 5: The Role of Stiffness in Tropomyosin Function

5.1 Introduction

The relationship between Tpm and Tn along actin filaments highlights a link between Tpm stiffness and its function. In order for Tpm to work with Tn to regulate myosin binding to actin, Tpm needs to move between three positions along the actin filament. This requires Tpm to be flexible enough to move between these positions, but also have a degree of stiffness in order to stabilise the actin and confer cooperative myosin binding (Mckillop, Geeves 1993, Hitchcock-DeGregori 2008, Stewart 2001). As a result, much interest lies in exploring the stiffness of Tpm, relative to its function in muscle. Stiffness can be quantified by looking at the persistence length (L_p) of Tpm monomers (Trachtenberg, Hammel 2010).

The apparent persistence length is measured as deviations from a straight line, whereas dynamic persistence lengths take into account the average curvature of a molecule. Polymers with a larger persistence length have lower flexibility. A simple analogy is spaghetti. Uncooked spaghetti is stiff and given a hypothetical L_p of 1 m. Cooked spaghetti is less stiff, and more floppy, ergo its relative hypothetical L_p is 1 cm, shown in figure 5.1.1.

Figure 5.1.1. Visual representation of L_p using cooked and uncooked spaghetti. Cooked spaghetti has a much lower L_p than uncooked spaghetti. The difference in L_p is reflective of the difference in stiffness between cooked and uncooked.

The average contour length (L_c) of Tpm is ~40 nm (Perry, 2001). Previous AFM data presented for recombinant human cardiac α Tpm provided an L_p comparable to the L_c, at just 1-1.3 times the length (39.5 – 45.8 nm) (Loong, Zhou et al. 2012a). It was suggested that measurements with <100 molecules led to an overestimation of L_p, requiring large data sets for such experimental analysis.

An EM study using bovine cardiac α Tpm calculated an average L_p of ~104 nm from 16 molecules of the protein (Li, Holmes et al. 2010). The low number of particles measured leaves greater room for error, and as suggested by Loong, Zhou et al., leads to an overestimation of persistence length. These measurements of persistence length for tropomyosin, assumed it was straight on average and suggested the protein was flexible. However, measurements of a "dynamic" L_p, suggested Tpm is a semi rigid polymer with an L_p of 460 ± 40 nm (Li, Holmes et al. 2010, Li, Lehman et al. 2010).

Data collected via AFM and EM studies show significant differences in values for persistence length. AFM studies calculated the L_p to be 1-1.3 times the contour

168

length of Tpm, while EM studies calculated the L_p to be ~3 times the contour length. The differences between these values lead to differing conclusions on the stiffness of Tpm and thus its role in regulation of actomyosin interactions.

The discrepancies between data collected via AFM and EM could be as a result of the different imaging techniques, different deposition techniques and surfaces, or it could arise from different analysis methods. The aim within this study was to determine and compare the L_p for α and β Tpm isoforms, with a view to explore these inconsistencies and differences in surfaces and analysis.

Here, we used an AFM image analysis approach to determine the persistence length of α and β Tpm, and therefore study the stiffness of the protein. The results were compared with persistence length values obtained by TEM and previous data reported for AFM. Image data obtained from AFM were analysed using MATLAB to trace the contours of single molecules of Tpm deposited on mica, which was used to calculate the persistence length. The persistence length provides insight into the stiffness and flexibility of the protein, and thus its role in muscle regulation.

5.2 Method

5.2.1 Sample deposition

Tropomyosin was imaged at room temperature on untreated, freshly cleaved mica in low salt buffer (500 μM KCl, 20 mM KPi, 5 mM $MgCl_2$, 1 mM NaN_3, pH7).

Tpm samples were not subjected to repeated freeze thawing. Once expressed and purified from *E.coli*, aliquots were frozen at ~100 nM concentration, in small volumes, to allow single use of aliquots and minimise protein waste. This also ensured samples were monomeric and fresh each use. The mica was freshly cleaved before depositing 5 nM Tpm. Tpm was incubated on the mica before being rinsed with dH$_2$O and dried with N$_2$ gas. Imaging of Tpm on poly-l-lysine coated mica surface was also carried out as per Loong et al. ((Loong, Zhou et al. 2012a).

5.2.2 AFM Imaging

Samples were scanned using ScanAsyst PeakForce Tapping mode on a MultiMode 8 SPM. The majority of images were acquired at scan size 500 nm. The probe used was a ScanAsyst-Air silicon tip on nitride lever (nominal parameters: thickness: 650 nm, length 115 μm, width 25 μm, resonant frequency 70kHz, spring constant 0.4 N/m). Scan parameters of were: Auto z limit 1 μM, ScanAsyst noise threshold 0.1 nm, scan line 2048, scan rate 0.977 Hz. Larger scans scaled up the lines per scan accordingly, to preserve the xyz pixel/nm.

AFM scans have two axes: fast scan and slow scan, fig 5.2.2.1. Line defects are usually parallel to the fast scan axis and samples appear longer in the fast scan axis and shorter in the slow scan axis. Samples were subsequently scanned at 45 degrees to help the scanner reach equilibrium faster.
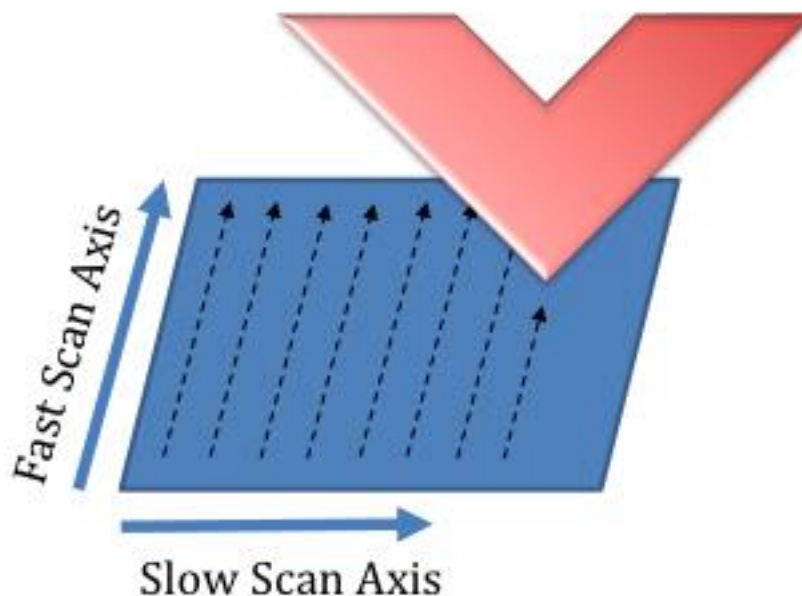
Figure 5.2.2.1. Scan axes of AFM. The probe (red) traces the sample surface from left to right (black dotted arrows), which is the fast scan axis. This motion is repeated down the sample and each line builds the slow scan axis.

The piezoelectric scanner was subject to thermal drift, to minimise this problem, prior to scanning a sample, the AFM was set to scan blank mica at 512 samples/line. This effectively calibrated the scanner to the ambient conditions. Samples were scanned three times, as this showed reduced drift of Tpm in images, figure 5.2.2.2.
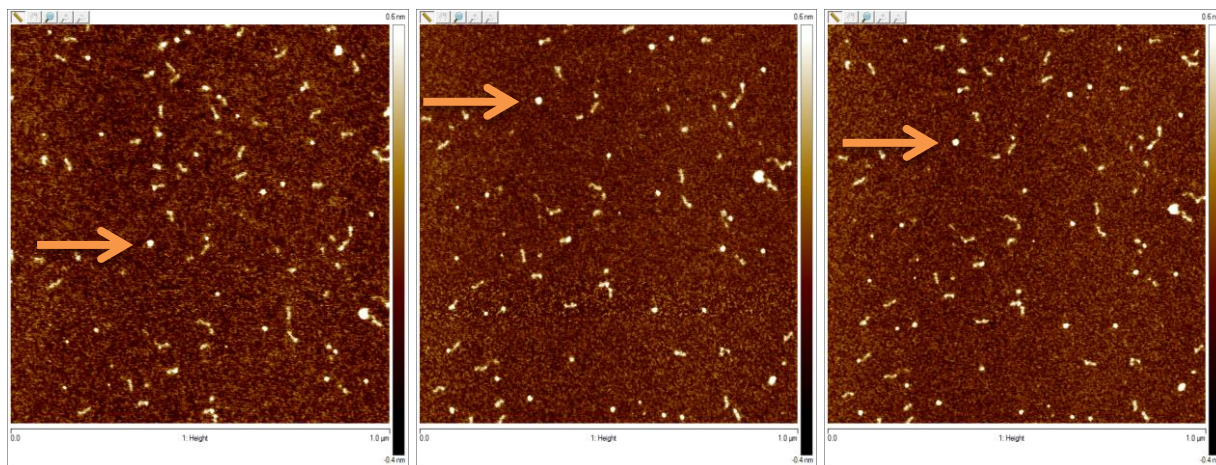
Figure 5.2.2.2. Repeated scans of 1.5 nm Tpm from left to right. Scan size 1 μM, scan rate 0.977 Hz, samples/line 1024, lines 1024. The orange arrow indicates a particle, used for location reference.

Scans up to 1x1 μm were performed using a NanoScope E scanner (S/N: 10001EVLR). This gave good resolution with minimal noise, owing to the compact nature of the piezo scanner. Scans larger than 4x4 μm were performed using a NanoScope J scanner (S/N: 9759JVLR). A hood/muffler was used for larger scans to dampen extra noise. This hood can lead to increased thermal drift, due to an increase in the ambient temperature.

AFM images were processed in Bruker NanoScope software. Images were flattened to remove tilt and scan bow, by identifying background, generating a mask and fitting to a polynomial. Images were flattened in the 0th polynomial order, which subtracts the average Z value for the unmasked segment to remove the Z offset between every point in the scan line. The Z< thresholding direction defines the range in the image for the polynomial calculation relative to the lowest point in the whole image. The thresholding was then applied to the whole

image to mask segments we aimed to trace and flattened the unmasked background noise. These processed ASCII files were then exported to MATLAB for analysis.

5.2.3 MATLAB analysis

Processed AFM images were analysed using a semi-automated image analysis MATLAB script written by Dr Wei-Feng Xue, summarised in figure 5.2.3.1. Briefly, processed AFM images were imported into MATLAB and converted into a square matrix. Polymers were then traced using the MATLAB script. Polymer ends were manually selected and trace parameters defined. The "appWidth" defines the apparent width in pixels. The maxSearchPhi is the search radius in degrees per pixel, for example 30 degrees is 30 + 30 = 60 degrees radius. The zBgThreshold is the background noise thresholding limit.

Polymers are automatically traced and retraced, before displaying the traced polymer on the image as well as a height plot and θ angle plot. The user then manually accepts and saves each individual trace if appropriate. The features from each trace are extracted subsequently. The extracted features show the contour length for each polymer, from which the mean is calculated and histogram plotted. The persistence length is calculated using equation 5.2.3.1.
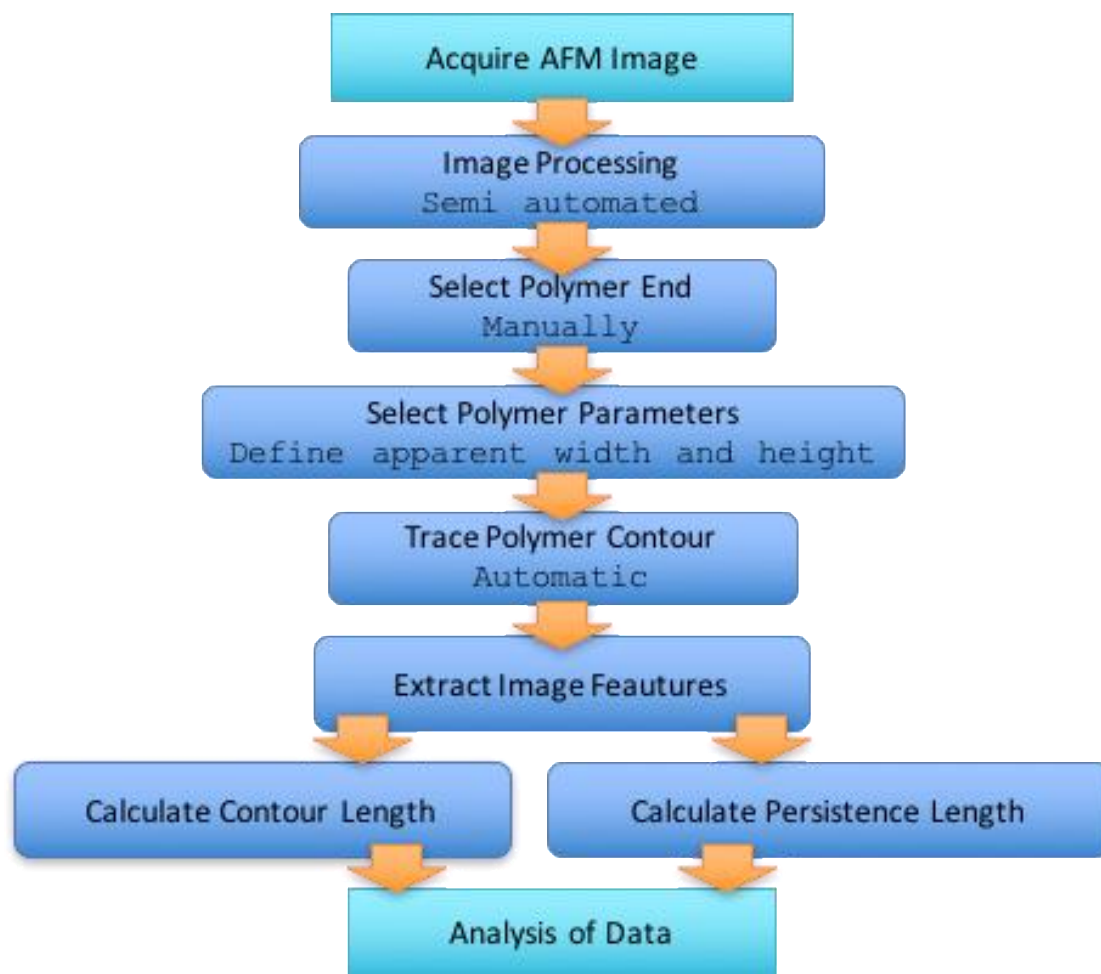
Figure 5.2.3.1. Overview of polymer tracing from AFM images using MATLAB script.

From the AFM images imported into MATLAB, particles are converted to a height colourmap, which helps define the ends of the polymer for tracing, figure 5.2.3.2. The Z axis/height plot shows the Tpm monomer distinct from the background noise, which is flattened in NanoScope Analysis.
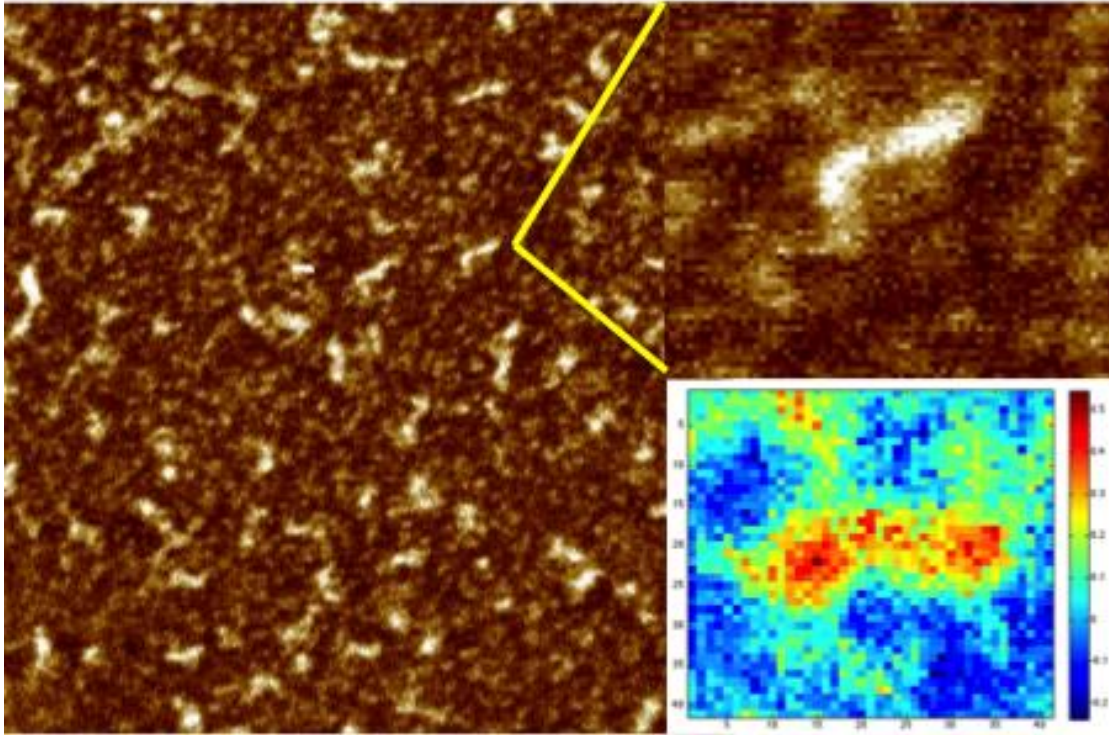
Figure 5.2.3.2. 1 μM scan of α Tpm under normal AFM conditions. Inset: a zoomed in, single Tpm monomer, and below, the same monomer is converted to a colourmap to highlight the height of Tpm in relation to the background noise, which enables detection of ends and tracing of the polymer.

The equation used to describe the persistence length was derived from the wormlike chain model for semi-flexible polymers, equation 5.2.3.1.

$$P\left(\theta_{2D}(L)\right) = \sqrt{\frac{L_P}{2\pi L}}\, e^{\frac{-L_P\theta_{2D}^2}{2L}}$$

<div align="right">Equation 5.2.3.1.</div>

Lp is the persistence length of a semi flexible chain, P is the probability, θ is the angle, and L is the contour length between two points. The probability of finding a bend angle over a given length is a function of L_p.

$$< \cos(\theta_{2D}) > = e^{-\frac{L}{2L_P}}$$

<div align="right">Equation 5.2.3.2.</div>

From equation 5.2.3.2, the average cosine of bend angle theta as a function of contour length is then equal to an exponential decay. Equation 5.2.3.2 assumes the Tpm polymer reaches equilibrium on a 2D plane. For Tpm, a small polymer, equilibration is fast therefore 2D is appropriate. The difference between 2D and 3D projection is a factor of two, and for this comparison it is not significant, given the assumption that α and β do not equilibrate at a different rate.

Previous work published for L_p analysis of DNA using EM and AFM stated that molecules were equilibrated onto a 2D plane up to ~120 nm and 300 nm, respectively. The use of a 2D model was validated using Monte Carlo simulations of DNA molecules following wormlike chain statistics in plane (Faas, Rieger et al. 2009). Given that Tpm is ~40 nm in length, it fits within the length threshold specified for analysis of particles using AFM.

5.3 Optimising imaging conditions

Previous AFM imaging of Tpm in the Geeves & Xue lab was explored at a range of Tpm concentrations from 0.1 nM – 120 μM, and a range of KCl concentrations from 0.105 mM – 500 mM. It was concluded that Tpm traced in low salt concentrations <25 nM had contour lengths closer to the expected contour length of 40 nm than samples traced in high salt buffers; e.g. 500 mM KCl. Optimal coverage of Tpm was obtained by decreasing Tpm concentration,

although even at 50 nM, Tpm was very dense on mica surfaces, making tracing of single Tpm polymers difficult. Optimal imaging conditions were yet to be standardised, however.

There are a multitude of factors that will affect images obtained using AFM. The conditions we chose to standardise were: sample deposition, sample concentration and salt concentration.

Tpm had previously been stored and imaged in high salt (500 mM KCl) buffer, as this prevented polymerisation and aggregation of Tpm. However, it was seen that these high salt conditions altered the stability of Tpm and thus did not give good images on AFM. It is of interest to explore Tpm at physiological conditions, so a range of salt concentrations were explored to standardise best imaging conditions along with more physiological conditions. Salt concentrations were explored at 300 mM, 150 mM, 50 mM and 500 μM KCl buffer containing 20 mM KPi, 5 mM $MgCl_2$, 1 mM NaN_3, pH 7. All samples were explored at 50 nM Tpm, shown in figure 5.3.1.
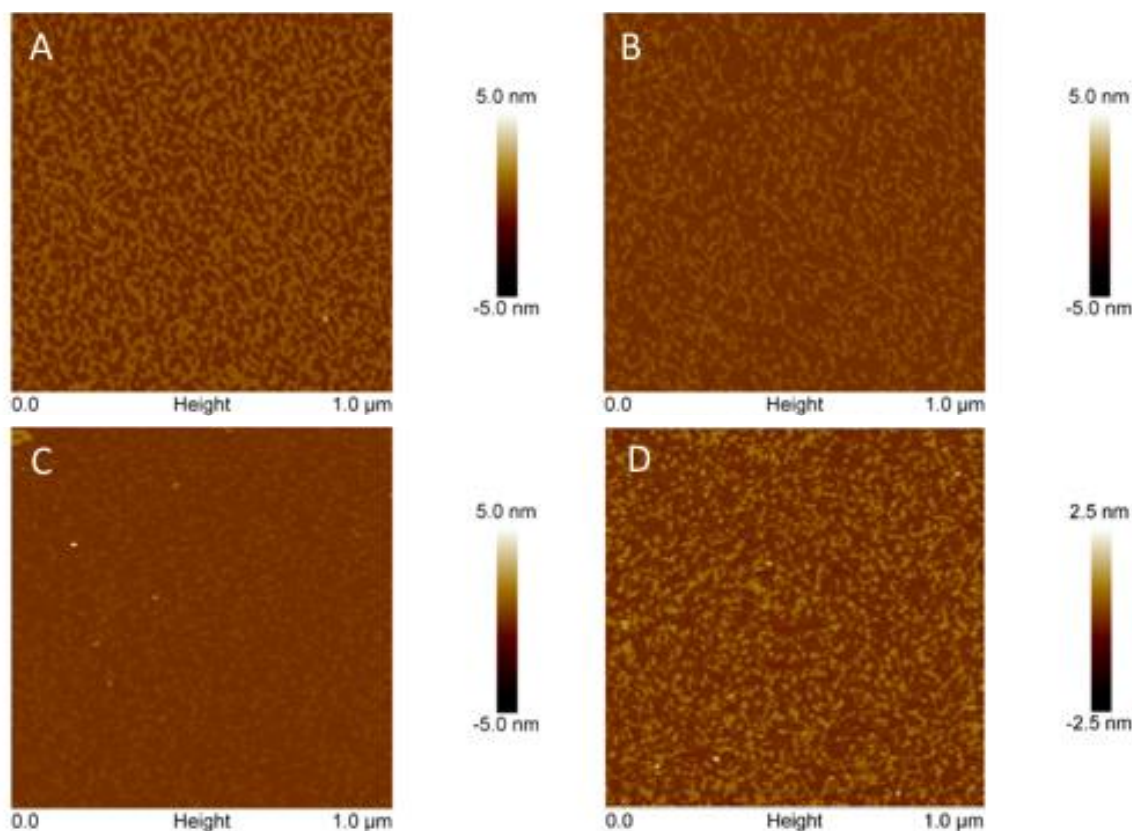
Figure 5.3.1. AFM images of 50 nM α Tpm molecules on mica surfaces. Samples were as follows - A: 300 mM KCl, B: 150 mM KCl, C: 50 mM KCl, 500 μM KCl.

Converse to expectation, samples in buffers with salt concentrations $\geq$ 150 mM KCl, figure 5.3.1.A – C, showed Tpm polymers and clumps, while Tpm imaged at 500 μM KCl, figure 5.3.1.D, showed single Tpm particles. This is unusual as high salt is normally used to prevent Tpm polymerisation. The coverage of Tpm on the surface was too dense to be able to easily trace single particles for all salt concentrations. This indicated that salt concentration did not affect the coverage of Tpm, but did affect Tpm polymerisation. Sample deposition in 500 μM KCl buffers were then explored by changing incubation duration and sample rinsing, as this salt concentration provided the best single particle coverage of Tpm.

The original deposition protocol for Tpm on freshly cleaved mica was 5 minutes incubation, followed by a wash with 1 x 1000 μL of dH$_2$O. Given that coverage was too high following these deposition methods, incubation time and washings were standardised, summarised in table 5.3.1. First, incubation time was decreased to see if this would decrease coverage, and increased washes with dH$_2$O were also explored. Samples were incubated for 2 minutes, and then washed with 1 x 1000 μL or with 10 x 1000 μL. For both conditions, Tpm was not detectable on the mica, so imaging was repeated at longer incubations, but with greater numbers of rinsing.

Samples were incubated for 1 hour and washed with 5 x 1000 μL dH$_2$O. Again, nothing was seen on these surfaces. Incubation time was increased to 2.5 hours, with 3 x 1000 μL dH$_2$O washes, and again, Tpm could not be seen. It was concluded that perhaps the sample was rinsed too often, so Tpm incubated for 3 hours was subjected to 1 x 1000 μL was with dH$_2$O and imaged, but nothing was visible once again.

Imaging was repeated for Tpm in original conditions, with Tpm incubated for 5 minutes before being washed with 1 x 1000 μL dH$_2$O, to check the Tpm sample was not the problem. As before, coverage was too dense to easily detect single Tpm particles. Given that altering incubation times significantly, resulted in no detectable Tpm, imaging was repeated for 5 minutes incubation but washes were increased to 5 x 1000 μL to try to reduce Tpm coverage. There was no visible change in coverage of Tpm, so it was concluded that rinsing did not have a

significant effect. Sample incubation was decreased to 4 minutes with 1 x 1000

μL dH$_2$O wash, but once again, no Tpm was detectable on the mica surface.

It was interesting that sample deposition was so variable to changes in

incubation and washing. It was expected that Tpm deposition would change for

each condition, but not in the simple black and white sense of no Tpm vs dense

coverage. Given the extensive conditions tested, it was concluded that 5 minutes

incubation with 1 x 1000 μL dH$_2$O wash was optimal, so the concentration of

Tpm was next explored to find optimal coverage.

Tpm was imaged at 50 nM, 25 nM, 20 nM, 15 nM, 5 nM and 2.5 nM as before, in

500 μM KCl, 20 mM KPi, 5 mM MgCl$_2$, 1 mM NaN$_3$, pH 7.
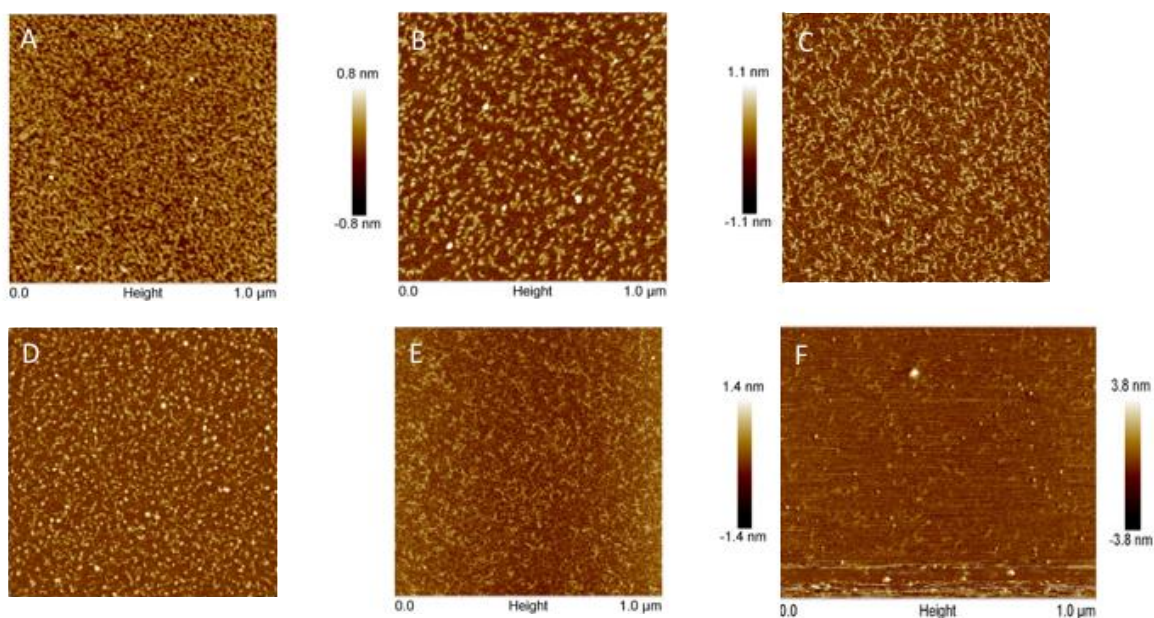
Figure 5.3.2. AFM images of α Tpm in 500 μM KCl buffer on freshly cleaved mica. Samples were as follows - A: 50 nM Tpm, B: 25 nM Tpm, C: 20 nM Tpm, D: 15 nM Tpm, E: 5 nM Tpm, F: 2.5 nM Tpm.

Samples were previously imaged at 50 nM, shown in figure 5.3.2. A. The coverage of this was too high to detect single Tpm particles. Samples viewed at 25, 20 and 15 nM (B, C, D, respectively) showed less coverage but were still too dense. There were also more Tpm clumps or artefacts present at these concentrations. Tpm imaged at 5 nM (E) showed a better coverage of single Tpm particles with minimal clumping, while samples at 2.5 nM (F) showed too little coverage. In figure 5.3.2.F it can be seen that the probe picks up a contaminant during the scan, thus creating an unclear image. The concentration that gave the best images was 5 nM α Tpm, so this was chosen for future work.

Standardisation of all conditions are summarised in table 5.3.1. After optimisation, the best conditions were chosen to be 5 nM Tpm in low salt buffer (500 μM KCl), with 5 minutes incubation and 1 x 1000 μL wash with dH_2O.

Incubation (minutes)	Wash dH$_2$O	[KCl]	[Tpm] (nM)	Result
5	1 x 1000 μL	300 mM	50	Dense polymers, no single particles
5	1 x 1000 μL	150 mM	50	Dense polymers, few single particles
5	1 x 1000 μL	50 mM	50	Less polymers, increased single particles
5	1 x 1000 μL	500 μM	50	Few polymers, dense single particles
2	10 x 1000 μL	500 μM	50	No sample visible
2	1 x 1000 μL	500 μM	50	No sample visible
1	5 x 1000 μL	500 μM	50	No sample visible
2.5	3 x 1000 μL	500 μM	50	No sample visible
3	1 x 1000 μL	500 μM	50	No sample visible
5	1 x 1000 μL	500 μM	50	Dense coverage
5	5 x 1000 μL	500 μM	50	Dense coverage
5	1 x 1000 μL	500 μM	25	Tpm dense, with some polymers and clumping
5	1 x 1000 μL	500 μM	20	Tpm dense, with some polymers and clumping
5	1 x 1000 μL	500 μM	15	Single Tpm dense coverage with some clumping
5	1 x 1000 μL	500 μM	5	Good coverage of single Tpm particles, minimal clumping
5	1 x 1000 μL	500 μM	2.5	Sparse Tpm coverage

Table 5.3.1. Standardisation of AFM imaging of β Tpm on mica surfaces. Optimal conditions are highlighted in yellow. Parameters changed were KCl concentration, sample deposition (incubation and washing) and Tpm concentration.

Incubation (minutes)	Wash dH$_2$O	[KCl]	[Tpm] (nM)	Result
5	1 x 1000 μL	500 μM	5	No sample visible
5	1 x 1000 μL	500 μM	25	Sparse Tpm coverage
5	1 x 1000 μL	500 μM	50	Good coverage of single Tpm particles, minimal clumping

Table 5.3.2. Standardisation of AFM imaging of α Tpm on mica surfaces. Optimal conditions are highlighted in yellow. Parameters for KCl concentration and sample deposition (incubation and washing) were kept the same and Tpm concentration was optimised.

Incubation (minutes)	Wash dH$_2$O	Buffer	[Tpm] (nM)	Result
5	1 x 600 μL	2mM MgCl$_2$, 5 mM NaCl, 20 mM TRIS-HCL, pH 7.5	1	Very dense polymers, no single particles
5	1 x 600 μL	2mM MgCl$_2$, 5 mM NaCl, 20 mM TRIS-HCL, pH 7.5	0.1	Dense polymers, few single particles

Table 5.3.2. Standardisation of AFM imaging of α Tpm on poly-l-lysine coated mica surfaces. Conditions as per Loong et al. are highlighted in pink (Loong, Zhou et al. 2012a)The parameter that was changed was Tpm concentration.

5.4 Primary properties of α Tpm

After optimisation trials, 50 nm α Tpm was imaged in low salt buffer (500 μM KCl, 20 mM KPi, 5 mM MgCl$_2$, 1 mM NaN$_3$, pH 7) using Brukers ScanAsyst PeakForce Tapping mode on freshly cleaved mica, prepared as described in the methods. Tpm at this concentration gave good, clear coverage, with easy distinction of single particles in the images.
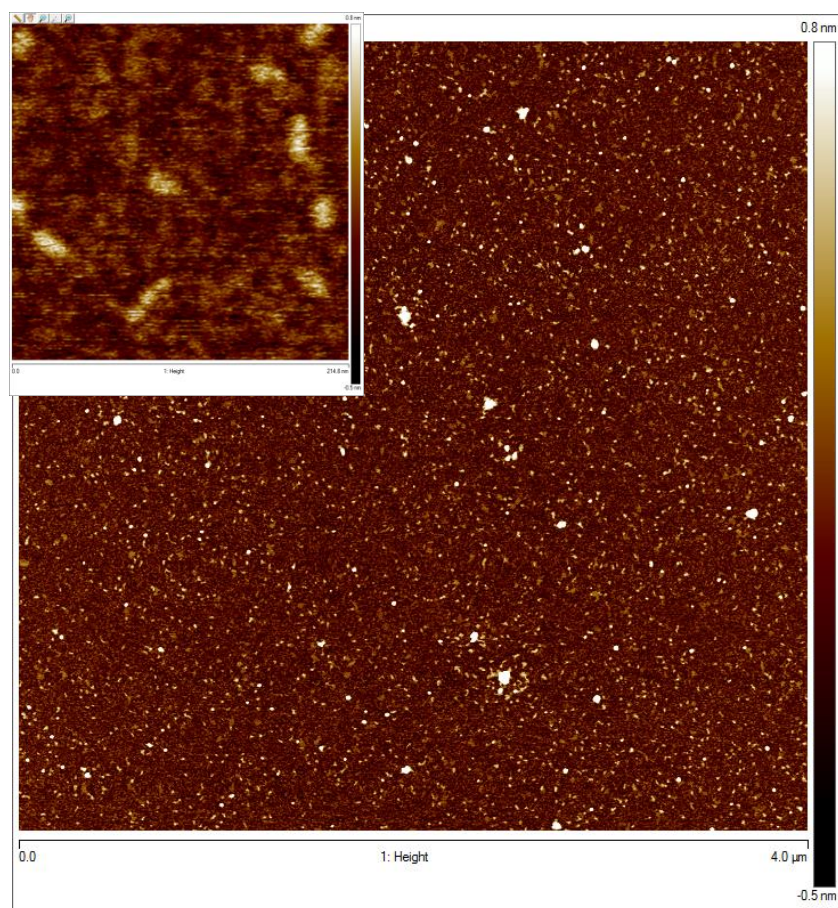
Figure 5.4.1. 50 nm α Tpm AFM scan: size - 4 μM, scan rate – 0.244 Hz, samples/line 4096, lines 4096. Inset: zoomed Tpm monomers

Coverage of α Tpm over the 4 μM scan was good; showing clear single particles, with a few clumps and polymers, figure 5.4.1. The inset shows a zoomed in section, highlighting the single Tpms.

The images were subjected to analysis as explained Section 5.2, to trace the particles. Analysis of the contour length showed α Tpm monomers to be ~20 nm ± 2.8 nm long (95 % confidence interval). There is a small second Gaussian population at roughly double the contour length for monomers (45 nm ± 2.8 nm). This second peak can be attributed to Tpm dimers, which can be expected to occur over time, as these samples were imaged in low salt (500 μM KCl) and in the absence of any reducing agents.
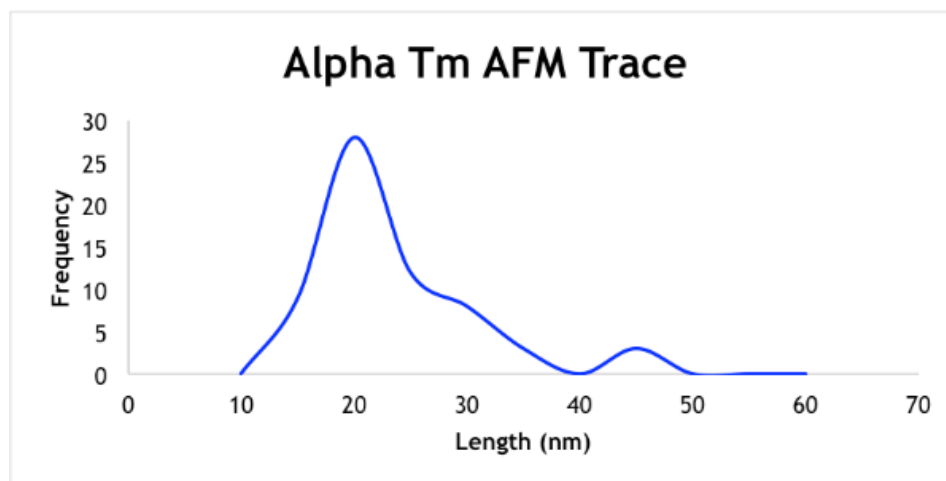
Figure 5.4.2. MATLAB trace data to measure contour length of α Tpm. The average length is ∼ 20 nm, with a second population at ∼ 45 nm, n = 63

The contour length is approximately half the expected length of Tpm. Which not only does not match expected, published values (40 nm), but is different to those previously calculated by both AFM and EM studies. It is also possible that the second, smaller peak is the real Tpm monomer length, and the particles traced at 20 nm are anomalous. The smaller peak could be fragments of Tpm or clumps of the protein. The raw data is shown in table A 11 (appendix) for clarity.

Nevertheless, MATLAB was used to calculate the persistence length, as a value with respect to the contour length. The calculated L_p for α Tpm was 135.7 nm. This measurement of L_p is ∼7 times longer than the contour length, suggesting Tpm is considerably stiff. EM and MD values for persitence length of α Tpm were calculated to be 104 nm and 106 nm, respectively; roughly 2.5 times the measured contour length (Li, Holmes et al. 2010, Li, Lehman et al. 2010). AFM of Tpm on poly-l-lysine coated surfaces on the other hand, revealed the persistence

length to be 1 – 1.3 times the contour length, which is again, much lower than calculated here (Loong, Zhou et al. 2012a).

In absolute terms, the L_p calculated here was similar to those stated in previous publications. However, the L_p relative to the contour length highlights a significant difference. As the contour length measured here was shorter than expected, this could account for structural changes that may affect the measured stiffness of Tpm.

From the MATLAB analysis a cos (θ) plot was generated, which plotted the segment length and bend angle data for α Tpm extracted from the AFM images. This was plotted against the fitted model for the average expectation value for $\cos(\theta)^2$ in relation to segment length, calculated using equation 5.2.3.2. The plot shows how well the model data fits the measured data.
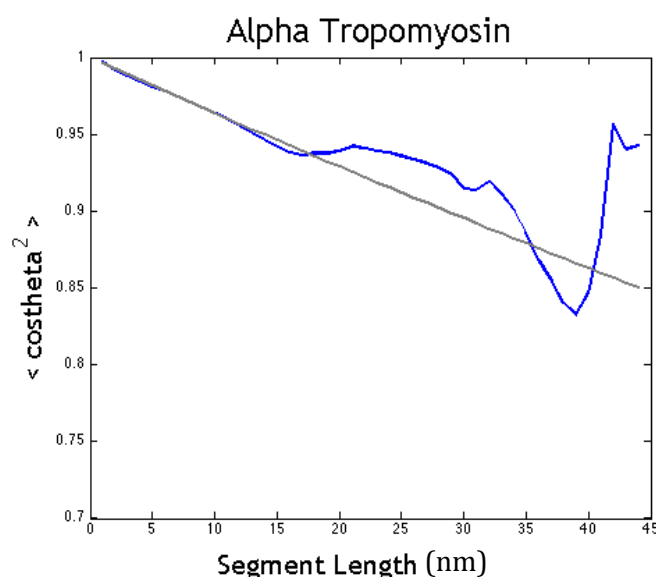
Figure 5.4.3. Fitted model for average expectation value for cos (θ)^2 in relation to segment length, equation 5.2.3.2 (black line) plotted together with α Tpm segment length and bend angle data extracted from AFM images (blue line).

The histogram plot of traced α Tpm, figure 5.4.2, showed the average contour length to be ~20 nm. The majority of particles traced were between 15-30 nm. It can be seen from figure 5.4.3 that the model we fitted to the data followed the data points very well for segment lengths up to 15 nm. There were few particles traced above 30 nm, meaning fewer data for the model to fit to, which will reduce the goodness of the fit. Segment lengths above 30 nm show greater variance from the model, which is expected given the lower number of long particles traced from the AFM images.

5.5 Primary properties of β Tpm

The sequence identity between α and β human Tpm is 85.6 %. Between the two isoforms, there are 39 amino acids substitutions (Heeley, Lohmeier-Vogel 2016). The majority of the changes are located in the C-terminal region. Charge change in the Tpm overlap region result in β Tpm being more negatively charged than α. Both isoforms have distinct properties from one another, so it is likely that the persistence length will be different for each too.

AFM images of 5 nm β Tpm were collected as before in low salt buffer (500 μM KCl, 20 mM KPi, 5 mM $MgCl_2$, 1 mM NaN_3, pH 7) on freshly cleaved mica.
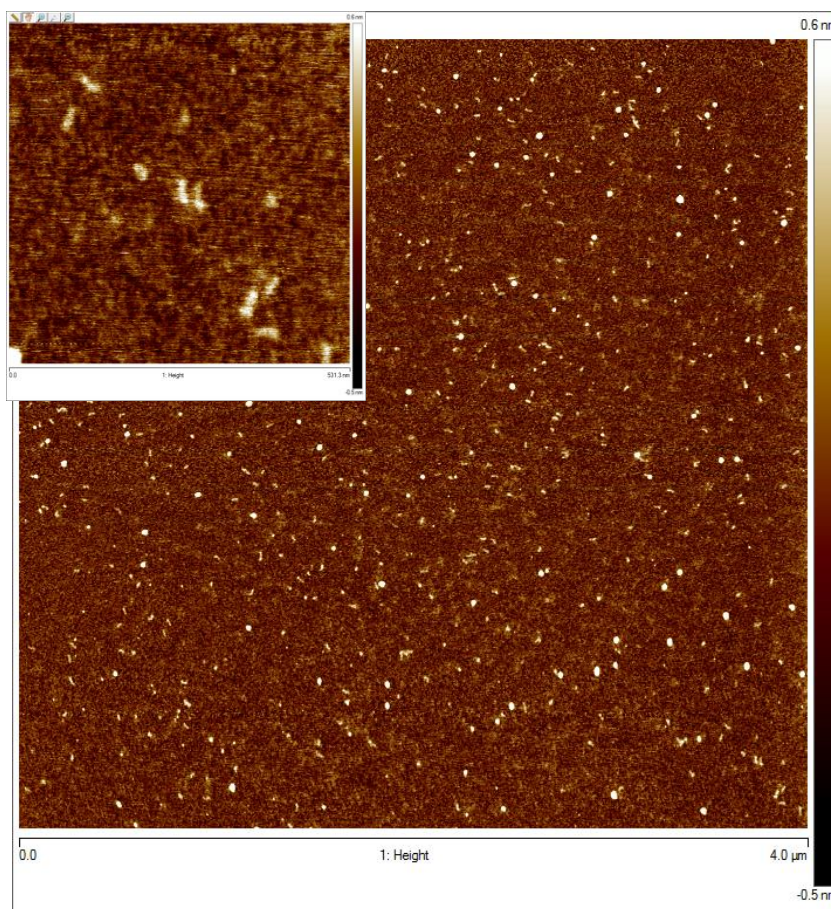
Figure 5.5.1. 5 nm β Tpm AFM scan: size - 4 μM, scan rate – 0.244 Hz, samples/line 4096, lines 4096. Inset: zoomed Tpm monomers

AFM images of β Tpm show good coverage of single Tpm particles, with minimal clumps and polymers, figure 5.5.1. The inset highlights zoomed in section of β Tpm monomers.

Images were subjected to analysis as before, and the average contour length of β Tpm was calculated to be ~ 30 nm ± 2 nm (95 % confidence interval), figure 5.5.2. There is a second small population of Tpm at ~ 55 nm ± 2 nm, which can be attributed to Tpm dimers. The contour length is closer to that stated in literature

than measured for α. As is the case with α Tpm, it is possible that the second Gaussian population is the true length for β Tpm.
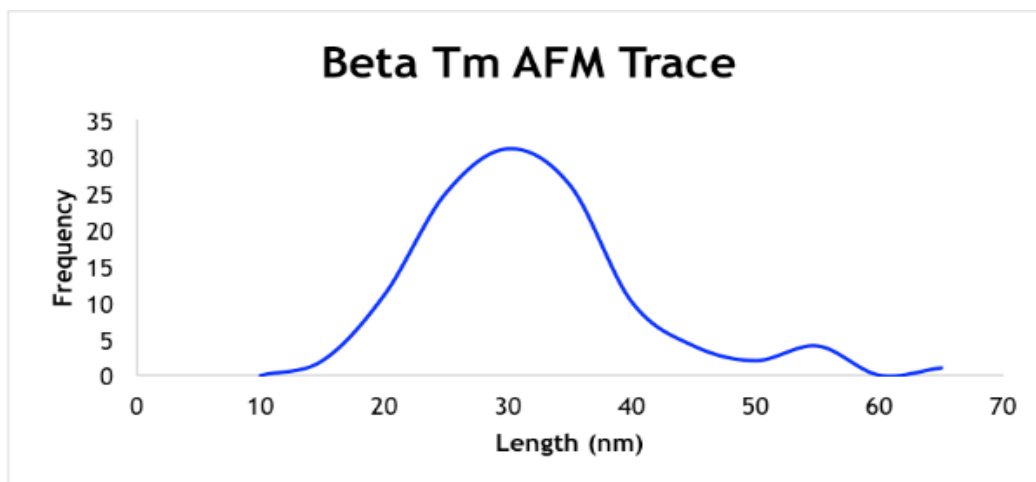
Figure 5.5.2. MATLAB trace data to measure contour length of β Tpm. The average length was ~ 30 nm, with a second population at ~ 55 nm, n = 116

The calculated L_p of β Tpm was 40.9 nm. This L_p measurement is 1.36 times longer than the contour length, which suggests that β Tpm is less stiff and more flexible. The persistence length calculated here matches data previously presented for α Tpm (Li, Lehman et al. 2010, Loong, Zhou et al. 2012a). The persistence length of β Tpm has not been explored previously, so we do not have literature to compare our values to. The raw data is shown in table A 12 (appendix) for clarity.

The segment length and bend angle data for β Tpm extracted from AFM images were plotted, figure 5.5.3. The fitted model for the average expectation value for $\cos(\theta)^2$ in relation to segment length was plotted against the data, showing how well the model data fits the measured data.
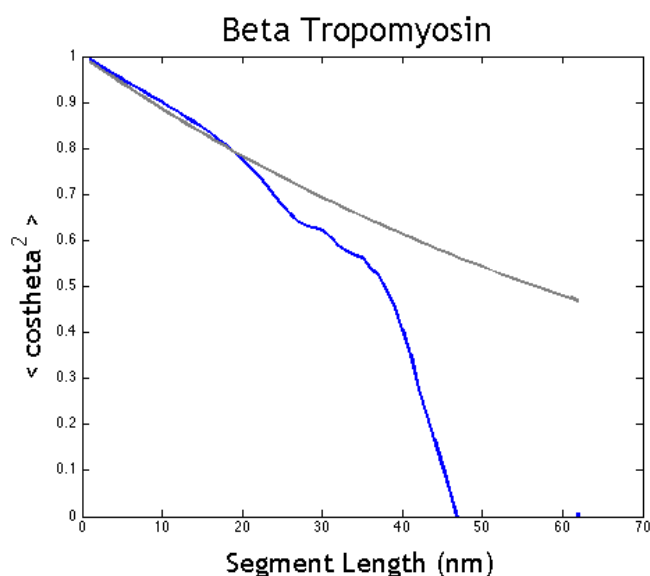
Figure 5.5.3. Fitted model for average expectation value for $\cos(\theta)^2$ in relation to segment length, equation 5.2.3.2 (black line) plotted together with β Tpm segment length and bend angle data extracted from AFM images (blue line).

The majority of particles traced were between 20 -40 nm, with few particles >40 nm traced. As explained earlier, less particles traced at longer lengths means the model data has less measured data to fit to, leading to a decrease in the goodness of the fit.

Up to 20 nm the measured data fits the model data very well. Between 20 nm and 40 nm, there is some deviation from the model data. Above 40 nm, the measured data does not fit the model well, owing to a lack of longer particles that were actually measured.

The α and β isoforms behave somewhat differently when imaging using AFM. It can be seen that α Tpm monomers look shorter and more "blob like" than β, but on the other hand, coverage of β is less than α at the same concentration.

The contour length of β is 10 nm (1.5 times) longer than α Tpm, table 5.5.1. The calculated persistence length of β is one third of α, indicating that β, while longer than α, is significantly less stiff than α.

	Alpha (nm)	Beta (nm)
Persistence Length	136	41
Contour Length	20 ± 2.8	30 ± 2

Table 5.5.1 The measured contour length and calculated persistence length of α and β Tpm. The higher the persistence length, the greater the stiffness and lower flexibility. Errors shown are calculated using a 95 % confidence interval.

5.6 Repeated Loong and Chase protocol for AFM using poly-l-lysine coated surfaces

Data presented here did not match the values stated in the literature for α Tpm, there is no published data for the β isoform. For both α and β Tpm, the contour length was shorter than expected. The calculated L_p for α Tpm was close to that stated in literature in absolute terms (Li, Holmes et al. 2010, Li, Lehman et al. 2010), but proportionally to the contour length, was very different. To ascertain whether or not the difference lay in the data itself or the analysis, the data was

reproduced from Loong et al. imaging of human cardiac α Tpm on poly-l-lysine

coated mica surfaces.

AFM images of 1 nm α Tpm were collected as per Loong et al. 2012, in 2mM

$MgCl_2$, 5 mM NaCl, 20 mM TRIS-HCL, pH 7.5, on 0.01 % poly-l-lysine coated mica.
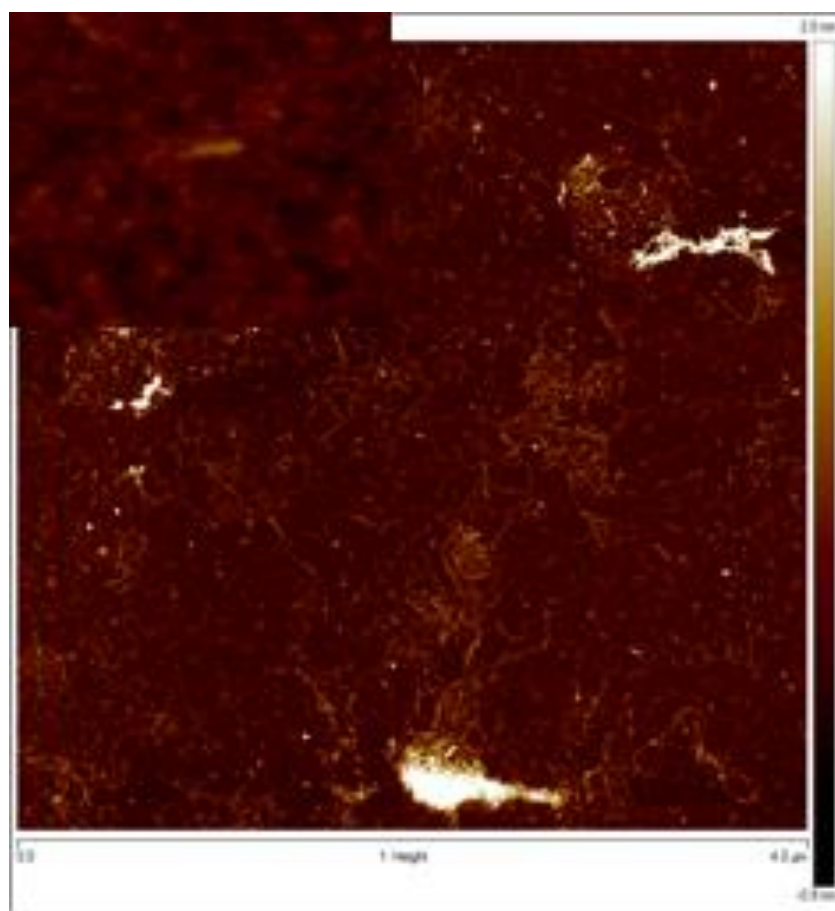
Figure 5.6.1. 1 nM α Tpm on poly-l-lysine coated mica surface. Scan size: 4 μM, scan rate 0.244 Hz, samples/line 4096, lines 4096. Inset: single Tpm monomer

Coverage of Tpm was very dense on poly-l-lysine surfaces, with significant

polymerization and clumping of the protein. There were not many single Tpm

particles that could be easily traced, shown inset figure 5.5.1. Of the particles

traced (n = 8) the contour length was calculated as before to be 20 nm, and the

persistence length was calculated to be 853 nm. There were very few single Tpm monomers to trace, so the protocol was repeated but at a tenfold dilution of Tpm, to try and reduce coverage, thus increasing the number of single Tpm for tracing.
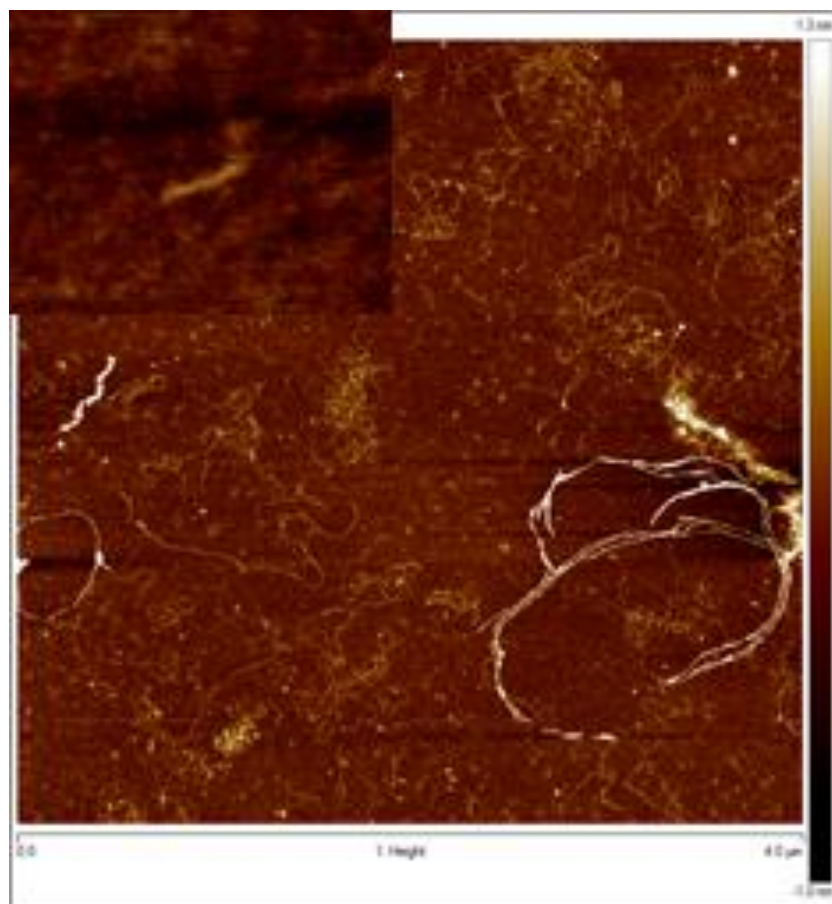
Figure 5.6.2. 0.1 nM α Tpm on poly-l-lysine coated mica surface. Scan size: 4 μM, scan rate 0.244 Hz, samples/line 4096, lines 4096. Inset: zoomed single Tpm

Once again, the coverage of Tpm was too high to be able to easily trace individual particles. There was significant polymerization and clumping of Tpm on the surface. Single Tpm particles were traced, n = 11, and the contour length persistence length were measured and calculated as before. The measured contour length was 29.8 nm and the L_p was 485.6 nm.

There was significant difference between values obtained at 1 nM and 0.1 nM Tpm. The contour length varied by ~ 10 nm (50 %) and there was a twofold difference between the calculated persistence lengths. On top of this, no values, either at 1 nM or 0.1 nM Tpm, matched the data published by Loong et al. (L_c ~ 40 nm, L_p ~ 40 – 50 nm). The number of particles traced here was very low, (n = 8 & 11) and the data was not easily reproducible. As a result, analysis of images was explored to further understand difference between our data and that presented by Loong et al.

To evaluate the differences between analysis used in this chapter and the analysis performed by Loong et al., AFM images of α Tpm presented by Loong, et al. were imported into our MATLAB script and analyzed in the same way as before. The contour length measured from these images were then compared to those published by Loong et al. The average contour length measured was ~ 25 nm. This was much lower than the contour length presented in their publication of ~ 40 nm. The contour length calculated by Loong, et al. included corrections of 4.1 – 4.8 nm to compensate for chain length beyond the end 2 pixels.
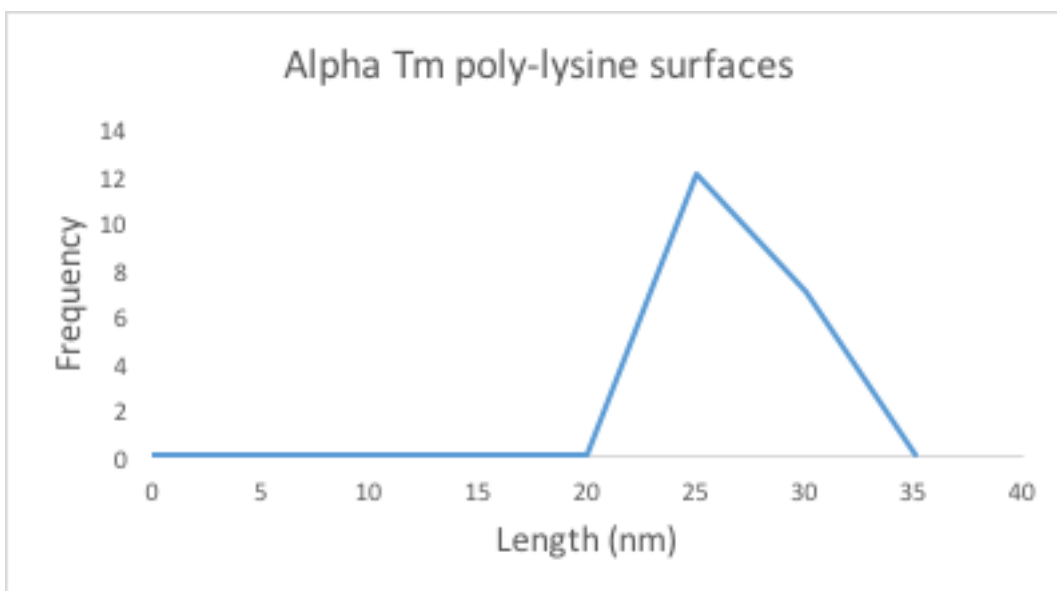
Figure 5.6.3. MATLAB trace data to measure contour length of α Tpm images produced by Loong et al. on poly-lysin coated mica. The average length was ~ 25 nm, n = 19

Polymer end detection was the first difference between our data analysis. The ends of a polymer were detected according to the height profile in relation to the ends on the polymer and will underestimate the contour length slightly, to account for any background noise, as explained in figure 5.2.3.2. This is in contrast to Loong et al. who compensate for polymer end length being underestimated.

Once the polymer has been traced, the user is required to check manually, by eye, that it is a good fit for the protein and that the software correctly followed the center line for each particle. Loong et al. state that their MATLAB script is semi-automated, and that Tpm molecules were manually selected before automated MATLAB filtering and analysis. It also stated that the number of Tpm particles were manually counted, including estimating the number of single Tpm molecules in a long polymer, and counting Tpm at the edges of the image frame, as long as more than half the length was in frame. Whereas in our analysis, only

clear single Tpm molecules were counted, any polymers or incomplete molecules were discounted.

The most significant changes in data analysis are those for the persistence length. Loong et al. state 3 different methods by which they calculate the persistence length; by tangent angle correlation, by l_{e-e} distribution (end-to-end length distribution) and by tangent angle second moment analysis. The L_p was calculated for samples incubated over a range of times. For tangent angle correlation the L_p was calculated to be 40.6 – 45.8 nm. Fitting of the L_{e-e} distribution to the wormlike chain model gave L_p values of 41.7 – 51.6 nm. For tangent angle second moment analysis, the L_P was calculated to be 39.5 – 44.5 nm (Loong, Zhou et al. 2012a). There did not appear to be a correlation between incubation time and L_p calculated. The l_{e-e} distribution scaled l_{e-e} by its L_c to account for variability between Tpm. During polymer detection and image skeletonization, parts of Tpm were likely to be missed. The L_c was compensated in length by fitting the height profile beyond the skeleton lengths with half the 2D elliptical Gaussian function.

In comparison to the published data, the persistence length measured in our work from AFM images collected on poly-l-lysine surfaces at 1 nM and 0.1 nM α Tpm was 853 nm and 485.6 nm, respectively. This is as least 10 times larger than the values published by Loong et al.

To conclude, data for α Tpm on poly-l-lysine coated mica was not easily reproduced. Analysis of images published by Loong et al. showed differences in

the analysis of data they used compared to our values for both tracing polymer contour length but also in calculating the persistence length. Data for contour length and persistence length are summarized in table 5.6.1.

	Condition	Number particles	L_c (nm)	L_p (nm)
1	AFM α	63	20 & 45	136
2	AFM β	116	30 & 55	41
3	AFM poly-l-lysine α	8 & 11	25	853 & 486
4	EM & MD α	109	40	102 & 101
5	EM & MD α	16	40	104 & 106
6	AFM poly-l-lysine α	199 – 1852	40	~40 – 50

Table 5.6.1. Contour length (L_c) and persistence length (L_p) for Tpm, as presented in our work (grey) and published data (white). 1: Our AFM data for 50 nM α Tpm on mica 2: Our AFM data for 5 nM β Tpm on mica 3: Our AFM data for 1 nM and 0.1 nM α Tpm on poly-l-lysine coated mica, as per Loong et al. 2012 4: EM and MD data for α Tpm on mica(Li, Holmes et al. 2010, Sousa, Cammarato et al. 2010)5. EM and MD data for α Tpm(Li, Holmes et al. 2010)6. AFM data for α Tpm on poly-l-lysine coated mica(Loong, Zhou et al. 2012a)

5.7 Conclusion

5.7.1 Sample deposition may result in small distortions

While values of contour length and persistence length of α and β may not match those stated in literature, isoforms can be compared with respect to one another. The contour length of β Tpm measured 30 nm compared to 20 nm for α. These changes can arise from the stability of the protein in general. As shown in earlier chapters, β Tpm has a significantly lower thermal stability than α. These changes will affect how the sample behaves during deposition at imaging. Differences

between isoforms were seen during sample deposition, as α Tpm was used at 50 nM to achieve optical imaging density while β Tpm was used at 5 nM.

Tpm was imaged on freshly cleaved mica. Mica is typically associated with the chemical formula $KAl_2(SiAl)O_{10}(OH)_2$. Cleavage occurs by breaking the weak bonds between potassium ions and the adjacent aluminosilicate layers. The cleaved surface contains Si and O atoms, interspersed with K^+ ions. Freshly cleaved mica has been shown to contain a contaminant layer, even after washing and drying, because upon cleavage, potassium ions in the mica react strongly with carbonaceous gases in the atmosphere to produce a carbon-containing layer of 0.3 – 0.4 nm. This contamination is created upon washing with H_2O, creating potassium carbonate, thus reducing the surface charge of mica. The potassium carbonate forms crystals on the surface upon drying of the mica. So, while mica is chosen to create a flat substrate surface over graphite, conditions should be explored to remove surface charges and thus, contaminants, to provide a better imaging surface (Ostendorf, Schmitz et al. 2008). A flatter background will reduce the need for image processing and thresholding, and thus may produce better 3D data for Tpm. Given the 1 nm height for Tpm, slight background noise and contaminant layers may result in polymers being shown as shorter and underestimating the ends of the polymer.

The charged surface of mica may dissipate quickly, owing to the washing and drying of the surface, on the other hand, residual surface charges may be responsible for stronger binding with β Tpm, given its stronger negative charge. Differences in interactions with mica may result in Tpm distortions due to

stronger or weaker binding, thus giving rise to differences in contour length measured.

5.7.2 α and β isoforms have different persistence length

The persistence length of α Tpm is much greater than that of β Tpm, 135.7 nm and 40.9 nm, respectively. This suggests that the functional regulatory unit for β Tpm is approximately the same length as one structural regulatory unit (1 Tpm along 7 actin subunits). On the other hand, given the measured L_c for α, the functional regulatory unit with respect to the L_p is approximately 7 times the size of the structural regulatory unit. These differences suggest that α Tpm is significantly stiffer than β and confers Ca^{2+} sensitivity and cooperativity over a long range along muscle filaments. On the other hand, the increased flexibility of β communicates regulation over a short range for individual regulatory units, impeding propagation of activation. The changes in stiffness for each isoform could provide insight into dimerization of Tpm. It can be hypothesised that heterodimers would have an intermediate stiffness between α and β homodimers, and therefore provide an intermediate cooperative activation of the thin filament. It can also be suggested that at low calcium, the increased flexibility of β Tpm means it is more likely to be activated in comparison to α (Loong, Zhou et al. 2012b).

Analysis of α and β Tpm from rabbit skeletal muscle revealed differences in phosphorylation by 2D PAGE. The α isoform was ~10 % phosphorylated, while β was nil (Heeley, Lohmeier-Vogel 2016) . Phosphorylation has been shown to

increase the stiffness of head-to-tail overlap regions, and thus enhance muscle activation (Lehman, Medlock et al. 2015) . The increased stiffness for α Tpm against β Tpm calculated here reflects these biological properties.

Changes in measured contour lengths for α and β isoforms could be due to sample deposition and drying out of the protein. It is possible to study proteins in solution using AFM in tapping mode. The benefits of exploring a protein in liquid is that it prevents any distortion of the protein from drying out and also enables proteins to be studied under more physiological conditions. Imaging in liquids may also reduce potassium crystal artefacts on the surface, as these are water soluble, thus creating a flatter surface to image on.

5.7.3 Future imaging conditions

Future directions may include in-fluid imaging, but it is not as simple as imaging in air. AFM imaging performed here used automatic calibration of the AFM, however, in liquid, cantilever frequency response has to be tuned and auto tuning is not recommended owing to the multiple peaks produced. The resonance of the tip in liquid is not only of the tip, but also the environment it is in, which can be complicated. Finally, AFM tip roughness can disrupt the tip-liquid-surface interface by introducing disorder and minimizing oscillatory forces (Ricci, Braga 2004).

Owing to the nature of hydrogen bonding, ionic interactions and hydrodynamic forces, approaching a sample can also cause problems. Viscous damping and

compression provide additional forces during imaging. The high quality factor (Q) decreases in liquid when compared to air and can lead to damage of samples and decreased resolution. The thermal properties of samples in liquid are liable to fluctuations, which can contribute to noise when imaging. Proper regulation of the thermal environment can prove troublesome too. The oscillatory forces of the liquid used can cause artefacts depending on the size of the liquid molecules. Viscosity has been shown to increase for confined liquid between the tip and sample, showing a positive correlation between tip approaching the surface and viscosity increasing. Suggesting that low Q may be an issue for non-contact AFM imaging in liquids (O'Shea 2001). Finally, slow scan speeds in liquid can cause the tip to stick to a surface, so scan speeds may have to be increased to avoid this risk, thus reducing image resolution (Füzik, Ulbrich et al.).

Imaging in liquid requires extensive standardisation, as outlined above. It is possible that differences in measured contour length arise from sample deposition. Imaging in liquid, so as to preserve features of the protein, could rectify these issues. Once an accurate L_c is measured for Tpm, a more thorough analysis of L_p can be undertaken.

5.7.4 Comparison of L_p with literature

One aim of this chapter was to explore the discrepancies between L_p data for Tpm produced by AFM and EM studies. The calculated persistence length for EM and MD studies describe Tpm as a semi-rigid polymer (Li, Holmes et al. 2010, Li, Lehman et al. 2010). The L_p was ~ 100 nm, which was not dissimilar to that

which we calculated for α Tpm at 136 nm. The main difference was in the L_p relative to the contour length, as we measured α Tpm to be 20 nm, which was roughly half the expected length. Therefore, α Tpm was defined as a stiff polymer, given that the L_p is almost 7 times the contour length. EM and MD studies stated Tpm to be a semi-rigid polymer. Conversely, AFM studies stated the L_p to be of a similar length to the contour length (40 – 50 nm), which indicated that Tpm is a flexible polymer, because the functional regulatory unit is roughly the same size as the structural regulatory unit (Loong, Zhou et al. 2012a).

While AFM image analysis here did not replicate published data, as we were unable to accurately measure contour lengths and thus define the true persistence length of Tpm, it has provided a means of comparison.

5.7.5 AFM imaging and analysis

The relatively slow scan speed of AFM can lead to thermal drift. While every precaution was taken to minimise this, it can still be an issue. The piezoelectric scanner can also lead to hysteresis of images between x, y and z axis, which requires filtering and processing with software (Ricci, Braga 2004). This image processing can flatten out topological features of a protein. Large scans performed here (4 μM) would take approximately 4 hours to run. Given that each scan was replicated 3 times to reduce this drift, it would take an entire day to capture one clear image. Loong, et al. (2012) stated tip convolution as the major limiting factor and did not mention thermal drift and measures taken to avoid it.

AFM imaging by Loong et al. was performed at phase angles (<90 degrees) to reduce cantilever contact with surface topography and images were flattened by subtracting background noise after a 1st order fit. On the other hand, our imaging was performed using ScanAsyst PeakForce Tapping mode at 45 degrees. A difference in cantilever contact with the sample can lead to discrepancies in measurements. The cantilever probe is subject to both repulsive and attractive forces of Van Der Waals forces and dipole-dipole interactions. These short-range interactions effect resonance frequency. Attractive forces reduce resonance frequency of the cantilever by adding to spring tension on the tip. Repulsive forces increase resonance frequency of the cantilever by increasing spring compression on the tip (O'Shea 2001). This can lead to sample deformation, which will affect values obtained by image analysis.

Another difference between our initial work and that presented by Loong et al. is sample deposition. We used freshly cleaved mica, while Loong et al. used a poly-l-lysine coated surface. To see if the image acquisition or image analysis was the source of our differences in values obtained and calculated, we repeated the Loong et al. protocol, as published (Loong, Zhou et al. 2012a).

Upon testing the poly-l-lysine protocol, the first issue arose in the density of sample deposition, and even at a tenfold reduction of Tpm concentration, it was difficult to find single Tpm particles. Of the ~10 particles traced for each Tpm concentration, the length was 20 and 30 nm and the persistence length was 853 nm and 486 nm for 1 nM and 0.1 nM Tpm, respectively. Data published for α

Tpm on poly-l-lysine coated mica suggested that the persistence length of Tpm was similar to the contour length. On the other hand, data presented here revealed the persistence length to be 10 – 20 times the contour length, indicating that α Tpm is incredibly stiff and able to confer cooperativity long range. The number of Tpm particles traced was very low, and the high degree of variance for values measured between the two concentrations of Tpm used indicates that our data may not provide reliable insight for these conditions.

Data presented here did not match those in the literature. The original images published by Loong et al. for α Tpm on poly-l-lysine coated mica were subjected to analysis using our MATLAB script. The difference in analysis methods was highlighted when tracing L_c for Tpm of published AFM images stated as being 40 nm long, and our analysis was 15 nm shorter, table 5.6.1.

Loong et al. overestimated L_c in their analysis to account for end loss during skeletonization processing, while our script underestimated L_c to account for background noise and more accurately detect ends using a height profile map. In addition to this, our semi-automated script automatically detected polymer ends but required polymer tracing to be confirmed by eye manually, whereas the semi-automated script used by Loong et al. required the user to manually select Tpm monomers, and to estimate the number of Tpm monomers in a polymer. It was seen in our analysis that occasionally Tpm traces would take a "shortcut" when tracing a particle, rather than following the contour, so manual approval of traces reduced such errors in analysis. Instead of estimating monomers from

polymer chains, our analysis included all traceable particles, thus creating a second peak of Tpm contour length, which accounted for polymer chains.

5.7.6 Comparison to EM imaging and analysis

Electron microscopy (EM), while much faster than AFM, generally provides much lower quality images and only produces two-dimensional images. Given the 1 nm height of Tpm, end particle detection is not as easily defined when working with a 2D image. EM studies of Tpm require the sample to be dried on mica, before being coated in evaporated platinum under vacuum and transferred onto a carbon support and copper grid (Sousa, Cammarato, et al. 2010). Sample deposition may lead to deformation and alteration of Tpm structure, thus affecting the calculations of persistence length. While one study of Tpm with EM only had 16 particles (Sousa, Cammarato et al. 2010), another EM paper of Tpm stated similar values for L_p and had over 100 particles in the study (Li, Holmes et al. 2010). This questions the impact of low numbers of molecules leading to overestimation of L_p (Loong, Zhou et al. 2012a).

Analysis of Tpm images acquired by EM used the tangent angle correlation to determine the apparent L_p and assumed the starting shape of the particle was straight (Li, Holmes et al. 2010, Sousa, Cammarato et al. 2010). Li et al. calculated a "central " L_p, however, which excluded 15 residues at each termini during analysis. The reasoning for this was to exclude perturbations of the coiled-coil axis at the termini over 2 heptad repeats, while being short enough to only exclude 5 % of the total length. However, as they stated by Sousa et al., the

mechanical properties of Tpm is different for the central and distal parts of the protein (L_p 63 nm and 108 nm, respectively), and given that L_p is a measurement of the entire protein, excluding the residues at the termini may alter the calculated L_p (Sousa, Cammarato et al. 2010).

Reported measurements for a dynamic L_p that assumed the particle was curved revealed the L_p to be 12 times the L_c (343 nm), in comparison to the apparent L_p (Li, Holmes et al. 2010). Sousa et al. also stated an underestimation of their values by a factor of 4 – 5, given the proteins inherent curvature. On the contrary, data presented here did not assume Tpm was straight, but the calculated L_p was similar to the apparent L_p published, instead of the dynamic L_p. This could be as a result of under analyzing data by excluding 15 residues at each termini. However, in absolute terms, data presented for Tpm analysis using EM was comparable to the values which we obtained. Both EM analysis and that presented here underestimated Tpm length to ensure a more accurate trace and analysis, whereas AFM data presented by Loong et al. overestimated L_c and reports a much smaller L_p.

5.7.8 Final thoughts

There are numerous other variables that can be explored for imaging using AFM, including low force imaging and trying different types of cantilever and tips. These variables are most likely to increase the resolution of images, but not necessarily alter the contour lengths measured for each isoform, so as to match the expected values. It is likely though, that sample deposition contributed to

discrepancies in our data, and therefore for future work I would suggest exploring imaging in liquid as the best option. It became clear that image processing and analysis of images acquired was a source of discrepancies for values reported for Tpm. This was seen when published data was subjected to the analysis method used here. It would be interesting to do the reverse analysis, and subject the data presented here to the same analysis methods as those published by Loong et al. and Li et al. to see the impact on L_p and L_c for our data.

Chapter 6: Conclusions and future work

6.1 Conclusions

The properties of α and β Tm were explored using AFM and CD. α and β Tm showed very distinct properties during AFM studies. Samples deposited differently on mica, leading to differences in contour lengths being measured. Persistence length calculations determined that α Tm was significantly stiffer than the β isoform. Changes in stiffness alter the function of Tm to cooperatively activate the thin filament. It could provide an explanation into the preferential assembly of dimers in muscle, in relation to calcium sensitivity and cooperative activation. During CD studies, β Tm was seen to have a significantly lower thermal stability in comparison to α Tm over 5 – 65 ℃, most significantly at temperatures up to 35 ℃. The decrease in thermal stability at physiological temperatures, alongside decreased stiffness, could provide insight into the lower prevalence of the β homodimer *in vivo.*

Buffer conditions were explored and contrary to expectation, high salt concentrations increased the thermal stability of Tm. This stability followed Hofmeister predictions, as well the positive correlation between thermal stability and salt concentration, indicating this was not an electrostatic effect.

Protein modifications such as His-tags and cross-linking were explored. His-tagged protein showed a decrease of thermal stability at temperatures above 55 ℃, which was compounded for both dimers being tagged. The stabilising effect of high salt buffers was

reduced when exploring His-tagged Tm. On the other hand, the cross-linked proteins showed an overall increase in thermal stability. This increase in stability was not reflected in other experimental data however. During dimer exchange studies, particularly when exploring heterodimers and cardiomyopathy mutants, cross-linked samples were liable to precipitation and smearing on SDS PAGE. Also, mass spectrometry analysis of chemically cross-linked dimers revealed protein degradation and lots of heterogeneity in samples. These results highlight the need to minimise use of cross-linking experimentally, but also caution when using even a relatively small tag, such as a His-tag.

Dimer exchange studies showed a lack of exchange between dimers up to 20 ℃. Experimentally, this removes the need for harsh, chemical cross-linking of the protein to fix heterodimer populations. This was important for CD studies of heterodimers, to be sure of dimer content for first melting curves.

Exchange was seen between homodimers to form heterodimers within just 1-hour incubation at 37 ℃, however heterodimers did not show reverse exchange to form homodimers. This gave indication to a preferential assembly of heterodimers, but required more in depth analysis given the problems caused by cross-linking for SDS PAGE analysis. Exchange at 37 ℃ may prove useful experimentally, such as protein labelling and heterodimer formation.

Cardiomyopathy mutant E54K was explored. Exchange of the heterodimer Hisα-E54K showed a lack of exchange to form homodimers, as for α-Hisα heterodimers. The apparent increased stability of the mutant heterodimer conflicted with thermal stability data, which

showed E54K-Hisα had reduced stability at temperatures up to ~ 35 °C. On the other hand, E54K-α heterodimer only showed a significant decrease in thermal stability at temperatures above ~55 °C. This highlighted the unpredictable effect of this mutation and also the effect of His-tags on Tm thermal stability.

While thermal melting data provided some insight into the unfolding events of Tm, the behaviour of the protein is still too complex to accurately assign these peaks to specific unfolding events, given that changes are communicated both locally and globally in the protein.

6.2 Future Work

The work presented here could be further explored by carrying out additional experiments. Repeating the experiments in the presence of Tn and varying levels of calcium, to explore the role of regulatory components on the dimer stability, could further explore exchange of monomers in dimers. The exchange of pyrTm on actin could be repeated at 37 °C to explore exchange at physiological conditions. Preferential assembly of heterodimers could be further explored by studying the exchange of WT and E54K homodimers to compare with heterodimeric results. Different cross-linking conditions could also be explored to try and minimise protein degradation, thus enabling clearer imaging of dimers on polyacrylamide gels.

The thermal stability of Tm could be further explored by studying the potential stabilising effects of actin presence. While CD and TSA studies were not suitable for this, DSC may

provide an alternate method to explore this. DSC is more suited to actin+Tm samples as it measures the heating rate of the sample as a whole compared to a reference, while CD measures protein unfolding by looking at the proteins secondary structure. DSC provides a thermal melting curve similar to CD, which will provide insight on the thermal stability of Tm when bound to actin. The thermal stability of E54K homodimers could also provide insight into the behaviour of the mutation, given the unusual behaviour of the untagged vs. His-tagged heterodimer.

Data from AFM imaging of Tm provided interesting insight into differences between α and β isoforms. Known cardiomyopathy mutants could be compared with our values obtained for the persistence length, to explore the change relative to wild type isoforms. So far, only homodimers have been explored. The stiffness of Tm could be further explored by imaging heterodimers.

Discrepancies between values obtained here and those previously published could be explored. Imaging Tm in liquid may provide a more insight into how the protein behaves *in vivo*. More physiological conditions could be explored, such as changing temperature and salt conditions.

The effect of the persistence length on the function of Tm can be further explored by looking at the calcium regulation of actin filaments. Stopped flow experiments can be utilised to explore changes in pCa curves relative to the persistence length of Tm. This will provide insight into the connection between stiffness and calcium regulation and cooperative activation of the thin filament.

Experiments with cardiac tissue from transgenic mice showed promise for identifying the dimer content of the tissue. Though we proved detection of heterodimers was possible with the use of His-tags, cardiomyopathy point mutations prove challenging, given the incredibly small change in molecular mass, thus rendering detection using SDS PAGE impossible. Future work could explore alternative methods for cross-linking of Tm to reduce protein deformation, thus reducing heterogeneity in mass spectrometry results.

References

Report of the 1995 World Health Organization/International Society and Federation of Cardiology Task Force on the Definition and Classification of Cardiomyopathies. 1996. *Circulation,* **93**(5), pp. 841-842.

ALLISON, D.P., MORTENSEN, N.P., SULLIVAN, C.J. and DOKTYCZ, M.J., 2010. Atomic force microscopy of biological samples. *Wiley Interdisciplinary Reviews: Nanomedicine and Nanobiotechnology,* **2**(6), pp. 618-634.

BAI, F., WANG, L. and KAWAI, M., 2013. A study of tropomyosin's role in cardiac function and disease using thin-filament reconstituted myocardium. *Journal of muscle research and cell motility,* **34**(0), pp. 10.1007/s10974-013-9343-z.

BALDWIN, R.L., 1996. How Hofmeister ion interactions affect protein stability. *Biophysical journal,* **71**(4), pp. 2056-2063.

BARUA, B., WINKELMANN, D.A., WHITE, H.D. and HITCHCOCK-DEGREGORI, S.E., 2012. Regulation of actin-myosin interaction by conserved periodic sites of tropomyosin. *Proceedings of the National Academy of Sciences,* **109**(45), pp. 18425-18430.

BARUA, B., PAMULA, M.C. and HITCHCOCK-DEGREGORI, S.E., 2011. *Evolutionarily conserved surface residues constitute actin binding sites of tropomyosin.* **108**(25), pp. 10150-10155

BEAULIEU-BOIRE, I., LEBLANC, N., BERGER, L. and BOULANGER, J., 2013. Troponin Elevation Predicts Atrial Fibrillation in Patients with Stroke or Transient Ischemic Attack. *Journal of Stroke and Cerebrovascular Diseases,* **22**(7), pp. 978-983.

BEHRMANN, E., MÜLLER, M., PENCZEK, P., MANNHERZ, H., MANSTEIN, D. and RAUNSER, S., 2012. Structure of the Rigor Actin-Tropomyosin-Myosin Complex. *Cell,* **150**(2), pp. 327-338.

BIESIADECKI, B.J., TACHAMPA, K., YUAN, C., JIN, J.-., DE TOMBE, P.P. and SOLARO, R.J., 2010. Removal of the cardiac troponin I N-terminal extension improves cardiac function in aged mice. *Journal of Biological Chemistry,* **285**(25), pp. 19688-19698.

BINNIG, G., QUATE, C.F. and GERBER, C., 1986. Atomic force microscope. *Physical Review Letters,* **56**(9), pp. 930-933.

BLOEMINK, M.J., DEACON, J.C., RESNICOW, D.I., LEINWAND, L.A. and GEEVES, M.A., 2013. The Superfast Human Extraocular Myosin Is Kinetically Distinct from the Fast Skeletal IIa, IIb, and IId Isoforms. *Journal of Biological Chemistry,* **288**(38), pp. 27469-27479.

BRONSON, D.D. and SCHACHAT, F.H., 1982. Heterogeneity of contractile proteins. Differences in tropomyosin in fast, mixed, and slow skeletal muscles of the rabbit. *The Journal of biological chemistry,* **257**(7), pp. 3937-3944.

BROWN, H.R. and SCHACHAT, F.H., 1985. Renaturation of skeletal muscle tropomyosin: implications for in vivo assembly. *Proceedings of the National Academy of Sciences,* **82**(8), pp. 2359-2363.

BROWN, J.H., KIM, K., JUN, G., GREENFIELD, N.J., DOMINGUEZ, R., VOLKMANN, N., HITCHCOCK-DEGREGORI, S.E. and COHEN, C., 2001. Deciphering the design of the tropomyosin molecule. *Proceedings of the National Academy of Sciences,* **98**(15), pp. 8496-8501.

CENSULLO, R. and CHEUNG, H.C., 1994. Tropomyosin length and two-stranded F-actin flexibility in the thin filament. *Journal of Molecular Biology,* **243**(3), pp. 520-529.

CORBETT, M.A., ANTHONY AKKARI, P., DOMAZETOVSKA, A., COOPER, S.T., NORTH, K.N., LAING, N.G., GUNNING, P.W. and HARDEMAN, E.C., 2005. An αTropomyosin mutation alters dimer preference in nemaline myopathy. *Annals of Neurology,* **57**(1), pp. 42-49.

CORRÊA, F., SALINAS, R.K., BONVIN, A.M.J.J. and FARAH, C.S., 2008. Deciphering the role of the electrostatic interactions in the ?-tropomyosin head-to-tail complex. *Proteins: Structure, Function, and Bioinformatics,* **73**(4), pp. 902-917.

CRICK, F.H.C., 1953. The Packing of a-Helices: Simple Coiled-Coils. *Acta Crystallographica,* **6**, pp. 689-697.

DATE, M.S. and DOMINY, B.N., 2011. Modeling the Influence of Salt on the Hydrophobic Effect and Protein Fold Stability. *Communications in Computational Physics,* **13**(1), pp. 90-106.

DAVIS, J.P. and TIKUNOVA, S.B., 2008. Ca2+ exchange with troponin C and cardiac muscle dynamics. *Cardiovascular research,* **77**(4), pp. 619-626.

DEACON, J.C., BLOEMINK, M.J., REZAVANDI, H., GEEVES, M.A. and LEINWAND, L.A., 2012. Identification of functional differences between recombinant human a and ß cardiac myosin motors. *Cellular and Molecular Life Sciences,* **69**(13), pp. 2261-2277.

DEHNICKE, K., 1976. The Chemistry of Cyano Complexes of the Transition Metals. Organometallic Chemistry - A Series of Monographs. Von A. G. Sharpe. Academic Press, London-New York-San Francisco 1976. 1. Aufl., XI, 302 S., geb. *Angewandte Chemie,* **88**(22), pp. 774-774.

DOMINGUEZ, R. and HOLMES, K.C., 2011. Actin Structure and Function. *Annual Review of Biophysics,* **40**(1), pp. 169-186.

EAST, D.A., SOUSA, D., MARTIN, S.R., EDWARDS, T.A., LEHMAN, W. and MULVIHILL, D.P., 2011. Altering the stability of the Cdc8 overlap region modulates the ability of this tropomyosin to bind co-operatively to actin and regulate myosin *Biochemical Journal,* **438**(2), pp. 265-273.

EDWARDS, B.F. and SYKES, B.D., 1981. Analysis of cooperativity observed in pH titrations of proton nuclear magnetic resonances of histidine residues of rabbit cardiac tropomyosin. *Biochemistry,* **20**(14), pp. 4193-4198.

FAAS, F.G.A., RIEGER, B., VAN VLIET, L.J. and CHERNY, D.I., 2009. *DNA Deformations near Charged Surfaces: Electron and Atomic Force Microscopy Views.* **97**(4), pp.1148-1157.

FARAH, C.S. and REINACH, F.C., 1995. The troponin complex and regulation of muscle contraction. *The FASEB Journal,* **9**(9), pp. 755-767.

FILATOV, V.L., KATRUKHA, A.G., BULARGINA, T.V. and GUSEV, N.B., 1999. REVIEW: Troponin: Structure, Properties, and Mechanism of Functioning. *Biochemistry,* **64**(9), pp. 969-985.

FOTIADIS, D., 2012. Atomic force microscopy for the study of membrane proteins. *Current opinion in biotechnology,* **23**(4), pp. 510-515.

FRASER, I.D.C. and MARSTON, S.B., 1995. In vitro motility analysis of actin-tropomyosin regulation by troponin and calcium. The thin filament is switched as a single cooperative unit. *Journal of Biological Chemistry,* **270**(14), pp. 7836-7841.

FÜZIK, T., ULBRICH, P. and RUML, T., Imaging of biological samples in liquid environment.

GEEVES, M.A. and RANATUNGA, K.W., 2012. Tuning the Calcium Sensitivity of Cardiac Muscle. *Biophysical journal,* **103**(5), pp. 849-850.

GEEVES, M.A., HITCHCOCK-DEGREGORI, S. and GUNNING, P.W., 2014. A systematic nomenclature for mammalian tropomyosin isoforms. *Journal of muscle research and cell motility,* **36**(2), pp. 147-153.

GEEVES, M.A. and HOLMES, K.C., 2005. The Molecular Mechanism of Muscle Contraction. *Advances in Protein Chemistry.* Academic Press, **71**, pp. 161-193.

GORDON, A.M., HOMSHER, E. and REGNIER, M., 2000. Regulation of Contraction in Striated Muscle. *Physiological Reviews,* **80**(2), pp. 853-924.

GREENFIELD, N.J., 2006. Using circular dichroism spectra to estimate protein secondary structure. *Nature Protocols,* **1**(6), pp. 2876-2890.

GROSS, L., 2009. The Chemical Structure of a Molecule Resolved by Atomic Force Microscopy. *Science (New York, N.Y.),* **325**(5944), pp. 1110-1114.

GUNNING, P.W. and HARDEMAN, E.C., 2017. Tropomyosins. *Current Biology,* **27**(1), pp. R8-R13.

GUNNING, P., O'NEILL, G. and HARDEMAN, E., 2008. Tropomyosin-Based Regulation of the Actin Cytoskeleton in Time and Space. *Physiological Reviews,* **88**(1), pp. 1-35.

HEAD, J.G., RITCHIE, M.D. and GEEVES, M.A., 1995. Characterization of the equilibrium between blocked and closed states of muscle thin filaments. *European Journal of Biochemistry,* **227**(3), pp. 694-699.

HEALD, R.W. and HITCHCOCK-DEGREGORI, S.E., 1988. The structure of the amino terminus of tropomyosin is critical for binding to actin in the absence and presence of troponin. *Journal of Biological Chemistry,* **263**(11), pp. 5254-5259.

HEELEY, D.H. and LOHMEIER-VOGEL, E.M., 2016. Biochemical Comparison of Rabbit Skeletal Muscle Alpha and Beta Tropomyosin Isoforms. *Biophysical journal,* **110**(3), pp. 276a.

HERSHBERGER, R.E., HEDGES, D.J. and MORALES, A., 2013. Dilated cardiomyopathy: the complexity of a diverse genetic architecture. *Nat Rev Cardiol,* **10**(9), pp. 531-547.

HERSHBERGER, R.E., NORTON, N., MORALES, A., LI, D., SIEGFRIED, J.D. and GONZALEZ-QUINTANA, J., 2010. Coding Sequence Rare Variants Identified in MYBPC3, MYH6, TPM1, TNNC1, and TNNI3 From 312 Patients With Familial or Idiopathic Dilated Cardiomyopathy. *Circulation: Cardiovascular Genetics,* **3**(2), pp. 155-161.

HITCHCOCK-DEGREGORI, S.E., 2008. Tropomyosin: Function Follows Structure. In: P. GUNNING, ed, *Tropomyosin Advance in experimental medicine and biology Volume 644.* Landes Bioscience, pp. 60-72.

HITCHCOCK-DEGREGORI, S. and BARUA, B., 2017. Tropomyosin Structure, Function, and Interactions: A Dynamic Regulator. In: D.A.D. PARRY and J.M. SQUIRE, eds, *Fibrous Proteins: Structures and Mechanisms.* Cham: Springer International Publishing, pp. 253-284.

HOLMES, K.C. and LEHMAN, W., 2008. Gestalt-binding of tropomyosin to actin filaments. *Journal of muscle research and cell motility,* **29**(6), pp. 213-219.

HOLTZER, M.E., KIDD, S.G., CRIMMINS, D.L. and HOLTZER, A., 1992. ββ homodimers exist in native rabbit skeletal muscle tropomyosin and increase after denaturation–renaturation. *Protein Science,* **1**(3), pp. 335-341.

ISHII, Y., HITCHCOCK- DEGREGORI, S., MABUCHI, K. and LEHRER, S.S., 1992. Unfolding domains of recombinant fusion αα- tropomyosin. *Protein Science,* **1**(10), pp. 1319-1325.

ISHII, Y. and LEHRER, S.S., 1990. Excimer fluorescence of pyrenyliodoacetamide-labeled tropomyosin: a probe of the state of tropomyosin in reconstituted muscle thin filaments. *Biochemistry,* **29**(5), pp. 1160-1166.

ISHII, Y., 1994. The local and global unfolding of coiled-coil tropomyosin. *European Journal of Biochemistry,* **221**(2), pp. 705-712.

JANCO, M., KALYVA, A., SCELLINI, B., PIRODDI, N., TESI, C., POGGESI, C. and GEEVES, M.A., 2012. a-Tropomyosin with a D175N or E180G mutation in only one chain differs from tropomyosin with mutations in both chains. *Biochemistry,* **51**(49), pp. 9880-9890.

JANCO, M., SUPHAMUNGMEE, W., LI, X., LEHMAN, W., LEHRER, S.S. and GEEVES, M.A., 2013. Polymorphism in tropomyosin structure and function. *Journal of muscle research and cell motility,* **34**(3-4), pp. 177-187.

JIN, Y., PENG, Y., LIN, Z., CHEN, Y., WEI, L., HACKER, T.A., LARSSON, L. and GE, Y., 2016. Comprehensive analysis of tropomyosin isoforms in skeletal muscles by top-down proteomics. *Journal of muscle research and cell motility,* **37**(1), pp. 41-52.

KALYVA, A., SCHMIDTMANN, A. and GEEVES, M.A., 2012. In vitro formation and characterization of the skeletal muscle a•ß tropomyosin heterodimers. *Biochemistry,* **51**(32), pp. 6388-6399.

KARIBE, A., TOBACMAN, L.S., STRAND, J., BUTTERS, C., BACK, N., BACHINSKI, L.L., ARAI, A.E., ORTIZ, A., ROBERTS, R., HOMSHER, E. and FANANAPAZIR, L., 2001.

Hypertrophic Cardiomyopathy Caused by a Novel a-Tropomyosin Mutation (V95A) Is Associated With Mild Cardiac Phenotype, Abnormal Calcium Binding to Troponin, Abnormal Myosin Cycling, and Poor Prognosis. *Circulation,* **103**(1), pp. 65-71.

KOHN, W.D., KAY, C.M. and HODGES, R.S., 1997. Salt effects on protein stability: two-strandedα-helical coiled-coils containing inter- or intrahelical ion pairs. *Journal of Molecular Biology,* **267**(4), pp. 1039-1052.

KOPYLOVA, G.V., SHCHEPKIN, D.V., BOROVKOV, D.I. and MATYUSHENKO, A.M., 2016. Effect of Cardiomyopathic Mutations in Tropomyosin on Calcium Regulation of the Actin–Myosin Interaction in Skeletal Muscle. *Bulletin of experimental biology and medicine,* **162**(1), pp. 42-44.

KREMNEVA, E., BOUSSOUF, S., NIKOLAEVA, O., MAYTUM, R., GEEVES, M.A. and LEVITSKY, D.I., 2004. Effects of Two Familial Hypertrophic Cardiomyopathy Mutations in α-Tropomyosin, Asp175Asn and Glu180Gly, on the Thermal Unfolding of Actin-Bound Tropomyosin. *Biophysical journal,* **87**(6), pp. 3922-3933.

LAKDAWALA, N.K., THUNE, J.J., COLAN, S.D., CIRINO, A.L., FARROHI, F., RIVERO, J., MCDONOUGH, B., SPARKS, E., ORAV, E.J., SEIDMAN, J.G., SEIDMAN, C.E. and HO, C.Y., 2012. Subtle Abnormalities in Contractile Function Are an Early Manifestation of Sarcomere Mutations in Dilated Cardiomyopathy. *Circulation: Cardiovascular Genetics,* **5**(5), pp. 503-510.

LAPSHIN, R.V., 2004. Feature-oriented scanning methodology for probe microscopy and nanotechnology. *Nanotechnology,* **15**(9), pp. 1135-1151.

LEHMAN, W., MEDLOCK, G., LI, X.E., SUPHAMUNGMEE, W., TU, A., SCHMIDTMANN, A., UJFALUSI, Z., FISCHER, S., MOORE, J.R. and GEEVES, M.A., 2015. Phosphorylation of Ser283 enhances the stiffness of the tropomyosin head-to-tail overlap domain. *Archives of Biochemistry and Biophysics,* **571**, pp. 10-15.

LEHMAN, W., ORZECHOWSKI, M., LI, X.E., FISCHER, S. and RAUNSER, S., 2013. Gestalt-binding of tropomyosin on actin during thin filament activation. *Journal of muscle research and cell motility,* **34**(0), pp. 155-163.

LEHRER, S.S. and JOSEPH, D., 1987. Differences in local conformation around cysteine residues in αα, αβ, and ββ rabbit skeletal tropomyosin. *Archives of Biochemistry and Biophysics,* **256**(1), pp. 1-9.

LEHRER S.S, Ly S & FUCH F., 2011 Tropomyosin is in a reduced state in rabbit psoas muscle. *J Muscle Res Cell Motil*, **32**, 19–21

LEHRER, S.S., QIAN, Y. and HVIDT, S., 1989. Assembly of the native heterodimer of Rana esculenta tropomyosin by chain exchange. *Science,* **246**(4932), pp. 926-929.

LEHRER, S.S. and QIAN, Y., 1990. Unfolding/refolding studies of smooth muscle tropomyosin. Evidence for a chain exchange mechanism in the preferential assembly of the native heterodimer. *Journal of Biological Chemistry,* **265**(2), pp. 1134-1138.

LEHRER, S.S. and STAFFORD III, W.F., 1991. Preferential assembly of the tropomyosin heterodimer: Equilibrium studies. *Biochemistry,* **30**(23), pp. 5682-5688.

LEVITSKY, D.I., ROSTKOVA, E.V., ORLOV, V.N., NIKOLAEVA, O.P., MOISEEVA, L.N., TEPLOVA, M.V. and GUSEV, N.B., 2000. Complexes of smooth muscle tropomyosin with F-actin studied by differential scanning calorimetry. *European Journal of Biochemistry,* **267**(6), pp. 1869-1877.

LI, X., HOLMES, K.C., LEHMAN, W., JUNG, H. and FISCHER, S., 2010. The Shape and Flexibility of Tropomyosin Coiled Coils: Implications for Actin Filament Assembly and Regulation. *Journal of Molecular Biology,* **395**(2), pp. 327-339.

LI, X., LEHMAN, W. and FISCHER, S., 2010. The relationship between curvature, flexibility and persistence length in the tropomyosin coiled-coil. *Journal of structural biology,* **170**(2), pp. 313-318.

LI, X., SUPHAMUNGMEE, W., JANCO, M., GEEVES, M.A., MARSTON, S.B., FISCHER, S. and LEHMAN, W., 2012. The flexibility of two tropomyosin mutants, D175N and E180G, that cause hypertrophic cardiomyopathy. *Biochemical and biophysical research communications,* **424**(3), pp. 493-496.

LOONG, C.K.P., BADR, M.A. and CHASE, P.B., 2012. Tropomyosin flexural rigidity and single Ca 2+ regulatory unit dynamics: Implications for cooperative regulation of cardiac muscle contraction and cardiomyocyte hypertrophy. *Frontiers in Physiology,* **3**(80), pp. 1-10.

LOONG, C.K.P., ZHOU, H.-. and CHASE, P.B., 2012. Persistence length of human cardiac a-tropomyosin measured by single molecule direct probe microscopy. *PLoS ONE,* **7**(6), e39676

LOONG, C.K.P., ZHOU, H. and BRYANT CHASE, P., 2012. Familial hypertrophic cardiomyopathy related E180G mutation increases flexibility of human cardiac α-tropomyosin. *FEBS letters,* **586**(19), pp. 3503-3507.

LY, S. and LEHRER, S.S., 2012. Long-range effects of familial hypertrophic cardiomyopathy mutations E180G and D175N on the properties of tropomyosin. *Biochemistry,* **51**(32), pp. 6413-6420.

MAK, A.S., SMILLIE, L.B. and STEWART, G.R., 1980. A comparison of the amino acid sequences of rabbit skeletal muscle alpha- and beta-tropomyosins. *Journal of Biological Chemistry,* **255**(8), pp. 3647-3655.

MAK, A., SMILLIE, L.B. and BÁRÁNY, M., 1978. Specific phosphorylation at serine-283 of alpha tropomyosin from frog skeletal and rabbit skeletal and cardiac muscle. *Proceedings of the National Academy of Sciences,* **75**(8), pp. 3588-3592.

MARSTON, S.B., COPELAND, O., MESSER, A.E., MACNAMARA, E., NOWAK, K., ZAMPRONIO, C.G. and WARD, D.G., 2013. Tropomyosin isoform expression and phosphorylation in the human heart in health and disease. *Journal of muscle research and cell motility,* **34**(3-4), pp. 1-9.

MATHUR, M.C., CHASE, P.B. and CHALOVICH, J.M., 2011. Several cardiomyopathy causing mutations on tropomyosin either destabilize the active state of actomyosin or alter the binding properties of tropomyosin. *Biochemical and biophysical research communications,* **406**(1), pp. 74-78.

MATSUMURA, F. and YAMASHIRO-MATSUMURA, S., 1985. Purification and characterization of multiple isoforms of tropomyosin from rat cultured cells. *Journal of Biological Chemistry,* **260**(25), pp. 13851-13859.

MATYUSHENKO, A.M., ARTEMOVA, N.V., SHCHEPKIN, D.V., KOPYLOVA, G.V., NABIEV, S.R., NIKITINA, L.V., LEVITSKY, D.I. and BERSHITSKY, S.Y., 2017. The interchain disulfide cross-linking of tropomyosin alters its regulatory properties and interaction with actin filament. *Biochemical and biophysical research communications,* **482**(2), pp. 305-309.

MAYNARD, S.J., MENOWN, I.B.A. and ADGEY, A.A.J., 2000. Troponin T or troponin I as cardiac markers in ischaemic heart disease. *Heart,* **83**(4), pp. 371-373.

MCKILLOP, D.F. and GEEVES, M.A., 1991. Regulation of the acto.myosin subfragment 1 interaction by troponin/tropomyosin. Evidence for control of a specific isomerization between two acto.myosin subfragment 1 states. *Biochemical Journal,* **279**, pp. 711-718.

MCKILLOP, D.F.A. and GEEVES, M.A., 1993. Regulation of the interaction between actin and myosin subfragment 1: Evidence for three states of the thin filament. *Biophysical journal,* **65**(2), pp. 693-701.

MCLACHLAN, A.D. and STEWART, M., 1976. The 14-fold periodicity in α-tropomyosin and the interaction with actin. *Journal of Molecular Biology,* **103**(2), pp. 271-298.

MIJAILOVICH, S.M., KAYSER-HEROLD, O., LI, X., GRIFFITHS, H. and GEEVES, M.A., 2012. Cooperative regulation of myosin-S1 binding to actin filaments by a continuous flexible Tm-Tn chain. *European Biophysics Journal,* **41**(12), pp. 1015-1032.

MIJAILOVICH, S.M., LI, X., GRIFFITHS, R.H. and GEEVES, M.A., 2012. The hill model for binding myosin S1 to regulated actin is not equivalent to the McKillop-Geeves model. *Journal of Molecular Biology,* **417**(1-2), pp. 112-128.

225

MIKI, M., KOBAYASHI, T., KIMURA, H., HAGIWARA, A., HAI, H. and MAÉDAT, Y., 1998. Ca^{2+}-Induced Distance Change between Points on Actin and Troponin in Skeletal Muscle Thin Filaments Estimated by Fluorescence Energy Transfer Spectroscopy. *The Journal of Biochemistry,* **123**(2), pp. 324-331.

MIKI, M., MIURA, T., SANO, K., KIMURA, H., KONDO, H., ISHIDA, H. and MAEDAT, Y., 1998. Fluorescence Resonance Energy Transfer between Points on Tropomyosin and Actin in Skeletal Muscle Thin Filaments: Does Tropomyosin Move? *The Journal of Biochemistry,* **123**(6), pp. 1104-1111.

MINAKATA, S., MAEDA, K., ODA, N., WAKABAYASHI, K., NITANAI, Y. and MAÉDA, Y., 2008. Two-Crystal Structures of Tropomyosin C-Terminal Fragment 176–273: Exposure of the Hydrophobic Core to the Solvent Destabilizes the Tropomyosin Molecule. *Biophysical journal,* **95**(2), pp. 710-719.

MIRZA, M., ROBINSON, P., KREMNEVA, E., COPELAND, O., NIKOLAEVA, O., WATKINS, H., LEVITSKY, D., REDWOOD, C., EL-MEZGUELDI, M. and MARSTON, S., 2007. The effect of mutations in alpha-tropomyosin (E40K and E54K) that cause familial dilated cardiomyopathy on the regulatory mechanism of cardiac muscle thin filaments. *The Journal of biological chemistry,* **282**(18), pp. 13487-13497.

MIRZA, M., MARSTON, S., WILLOTT, R., ASHLEY, C., MOGENSEN, J., MCKENNA, W., ROBINSON, P., REDWOOD, C. and WATKINS, H., 2005. Dilated Cardiomyopathy Mutations in Three Thin Filament Regulatory Proteins Result in a Common Functional Phenotype. *Journal of Biological Chemistry,* **280**(31), pp. 28498-28506.

MIRZA, M., ROBINSON, P., KREMNEVA, E., COPELAND, O., NIKOLAEVA, O., WATKINS, H., LEVITSKY, D., REDWOOD, C., EL-MEZGUELDI, M. and MARSTON, S., 2007. The Effect of Mutations in a-Tropomyosin (E40K and E54K) That Cause Familial Dilated Cardiomyopathy on the Regulatory Mechanism of Cardiac Muscle Thin Filaments. *Journal of Biological Chemistry,* **282**(18), pp. 13487-13497.

MURAKAMI, K., STEWART, M., NOZAWA, K., TOMII, K., KUDOU, N., IGARASHI, N., SHIRAKIHARA, Y., WAKATSUKI, S., YASUNAGA, T. and WAKABAYASHI, T., 2007.

Structural basis for tropomyosin overlap in thin (actin) filaments and the generation of a molecular swivel by troponin-T. *Proceedings of the National Academy of Sciences of the United States of America,* **105**(20), pp. 7200-7205.

MUTHUCHAMY, M., BOIVIN, G.P., GRUPP, I.L. and WIECZOREK, D.F., 1998. *β*-Tropomyosin Overexpression Induces Severe Cardiac Abnormalities. *Journal of Molecular and Cellular Cardiology,* **30**(8), pp. 1545-1557.

NAKAJIMA-TANIGUCHI, C., MATSUI, H., NAGATA, S., KISHIMOTO, T. and YAMAUCHI-TAKIHARA, K., 1995. Novel missense mutation in α-tropomyosin gene found in Japanese patients with hypertrophic cardiomyopathy. *Journal of Molecular and Cellular Cardiology,* **27**(9), pp. 2053-2058.

NARA, M., MORII, H. and TANOKURA, M., 2013. Infrared study of synthetic peptide analogues of the calcium-binding site III of troponin C: The role of helix F of an EF-hand motif. *Biopolymers,* **99**(5), pp. 342-347.

NEUMAN, K.C. and NAGY, A., 2008. Single-molecule force spectroscopy: optical tweezers, magnetic tweezers and atomic force microscopy. *Nature Methods,* **5**(6), pp. 491-505.

ODA, T., IWASA, M., AIHARA, T., MAÉDA, Y. and NARITA, A., 2009. The nature of the globular- to fibrous-actin transition. *Nature,* **457**(7228), pp. 441-445.

O'SHEA, S.J., 2001. Oscillatory forces in liquid atomic force microscopy. *Japanese Journal of Applied Physics,* **40**(6S), pp. 4309-4313.

O'SHEA, E.K., RUTKOWSKI, R., STAFFORD III, W.F. and KIM, P.S., 1989. Preferential heterodimer formation by isolated leucine zippers from Fos and Jun. *Science,* **245**(4918), pp. 646-648.

OSTENDORF, F., SCHMITZ, C., HIRTH, S., KÜHNLE, A., KOLODZIEJ, J. and REICHLING, M., 2008. How flat is an air-cleaved mica surface? *Nanotechnology,* **19**(30), pp. 1-6.

PACE, C.N., SHIRLEY, B.A. and THOMSON, J.A., 1989. Measuring the conformational stability of a protein. In: T.E. CREIGHTON, ed, *Protein Structure, a practical approach.* IRL Press, pp. 311-330.

PANDURANGACHAR, M., KUMARA SWAMY, B.E., CHANDRASHEKAR, B.N., GILBERT, O., REDDY, S. and SHERIGARA, B.S., 2010. Electrochemical investigations of potassium ferricyanide and dopamine by 1-butyl-4-methylpyridinium tetrafluoro borate modified carbon paste electrode: A cyclic voltammetric study. *International Journal of Electrochemical Science,* **5**(8), pp. 1187-1202.

PERRY, S.V., 2001. Vertebrate tropomyosin: distribution, properties and function. *Journal of Muscle Research & Cell Motility,* **22**(1), pp. 5-49.

POOLE, K.J.V., LORENZ, M., EVANS, G., ROSENBAUM, G., PIRANI, A., CRAIG, R., TOBACMAN, L.S., LEHMAN, W. and HOLMES, K.C., 2006. A comparison of muscle thin filament models obtained from electron microscopy reconstructions and low-angle X-ray fibre diagrams from non-overlap muscle. *Journal of structural biology,* **155**(2), pp. 273-284.

POTEKHIN, S.A. and PRIVALOV, P.L., 1982. *Co-operative blocks in tropomyosin.* **159**(3), pp. 519-535.

RAO, V.S., MARONGELLI, E.N. and GUILFORD, W.H., 2009. Phosphorylation of tropomyosin extends cooperative binding of myosin beyond a single regulatory unit. *Cell motility and the cytoskeleton,* **66**(1), pp. 10-23.

REDWOOD, C. and ROBINSON, P., 2013. Alpha-tropomyosin mutations in inherited cardiomyopathies. *Journal of muscle research and cell motility,* **34**(3-4), pp. 285-294.

RICCI, D. and BRAGA, P.C., 2004. Recognizing and avoiding artifacts in AFM imaging. *Methods in molecular biology (Clifton, N.J.),* **242**, pp. 25-37.

ROBASZKIEWICZ, K., OSTROWSKA, Z., CYRANKA-CZAJA, A. and MORACZEWSKA, J., 2015. Impaired tropomyosin–troponin interactions reduce activation of the actin thin

filament. *Biochimica et Biophysica Acta (BBA) - Proteins and Proteomics,* **1854**(5), pp. 381-390.

ROBASZKIEWICZ, K., OSTROWSKA, Z., MARCHLEWICZ, K. and MORACZEWSKA, J., 2016. Tropomyosin isoforms differentially modulate the regulation of actin filament polymerization and depolymerization by cofilins. *FEBS Journal,* **283**(4), pp. 723-737.

ROPPOLO, L.P., FITZGERALD, R., DILLOW, J., ZIEGLER, T., RICE, M. and MAISEL, A., 1999. A comparison of troponin T and troponin I as predictors of cardiac events in patients undergoing chronic dialysis at a Veteran's Hospital: A pilot study. *Journal of the American College of Cardiology,* **34**(2), pp. 448-454.

SANBE, A., 2013. Dilated Cardiomyopathy: A Disease of the Myocardium. *Biological and Pharamceutical Bulletin,* **36**(1), pp. 18-22.

SCHEVZOV, G., WHITTAKER, S.P., FATH, T., LIN, J.J.C. and GUNNING, P.W., 2011. Tropomyosin isoforms and reagents. *Bioarchitecture,* **1**(4), pp. 135-164.

SCHULZ, E.M., WILDER, T., CHOWDHURY, S.A.K., SHEIKH, H.N., WOLSKA, B.M., SOLARO, R.J. and WIECZOREK, D.F., 2013. Decreasing Tropomyosin Phosphorylation Rescues Tropomyosin Induced Familial Hypertrophic Cardiomyopathy. *Journal of Biological Chemistry,* **288**(40), pp. 28925-28935.

SENSKE, M., CONSTANTINESCU-ARUXANDEI, D., HAVENITH, M., HERRMANN, C., WEINGARTNER, H. and EBBINGHAUS, S., 2016. The temperature dependence of the Hofmeister series: thermodynamic fingerprints of cosolute-protein interactions. *Physical Chemistry Chemical Physics,* **18**(43), pp. 29698-29708.

ŚLIWIŃSKA, M. and MORACZEWSKA, J., 2013. Structural differences between C-terminal regions of tropomyosin isoforms. *PeerJ,* **1**(e181),.

SMILLIE, L.B., 1996. Chapter 5 - Tropomyosin. In: M. BÁRÁNY, ed, *Biochemistry of Smooth Muscle Contraction.* San Diego: Academic Press, pp. 63-75.

SOKOLOV, D.V., 2013. Atomic force microscopy for protein nanotechnology. *Methods Mol Bio,* **996**, pp. 323-367.

SOUSA, D., CAMMARATO, A., JANG, K., GRACEFFA, P., TOBACMAN, L.S., LI, X. and LEHMAN, W., 2010. Electron Microscopy and Persistence Length Analysis of Semi-Rigid Smooth Muscle Tropomyosin Strands. *Biophysical journal,* **99**(3), pp. 862-868.

SQUIRE, J.M., PAUL, D.M. and MORRIS, E.P., 2017. Myosin and Actin Filaments in Muscle: Structures and Interactions. In: D.A.D. PARRY and J.M. SQUIRE, eds, *Fibrous Proteins: Structures and Mechanisms.* Cham: Springer International Publishing, pp. 319-371.

STEVENS, R., STEVENS, L. and PRICE, N.C., 1983. *Biochemical education,* **11**(2), pp. 70.

STEWART, M., 2001. Structural basis for bending tropomyosin around actin in muscle thin filaments. *Proceedings of the National Academy of Sciences,* **98**(15), pp. 8165-8166.

STRAUSSMAN, R., SQUIRE, J.M., BEN-YA'ACOV, A. and RAVID, S., 2005. Skip Residues and Charge Interactions in Myosin II Coiled-coils: Implications for Molecular Packing. *Journal of Molecular Biology,* **353**(3), pp. 613-628.

STRENG, A.S., DE BOER, D., VAN DER VELDEN, J., VAN DIEIJEN-VISSER, M.P. and WODZIG, W.K.W.H., 2013. Posttranslational modifications of cardiac troponin T: An overview. *Journal of Molecular and Cellular Cardiology,* **63**(0), pp. 47-56.

STURTEVANT, J.M., HOLTZER, M.E. and HOLTZER, A., 1991. A scanning calorimetric study of the thermally induced unfolding of various forms of tropomyosin. *Biopolymers,* **31**(5), pp. 489-495.

SWENSON, C.A. and STELLWAGEN, N.C., 1989. Flexibility of smooth and skeletal tropomyosins. *Biopolymers,* **28**(5), pp. 955-963.

SZELTNER, Z. and POLGÁR, L., 1996. Conformational Stability and Catalytic Activity of HIV-1 Protease Are Both Enhanced at High Salt Concentration. *Journal of Biological Chemistry,* **271**(10), pp. 5458-5463.

TAKEDA, S., YAMASHITA, A., MAEDA, K. and MAEDA, Y., 2003. Structure of the core domain of human cardiac troponin in the Ca2+-saturated form. *Nature,* **424**(6944), pp. 35-41.

THIERFELDER, L., WATKINS, H., MACRAE, C., LAMAS, R., MCKENNA, W., VOSBERG, H., SELDMAN, J.G. and SEIDMAN, C.E., 1994. α-tropomyosin and cardiac troponin T mutations cause familial hypertrophic cardiomyopathy: A disease of the sarcomere. *Cell,* **77**(5), pp. 701-712.

TRACHTENBERG, S. and HAMMEL, I., 2010. Determining the persistence length of biopolymers and rod-like macromolecular assemblies from electron microscope images and deriving some of their mechanical properties. *Microscopy: Science, Technology, Applications and Education,* **3**, pp. 1690-1695.

VEIGEL, C. and SCHMIDT, C.F., 2011. Moving into the cell: Single-molecule studies of molecular motors in complex environments. *Nature Reviews Molecular Cell Biology,* **12**(3), pp. 163-176.

VIBERT, P., CRAIG, R. and LEHMAN, W., 1997. Steric-model for activation of muscle thin filaments. *Journal of Molecular Biology,* **266**(1), pp. 8-14.

VICENTE-MANZANARES, M., MA, X., ADELSTEIN, R.S. and HORWITZ, A.R., 2009. Non-muscle myosin II takes centre stage in cell adhesion and migration. *Nature reviews.Molecular cell biology,* **10**(11), pp. 778-790.

VINOGRADOVA, M.V., STONE, D.B., MALANINA, G.G., KARATZAFERI, C., COOKE, R., MENDELSON, R.A. and FLETTERICK, R.J., 2005. Ca2+-regulated structural changes in troponin. *Proceedings of the National Academy of Sciences of the United States of America,* **102**(14), pp. 5038-5043.

VOLKMANN, N. and HANEIN, D., 2000. Actomyosin: law and order in motility. *Current opinion in cell biology,* **12**(1), pp. 26-34.

WALKER, J.S., LI, X. and BUTTRICK, P.M., 2010. Analysing force-pCa curves. *Journal of muscle research and cell motility,* **31**(1), pp. 59-69.

WANG, L., CHEN, T., ZHOU, X., HUANG, Q. and JIN, C., 2013. Atomic force microscopy observation of lipopolysaccharide-induced cardiomyocyte cytoskeleton reorganization. *Micron,* **51**(0), pp. 48-53.

WEI, B. and JIN, J.-., 2011. Troponin T isoforms and posttranscriptional modifications: Evolution, regulation and function. *Archives of Biochemistry and Biophysics,* **505**(2), pp. 144-154.

WIECZOREK, D.F., JAGATHEESAN, G. and RAJAN, S., 2008. The role of tropomyosin in heart disease. *Tropomyosin.* Springer, pp. 132-142.

WILLIAMS, D.L. and SWENSON, C.A., 1981. Tropomyosin stability: assignment of thermally induced conformational transitions to separate regions of the molecule. *Biochemistry,* **20**(13), pp. 3856-3864.

WOODS, E.F., 1967. Molecular Weight and Subunit Structure of Tropomyosin B. *Journal of Biological Chemistry,* **242**(12), pp. 2859-2871.

WRABL, J., HOLTZER, M.E. and HOLTZER, A., 1994. Thermal unfolding equilibria in homodimeric chicken gizzard tropomyosin coiled coils. *Biopolymers,* **34**(12), pp. 1659-1667.

XUE, W., HOMANS, S.W. and RADFORD, S.E., 2009. Amyloid fibril length distribution quantified by atomic force microscopy single-particle image analysis. *Protein Engineering Design and Selection,* **22**(8), pp. 489-496.

YACOUB, M.H., 2014. Decade in reviewmdash]cardiomyopathies: Cardiomyopathy on the move. *Nat Rev Cardiol,* **11**(11), pp. 628-629.

YANG, S., BARBU-TUDORAN, L., ORZECHOWSKI, M., CRAIG, R., TRINICK, J., WHITE, H. and LEHMAN, W., 2014. Three-dimensional organization of troponin on cardiac muscle thin filaments in the relaxed state. *Biophysical journal,* **106**(4), pp. 855-864.

YUROV, V.Y. and KLIMOV, A.N., 1994. Scanning tunneling microscope calibration and reconstruction of real image: Drift and slope elimination. *Review of Scientific Instruments,* **65**(5), pp. 1551-1557.

ZHENG, W., HITCHCOCK-DEGREGORI, S. and BARUA, B., 2016. Investigating the effects of tropomyosin mutations on its flexibility and interactions with filamentous actin using molecular dynamics simulation. *Journal of muscle research and cell motility,* **37**(4), pp. 131-147.

ZOT, A.S. and POTTER, J.D., 1987. Structural aspects of troponin-tropomyosin regulation of skeletal muscle contraction. *Annual Review of Biophysics and Biophysical Chemistry,* **16**, pp. 535-559.

Appendix

Isoform	Conditions	Peak 1	Peak 2	Peak 3
αα	100 mM KCl + DTT	38.5	45.2	50.7
αα	100 mM KCL + MOPS + DTT	39.6	45.2	50.0

Table A1. First differential analysis of α Tpm in standard salt buffer containing MOPS, against α Tpm in standard salt buffer containing KPI, in the presence of DTT. Peak heights 1 – 3 represent the three unfolding events at low, mid-range and high temperatures

Isoform	Conditions	Peak 1	Peak 2	Peak 3
αα	400 mM KCl + DTT	40.5	46.9	52.4
ßß	400 mM KCl + DTT	15.4	39.2	46.8

Table A2. Changes in thermal stability of β Tpm in reference to α Tpm in 400 mM KCl, 20 mM KPi, 5 mM MgCl2, 1 mM NaN3 pH7. Peaks 1 – 3 represent thermal unfolding events at low, middle and high temperature ranges.

Isoform	Conditions	Peak 1	Peak 2	Peak 3
αα	100 mM KCl + DTT	38.5	45.2	50.7
αHisα	100 mM KCl + DTT	37.7	44.9	49.2
HisαHisα	100 mM KCl + DTT	39.0	44.7	48.1

Table A3. Changes in thermal stability of Hisα homodimer and αHisα heterodimer Tpm in reference to α Tpm in 100 mM KCl, 20 mM KPi, 5 mM MgCl2, 1 mM NaN3 pH7, 1 mM DTT. Peaks 1 – 3 represent thermal unfolding events at low, middle and high temperature ranges.

Isoform	Conditions	Peak 1	Peak 2	Peak 3
αα	100 mM KCl + DTT	38.5	45.2	50.7
αα	400 mM KCl + DTT	40.5	46.9	52.4
αα	500 mM KCl + DTT	41.2	48.7	54.7

Table A4. First differential analysis of α Tpm in 500 mM KCl and 400 mM KCl compared to 100 mM KCl. Thermal stability is increased across all three peaks, and increases with increased salt.

Isoform	Conditions	Peak 1	Peak 2	Peak 3
αHisα	100 mM KCl + DTT	37.7	44.9	49.2
αHisα	500 mM KCl + DTT	39.6	45.8	50.7

Table A5. First differential analysis of His α Tpm in 500 mM KCl compared to 100 mM KCl. Thermal stability is increased across all three peaks, and increases with increased salt.

Isoform	Conditions	Peak 1	Peak 2	Peak 3
αα	33 mM CaCl2.2H2O + DTT	29.3	47.6	57.8
αα	100 mM KCl + DTT	38.5	45.2	50.7
αα	100 mM KCL + MOPS + DTT	39.6	45.2	50.0
αα	100 mM NH3Cl + MOPS + DTT	43.5	47.7	54.3

Table A6. Changes in thermal stability when 100 mM KCl was substituted for 100mM NH$_3$Cl and 33 mM CaCl$_2$. NH$_3$Cl increased thermal stability over the entire temperature range, which CaCl$_2$ decreased thermal stability of peak 1 and increased thermal stability of peak 2 and 3.

Isoform	Conditions	Peak 1	Peak 2	Peak 3
αα x link	100 mM KCl - DTT	35.0	48.3	55.6
αα x link	100 mM KCl + DTT 1	35.1	45.8	51.8
αα x link	100 mM KCl + DTT 2&3	37.7	44.6	49.0

Table A7. The effect of cross-linking α Tpm on thermal stability in standard salt buffer (100 mM KCl). The first melt after addition of 1 mM DTT (reducing the cross-link) showed a decrease in thermal stability of peaks 2 and 3 (mid to high temperatures). There effects were amplified for melts 2 and 3 of the same sample (fully reduced). Peak 1 showed an increase in thermal stability, only upon full reduction of the cross-link.

Isoform	Conditions	Peak 1	Peak 2	Peak 3
hisαhisα x link	100 mM KCl - DTT	32.7	53.7	57.0
hisαhisα x link	100 mM KCl + DTT 1	34.4	47.3	54.0
hisαhisα x link	100 mM KCl + DTT 2&3	38.2	45.0	48.9

Table A8. The effect of cross-linking Hisα Tpm on thermal stability in standard salt buffer (100 mM KCl). The first melt after addition of 1 mM DTT (reducing the cross-link) showed a decrease in thermal stability of peaks 2 and 3 and an increased thermal stability of peak 1. There effects were amplified for melts 2 and 3 of the same sample (fully reduced).

Isoform	Conditions	Peak 1	Peak 2	Peak 3
αα	100 mM KCl -DTT	39.6	45.1	54.4
αE54K	100 mM KCl -DTT	38.5	45.4	51.9

Table A9. Changes in thermal stability of E54Kα Tpm in standard salt buffer (100 mM KCl) in the absence of DTT, against αα Tpm under the same conditions. The mutant heterodimer decreased thermal stability of peak 3.

Isoform	Conditions	Peak 1	Peak 2	Peak 3
αHisα	100 mM KCl -DTT	37.5	46.6	56.0
HisαE54K	100 mM KCl -DTT	36.0	44.8	55.5

Table A10. Changes in thermal stability of E54KHisα Tpm in standard salt (100 mM) in the absence of DTT, against the thermal stability of αα Tpm under the same conditions. The mutant heterodimer showed a significant decrease in the thermal stability of peak 1.

Bin	Frequency
10	0
15	8
20	25
25	12
30	8
35	3
40	0
45	3
50	0
55	0
60	0

Table A11. Histogram binned data of MATLAB traces to measure contour length of α Tpm.

Bin	Frequency
10	0
15	2
20	11
25	25
30	31
35	26
40	10
45	4
50	2
55	4
60	0
65	1

Table A12. Histogram binned data of MATLAB traces to measure contour length of β Tpm.